Queen Mary University of London

PhD Thesis

Thesis Submitted in Partial Fulfillment of the Requirements for the Degree of Doctor of Philosophy

Targeting Microvesicles to the Arthritic Joint Using Antibodies Specific to Damaged Cartilage

Miss Louise Mary Topping
BSc (Hons), MRes

Barts and The London
School of Medicine and Dentistry

Statement of Originality

I, Louise Mary Topping, confirm that the research included within this thesis is my own work or that where it has been carried out in collaboration with, or supported by others, that this is duly acknowledged below and my contribution indicated. Previously published material is also acknowledged below.

I attest that I have exercised reasonable care to ensure that the work is original, and does not to the best of my knowledge break any UK law, infringe any third party's copyright or other Intellectual Property Right, or contain any confidential material.

I accept that the College has the right to use plagiarism detection software to check the electronic version of the thesis.

I confirm that this thesis has not been previously submitted for the award of a degree by this or any other university.

Collaboration and publications:

- Vinci, C. *et al.,* 2019
- Topping, L. M *et al.,* 2019

Dr Bethan Thomas kindly performed the histological staining of the final experiment of this thesis.

This work was supported by the Queen Mary University of London Life Sciences Initiative.

Signature: Louise Topping

Date: 26th October 2018

Abstract

Rheumatoid arthritis (RA) is a systemic autoimmune disease and the second most common form of arthritis. The efficacy of current treatments for RA is limited by an increased risk of off target effects and a high percentage of non-responders. To try and overcome this, human antibodies that bind specifically to damaged arthritic cartilage, but not healthy cartilage, were developed for means of delivering drugs to the joints. The antibodies are specific to collagen type II (CII), the major cartilage protein, that has been post-translationally modified by reactive oxidants (ROS, resulting in ROS-CII), which is abundantly found in inflamed joints. It has previously been shown that fusing anti-ROS-CII antibodies to either a mouse version of etanercept or viral-IL-10 significantly enhanced the therapeutic effect on the inflamed knee in a mouse model of arthritis.

Herein, a new treatment modality was created to attempt to utilise the anti-ROS-CII antibodies to target biological scaffolds to the arthritic joint. As a biological scaffold, microvesicles (MV), a subset of extracellular vesicles released from the plasma membrane of nearly all cells, were utilised. Specifically, MV derived from neutrophils (PMN) were used. MV from PMN have been previously shown to penetrate cartilage and exert chondro-protective effects in the context of inflammatory arthritis.

Antibodies specific to ROS-CII retained their binding capabilities after enrichment upon MV, and anti-ROS-CII enriched MV exhibited the ability to localise specifically in the arthritic joint in vivo. The targeted MV were then co-loaded with anti-inflammatory

therapeutics to deliver a pro-resolving ‘magic bullet’ to the arthritic knee in vivo. Importantly, targeting MV with anti-ROS-CII alongside combined treatments led to the complete amelioration of knee inflammation.

Overall, this study demonstrates the attainability of targeting a pro-resolving biological scaffold to the arthritic joint. The potential of co-delivering MV alongside anti-inflammatory therapeutics is beneficial to simultaneously protect cartilage and reduce inflammation.

“You’re going to university, you have no choice in the matter.”

Mum

Acknowledgements

Foremost, I would like to thank Professor Ahuva Nissim for her constant support, guidance and wisdom throughout my PhD. I have thoroughly enjoyed my time with you and I know I will enjoy your friendship for long to come. My thanks also to Dr Helena Azevedo, without whom this PhD wouldn't exist, and Dr Lucy Norling for their co-supervision. I would also like to mention Professor Mauro Perretti, who has shared his experience and guidance throughout this process. I would additionally like to thank my funding body, the QMUL Life Sciences Initiative, for providing the opportunity for me to complete this PhD.

I must extend my love and thanks to the whole of Biochemical Pharmacology (AKA Biopharmily), both current and past members. It has been a joy to work in this environment for 3 years, and I have really made some special, life-long friends. I must give a particular shout-out to Dr Chiara Vinci, Dr Danilo Cucchi, Dr Michelle Sugimoto, Dr Hefin Rhys, Laura Medrano-Gonzalez, Hannah Law, Dr Patricia de Souza and Ula Stopka-Farooqui who all played an important part in my journey, and to whom I am very grateful. Chiara must get extra special recognition for being such a patient, helpful, practical and wonderful ally since day one. I must also thank everyone who gave their time to teach me within the lab, including Hefin, Lucy, Dr Ngee Han Lim, Dr Bethan Thomas and Dr Dianne Cooper. Thanks also to Bethan and Dr Mike Tranter for proof reading this thesis!

Additional thanks to the other members of the William Harvey Research Institute who have helped contribute and/or support in one way or another: all the healthy blood donors, Charterhouse Square flow cytometry unit, Barts and the London genome centre, Charterhouse Square BSU, everyone on the William Harvey Research Institute postgraduate research committee, Arif Mustafa, Martin Goss, Professor Mike Seed, Dr Jordi Lopez-Tremoleda, Dr Mathieu-Benoit Voisin, Dr Lucas Jagemann, Dr Giovanna Nalesso, Dr Elisa Corsiero and Pedro Alves.

I would like to thank some of the people who have played an important part in my educational journey since secondary school, and have inspired me to continue to a PhD: Victoria Gamble (Matthews), Hannah Sillars, Nishanthi Palakrishnan, Professor Matteo Santin and Dr Mariagemiliana Dessi. I am also lucky to have a wonderful group of friends whom I should thank, who have been there consistently for over 10 years and continue to inspire me with their own successes: Lucy Butt, Lacey Hailstones, Mabel Newton and Sophie Snook.

I would also like to acknowledge Elle Woods (regardless of the fact that she is a fictional character) for being a fabulous inspiration to me since 2001.

A big acknowledgement must go to my better half, Chris. I doubt I could have done this without your support. You've been there consistently since A levels to now PhD, and believed in and supported me unconditionally, at every step along the way. Thank you for understanding the craziness that comes with doing a PhD. I am so grateful to have you supporting me in every way, from reassuring me when things get tough, to cooking our tea every night because I get home so late! Thank you!

It's impossible to put into words the gratitude I have for my whole family, who have fiercely supported me throughout this whole process. They have all supported me in different ways and kept me sane when I most needed it, and I appreciate each and every one of them. Particular thanks to Mum and Stevie who have always helped in every way they possibly can. Thanks also to Dave for always willing to help your little sister when in need!

Table of Contents

List of Figures

List of Tables

List of Acronyms

°C	Degrees celcius
µM	Micromolar
µg	Microgram
µm	Micrometer
ACAN	Aggrecan
ACPA	Anti-citrullinated protein/peptide antibodies
ADAMTS	A disintegrin and metalloproteinase with thrombospondin motifs
AGE	Advanced glycation end products
AIA	Antigen induced arthritis
ANOVA	Analysis of variance
Anti-mTNF	Antibody specific to mouse tumour necrosis factor
Anti-ROS-CII	Antibody specific to ROS-CII
AnxA1	Annexin A1
BODIPY Maleimide	Boron-dipyrromethene maleimide
BSA	Bovine serum albumin
CII	Collagen type II
CD	Cluster of differentiation
cDNA	Coding DNA
CFA	Complete Freund's adjuvant
CIA	Collagen induced arthritis
COL2A1	Type II collagen
Ct	Cycle threshold
DAPI	4’,6-diamidino-2-phenylindole
dH2O	Distilled water
DMARDs	Disease modifying anti-rheumatic drugs
DMM	Destabilisation of the medial meniscus
DNA	Deoxyribonucleic acid

E. coli	*Escherichia coli*
ECM	Extracellular matrix
EDTA	Ethylene-(2,2)-diamine-tetracetic acid
ELISA	Enzyme-linked immunosorbent assay
FBS	Foetal bovine serum
Fc	Fragment crystallisable
FPR	Formyl peptide receptor
G	Gauge (needle size)
g	Gravitational acceleration
Gly CII	Glycated collagen II
H&E	Haematoxylin and eosin
H_2O_2	Hydrogen peroxide
H_2SO_4	Sulphuric acid
HCl	Hydrochloric acid
HEL	Hen egg lysozyme
HLA	Human leukocyte antigen
HOCl CII	Chlorinated collagen II
HRP	Horse radish peroxidase
IgG	Immunoglobulin G
IgM	Immunoglobulin M
IL	Interleukin
IL-1β	Interleukin 1β
IL-4	Interleukin 4
IL-6	Interleukin-6
IL-8	Interleukin-8
IL-10	Interleukin-10
IPTG	Isopropyl β-D-thiogalactoside
ISX	ImageStreamX
IVIS	*In vivo* imaging system

mBSA	Methylated bovine serum albumin
mL	Millilitre
mM	Millimolar
mm	Millimetre
MMP	Matrix metalloproteinase
mRNA	Messenger ribonucleic acid
mTNF	Mouse tumour necrosis factor
MV	Microvesicles
NaCl	Sodium chloride
NaOH	Sodium hydroxide
NF-κB	Nuclear factor kappa B
nm	Nanometre
NO	Nitric oxide
NTA	Nanoparticle tracking analysis
OA	Osteoarthritis
OCT	Optimal cutting temperature compound
OD	Optical density
OH	Hydroxide
PAD	Peptidyl arginine deiminase
PAGE	Polyacrylamide gel electrophoresis
PBMC	Peripheral blood mononuclear cells
PBS	Phosphate buffered saline
PCR	Polymerase chain reaction
PFA	Paraformaldehyde
PMN	Polymorphonuclear cells
qPCR	Quantitative PCR, real-time PCR
RA	Rheumatoid arthritis
RF	Rheumatoid factor
RNA	Ribonucleic acid

ROI	Region of interest
ROS	Reactive oxygen species
ROS-CII	CII post translationally modified by ROS
RPL32	Ribosomal protein L32
RPM	Rotations per minute
scFv	Single chain variable fragment
SD	Standard differentiation
SDS	Sodium dodecylsulphate
SEM	Standard error of the mean
SOX9	Sex determining region y-box 9
SSC	Side scatter
TEMED	Tetramethylethlenediamine
TMB	3, 3', 5, 5'-tetramethylbenzidine
TGF-β	Transforming growth factor β
TNFα	Tumour necrosis factor α
V	Volts
vIL-10	Viral interleukin 10
v/v	Volume to volume
VEGF	Vascular endothelial growth factor
w/v	Weight to volume

Chapter 1: Introduction

1.1 Arthritis

Around 10 million people in the United Kingdom currently have a form of arthritis, with an estimated global incidence of around 350 million individuals. Arthritis is a group of diseases that cause pain and inflammation in the joints. It is a leading cause of disability and results in a reduced quality of life with significant morbidity. Not only does arthritis cause a severe, detrimental impact to the sufferer, but it also carries a heavy socio-economic burden [1].

The two most common subtypes of arthritis are osteoarthritis (OA) and rheumatoid Arthritis (RA). The variance between these two subtypes is great, with RA classically referred to as 'inflammatory arthritis', typically caused by a loss of tolerance and subsequent autoimmune disease in an individual. OA has often been recognized as 'non-inflammatory arthritis' due to the nature of its onset, often caused by injury or wearing of cartilage. Nonetheless, the involvement of an inflammatory component in OA has become more recognized over the past decade [2].

1.1.1 Rheumatoid Arthritis

RA is a chronic, systemic inflammatory disease affecting around one percent of the population. It is a complex, multifactorial disease and unlike many inflammatory diseases has little known regarding etiology. Autoantigens in RA have been identified, as have genetic and environmental risk factors, however the underlying mechanism of disease is still unclear.

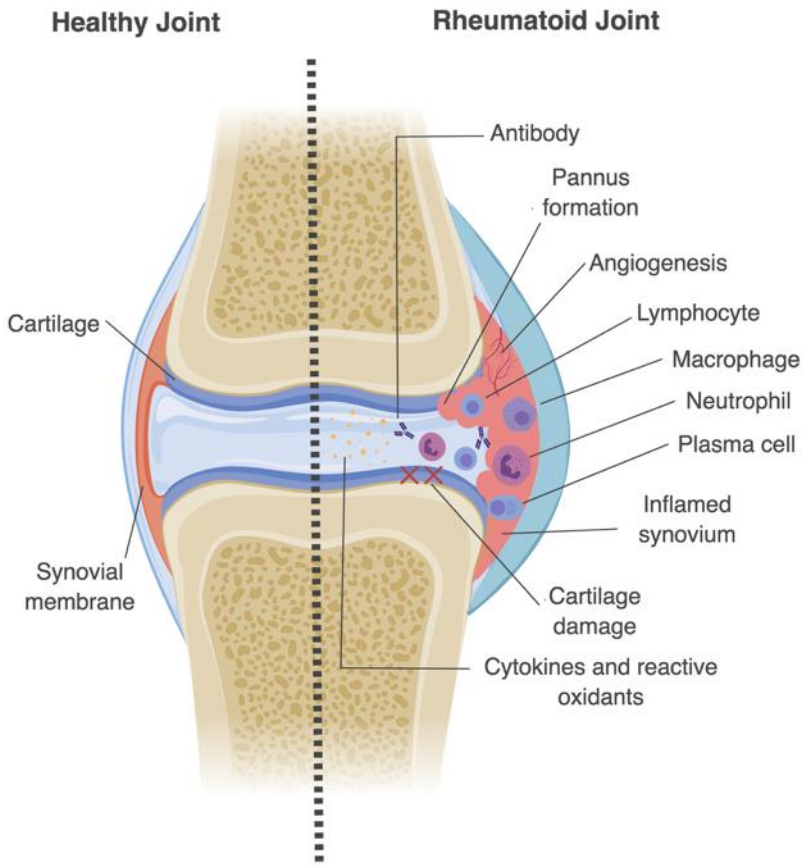

Figure 1. Comparison of a healthy and rheumatic joint. Rheumatic joints are characterized by the infiltration of immune cells, synovial changes, cartilage destruction and the excessive production of cytokines and reactive oxidants. Image created with Biorender.

1.1.1.1 Aetiology

RA involves a complex interplay of genetic factors and environmental triggers. There has been a long-established, well documented association of the HLA-DRB1 locus, which codes for a human leukocyte antigen [1]. The common amino acid motif 'QKRAA" found in HLA-DRB1 alleles indicates a susceptibility to developing RA, suggesting that predisposition in human leukocyte antigens, potentially including T-cell repertoire selection, antigen presentation, or

alteration in peptide affinity, have a role in the development and promotion of disease [3,4]. Moreover, like many autoimmune diseases, there is an imbalance between sexes, with the ratio of females being diagnosed roughly 3:1 compared to males [5]. Observational studies have also implied that females with RA overall do worse than men with disease [6]. This has been attributed to X-linked genetic factors and hormonal differences, although a direct mechanism is unclear [5,7].

Certain environmental triggers have been established in RA, in both HLA-DRB1 allele positive individuals and in those without susceptibility genotypes. Smoking was first paired with increased risk in 1987, when an association between smoking and hospitalisation due to RA was observed in a gynaecological study [8]. Henceforth, there were numerous clinical studies supporting the association and it has become the most prominent environmental factor in RA pathogenesis [9]. Additional environmental triggers come from infectious agents such as Epstein-Barr virus, *Escherichia coli,* cytomegalovirus and their by-products [1,10]. Such infectious agents have been long linked to RA and are thought to pose a threat due to molecular mimicry, resulting in a loss of tolerance- although unifying mechanisms remain elusive. Many contributing genetic and environmental factors have been established in RA, however some of the fundamental underlying mechanisms of disease are still unknown. These gaps in the knowledge mean that a cure for RA is currently non-existent, and current treatment and therapies aim to relieve the symptoms of disease but often fall short.

1.1.1.2 Pathogenesis

Several different cell types are thought to be responsible for the pathogenesis of RA, as demonstrated in Figure 1. The adaptive autoimmune response, mediated by T cells and B cells, is known to be a major contributing factor to the initializing of the inflammatory cascade. Both T cells and B cells, as well as members of the innate immune system such as macrophages and neutrophils, migrate into the synovial tissue, leading to the production of immune mediators and degradative molecules. This production results in degradation of the extracellular matrix within the joint, as well as degradation of healthy cartilage. Within the inflamed arthritic joint there are detrimental changes to the native cells that reside in the synovium and bone. Synoviocytes undergo hyperplasia, angiogenesis occurs and the differentiation of mature osteoclasts results in bone erosion [11]. Synovial hyperplasia is incompletely understood, however cytokines are known to be crucial to the process [12]. Synovial fibroblasts become activated because of the abnormal presence of pro-inflammatory cytokines in the arthritic joint, of which tumour necrosis factor alpha (TNFα) and interleukin-1 Beta (IL-1β) are paramount. Exposure to such cytokines results in the synovial fibroblasts in turn producing TNFα and IL-1β, which induces the production of degradative enzymes by chondrocytes residing in cartilage, such as matrix metalloproteases (MMP), aggrecanases and cathepsins- enzymes which play the main role in the destruction of cartilage in arthritis [12,13].

The presence of autoantibodies in RA is a prominent feature and has become an important part of diagnosis. There have been many reports on autoantibodies to several varying

proteins in RA, however rheumatoid factor (RF) and anti-citrullinated protein/peptide antibody (ACPA) are the most clinically relevant to date. RF was the first described human autoantibody and is found in around 70-80% of RA patients [14,15]. RF is specific to the Fc region of Immunoglobulin G (IgG) antibodies, and themselves usually exist as Immunoglobulin M (IgM) isotypes [15]. RF can be detected in up to 10% of healthy individuals, however the nature of RF found in healthy individuals to those found in RA differs, with healthy RF showing low affinity for IgG and polyreactivity [15].

Within the rheumatoid synovium, high affinity RF are produced by B cells which contain multiple replacement mutations in their complementarity-determining region (CDR), which indicates the role of T-cell help. Furthermore, synovial fibroblasts have been found to support the accumulation and survival of B-cells in the rheumatoid synovium, hence encouraging the production of RF and autoantibodies [16]. RF also plays a major role in the formation of immune complexes in RA. Immune complexes, comprised of immunoglobulins bound to their cognate antigens, have long known to be found in patients with RA. In the rheumatoid synovium, most immune complexes are composed of antibodies with RF specificity [17].

ACPA are highly specific for RA and have thus become an important aspect of diagnosis. As well as a useful diagnostic tool, there is sufficient evidence to suggest ACPA play a role in the pathophysiologic process of RA. For many years, these antibodies were referred to by numerous names including anti-perinuclear factor, anti-keratin antibodies and anti-filaggrin

antibodies, until the crucial finding was discovered that linked each of the antibodies. Each antibody targets epitopes in which arginine has been post-translationally converted to citrulline by the action of peptidyl arginine deiminase (PAD) enzymes [18,19]. Although citrullination does not exist exclusively in RA, it has become a hallmark of disease. The pooled sensitivity and specificity of ACPA analysis in RA is around 67% and 95% respectively [20]. Not all RA patients are ACPA positive, which explains the low sensitivity in the ACPA analysis. However, the high specificity of ACPA analysis out performs RF for diagnosing RA [20].

The pathogenesis of RA has been further understood in the development of murine models of inflammatory arthritis. Multiple models exist, all of which replicate areas of human disease. Collagen induced arthritis (CIA) shares multiple similarities of human RA, including a breach of tolerance and the production of autoantibodies. CIA involves immunization of type II collagen in complete Freund's adjuvant (CFA), creating an autoimmune response towards articular cartilage within the joint. The result is a polyarthritic disease, characterized by synovial inflammatory infiltration, cartilage and bone erosion and synovial hyperplasia similar to human RA [21,22]. Furthermore, the transfer of serum from CIA mice to non-immunized recipient mice results in the development of arthritis [23]. Such models using antibody cocktails against CII are referred to as collagen-antibody-induced arthritis and demonstrate a strong role of the innate immune system in the development of RA.

Additional models using immunization with CFA exist, including the methylated bovine serum albumin (mBSA) model. This model involves priming the immune system using mBSA in CFA,

followed by locally administering mBSA alone within the knee joint. The result is pathology comprising immune complex mediated inflammation, followed by articular T cell mediated responses [24]. The inflammation is localized to the site of mBSA injection, so the model is often used as a monoarticular model with one single knee joint inflamed. Although the mBSA model has fewer similarities to human RA, the characteristic of localized inflammation has proved useful in a murine model. Additional murine models of RA include transgenic murine models, such as the TNF-α transgenic model in which the overexpression of TNF-α results in spontaneous arthritis, and the K/BxN model, in which crossing the TCR transgenic KRN line with mice expressing the MHC class II molecule Ag7 results in spontaneous arthritis [25].

1.1.1.3 Current Therapies

The traditional therapies for RA are disease modifying anti-rheumatic drugs (DMARDs), non-steroidal anti-inflammatory drugs (NSAIDs) and glucocorticoids [26]. Over recent years the development of small molecules and biologics have been instrumental in managing disease in a proportion of RA patients [27–31], however there are still hurdles existing in treating the disease that need to be overcome.

To manage the pain and stiffness associated with RA, NSAIDs and analgesics are administered. The use of NSAIDs is greatly supported, however their role of first line treatment has reduced due to concerns about limited effectiveness, inability to modify the disease and off target side effects, such as in both the gastrointestinal and cardiovascular systems [32]. NSAIDs are often needed to be administered alongside proton-pump inhibitors

for gastro-protection [32]. DMARDs are the main course of treatment for a patient with RA. They are a heterogeneous group of drugs, with varying mechanisms of action- some of which are still incompletely understood. Overall, DMARDs reduce joint swelling and pain, limit progressive joint damage and decrease acute-phase markers [32]. Examples of DMARDs used for the management of RA include methotrexate, sulfasalazine and leflunomide. DMARDs are used individually or in combination to manage the symptoms and disease progression in RA with combinations varying across different countries [32]. Adverse effects of DMARD's can be minor, for example nausea, or serious, including hepatotoxicity. To monitor serious side effects patients are required to have regular blood tests and liver function tests whilst taking DMARDs long term.

The first biological agents to be licensed for the treatment of RA were TNF inhibitors, including infliximab and etanercept. Anti-TNF treatment plays a key role in the current treatment of RA by either blocking the TNF receptor or by inhibitor binding to TNF, ultimately inhibiting the pro-inflammatory cascade. Other key examples of biologics include: (i) abatacept, a fusion protein composed of the Fc portion of an IgG1 with the extracellular domain of CTLA-4. Abatacept works by preventing T-cell activation by inhibiting CD80/CD86 binding by antigen presenting cells [33]; (ii) rituximab, or sometimes known as anti-CD20, is a chimeric mouse/human antibody. Rituximab induces B-cell death by a mechanism that isn't fully understood, however direct signalling, complement dependent cellular cytotoxicity and antibody dependent cellular cytotoxicity all appear to play a role [34]; and tocilizumab, also

referred to as anti-IL-6. Tocilizumab is a humanized monoclonal antibody that inhibits IL-6, a pro-inflammatory cytokine involved in the pathogenesis of RA [35].

Biologics are conventionally combined with DMARDs to limit disease and associated symptoms; however over the years it has become apparent that what works in one patient may not be efficacious for another. For example, around 30-40% of patients do not respond to anti-TNF therapy and will likely be subsequently treated with alternative biologics, such as tocilizumab and abatacept [36]. Studies have also suggested the overall rate of non-responders to biologics is around 30-40%, which is a major drawback of the therapy [37]. The high rate of non-response results in undesirable side effects with no therapeutic benefit to the patient. The reasoning of patient non-response to biologics has been an area of investigation for some time, and the ability to predict non-responders before initiating treatment would be beneficial for both the patient and healthcare provider. There are many contributing factors that have been proposed to influence response to biologics, including prior treatments, genomics, smoking status and serum biomarker profile [38]. An alternative proposed theory of non-response is due to the high systemic concentrations of the biological agent and inadequate local concentrations in the arthritic joints [39]. The high systemic concentrations result in off target side effects, such as opportunistic infections [33,40,41]. Furthermore, the heterogeneic nature of RA adds additional complexity when treating patients. One study found that heterogeneity in early pathological characterization of the synovial tissue from RA patients has a relationship with the likelihood of responding to biologics [42].

The introduction of biologics drastically changed the treatment of RA for the better. The standard of care for patients has improved greatly, with better clinical results and a greater knowledge of the pathogenesis of RA. However, many patients still have inadequate control of their arthritis activity due to non-response or becoming resistant to the beneficial effects of therapies. There is still a great need for additional and alternative treatment options, specifically to target the subset of patients of whom biologics are inefficient to control their disease.

1.1.2 Osteoarthritis

Osteoarthritis (OA) is the most common subtype of arthritis, affecting around 8 million people in the UK alone [43]. OA isn't an epidemic that is exclusive to the UK, and is a major source of pain, disability and socio-economic burden worldwide. OA is a complex, multifactorial disease with many genetic, biological and biomechanical components at play. Although the focus of current research is early intervention and disease prevention, the most effective treatment for severe osteoarthritis remains to be joint replacement, which comes with a plethora of drawbacks.

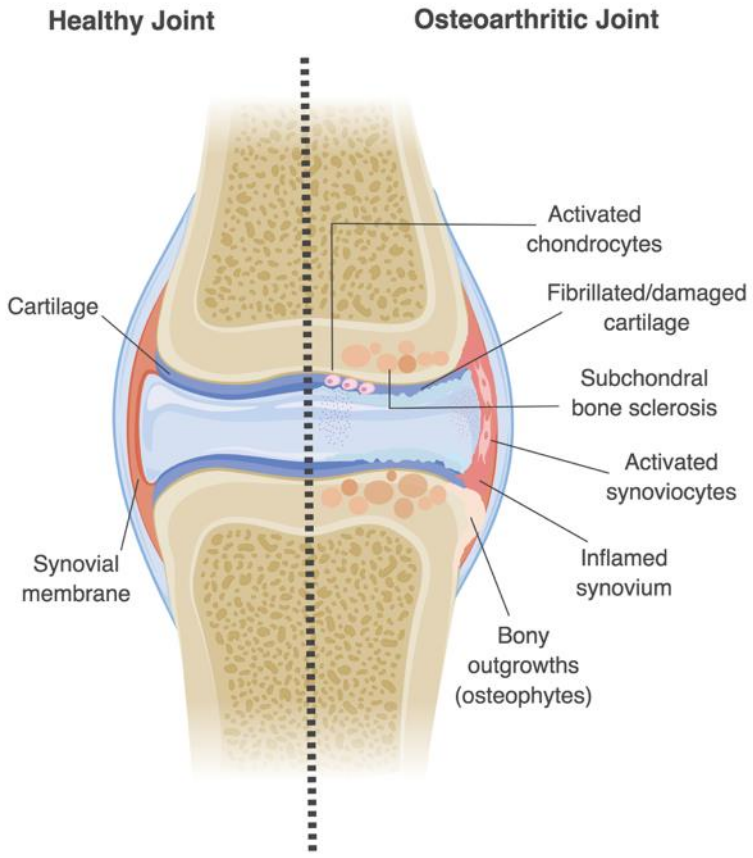

Figure 2. Schematic representing the changes in the joint due to severe osteoarthritis. Osteoarthritic joints are characterised by a loss of cartilage, the formation of osteophytes and an inflamed synovium. Image created with Biorender.

1.1.2.1 Aetiology

OA is primarily considered a disease of age related wear-and-tear of cartilage in the joints and hands, however over recent years the aetiology of OA has found to have a genetic component. OA is a widely heterogeneous disease, and the search for specific genes that give rise to OA has been formidable. Inheritance studies involving families and twin pairs have been able to demonstrate that genetic factors can be attributable to the development of OA in between 39-78% of cases [44–46].

There are many known environmental factors that drastically increase both risk and progression of OA. The most prevalent is age, however obesity and previous knee injury are also important risk factors. One study identified the lifetime risk of a person developing symptomatic knee OA to be nearly 1 in 2, and more than 1 in 2 if a history of knee injury is present [47]. For obese individuals the risk increased to nearly 2 in 3 [47]. The study also found that a higher body mass index at later ages accounted for the greatest variability in lifetime risk estimates [47]. There is also a gender bias involved, with OA being more common in women than men. Around 18% of women over the age of 60 suffer from OA compared to around 10% of men [48,49]. The role of oestrogen in the development of OA has been widely investigated, however a direct mechanism remains unclear [49].

One of the biggest challenges in managing and treating OA is the variability of disease. As aforementioned, it is an incredibly heterogeneous disease, which has no single aetiology.

Many risk factors are known; however, it remains to be an unpreventable disease that's difficult to treat successfully.

1.1.2.2 Pathogenesis

Until recently, OA has been typically viewed as a non-inflammatory disease due to the strong association with damaged cartilage and early observations noting fewer leukocytes within the synovium when compared to RA [50]. Despite this classification, over the past few decades the role of inflammation within OA progression has become better understood, as demonstrated in Figure 2, and the disease is recognised as more than simply 'wear and tear'.

OA is often classified into primary and secondary subtypes. The difference between primary and secondary OA depends on a known cause- secondary OA has developed following an obvious injury or trauma to a joint whereas primary OA has no known cause. With increased understanding of the multifactorial nature of OA, the primary and secondary classification may oversimplify the disease. For example, the risk of post-traumatic OA following meniscal injury of the knee joint is strongly linked to family history of arthritis and the other risk factors previously aforementioned [51]. However, for both primary and secondary OA, the immune system is now known to play a pivotal role in the progression of disease. The tissue that has long attracted great attention with regards to the pathogenesis of OA is articular cartilage. This is due to the striking changes that occur in the tissue throughout the progression of OA, often resulting in a complete loss of articular cartilage in affected joints. Cartilage is a unique tissue of the human body; it contains no nerves or blood vessels, unlike

the subchondral bone beneath it. The lack of vasculature means the tissue is naturally hypoxic. It has one primary cell type, namely chondrocytes, which make up only 5% of the total tissue. Most of the tissue is composed of a specially adapted extracellular matrix (ECM) maintained by the native chondrocytes, which is abundant in collagen and proteoglycans. The quality of the ECM is crucial for the maintenance of healthy cartilage and thus healthy joints. There are known changes that occur in cartilage during OA, both to the chondrocytes and the all-important matrix.

It is known that upon activation, chondrocytes produce several pro-inflammatory cytokines including IL-1β, IL-6 and TNFα. Activated chondrocytes also produce reactive oxygen species (ROS) and matrix degrading enzymes, including metalloproteases- some of which have apparent beneficial matrix remodelling roles in healthy cartilage and some of which are pathogenic [49]. The release of pathogenic matrix metalloproteases (MMP), including MMP1, MMP3 and MMP13, causes destruction of the ECM, which leads to a physiological alteration of articular cartilage and can result in the progressive degradation of cartilage [52]. Furthermore, the production of ROS by chondrocytes and other cells within the inflamed joint results in an imbalance of oxygen within the cartilage. Chondrocytes, which are adapted to thrive in the hypoxic environment, undergo cell death when exposed to excessive ROS. ROS also plays a strong role in ECM degradation, and studies have shown matrix degradation and cartilage loss in animal models treated with ROS scavengers is slowed [53].

It is unknown what causes chondrocyte activation in OA, and as the disease is so heterogeneous it is likely the source of activation will vary between patients. Chondrocyte activation is hypothesised to occur as a result of inflammatory signalling from other origins within the joint, for example from the synovium or subchondral bone [49]. Synovitis is a common feature of OA, even within the early stages of disease. Common features include the proliferation of synovial fibroblasts (also known as synoviocytes), tissue hypertrophy and increased vascularity [54]. One function of synoviocytes is to synthesise natural lubricants for the joint, such as hyaluronic acid. In situations such as arthritis, this should benefit the damaged knee, however it has been found that OA patients show a deficiency in the production and have reduced lubricating capabilities [49,55]. Similarly to chondrocytes, synoviocytes become activated and release pro-inflammatory cytokines, degradative enzymes and ROS. It is speculated that the activation is likely to be secondary to the pro-inflammatory mediators released during an initial insult to the joint. Following an initial insult, synovial tissue drives the degeneration of the joint through a positive feedback cycle [49,54]. The presence and extent of synovitis is also predictive of the progression of OA and cartilage loss [56], although there is a less consistent relationship with structural changes of the joint [49]. Although OA is an incredibly heterogeneous disease, the role of synovitis is crucial in the disease progression of most patients.

1.1.2.3 Current Therapies

The mainstay of current treatments for OA involve physical measures, drug therapy and surgery for late stage disease [57]. There is a strong emphasis on physical measures and

lifestyle changes in the treatment of OA, as pharmacological interventions to modify the disease are lacking, especially in comparison to RA treatment. The pharmacological therapies that are available only have the potential to reduce symptoms, particularly pain. None of the existing treatments are capable of reversing cartilage damage or protecting cartilage from further degradation [57].

A large proportion of OA treatment comes in the environmental changes that can be made to improve symptoms and slow the progression of disease. Weight loss is suggested, particularly in individuals with an overweight or obese body mass index. Weight loss can help to adjust the unbalanced mechanical stress on the joint, reduce pain and also reduce OA risks [57,58]. Additionally, moderate exercise has been identified to strengthen the muscles surrounding the joint and potentially delay the progression of OA [59].

Surgery will only be considered for severe cases of OA and joint replacement is the most extreme intervention. Additional surgical procedures, such as arthroscopic irrigation and debridement are able to temporarily relieve pain, but are not considered beneficial for long term recovery [57,60]. Microfracture is a technique that aims to penetrate the underlying subchondral bone to induce bone marrow stromal cells to repair the damaged bone and cartilage. This technique is widely associated with the production of fibrocartilage, an inferior and less durable cartilage compared to the native form [57]. As aforementioned, total joint replacement (or arthroplasty) is the most extreme intervention, but is also regarded as the best option for advanced OA, with the ability to eliminate pain and reinstate joint function in

a high proportion of patients. The artificial implant has a limited lifespan of around 10-15 years, which is one of the reasons why arthroplasty isn't recommended for young patients. Additionally, the outcome of arthroplasty also varies depending on which joint is being replaced, resulting in long term outcomes varying significantly [61].

There are five subtypes of pharmacological intervention currently used for the treatment of OA: acetaminophen, NSAIDs, serotonin-norepinephrine reuptake inhibitors (SNRIs), opioid analgesics and intra-articular injections [57]. Acetaminophen, more commonly known as paracetamol, is a common, 'over-the-counter' painkiller used to treat arthritis as well as a variety of other ailments. Acetaminophen is considered relatively safe and effective, and so it the first line oral-analgesic for mild to moderate OA. Patients with severe symptoms or those who do not respond to treatment will likely be introduced onto stronger analgesics. As previously discussed, NSAIDs are a group of drugs that provide both anti-inflammatory actions as well as analgesic effects. In randomized control studies, NSAIDs have continually outperformed acetaminophen for pain relief in OA patients. However, there are concerns with adverse events such as in individuals taking regular NSAIDs, with an estimated occurrence in 30% of patients [57,62]. Opioids are being increasingly used for the treatment of moderate and severe OA to manage the associated pain. One meta-analysis study found that the numbers of OA patients in the United States being prescribed opioids has steadily increased, from 31% in 2003, to 39% in 2006 and 40% in 2009 [63]. Opioids are associated with a range of common adverse side effects however, including nausea, vomiting and dizziness, which in some patients can outweigh the beneficial pain relief effects of the drugs [57]. SNRI's

primary use are in the treatment of depression, but SNRI are also now FDA approved for the management of chronic musculoskeletal pain, including OA [57]. Drugs such as Duloxetine have shown promising results in blinded, placebo controlled studies [64]. It holds potential as an alternative drug to alleviate OA pain for patients who do not respond well to the more commonly used drugs. Intra-articular injections are selectively used to treat OA. Corticosteroids and hyaluronic acid are both used to alleviate pain and to visco-supplement the joint, respectively. Corticosteroid injections are used in patients with moderate to severe OA who do not respond well to the other treatment options mentioned, whereas hyaluronic acid injections are recommended for treatment of hip or knee OA. The efficacy of hyaluronic acid injections have come under scrutiny in previous years and hence the recommendation for injection has been downgraded from an inconclusive level to a non-affirming level [57].

There are currently drugs in the pipeline that hope to overcome the unsatisfactory and unwanted side effects that occur with the current standard of pharmacological treatment. The ideal therapy for OA should alleviate pain whilst also reducing symptoms and restoring the normal function of the joint. Bone morphogenetic protein 7 (BMP7) is a biological agent that is FDA approved for the treatment of bone nonunions and spinal fusion. BMP7 has entered clinical trials for the treatment of symptomatic knee OA and passed phase one with no dose-limiting toxicity found [57].

A drug consisting of fibroblast growth factor (FGF), namely sprifermin, underwent a proof of concept study to evaluate efficacy and safety whilst administered intra-articularly. Treatment

with sprifermin reduced the loss of cartilage thickness and volume [65]. Sprifermin also reduced joint space narrowing in a dose dependent manner with no significant difference in adverse events between the control and experimental groups [65]. The local administration of sprifermin by intra-articular injection likely attributes to the lack of adverse events and high therapeutic potential. Additional studies are needed to understand greater this novel OA biologic, however the initial findings are extremely promising.

1.2 Cartilage

Cartilage is one of the key components of synovial joints, and plays an important role in the mechanical load-bearing function of the joint. As discussed, the etiologies of RA and OA differ, however in both diseases the destruction of cartilage is part of the underlying pathophysiology.

1.2.1 Healthy Articular Cartilage

Healthy adult articular cartilage is an avascular tissue, composed of a complex extracellular matrix (ECM) comprised of collagen, proteoglycans and other non-collagen proteins [66]. The native environment of cartilage is unlike any other tissue within the body. It is an avascular, hypoxic tissue composed abundantly of ECM. As shown in Figure 3, articular cartilage is subdivided into three distinctive zones; superficial, intermediate and deep zones [66]. The cartilage morphology within each of these zones differs, and likely reflect the differences in ECM composition. There is only one cell type found in cartilage, the chondrocyte, which make up around only 1-5% of the total tissue mass [67]. Chondroblasts, which are

mesenchymal progenitor cells *in situ*, are found in the superficial layers of the cartilage. Chondroblasts will form into chondrocytes embedded within lacunae upon migration into deeper layers of cartilage. Chondroblasts are important for ECM production, particularly collagen II synthesis. Chondrocytes are found within the superficial, intermediate and deep zones. The tidemark represents the area where cartilage meets bone, and is often referred to as calcified cartilage due to the chondrocyte derived collagen II fibres becoming structurally cemented to collagen I deposited by osteoblasts [68]. The composition and structure of important ECM proteins also changes when moving into deeper cartilage layers.

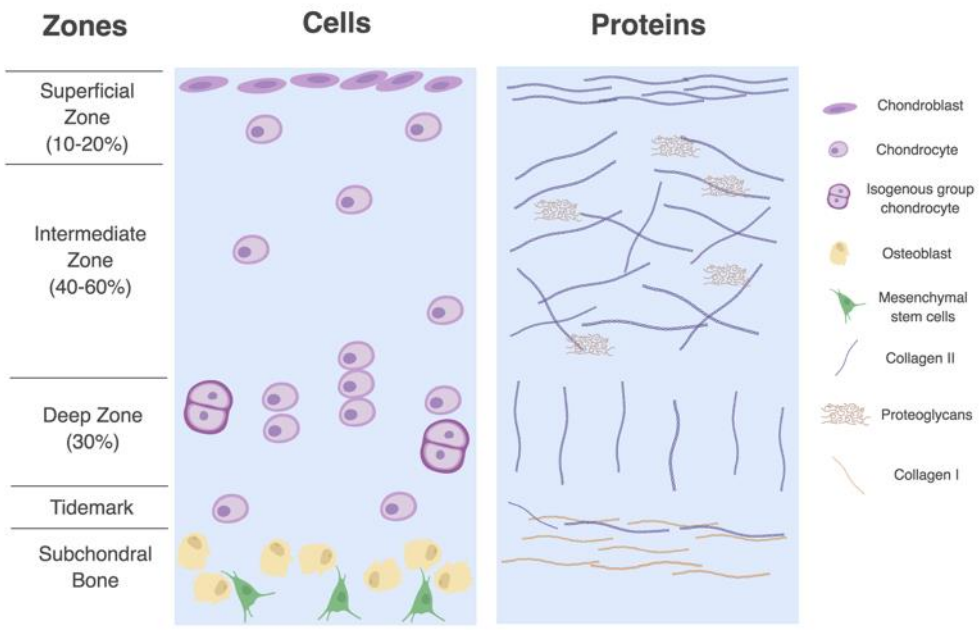

Figure 3. Schematic showing the structure of healthy articular cartilage. Cartilage is sectioned into three different zones: superficial, intermediate and the deep zones. The tidemark represents the area where cartilage meets bone. Chondrocytes are the only cell type within articular cartilage and are responsible for the maintenance of the extracellular matrix through the production of collagen II and proteoglycans. Image created with Biorender.

1.2.1.1 Chondrocytes

Chondrocytes are sparsely embedded within the ECM with no vasculature to provide nutrients, hence they rely on the diffusion of nutrients and metabolites from the articular surface [67]. Chondroblasts and chondrocytes within the superficial zone have a small and flattened morphology, chondrocytes within the middle zone are rounded and within the deep zone group into clusters [66]. The main function of chondrocytes within the superficial and middle zones is the maintenance of the ECM. Chondrocytes have an important role of maintaining the ECM by homeostatic low turnover replacement. Damage to articular cartilage leads to the degradation of ECM, and in many situations the rate of loss of ECM proteins is greater than the capacity for the native chondrocytes to replenish them.

The well-defined structural composition of articular cartilage is maintained through the actions of the mechanically sensitive chondrocytes. Chondrocytes have been described as residing in a 'resting', yet metabolically active, state. Chondrocytes react to small changes in the ECM to appropriately assemble and degrade components accordingly. This interaction is paramount for cartilage homeostasis and the phenotypic changes of chondrocytes observed in arthritis play a key role in the degradation of cartilage.

1.2.1.2 Collagens

Collagen is the most abundant macromolecule found in cartilage ECM, making up around 60% the tissue [67]. Of this dense collagen presence within the ECM, 90-95% is collagen type II (CII), but collagens III, VI, IX, X, XI, XII and XIV all contribute to form the ECM [69]. Within

articular cartilage, collagen is arranged into vast fibrils with a range of 20nm to 120nm in the superficial zone and deep zone, respectively.

CII is formed of 3 α chains. There are around 34 genes associated with collagen formation. Collagen synthesis usually begins with the transcription of genes associated with the formation of an alpha peptide, thus alpha 1, 2 or 3. Translation of the mRNA then occurs to produce pre-propeptides. Three modifications of the pre-propeptide occur which lead to the formation of the alpha peptide: (i) the signal peptide on the N-terminal dissolves to form propeptide, (ii) lysines and prolines on the propeptide are hydroxylated by hydroxylase enzymes, which aids cross linking, and (iii) glycosylation occurs at the hydroxyl groups on the lysines. Following these three modifications, the hydroxylated and glycosylated propeptides form a triple helix, making procollagen as shown in Figure 4. Once outside the cell, collagen peptidases then act upon the procollagen to form tropocollagen. Collagen fibrils are then formed through the actions of lysyl oxidase on the tropocollagen, which acts on lysines and hydroxylysines resulting in the covalent bonding between tropocollagen molecules.

As demonstrated in Figure 4, the 3 α chains of CII all contain the (Gly-X-Y)n, but vary in their amino acid sequence. Of the other collagen types, collagen IX and XII have been found to associate with CII fibres and contribute to their crosslinking. Collagen VI has been identified in the pericellular regions of cartilage and Collagen X is expressed by hypertrophic chondrocytes, so often found in the growth plate [69].

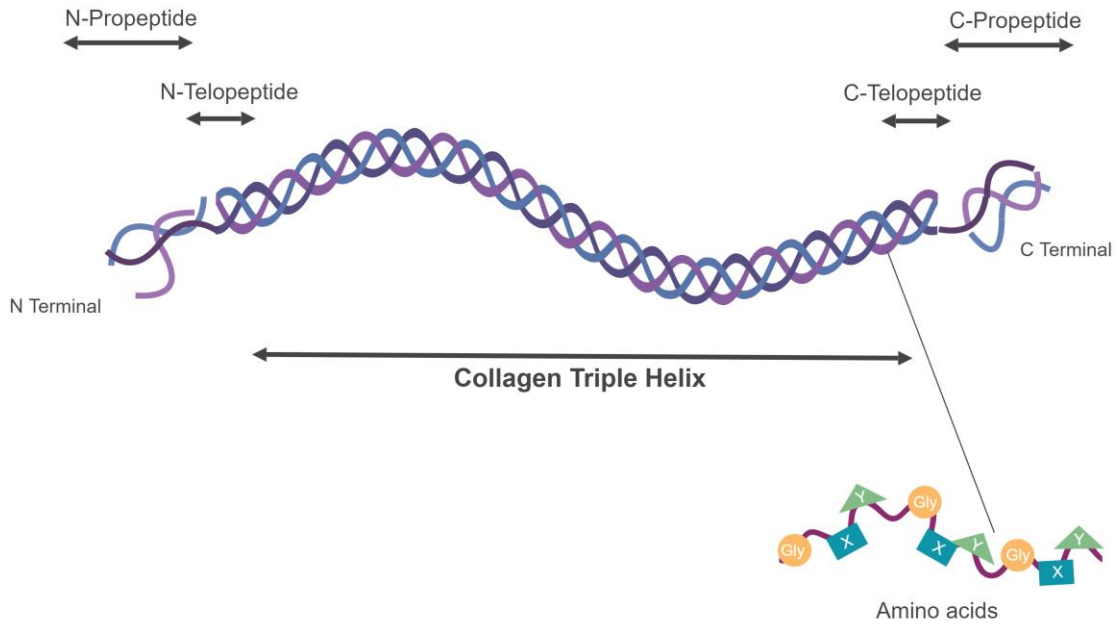

Figure 4. The triple helix structure of procollagen. Collagen is composed of three alpha chains formed through the formation of propeptide. Telopeptides are important for collagen crosslinking and are a site for cleavage by proteases. Image created with Biorender.

1.2.1.3 Proteoglycans

The most predominant proteoglycan present in cartilage is the large chondroitin sulphate proteoglycan aggrecan. As suggested by its name, following secretion aggrecan self assembles in an aggregating fashion with hyaluronan into a supramolecular structure. The core protein of aggrecan has a high molecular weight (230 kDa) and consists of three globular domains, G1, G2 and G3 [69]. Aggrecan also has three interglobular domains, keratin

sulphate and chondroitin sulphate glycasminoglycan attachment domains and a short interglobular domain between G1 and G2. The ability of aggrecan to bind to hyaluronan in the ECM is important for providing a mechanism for the fixation of aggregation within the matrix. Aggrecan and hyaluronan have also been found to be important for pericellular matrix formation and maintenance of matrix homeostasis [69].

Decorin, biglycan and fibromodulin are smaller, non-aggregating proteoglycans found in cartilage in similar molar quantities as aggrecan [70]. Decorin and fibromodulin interact with type II collagen fibrils within the ECM and have a role in fibrillogenesis and interfibril interactions [70]. Biglycan surrounds chondrocytes and is thought to have an interactive role with collagen VI [70]. Figure 5 summarises these interactions of proteoglycans either with each other, or with CII.

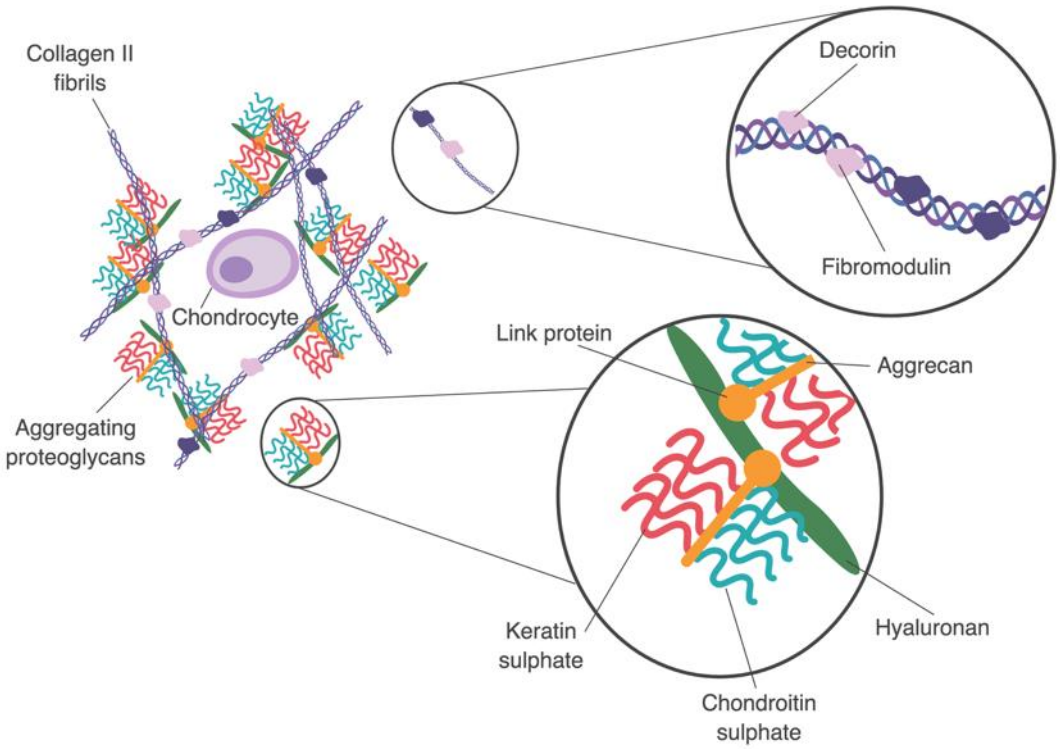

Figure 5. Schematic of proteoglycan aggregation and interaction with collagen II. Aggrecan self assembles with hyaluronan into a supramolecular structure. Keratin sulphate and chondroitin sulphate bind to aggrecan through attachment domains. Decorin and fibromodulin interact with collagen II fibrils. Image created with Biorender.

As previously mentioned, the turnover of CII is very low, with a half-life greater than 100 years. Although collagen has a very low turnover, aggrecan and other proteoglycans continue to be regularly synthesized within the ECM.

1.2.1.4 Water

The most abundant component of cartilage, contributing up to 80% of its wet weight, is water. Water is found predominantly in the intrafibrillar space within the collagen, as well as in low levels the intercellular space. The remainder is located in the pore space of the ECM [70,71].

Water in articular cartilage plays an incredibly important role for both nutrient transport and weight bearing. The relative water concentration decreases from 80% at the superficial zone to 65% in the deep zone. The flow of water through the cartilage zones is important to transport and distribute nutrients to the resident chondrocytes. The frictional resistance to water flow and combined pressurization of water within the matrix forms the two basic mechanisms by which cartilage is able to withstand significant loads [70].

1.2.2 Arthritic Cartilage

Cartilage damage is a key feature of degenerative joint diseases, including RA and OA. The mechanisms underlying the degradation of cartilage in arthritis have been elucidated in recent years, with a complex combination of factors playing a pivotal role.

1.2.2.1 Cell Activation

Cell activation plays a central role in cartilage degradation, particularly in RA. Destruction of cartilage is primarily mediated through proteolytic enzymes, which are produced by activated cells within the joint in response to the release of local mediators. Such mediators can include cytokines, prostaglandins, matrix breakdown products, complement, reactive oxygen species and neuropeptides; all of which are involved in chronic inflammation [72].

Chondrocyte phenotype and dedifferentiation has been recognised as a potential initiating event for cartilage loss [73]. As shown in Figure 6, the dedifferentiation of chondrocytes results in a fibroblast-like cell, and reduced production of important anabolic products such as CII and aggrecan [74]. Sox9 is a transcription factor that is essential for early chondrogenesis and the fate of chondrocytes. Sox9 inhibits the progression of chondrocytes from proliferation to prehypertrophy, and the acquisition of an osteoblast like phenotype [75]. Sox9 is expressed highly in healthy articular cartilage, but this high expression can be lost during arthritis [75]. Additionally, exposure of chondrocytes to excessive pro-inflammatory mediators can result in activation. For example, exposure of chondrocytes to IL-1β and TNF results in reduction of

the synthesis of ECM components, such as CII and aggrecan [76,77]. In addition, MMP1, MMP3 and MMP13 are overproduced, as well as a disintegrin and metalloproteinase with thrombospondin motifs 4 (ADAMTS4) [78]. Furthermore, exposure to pro-inflammatory mediators results in ageing and apoptosis of chondrocytes [76].

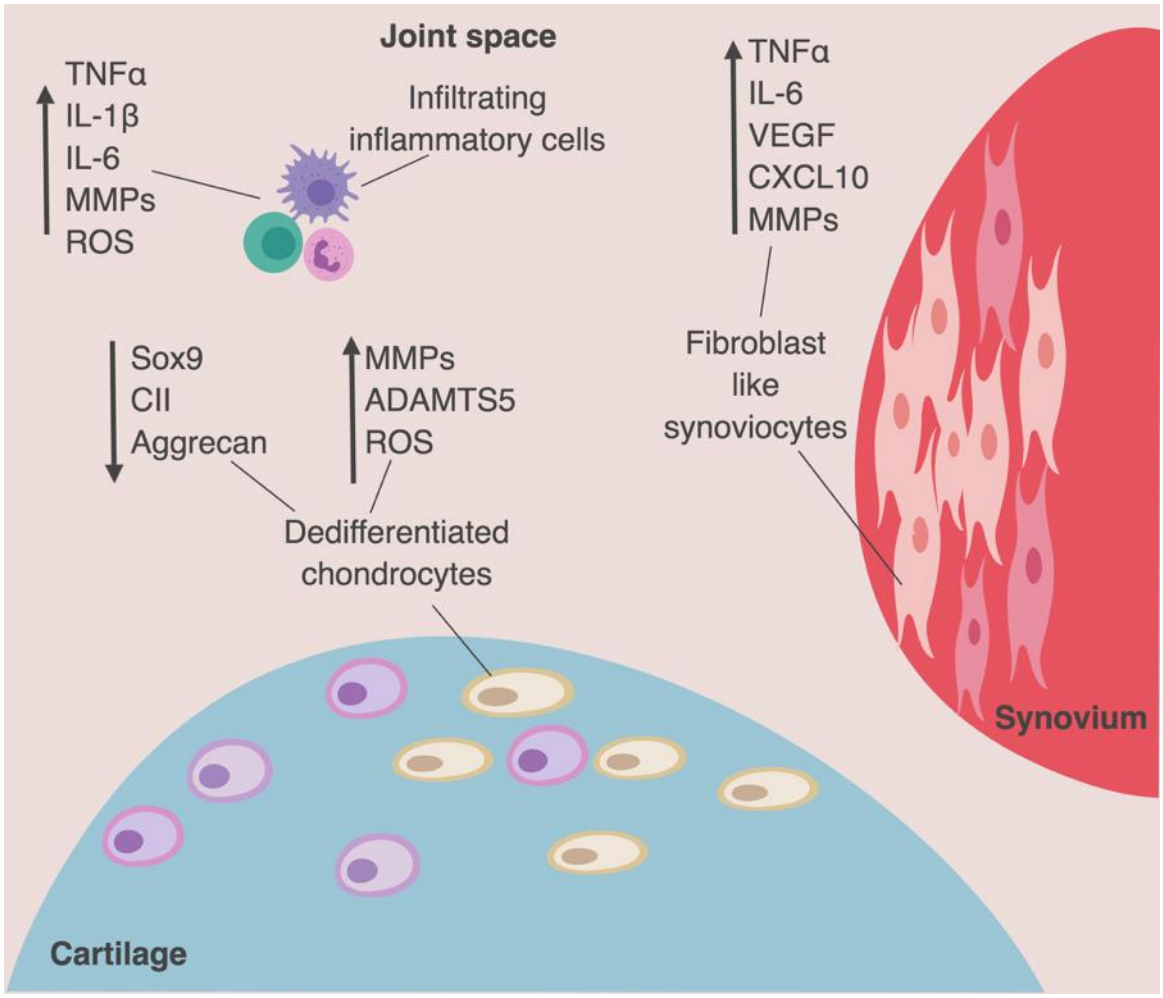

Figure 6. Schematic of the cellular and secretory changes in the arthritic joint. The exposure of chondrocytes and synoviocytes to inflammatory cytokines from invading immune cells results in phenotypic changes. Chondrocyte dedifferentiation occurs, resulting in reduced production of extracellular matrix proteins and increased reduction of matrix metalloproteases. Synoviocytes undertake an aggressive phenotype and become fibroblast-like synoviocytes (FLS). FLS produce excessive levels of inflammatory cytokines and pro-angiogenic factors. Image created with Biorender.

Fibroblast-like synoviocytes (FLS) are known to play an extremely important role in arthritic cartilage destruction. The activation of synoviocytes is well documented, and there is a phenotypic switch, which is often likened to that of a tumour cell. As highlighted in the schematic in Figure 6, the chronic exposure of synoviocytes to inflammatory cytokines such as TNF results in the continuous stimulation of synoviocytes towards an aggressive FLS phenotype [13]. FLS upregulate adhesion molecules, which results in FLS cells interacting with ECM and subsequently the destruction of cartilage and bone. Synovial invasion is characterized by the attachment of the synovial pannus to cartilage, and is mediated through the upregulation of adhesion molecules on FLS, such as vascular cell adhesion protein 1 (VCAM-1).

Pro-inflammatory mediators secreted by FLS cause detrimental changes in bone remodeling, particularly in RA. As demonstrated in Figure 7, in healthy bones, signalling via the classical Wnt pathway is critical for bone deposition and remodeling. Bone remodeling begins with activation mediated through cells of the osteoblast lineage. These cells undergo structural changes and express receptor activator of NF-κB ligand (RANKL) [79]. RANKL interacts with a receptor present on the osteoclast precursors, called RANK. This interaction of RANKL with RANK causes activation and differentiation of hematopoietic cells into osteoclast lineage, and hence the process of resorption begins [79]. RANKL is blocked by osteoprotegerin (OPG), which is secreted from osteoblasts and other bone marrow derived cells. OPG regulates bone resorption by inhibiting the final differentiation of osteoclasts, and instead activating their apoptosis [79].

Wnt signalling is mediated through multiple endogenous mechanisms, including Dickkopf proteins (Dkk). It has been identified that overexpression of Dkk-1 leads to excessive inhibition of Wnt signalling and is critical for bone erosion in RA [80] . Excessive levels of pro-inflammatory cytokines, including TNF-α, by activated FLS and infiltrating immune cells causes overexpression of Dkk-1 and hence inhibition of Wnt signalling. As a result, RANKL is overexpressed and activation and differentiation of osteoclasts occurs. The chronic presence of pro-inflammatory cytokines means the balance of resorption and deposition is lost, and bone resorption occurs at a high rate, which over time can cause joint deformity and functional disability [80,81].

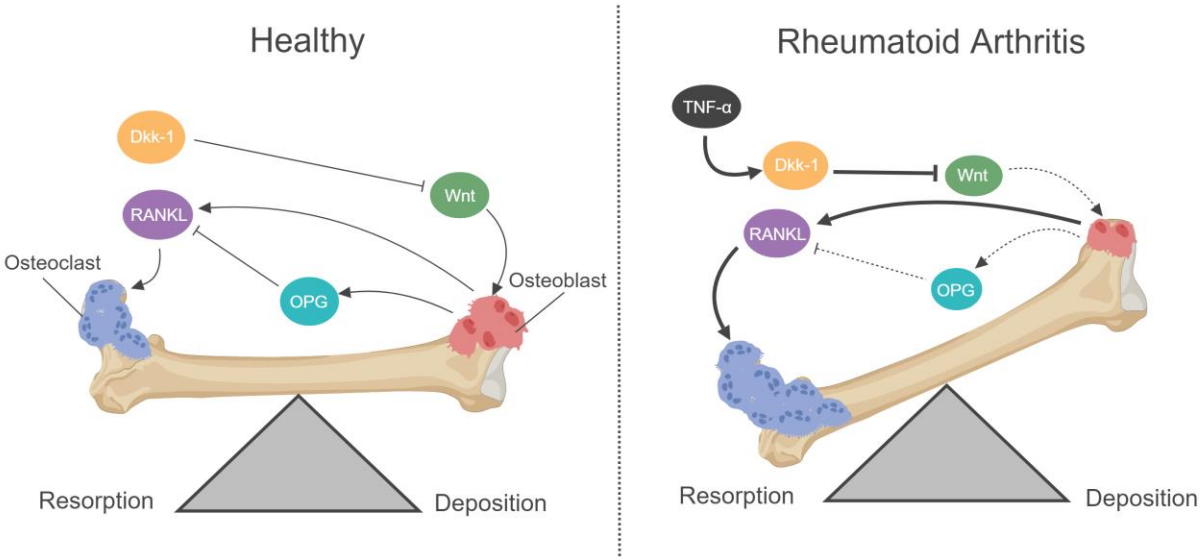

Figure 7. Schematic showing the differences in resorption and deposition in healthy and rheumatoid bones. In healthy individuals, the balance of resorption and deposition is maintained through the actions of osteoclasts and osteoblasts. Pro-inflammatory cytokines produced by the activated synovium results in Dkk-1 overexpression and an inhibition of Wnt signalling, and hence inhibition of osteoblast deposition. These signalling events inhibit osteoblast activity whilst enhancing osteoclast activity. Image created with Biorender.

1.2.2.2 Catabolic Factors

Cartilage breakdown is mediated through catabolic factors, particularly the overproduction of proteolytic enzymes. The production and expression of proteolytic enzymes are regulated through local mediators, such as cytokines, growth factors, reactive oxygen species and prostaglandins [72]. The metalloproteinase (MMP) family are a group of over 20 proteins with important roles in cartilage homeostasis and breakdown. They are divided into five categories: collagenases, stromelysins, gelatinases, membrane type MMPs and aggrecanases. The first four categories make up the matrix MMPs, whereas aggrecanases belong to the ADAMTS family (a disintegrin and metalloproteinase with thrombospondin motifs).

Due to the role MMPs have in degrading collagen II and aggrecan, they play a central role in cartilage destruction in arthritis. Collagen II degradation occurs early in the pathogenesis of arthritis, and is an irreversible event that usually takes place in the superficial layer. Fibrillar CII is broken down by the collagenase subunit of MMP; MMP1 and MMP3 [82]. After initial proteolysis and denaturation of CII by MMP1 and MMP13, the collagen triple helix breaks into fragments, which act as substrates for other MMP including gelatinases [83].

As well as collagen degradation, the proteolysis of aggrecan is another major effect of MMPs. Aggrecan can be degraded by many enzymes and two cleavage sites have been identified: one between amino acids Asn341 and Phe342 and the other between amino acids Glu373 and Ala374 [72]. MMP1, MMP3, MMP13 and cathepsin B have been found to all cleave the Asn341-Phe342 site [72,84]. The Glu373-Ala374 site is characteristic of the proteolytic activity of

the ADAMTS family, particularly ADAMTS4 and ADAMTS5. ADAMTS5 has been shown to be most upregulated during arthritis and plays a dominant role in aggrecan degradation [85]. Deletion of the active protein has shown to protect against both an osteoarthritic mouse model and an inflammatory arthritis mouse model [86].

1.3 Loss of Tolerance in Autoimmune Disease as a result of Post-Translational Modification of Protein

It is estimated that between 50-90% of proteins in the human body are subject to post-translational modification [87]. Some of the most explored post-translational modifications in the literature include phosphorylation and glycosylation, which have important roles in enzyme activity and protein folding, respectively. Post-translational modifications can occur on the amino acid side chain or at the proteins C or N termini, and are usually a chemical or enzymatic process. Most post-translational modifications are essential for biological functions of the subjected protein; however, a proportion of such modifications are redundant and can bring detrimental side effects.

Post-translational modification can play a role in the loss of tolerance through the creation of neo-antigens, to which the immune system has never been exposed or tolerized to. Self-tolerance is an ingrained mechanism of the immune system to discriminate self from non-self. An intricate network of central and peripheral immune tolerance mechanisms to prevent an immune reaction against self-proteins. In most cases, this mechanism is

successful in avoiding a self-attack through the elimination of self-reactive T-cells in the thymus, deletion and receptor editing of autoreactive B-cells in the bone marrow, as well as numerous mechanisms in the periphery including anergy (functional unresponsiveness) and deletion (through induction of apoptosis) [88–90]. However, in cases where these mechanisms do not function correctly and self-reactive cells are not eliminated, there is a loss of self-tolerance which can culminate into autoimmune disorders. The loss of self-tolerance can result in a cascade of excessive, chronic inflammation targeted at host tissue. As discussed earlier, one way of detecting the role of post-translational modification in autoimmune diseases is to test for the presence of autoantibodies against post-translationally modified self-proteins. The presence of autoantibodies to post-translationally modified proteins in autoimmune diseases such as RA and type 1 diabetes supports the hypothesis that post-translational modification of protein plays an important role in disease progression [91–94].

Post-translational modification is categorized into two subtypes: (a) enzymatic and (b) chemical modifications. As will be detailed in the following chapters, my work has focused on chemical post-translational modification in the context of arthritis. In RA, enzymatic post-translational modifications of protein have been highlighted extensively in recent years. As aforementioned, ACPA are highly specific for RA and have thus become an important aspect of diagnosis. As well as a useful diagnostic tool, there is sufficient evidence to suggest ACPA play a role in the pathophysiologic process of RA. ACPA targets epitopes in which arginine has been post-translationally converted to citrulline by the action of peptidyl arginine deiminase (PAD) enzymes [18,19]. Although citrullination does not exist exclusively in RA, it has become a

hallmark of disease. The pooled sensitivity and specificity of ACPA analysis in RA is around 67% and 95% respectively [20]. Not all RA patients are ACPA positive, which explains the low sensitivity in the ACPA analysis.

1.3.1 Reactive Oxygen Species

Post-translational modifications of proteins have been identified to occur in the presence of excessive ROS. ROS are highly reactive small molecules, which at normal physiological levels have an important role in cell signalling. ROS either readily accept another electron or transfer their unpaired electron to another molecule [95]. They are a normal byproduct of cellular metabolism and an intricate oxidant/antioxidant system exists to regulate their levels and avoid oxidative stress [96]. The different varieties of ROS can be formed by both enzymatic and non-enzymatic reactions.

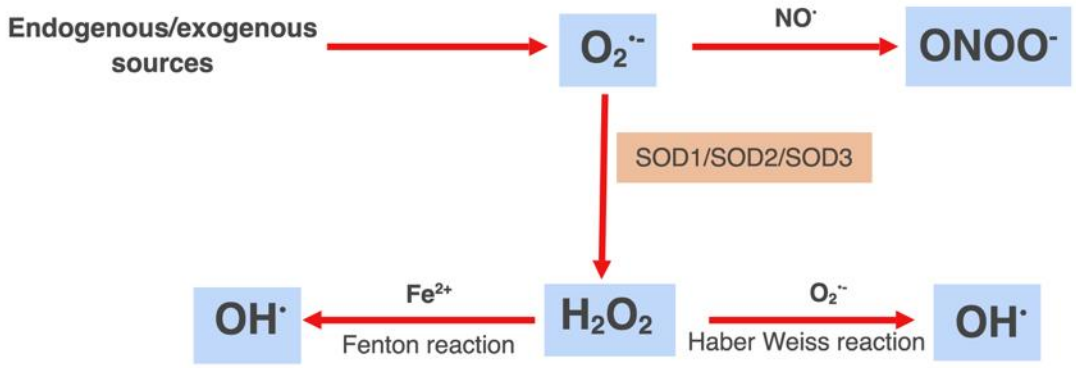

Figure 8. Schematic showing the reactions involved in the generation of reactive oxidant species. Superoxide anion ($O_2-\bullet$) is the precursor of most ROS. Hydrogen Peroxide (H_2O_2) is derived from $O_2-\bullet$ by dismutation. H_2O_2 can either be fully reduced to water, or partially reduced into another ROS, the hydroxyl radical OH•.

Although an antioxidant system exists, ROS are often produced in abnormally large quantities in the human body under many conditions, such as joint disease, asthma, ageing and cancer [95]. The reactivity of each ROS molecule varies widely, but the overproduction of ROS has shown to lead to the damage of DNA and proteins. [95]. Superoxide anion (O_2^-•) is the precursor of most ROS. O_2^-• is a pro-inflammatory compound that damages cells and the extracellular matrix of tissue. O_2^-• also promotes the recruitment of neutrophils to locations of inflammation [95]. As shown in Figure 8, Hydrogen Peroxide (H_2O_2) is derived from O_2^-• by dismutation, either spontaneously or by an enzyme called superoxide dismutase [97]. H_2O_2 can either be fully reduced to water, or partially reduced into another ROS, the hydroxyl radical OH•. The formation of OH• is catalyzed by reduced transition metals, forming one of the strongest oxidants in nature.

Neutrophils are key producers of ROS, especially in the context of inflammation. Neutrophils release an enzyme called Myeloperoxidase, which catalyzes a reaction between H_2O_2 and calcium ions, resulting in the production of the ROS compound hypochlorous acid.

An additional known oxidative post-translational modification in RA is glycation. Non-enzymatic glycation is a post-translational modification resulting in the spontaneous addition of a sugar molecule to a protein. Oxidative stress is associated with sugar oxidants that result from sequential oxidative reactions, and which generate advanced glycation end products (AGE). AGE have been found to play a physiological role in inflammatory autoimmune diseases, and this non-enzymatic glycation is evident in RA, despite the absence of

hyperglycemia. The relationship between AGE and oxidative stress has been highlighted, with AGE presence stimulating the production of ROS in neutrophils [98]. Figure 9 illustrates oxidative glycation that result in the formation of AGE. The carbonyl group of ribose sugar interacts with a free amine group on lysine, causing the formation of a Schiff base. The Schiff base rearranges into the more stable Amadori product, which is considered the first product of glycation [99]. Interaction of Amadori products with arginine causes the formation of pentosidine. Pentosidine is formed through metal-catalyzed oxidation of Amadori product in the presence of arginine [100]. Furthermore, high levels of pentosidine and carboxymethyllysine in the serum, synovial fluid, and urine of RA patients have been detected, and reflect the high levels of AGE compounds present within the body [101,102].

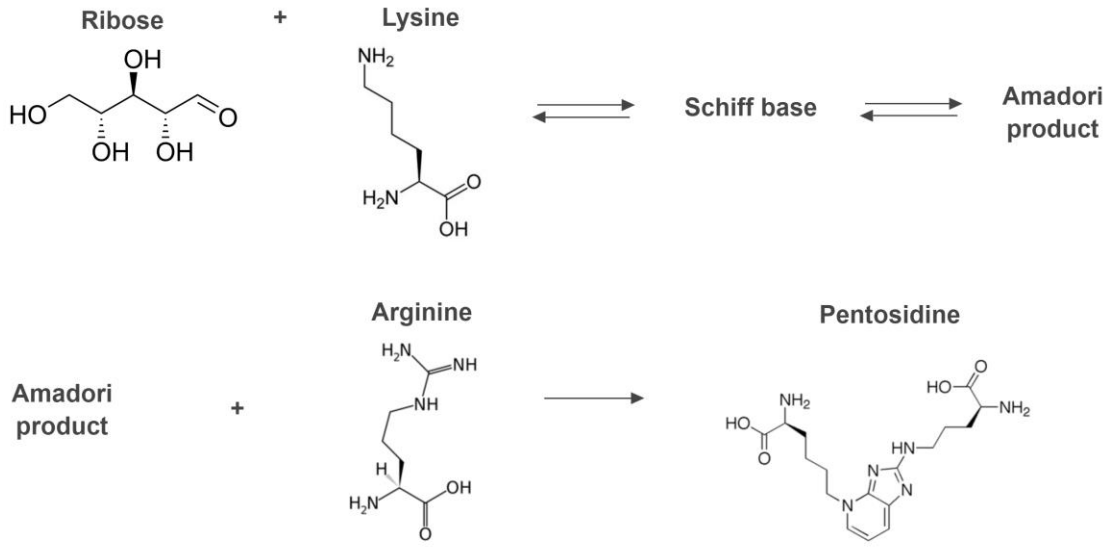

Figure 9. Representation of the formation of Amadori product and advanced glycation end products by oxidative glycation. When the carbonyl group of Ribose interacts with a free amine group on lysine, they form Schiff base, which is reversible. The Amadori product is considered the first glycation product. This undergoes spontaneously induced breakdown and rearrangement to form stable advanced glycation end products. The example of pentosidine is shown, which occurs when the lysine Amadori product cross links with arginine in collagen.

1.3.2 Post-Translational Modification of Protein by ROS

Inflammation is generally categorized into two subtypes: acute and chronic inflammation. Acute inflammation is short lived, self-resolving and usually beneficial for the host. Chronic inflammation occurs when there is a malfunction in the resolution stage of the process, resulting in a prolonged and dangerous activation of the immune system. The production of ROS is central to the progression of many inflammatory diseases [99]. The main producers of ROS within the family of immune cells are polymorphonuclear neutrophils (PMN). ROS

released by PMN can act as both a signalling molecule and a mediator of inflammation. During phagocytosis, neutrophils experience a 'respiratory burst' due to increased respiration, resulting in the generation of large quantities of ROS [100]. During RA, billions of PMN are found in the synovial fluid and therefore could be major contributors of extracellular ROS in the joint space [103,104].

Traditionally, ROS have been regarded to function primarily as anti-microbial agents, but their role as secondary messengers has become prevalent in recent years. ROS hold characteristics that are prerequisites for signalling molecules: they are small, diffusible and can be rapidly produced and degraded. There is strong evidence to suggest their role in homeostasis, cell proliferation and differentiation, and inflammatory response [100,105]. However, due to their toxicity there is only a narrow range in which they function as messengers effectively. The overproduction of ROS, as is often seen during chronic inflammation, can lead to direct injury to proteins, lipids and nucleic acids, resulting in cell death [106]. The overproduction of ROS during chronic inflammation has also been found to cause post-translational modification of matrix proteins. Post-translational modification of cysteine, methionine and tyrosine by ROS are well characterized and shown in Figure 10. Studies have previously demonstrated the importance of ROS post-translational modification in the context of arthritis and type I diabetes [94,107,108]. As will be discussed in the next chapter, collagen type II (CII) is the most abundant protein in cartilage, and therefore is an obvious target for modification by excessive levels of ROS within the inflamed, arthritic joint.

It was previously found that CII that has been post-translationally modified by reactive oxidants is a neoantigen in RA [108].

During inflammation, phagocyte NADPH oxidase (NOX2), inducible nitric oxide synthase (iNOS), and myeloperoxidase (MPO) are all primary sources of reactive oxygen, nitrogen and halide species, which are capable of post-translationally modifying proteins. A variety of reactive oxygen, nitrogen and chlorine species are able to post-translationally modify protein, including the hydroxyl radical (•OH), the carbonate radical (CO3•-), hypochlorite (OCl-) and products formed from reactions involving peroxynitrite (ONOO-). These reactive species are able to modify a wide range of amino acids within the protein. Cysteine residues are readily oxidized due to the existence of a free thiol (-SH) group. The free thiol group can be oxidized to form a disulfide bond with another thiol group. In the presence of oxidants such as •OH, cysteine can also be oxidised to cysteine sulfenic, sulfinic and sulfonic acid derivatives, as demonstrated in Figure 10(A). Methionine can also be oxidized in a similar manner to form methionine sulfone Figure 10(B). Other oxidative post-translational modifications include tyrosine oxidation to 3,4-dihydroxyphenylalenine, or inter- or intra-molecular di-tyrosine cross-linking via the formation of tyrosyl radicals Figure 10(C). Chlorination of proteins, mediated by HOCl produced by MPO, is another important modification that can occur on proteins which causes altered protein function. Chlorination has been most reported to occur on tyrosine residues, forming chlorotyrosine as seen in Figure 10(C). Chloramines on lysine and histidine residues constitute important intermediates in stable end products of chlorination.

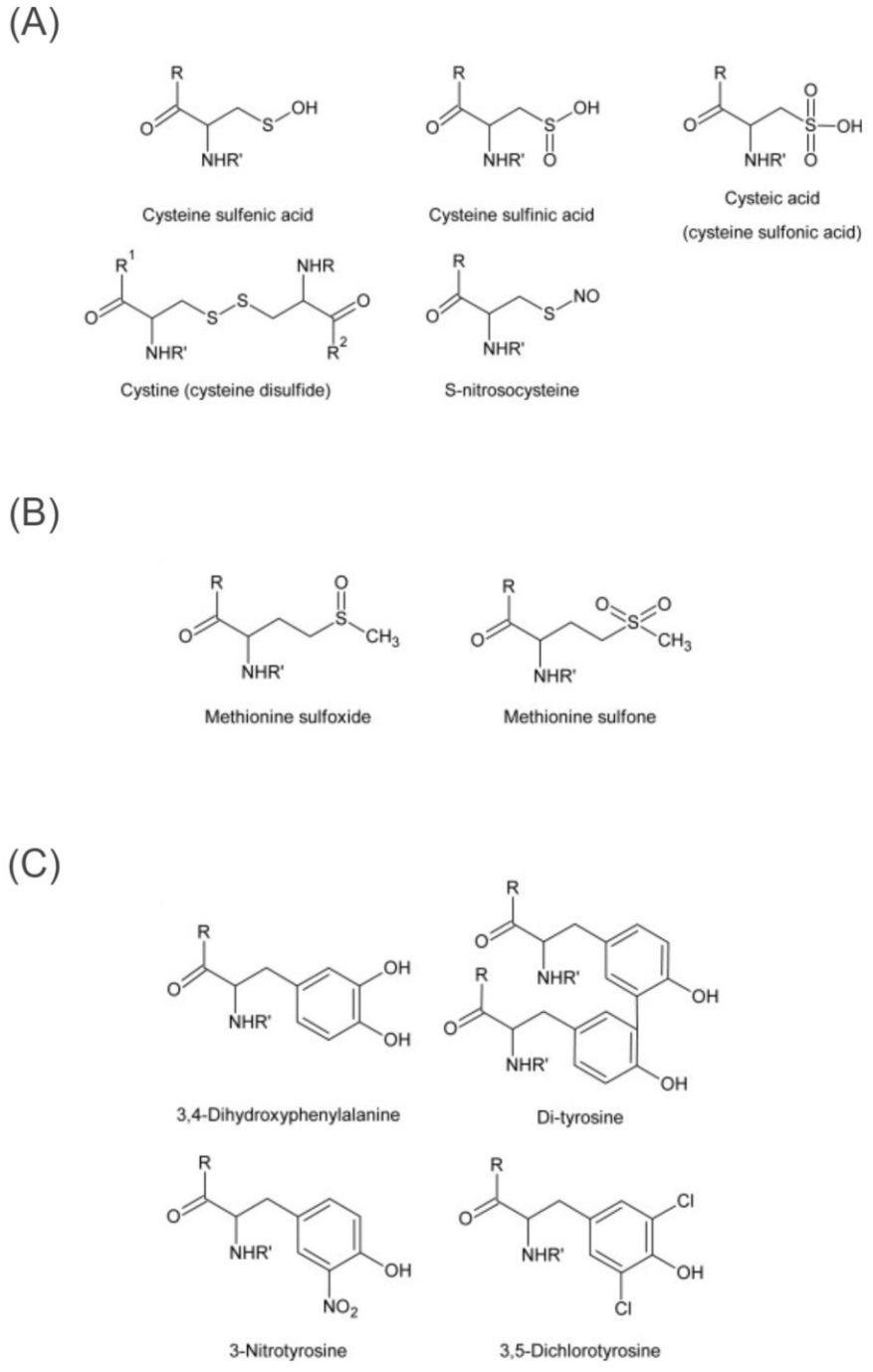

Figure 10. Structures of amino acids after post-translational modifications by reactive oxygen, nitrogen and chlorine species. Structures of some of the post-translationally modified forms of (a) cysteine residues, (b) methionine residues and (c) tyrosine residues. Adapted from Ryan *et al* [109].

1.4 Antibodies to Post-Translationally Modified Collagen II

1.4.1 Autoantibodies to Collagen II Post-Translationally Modified by Reactive Oxidants in Arthritis Patients

CII was first proposed as an autoantigen in RA in 1964 [110]. Autoreactivity to CII has been highlighted in the pathogenesis of RA, with autoantibodies found in between 3-27% of patients [111,112]. Most studies have shown the prevalence of autoantibodies to CII to be low, and the titers do not compare to the current gold standard biomarker of anti-CCP antibodies. The arthritogenic nature of CII is well established and is the basis for one of the most established models of murine RA. Collagen induced arthritis (CIA) involves immunizing rats and mice with CII in complete or incomplete Freund's adjuvant (CFA/IFA). The immunization results in polyarthritis, whereas similar immunizations with other collagen types does not have the same effect [113]. Furthermore, arthritis could be induced when using CII from a variety of sources (chicken, bovine and bovine vitreous), but not when CII was thermally denatured [113,114].

Although studies have highlighted the presence of autoantibodies to CII in a subset of patients with RA and the arthritogenic nature of CII is well established, the role of CII within the disease is still not understood. Given that only a small subset of patients present with autoantibodies to CII, it is now accepted that they are secondary to inflammation and not of pathological significance [113]. In recent years, CII that has been post-translationally modified

by ROS (ROS-CII) has been highlighted within the context of RA. In 2005, Nissim *et al* simulated the post-translational modifications of CII by ROS *in vitro*. This modified CII was used as the antigenic coating in an enzyme linked immunosorbent assay (ELISA) to test the reactivity of sera from patients with arthritis. The ELISA showed that sera from patients with RA were positive binders to ROS-CII (45.2%, with 22.6% considered strong binders), whereas only one sample bound strongly to CII (3.2%). Sera from non-RA patients showed minimal binding to ROS-CII (2.4%) and no binding to CII [108]. The study also assessed the binding of sera from CIA mice to native and ROS-CII by ELISA. The binding of sera from CIA mice was stronger to native CII but showed positive binding to modified CII. It was also observed that mice with a lower disease activity exhibited lower binding to modified CII [108]. Follow up studies by Nissim's group confirmed the presence of autoantibodies to ROS-CII in RA patients [92]. When stratifying patients, it was found that binding is particularly high in early RA subsets, with 92.9% of patients binding strongly to ROS-CII [92]. These studies have opened discussion regarding the role ROS-CII plays in arthritis, and have provided the basis for a potential additional biomarker of RA.

Interestingly, it has also previously been found that oxidative post-translationally modified CII is present in OA cartilage [115]. These results were unexpected as OA is considered a degenerative disease rather than an autoimmune disease, and generally very little is known about the importance, if any, of post-translational modification in the progression of disease. However, several studies have suggested the presence of autoantibodies to native proteins, suggesting a role of the adaptive immune system within the disease [116,117]. However, the

titration of autoantibodies in OA patients is often significantly lower than RA patients, hence why there is currently no biomarker diagnostic for OA [92].

1.4.2 Antibodies to Post-Translationally Modified Collagen II Raised from a Phage Display Library

Having found that autoantibodies to ROS-CII are present in a high number of RA patients, it was therefore likely that the antigen ROS-CII exists in the inflamed joint. This neoantigen was hypothesized to be found exclusively in the inflamed joint, where the high levels of ROS have modified CII. If this hypothesis was correct then it offers a novel way to target arthritic joints.

To target the potential neoantigen, Hughes *et al* produced single chain variable fragments (scFv) specific to ROS-CII from a semisynthetic phage display human library [118]. CII was exposed to $^{\cdot}OH$, HOCl, $ONOO^{-}$, or ribose to modify the protein *in vitro*. Using the phage display library, 3 rounds of subtractive selection (using native CII for subtraction) was performed to find scFv specific to the various ROS-CII. Soluble scFv were obtained from an infected, non-suppressor *Escherichia coli* HB2151 strain. To test the specificity of the produced scFv *in vitro,* immunostaining of tissue sections from RA and OA patients was performed. The immunostaining showed the scFv bound specifically to damaged cartilage, but not healthy cartilage. Interestingly, binding was present in both RA and OA samples, albeit with different patterns. RA samples showed a diffused staining throughout all layers of cartilage, whereas OA samples showed staining specifically at sites exhibiting features of

active OA. The scFv also showed strong staining to cartilage tissue from murine models of arthritis, both OA and RA [118].

The antibodies were also tested *in vivo* using optical imaging techniques. By fluorescently labelling the scFv, localisation could be observed using biofluorescence *in vivo* imaging system in arthritic mice. Models of monoarthritis were used to assess the specific localisation in the one inflamed joint or paw, and successful localisation was observed [39,118].

The production of scFv specific to ROS-CII gives potential for targeting therapeutics specifically to the arthritic joint. Hughes *et al* proved this concept by fusing vIL-10 to one of the anti-ROS CII scFv clones, namely 1-11E, and administering systemically in arthritic mice. A matrix metalloprotease (MMP) cleavage site meant the vIL-10 would only be released in the arthritic joint. The study found the antibody localised in the arthritic joint and reduced inflammation more effectively than vIL-10 fused to a non-specific scFv [39].

The specificity of these anti-ROS CII scFv mean therapeutics can be targeted specifically to the inflamed joint. This holds great importance as unwanted side effects can be potentially reduced, and novel anti-inflammatories can be delivered exactly to the site of the body they need them. The candidate antibody used in these studies, '1-11E', undergoes glycosylation of the binding site during production, which hinders its binding potential. This can be prevented with the use of an N-linked glycosylation inhibitor, such as tunicamycin, however the result is cell death during transfection and a large reduction in the overall antibody production. Translationally, the 1-11E antibody has a major disadvantage. To have another candidate

from the same library that shows similar binding patterns, without the issues of production, would be highly beneficial and is one of the major goals of my thesis.

1.5 Microvesicles

Intercellular communication is a hallmark of survival in a multicellular organism, and in the last two decades a new mode of communication has arisen in the form of extracellular vesicles (EV). EV have been found to act as vehicles for the transfer of membrane or cytosolic protein, lipids and RNA between cells [119]. It has only become apparent in recent years how physiologically relevant EV are, and the importance to understand both the mechanisms in which they are released and the effect they have on other cells.

In recent years, the nomenclature regarding the subtypes of extracellular vesicles has become more refined. The release of apoptotic bodies from cells undergoing apoptosis has been long known, however it is only recently appreciated that healthy cells shed vesicles from their plasma membrane [119]. These vesicles, ranging in size from around 100-1000nm [120], are referred to as microvesicles (but also known as microparticles, ectosomes and shedding vesicles). The term exosome was initially given to vesicles in the size range of 40-1000nm, but are now referred to as vesicles of 40-100nm released during reticulocyte differentiation as a consequence of multivesicular endosome (MVE) fusion with the membrane [119,121]. Exosomes and microvesicles (MV) are released through different mechanisms, however identification and differentiation after their release still proves difficult.

1.5.1 Microvesicle Formation and Function

For many years, the small vesicles shed from the surface of cells were considered nothing more than artifacts, however their importance is now becoming appreciated as their mechanisms attempt to be alluded. Microvesicles are speculated to be released by most, if not all, cell types [122], and increases in their production have been associated with certain diseases [123]. Before the shedding of MV from the cell membrane, budding of small cytoplasmic protrusions occurs, which then detach by fission of their stalk [122]. Protein accumulation in the membrane, and therefore in the content of the shed vesicle, has been shown to occur within the budding process [122]. The mechanism in which this occurs remains obscure and not well understood.

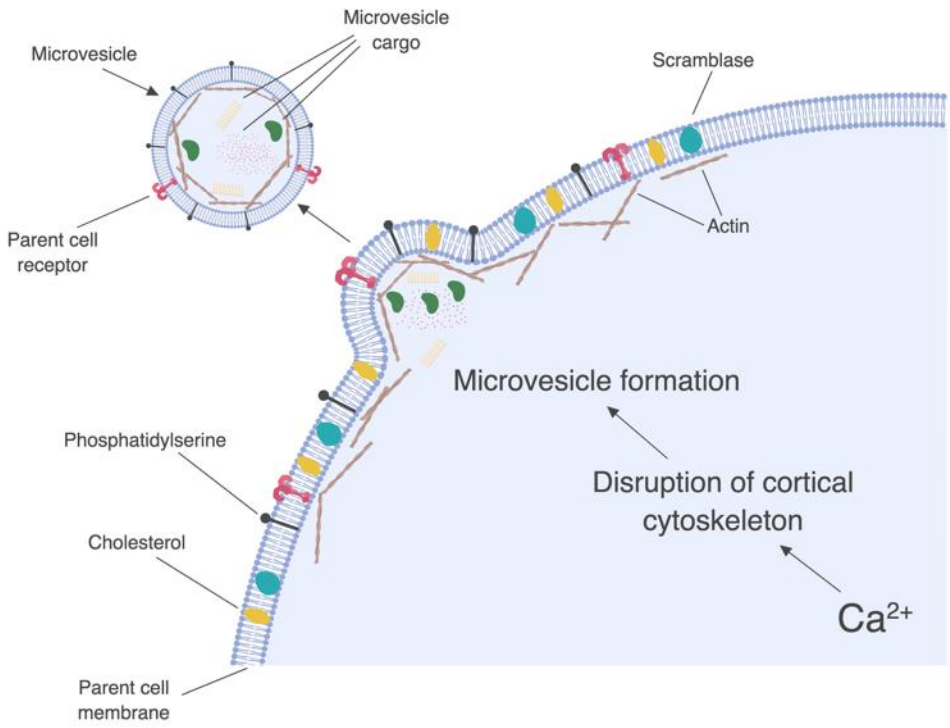

Figure 11. Illustration representing the formation of microvesicles from a cell membrane. The increase in intracellular calcium results in cytoskeletal rearrangement and the shedding of vesicles containing cargo molecules. Image created with Biorender.

Resting cells can shed MV, however the rate of shedding drastically increases upon stimulation. It is now accepted that calcium induces strong shedding rates. A sustained influx of calcium results in the cytoskeletal rearrangement, and calcium dependent proteases cleave talin and α-actinin, freeing the plasma membrane from the cytoskeleton [124,125]. Shedding of vesicles results in the constant removal of small portions of the plasma membrane, which must be replaced to protect the parent cell. Upon stimulation, the high rate of shedding must be compensated by a concomitant input from the cytoplasm. This mechanism is termed regulated exocytosis of non-secretory vesicles [122,126].

Upon shedding, many MV will not remain intact and will release their contents. This will occur within the extracellular space and the results of this release depend on the material contained within the vesicle. For example, a vesicle containing MMP can result in the destruction of extracellular matrix, a mechanism by which tumour cells increase their mobility [122]. The release of cargo can also be important for the release of signalling molecules. An example of this is the release of the pro-inflammatory cytokine IL-1β from vesicles derived from dendritic cells and macrophages [127]. Those vesicles that do not release their cargo following shedding will continue to interact with their target cell. It has been found that MV will not interact with any cell but only those that they recognize specifically [122]. An example of this is a study conducted by Losche *et al*, in which they discovered that the vesicles shed from platelets transfer tissue factor to monocytes, but not to neutrophils [128]. In many cases the interaction is limited to the cell surface, usually the MV binding to receptors present on the target cell. It is also recognised that MV can fuse into the plasma membrane of the target cell or be taken up into the cell by endocytosis, which will vary dependent on the cell type [122].

The function of MV during inflammation is becoming better characterized as time goes on. Inflammation is typically thought of as a cell driven process, either directly or indirectly by soluble mediators. The shedding of vesicles is now known to participate in the process of inflammation, acting in both a pro- and anti-inflammatory nature. MV from a single cell type can vary in its nature dependent on the stage of inflammation. For example, the MV shed by neutrophils in the early stages of inflammation stimulate macrophages to produce anti-inflammatory factors such as transforming growth factor ß (TGF-ß) and Interleukin-10 (IL-10)

and reduce pro-inflammatory factors such as TNF-α and Interleukin-8 (IL-8) [122,129]. During later time points, the MV shed from neutrophils can have a pro-inflammatory nature, stimulating the release of factors such as Interleukin-6 (IL-6) and monocyte chemotactic protein 1 (MCP1), which drive inflammation [130,131].

The overall function of MV cannot be simply summarized as it appears from the literature that both the cell type involved in the shedding and the microenvironment following release alter the overall function of the vesicle. In the context of inflammation, MV could be categorized into those which exhibit a pro-inflammatory nature and those that exhibit an anti-inflammatory nature, with one cell type capable of shedding both kinds of vesicle. The complexity of MV release is beginning to be dissected, but there are still many areas of vesicle biology that are not understood.

1.5.2 Neutrophil Derived Microvesicles and Arthritis

In 2004, Gasser and Schifferli first proposed that polymorphonuclear neutrophil (PMN) derived MV hold anti-inflammatory and immunosuppressive qualities, contradicting the proposed hypothesis that they would increase IL-8 and TNFα production [129]. Before these findings, MV from platelets, endothelial cells and monocytes were found to activate monocytes and endothelial cells in a pro-inflammatory manner [129]. Conversely, neutrophil derived MV increased the release of TGF-β in macrophages, and were able to actively inhibit inflammatory responses of macrophages to zymosan and lipopolysaccharide [129]. The

mechanism in which PMN MV elicit an anti-inflammatory response is now well characterized. Phosphatidylserine (PS) is present on the outer membrane of PMN derived MV, which was found to repress inflammation and promote anti-inflammatory pathways, in particular through the production of TGF-β [132]. Hoffmann *et al* presented that this phenomenon occurs through the interaction of PS with the PS receptor. Interestingly, PS liposomes did not inhibit bone marrow derived dendritic cell activation *in vitro,* but had a significant effect on the other adaptive immune cells used in the study. The authors state that bone marrow derived dendritic cells do not express PS receptor, strengthening the theory that PS exhibits its anti-inflammatory effects through the binding to PS receptor [132].

Later studies have also found that PMN MV inhibits the nuclear factor kappa-light-chain-enhancer of activated B cells (NF-κB) complex. PMN MV inhibits the NF-κB p65 translocation to the nucleus in macrophages, leading to the down regulation of pro-inflammatory genes, including TNFα, IL-1, IL-6 and IL-8 [133]. By using a blocking antibody, the authors showed that MerTK is centrally involved in the inhibition of NF-κB. This blockade was proposed to be through MerTK mediated activation of the PI3K/Akt pathway, resulting in negative regulation of the NF-κB complex [133]. The regulation of NF-κB via PI3K/Akt proves controversial however, with both negative and positive gene expression demonstrated.

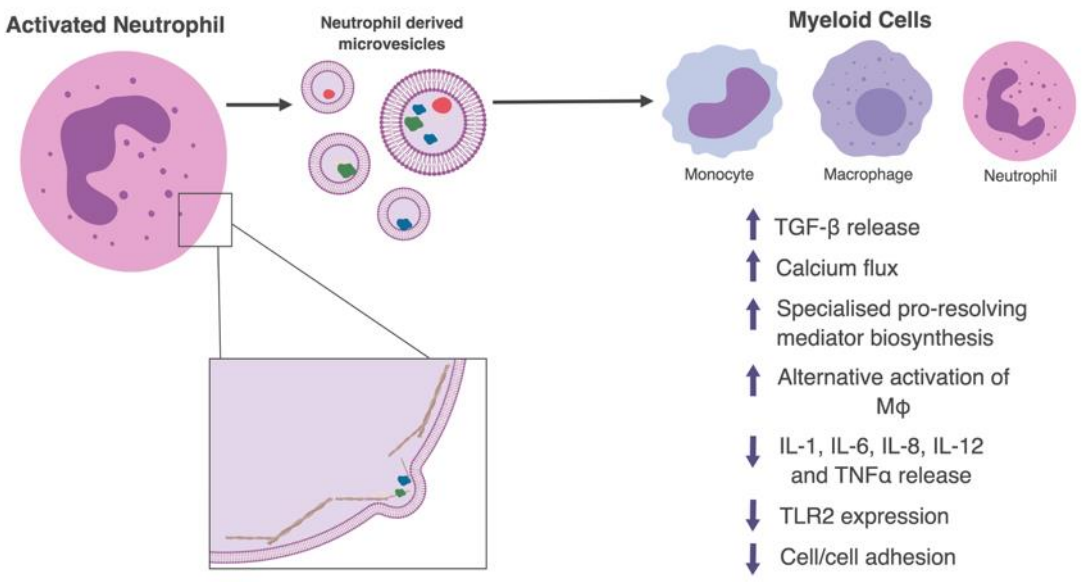

Figure 12. Summary of the descriptions in literature of the interaction of neutrophil derived microvesicles on various myeloid cells. The actions of neutrophil derived microvesicles on myeloid cells induces a pro-resolving phenotype. Image created with Biorender.

Studies over the past 10 years by members of our laboratory have extended the existing knowledge regarding PMN derived MV. In 2008, Dalli *et al* described the expression and functional activity of Annexin A1 (AnxA1) on PMN MV [134]. AnxA1 is an endogenous glucocorticoid-regulated protein that is able to potently counter-regulate inflammation [135]. The study also found the potent anti-migratory effect of PMN MV, which also relies on the presence of AnxA1 as shown by generating vesicles from AnxA1 knock out mice [134]. More recent studies by Headland *et al* uncovered the chondroprotective effects of PMN MV in a K/BxN mouse model of arthritis [136]. The studies also provided evidence of MV penetration into cartilage tissue, a property that is exclusive to PMN MV and not observed by PMN [136].

There is mounting evidence demonstrating the anti-inflammatory effects of PMN MV, contrary to the initial hypothesis based on MV derived from platelets and endothelial cells. The anti-inflammatory effects of PMN MV in inflammatory arthritis are significant, and the chondroprotective effects are important as no current existing therapy can penetrate and protect native cartilage. Hence, the use of PMN MV for therapeutic purposes is becoming an area of great interest for future studies.

1.5.3 Microvesicles as Therapeutic Vectors

The ability of PMN MV to enter cartila*g*e is a unique quality which has not previously been observed. The additional benefits of the described anti-inflammatory properties of PMN MV make them a viable therapeutic. MV have been exploited for therapy in experimental models multiple times in the literature. For example, MV derived from mesenchymal stem cells have been used to stimulate cardiac tissue repair in mice [137] and MV derived from dendritic cells have been used in cancer immunotherapy [138]. The notion that MV can play an efficacious role in the treatment of disease is becoming clear, and can potentially apply to PMN MV in the context of arthritis.

Microvesicles have previously been utilized as scaffolds for therapeutic purposes. In 2011, Norling *et al* enriched MV from human PMN with aspirin-triggered resolvin D1 or a lipoxin A4 analogue [139]. These enriched MV dramatically reduced polymorphonuclear cell influx in murine peritonitis, shortened resolution intervals and exhibited pro-resolving actions, therefore accelerating keratinocyte healing [139]. In 2013, Dalli *et al* administered alpha-2-macroglobulin (A2MG) enriched PMN MV to mice with microbial sepsis. Administration of A2MG-enriched-microparticles protected against hypothermia, reduced bacterial titres, elevated immunoresolvent lipid mediator levels in inflammatory exudates and reduced systemic inflammation [140]. These studies have shown the potential of using PMN MV as a pro-resolving scaffold. The enrichment of PMN MV with protein has been successful and efficacious in models of peritonitis and sepsis. In the context of arthritis, Headland *et al* found that the intravenous administration of PMN MV in arthritic mice was not sufficient to

reduce arthritic scores, and intra-articular injection was necessary to see a reduction in inflammation [141]. This slightly hinders the therapeutic potential of PMN MV in arthritis, as translationally a non-invasive administration such as intravenous injection would be preferred. Nonetheless, the study did not administer a range of doses, and it is likely a higher number of MV are needed to show efficacy when administered systemically.

Targeting the PMN MV to the arthritic joint by enriching the vesicles with antibodies specific to damaged cartilage proposes a viable way to deliver PMN MV systemically. Furthermore, MV could potentially be enriched with both antibodies that target and localize them to the arthritic joint and anti-inflammatory therapeutics. Enrichment of MV with antibodies has not been previously attempted and will form part of the basis of this thesis.

1.6 Hypothesis and Aims

A common feature of both OA and RA is cartilage damage. My primary supervisor's research group have developed antibodies specific to collagen type II that has been post-translationally modified by reactive oxygen species (ROS-CII), which selectively binds to damaged arthritic cartilage. Previous work has demonstrated that anti-ROS-CII could be used to direct therapeutics to the inflamed arthritic joints [39]. Importantly, the anti-ROS-CII-therapeutic fusion accelerated the reduction of inflammation in diseased joints, with similar features as healthy joints after treatment.

The main hypothesis of my thesis is that anti-ROS-CII can be used to deliver biological scaffolds specifically to arthritic joints. This will enable the development of potent yet safe treatments. The current study focused on utilizing neutrophil derived extracellular microvesicles (MV) as biological scaffolds; which exhibit inherent anti-inflammatory and pro-resolving properties and have been shown to penetrate and protect cartilage.

The main objectives of the thesis were to test and assess the specific targeting and therapeutic potential of anti-ROS-CII fortified PMN MV, additionally loaded with either single or combined therapeutics. The working hypothesis is that PMN MV enriched with anti-ROS-CII antibodies will be localized and retained within the arthritic joint. Incorporating combined therapies will help to resolve inflammation, whilst simultaneously the PMN MV scaffold will protect cartilage. Hence, anti-ROS-CII fortified PMN MV can be developed into a 'magic

bullet' combined treatment that can address the safety issue of systemic treatment by ensuring targeting specifically to the arthritic joint.

Specific aims:

In Vitro Assays

- Express new candidate antibody '3-11E' (scFv produced by bacterial expression and IgG/fusion antibodies by transient transfection)
- Analysis of new candidate antibody, including ELISA, SDS PAGE, and immunofluorescence
- Generate PMN MV *in vitro* and analyse by flow cytometry and nanoparticle tracking
- Fortify PMN MV with anti-ROS-CII antibodies by aqueous energy dissemination.
- Analyse the fortified MV by flow cytometry, ELISA, and immunofluorescence.

In Vivo Assays

A. Localization studies

- Analysis of the localisation of new candidate anti-ROS-CII antibody '3-11E' in mouse models of arthritis
- Localisation study of 3-11E fused to an anti-inflammatory cytokine
- Localisation study of PMN MV fortified with anti-ROS-CII

B. Treatment studies

- Treatment study of PMN MV fortified with anti-ROS-CII fused to an anti-inflammatory cytokine
- Treatment study of PMN MV fortified with multiple therapeutics

Chapter 2: Materials and Methods

2.1 Production of Antibodies to Post-Translationally Modified Collagen II

2.1.1 Production of scFv from *Escherichia Coli* HB2151

E. Coli (previously transformed by a member of the Nissim Lab with the plasmid of the scFv antibody) were cultured overnight in 5 mL OF 2xTY broth supplemented with 1% glucose and 100 µg/mL ampicillin at 37°C and 125 rpm. Following overnight incubation, cultures were diluted 1:100 in 2xTY broth supplemented with 0.1% glucose and 100 µg/mL ampicillin. Cultures were grown until optical density (OD) at 600 nm reached between 0.6 and 0.9. Induction of bacteria using 1 mM isopropyl β-D-thiogalactoside (IPTG, Sigma I5502) was conducted between OD 0.6 and 0.9 and cultures were incubated overnight at 30°C and 125 rpm. The following day, bacteria cultures were centrifuged at 4000*g* at 4°C for 15 minutes. Supernatant was collected and stored at 4°C. Bacterial pellets were resuspended in 1/20 of the original volume of 30 mM Tris pH 7.0, 20% sucrose and 1 mM EDTA and incubated on ice for 20 minutes. Resuspended pellets were then centrifuged at 10,800*g* at 4°C for 15 minutes. Supernatant was then collected and combined with the previously collected supernatant and stored at 4°C. Pellets were then resuspended in 5 mM magnesium sulfate solution and incubated on ice for 20 minutes. Resuspended pellets were then centrifuged at 10,800*g* at 4°C for 15 minutes. As previously described, supernatant was collected, combined with previous supernatant and stored at 4°C for purification.

2.1.2 Harvesting of Plasmid DNA

E. coli (previously transformed with the plasmid of interest) were cultured overnight in 250 mL of LB Broth (Sigma L3022) supplemented with 1% glucose and 100 µg/mL Ampicillin at 37°C and 125 rpm. Bacterial cultures were harvested by centrifugation at 6000*g* for 20 minutes. DNA isolation was conducted using a Qiagen QIAFilter Plasmid Maxi Kit according to the manufacturer's instructions. Briefly, bacteria were lysed and DNA was purified by the QIAGEN-tip containing a resin to bind plasmid DNA. Subsequent quantification of DNA was conducted using NanoDrop spectroscopy at 260 nm.

2.1.3 Production of IgG and Fusion Proteins by Transient Transfection

Transient transfection of IgG and vIL-10 fusion antibodies were conducted in Expi293f cells. Transfection was only performed in Expi293f cells below passage 20 and with a cell viability of >90%. Plasmid DNA isolation was conducted as described above. Firstly, 7.5×10^7 cells were seeded in 25.5 mL of Expi293f Expression Medium (Thermo Fisher A1435101) in a 125 mL sterile, disposable conical flask. Cells were counted using a hemocytometer and viability was assessed using Trypan Blue exclusion. For each 25.5 mL transfection, 30 µg of plasmid DNA was added to Opti-MEM® I reduced serum medium (Thermo Fisher 31985070) to a total volume of 1.5 mL. Following plasmid DNA dilution, 81 µL of ExpiFectamine™ 293 Reagent was diluted in Opti-MEM® I medium to a total volume of 1.5 mL. This was mixed gently and incubated for 5 minutes at room temperature. Following a 5-minute incubation, the diluted DNA was combined with the diluted ExpiFectamine and mixed gently. The mixture was

incubated for 20 minutes at room temperature to allow the DNA- ExpiFectamine™ 293 Reagent complexes to form. Following the incubation, the 3 mL mixture was added to the previously prepared cell suspensions. Cells were incubated for 20 hours at 37°C, 125 rpm and 8% CO_2 in air. Following 20 hours of culture, 150 µL of ExpiFectamine™ 293 Transfection Enhancer 1, and 1.5 mL of ExpiFectamine™ 293 Transfection Enhancer 2 were added to each flask. Cultures were incubated for 5 days to allow optimal expression. Harvesting of antibodies was conducted by centrifugation at 423*g* for 5 minutes. Supernatant was collected and stored at 4°C for purification.

2.1.4 Purification of Antibodies

IgG and vIL-10 fusion antibodies were purified by nickel column purification due to the presence of a histidine tag, whereas scFv antibodies were purified by protein A column purification.

2.1.4.1 Nickel Column Purification

Supernatants to be purified were treated with a 10x concentrated lysis buffer, composed of 50 mM monosodium phosphate, 300 mM sodium chloride and 10 mM imidazole. Ni-NTA slurry (Qiagen 1018244) was pre-incubated in 1x lysis buffer and centrifuged for 2 minutes at 423*g*. Ni-NTA slurry was resuspended in 1 mL of lysis buffer and was added to the supernatant containing the antibody. Supernatant + Ni-NTA resin was incubated at 4°C on a roller for 3 hours. Supernatant + Ni-NTA were then loaded into a 15 mL column with a tapped bottom outlet. Supernatant could flow through the column collecting the resin. Flow

through was stored at 4°C for SDS-PAGE analysis. Resin was then washed with 15 mL of wash buffer, composed of 50 mM monosodium phosphate, 300 mM sodium chloride, 20 mM imidazole plus 0.05% Tween 20. Wash fractions were stored at 4°C for SDS-PAGE analysis. Antibodies were then eluted using 50 mM monosodium phosphate, 300 mM sodium chloride and 250 mM imidazole into 0.5mL fractions and stored at 4°C for analysis. All collected samples were tested by SDS-PAGE and spectrophotometry at 280 nm.

2.1.4.2 Protein A Column Purification

Supernatants to be purified were treated with 10x binding buffer solution (200 mM sodium phosphate, pH 7.0). Protein A slurry (GE Healthcare 17-0780-01) was added to a 15 mL column with a tapped bottom outlet and was washed using phosphate buffer saline (PBS) and 1x binding buffer solution. Supernatant was then allowed to flow through the column twice at 4°C. Protein A resin was then washed with 25 mL volumes of PBS, PBS + 0.5 M sodium chloride, 0.2 M glycine solution pH 6.0 and finally with 0.2 M glycine solution pH 5.0. Each wash flow through was collected and stored at 4°C for analysis. Antibodies were then eluted using a 0.2 M glycine solution pH 3.0, and collected into fractions containing 200 µL of Tris pH 9.0 solution, to a total volume of 1 mL. Eluted fractions were stored at 4°C until analysis. All collected samples were tested by SDS-PAGE and spectrophotometry at 280 nm.

2.1.5 Sodium Dodecyl Sulphate Polyacrylamide Gel Electrophoresis

Resolving gels were produced with varying percentages of acrylamide depending on the known molecular weight of the antibody being analysed: for scFv with a molecular weight of

around 25-30 kDa a 15% solution was used; for scFv-vIL-10 fusion antibodies with a molecular weight of around 50 kDa a 12% solution was used and for IgG antibodies with heavy chain molecular weight of around 50 kDa and a light chain molecular weight of around 25 kDa a 10% solution was used. Following polymerization of the resolving gel, the stacking gel was prepared. The stacking gel was assembled with 0.75 mm combs to produce 10 wells. Following polymerization, the gel was assembled in an electrophoresis tank and filled with SDS running buffer. Samples were denatured using a 4x concentrated β-Mercaptoethanol solution and incubated for 5 minutes at 95°C. Protein ladder and samples were added to the wells in the stacking gel. The electrophoresis tank was assembled, and gels were run at 100 V for 1 hour and 30 minutes. Following electrophoresis, protein was visualized by an incubation with Coomassie brilliant blue solution (0.2% Brilliant blue Sigma B-7920, 45% methanol and 10% acetic acid) following by destaining (40% methanol and 10% acetic acid solution).

2.1.6 *In vitro* post-translational modification of Collagen II

Bovine sourced collagen II (CII) was diluted 1 mg/mL in 0.1M Acetic Acid for three hours at 4°C on a roller. Following three hours of incubation and dissolving of the CII, the acetic acid was replaced with PBS by dialysis using a Slide-A-Lyzer dialysis cassette (10,000 MWCO, Thermo Scientific). CII was post translationally modified *in vitro* to mimic native ROS modifications by the following incubations:

- 2 M of D-Ribose for 72 hours at 37°C to mimic non-enzymatic glycation.
- 1 mM Sodium hypochlorite for 10 hours at 37°C to mimic HOCl modification.

2.1.7 Enzyme Linked Immunosorbent Assay

Immunosorbent 96 well plates were coated with 100 µL of 10 µg/mL collagen II or ROS modified collagen II. Coatings were incubated overnight at 4°C. Following overnight incubation, plates were washed with 200 µL of PBS + 0.05% Tween 20 (PBST) and blocked with 2.5% powdered milk (Marvel) in PBST. Plates were blocked for 2 hours at room temperature. Primary antibody (anti-ROS-CII) was serially-diluted in blocking solution and added to the plate. Primary antibody was incubated for 2 hours at room temperature. Following incubation, plates were washed with 200 µL of PBST. Secondary antibody was diluted (anti-hIgG (Sigma A8792) 1:1000 dilution; anti-His Tag (Sigma A7058) 1:4000 dilution) and added to each well. The secondary antibody was incubated for 2 hours at room temperature before three washes with 200 µL of PBST. The ELISA was then developed using 100 µL of TMB solution (0.1 mg/mL TMB, 0.1M sodium acetate and 2 µL per 10mL of 30%

Hydrogen peroxide). The reaction was stopped using 50 µL of 20% Sulfuric acid and absorbances were read at 450 nm.

2.2 *In vivo* localisation studies of scFv, IgG and vIL10 Fusion Antibodies to Post-Translationally Modified Collagen II in Mouse Models of Arthritis

2.2.1 Labelling of Antibodies using a Cyanine Based Fluorophores

CyDye kits were purchased from GE Healthcare and used according to the manufacturer's instructions. For IgG and vIL10 fusion protein labelling, 1 mg of protein was labelled using one dye vial. For scFv protein labelling, 200 µg of protein was labelled using one dye vial. Different mass of protein was used depending on the molecular weight to ensure molar equivalence. The CyDye was resuspended in 400 µL of PBS. The appropriate volume of antibody (depending on concentration) was added to the 400 µL of dye alongside a 1/10 dilution of 1 M Sodium bicarbonate pH 9.0. Antibody + dye was incubated in the dark for 1 hour at room temperature with gentle agitation. To separate free dye after incubation, samples were run through a PD-10 desalting column (GE Healthcare). Antibody was eluted by adding 3 mL of PBS to the column and collecting the eluates.

The formulae used to calculate protein concentration uses absorbance at 280 nm, which is typical for protein quantification. The absorbance of the cyanine dye is also measured at the appropriate wavelength (678 nm) and multiplied by the amount absorbance of the cyanine

dye at 280 nm. This calculation removes the influence of the cyanine dye to give a true antibody concentration in mg/mL. To calculate the dye to protein ratios, the molar extinction coefficient of the antibody is divided by the molar extinction coefficient of the dye. This number is then used alongside the maximum absorbance of the dye and the absorbance of antibody concentration at 280 nm to calculate a value that represents the number of dye molecules per antibody.

2.2.2 Localisation of Antibodies in a Mouse Model of Rheumatoid Arthritis

Antigen induced arthritis (AIA) was performed on female, 10-week-old C57BL/6 mice. Mice were housed in groups of five in individually vented cages, maintained at 21 ± 2 °C on a 12-hour light/dark cycle and with food and water provided. All experimental protocols were performed in compliance with the UK Animals (Scientific Procedures) Act 1986 regulations for the handling and use of laboratory animals (Home Office project licence PPL no: 70/8264). Mice were anaesthetized using 2.5% isoflurane. Mice were primed on day 0 with subcutaneous injection of 100 µg of methylated bovine serum albumin (mBSA) in complete Freund's adjuvant (CFA). On day 21, mice were injected intra-articularly with 50 µg of mBSA in saline to stimulate inflammation in the knee joint. Inflammation was stimulated in only one knee, with contralateral knees acting as healthy controls.

As demonstrated in Figure 13, on day 22, 24 hours after stimulating inflammation in the knee joint, mice were administered Cy5.5 labelled anti-ROS-CII antibodies intravenously (10 µg of IgG and vIL-10 fusion antibody and 50 µg of scFv). Following intravenous administration, mice

were biofluorescently imaged by *in vivo* optical imaging at several time points, as described in 2.2.4. Fluorescence in the knee joints were analysed by creating Regions of interest (ROI) using Living Image 4.4 software and assessing average fluorescence intensity.

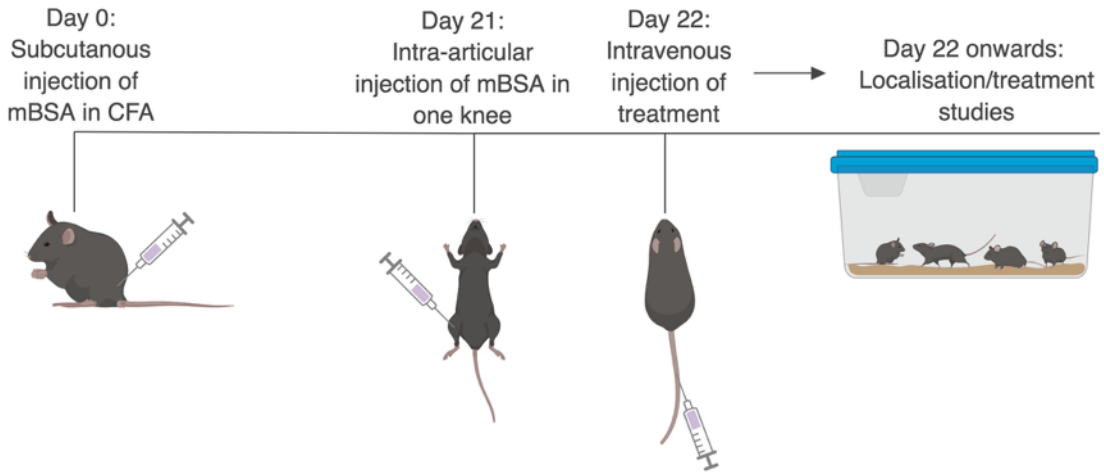

Figure 13. Timeline of the Antigen Induced Arthritis (AIA) mouse model. Mice were primed on day 0 by a subcutaneous injection at the base of the tail of methylated bovine serum albumin (mBSA) in complete Freund's adjuvant. On day 21, mice were challenged with an intra-articular injection of mBSA in one knee joint to induce inflammation. On day 22, mice were treated intravenously with antibody, followed by assessment from day 22 onwards. Image created with Biorender.

2.2.3 Localisation of Antibodies in a Mouse Model of Osteoarthritis

Destabilisation of the medial meniscus (DMM) performed on male, 10-week-old C57BL/6 mice in collaboration with the Kennedy Institute of Rheumatology, University of Oxford. Members of the Lim Lab at the Kennedy Institute of Rheumatology, University of Oxford, performed all surgeries. Mice were housed in groups of five in individually vented cages, maintained at 21 ± 2 °C on a 12-hour light/dark cycle and with food and water provided. All experimental protocols were performed in compliance with the UK Animals (Scientific Procedures) Act 1986 regulations for the handling and use of laboratory animals. Mice were

anaesthetised with 2.5% isoflurane. Following capsulotomy, the right meniscotibial ligament was transected, resulting in the release of the medial meniscus from its tibial attachment. Sham surgery consisted of capsulotomy alone. For pain relief, animals were given Vetergesic by subcutaneous injection prior to recovery from anaesthesia. Animals were monitored daily post-surgery.

At time points following DMM surgery (4 and 8 weeks post-surgery), mice were injected intra-articularly with 1µg of scFv antibody into both DMM and sham knees. Retention of the antibody within the knee joints was analysed by biofluorescence imaging by *In vivo* optical imaging at several time points. Fluorescence in the knee joints were analysed by creating regions of interest (ROI) using Living Image 4.4 software and assessing average fluorescence intensity as described in 2.2.4.

2.2.4 *In vivo* Imaging System

The knee area of mice was shaved before fluorescence imaging with IVIS Lumina III imager, using the excitation wavelength of 675 nm and an emission wavelength of 720 nm for Cy5.5 fluorescence (Perkin Elmer, Waltham, Massachusetts, USA) together with a black and white photograph for orientation. Images were taken at different time points up to 336 hours post-i.a. injection or 48 hours post-i.v. injection. Images were analysed using Living Image 4.4 (Perkin Elmer, Waltham, Massachusetts, USA) to obtain the average fluorescence intensities of a circular region of interest encompassing the knee joint. No background intensities were subtracted from the values; autofluorescence is only present in C57BL/6 mice in shaved

areas, and the data from the contralateral knee joints is shown in all figures and time points to indicate the nonspecific retention of antibody. Following the last imaging time point, mice were euthanized.

2.3 *In vitro* Analysis of Arthritic and Non-Arthritic Knee Joints Treated with vIL10 Fusion Antibodies

2.3.1 Processing of Knee Joints

Knee joints were removed from euthanized mice and incubated in 4% formalin at room temperature for 48 hours.

2.3.1.1 Decalcification of Bone and Paraffin Embedding

Following the 48-hour incubation in 4% formalin, knees were transferred into 10% ethylenediaminetetraacetic acid (EDTA) in PBS pH 7.0 solution. Knees were maintained in EDTA solution at room temperature whilst shaking for 4 weeks, with twice weekly changes of the EDTA solution. Following decalcification of bone, joints were embedded in paraffin wax in preparation for microtome cutting (paraffin embedding provided by Barts Cancer Institute Pathology Service, Charterhouse Square, Queen Mary University of London).

2.3.1.2 Section Cutting of Paraffin Embedded Joints

Paraffin embedded tissue blocks were chilled on ice and a water bath was preheated to 40°C prior to sectioning. The paraffin block was inserted into the holder of the microtome and orientated so the blade cut directly across the block. The block was trimmed to remove surrounding paraffin and until the tissue was exposed. The block was cut into 5 µM thick tissue sections. Each tissue section was transferred upon the preheated water. Charged

microscope slides were used to pick up sections and were placed in an oven at 37°C to dry. Following incubation at 37°C, the slides were as in 2.3.2 prior to immunostaining.

2.3.2 Histological Staining of Knee Joints

Prior to all immunostaining, slides were heated for 20 minutes at 60°C. All steps were conducted at room temperature unless stated otherwise. Paraffin wax was removed from the slides by two incubations in Histoclear (National Diagnostics HS-202) for 5 minutes. Slides were then dehydrated by two incubations in 100% Ethanol for 5 minutes. Samples were then rinsed briefly in distilled water before continuing staining as described in 2.3.2.1 and 2.3.2.2.

2.3.2.1 Safranin O Staining

A 0.2% safranin O solution (Sigma S8884, in dH_20) and 0.1% fast green solution (Sigma F7258, in dH_20) were prepared for staining. Slides were incubated in 0.1% Fast Green solution for 5 minutes. Slides were then incubated in a 1% acetic acid solution for 10 seconds and transferred to the 0.2% safranin O solution. Slides were incubated in safranin O for 5 minutes. Slides were then rinsed for 2-minutes in distilled water before dehydrated by two incubations for 5 minutes in 100% Ethanol and dewaxed by two incubations for 5 minutes in Histoclear. Slides were air dried before mounting using DePex (VWR 100503-836) and cover slips. Mounted slides were dried overnight in a fume hood.

2.3.2.2 Hematoxylin and Eosin Staining

A 1% Eosin solution (VWR341972Q) was prepared for staining. Meyer's Hematoxylin was purchased as a ready-to-use solution (Sigma MHS16). Slides were incubated in Harris Hematoxylin for 2 minutes. Slides were washed in distilled water for two minutes to remove all excess Hematoxylin. Slides were then incubated in acidic alcohol (1% hydrochloric acid (HCl) in 70% ethanol) for 10 seconds before being washed tap water for 2 minutes. Samples were then incubated in 1% Eosin solution for 2 minutes before washing in distilled water until the water was clear. Tissue was then dehydrated by two incubations for 5 minutes in 100% Ethanol and incubated twice for 5 minutes in Histoclear. Slides were air dried before mounting using DePex and cover slips. Mounted slides were dried overnight in a fume hood.

2.4 *In vitro* Analysis of Antibody Binding to Diseased and Healthy Tissues by Immunofluorescence

2.4.1 Mouse Models of Disease

Slides for mouse models of arthritis were obtained following embedding of knees following in house *in vivo* experiments (as previously described), or kindly donated by collaborators from the Kennedy Institute of Rheumatology.

2.4.2 Immunofluorescence Using Anti- Post-Translationally Modified Collagen II Antibodies

Slides were heated for 20 minutes at 60°C. All steps were conducted at room temperature unless stated otherwise. Paraffin wax was removed from the slides by two incubations in Histoclear for 5 minutes. Slides were then dehydrated by two incubations in 100% Ethanol for 5 minutes. Samples were then rinsed briefly in distilled water and air dried. Once fully dried, slides were fixed for 5 minutes using 4% Paraformaldehyde (PFA) in PBS. Slides were then washed twice on a shaker for 5 minutes with PBS. Solutions of 0.02 % HCl and 0.02 % HCl + 15 mg/mL pepsin (Sigma P7125) were pre-heated during the washes to 37°C in a water bath. After washing in PBS, slides were incubated in 0.02 % HCl for 15 minutes at 37°C. Following incubation in HCl, slides were transferred to 0.02 % HCl + 15mg/mL Pepsin solution and incubated for 45 minutes at 37°C. Slides were then washed briefly using PBS and distilled water and air dried. Tissue was then fixed again by incubating in 4 % PFA solution for 5 minutes. Slides were then washed twice on a shaker for 5 minutes with PBS, followed by two

incubations in 50 mM ammonium chloride solution for 5 minutes. Circles were drawn carefully around the samples using hydrophobic pen (DAKO) and non-specific sites were blocked using 20% Foetal Bovine Serum (FBS) in PBS + 1% Tween 20 for 1 hour. During the blocking stage, primary antibodies (fluorophore conjugated anti-ROS-CII and controls) were diluted to a maximum concentration of 10 μg/mL in blocking solution. Following completion of the blocking stage, primary antibodies were added to the samples and incubated overnight in the dark at 4°C. The following day, slides were washed three times for 10 minutes in PBS + 1% Triton X. Following the washes, slides were mounted using Fluoroshield with DAPI (Sigma F6057) and coverslips, and allowed to dry before storing at 4°C in the dark, prior to imaging on a classic motorised epifluorescence microscope (Olympus, BX61) equipped with a high-definition digital camera (Hamamatsu, Orca-R2). Images were acquired at room temperature using Cell P/Sense software. The acquisition parameters were determined using the positive and negative control slides to achieve the maximum sensitivity and specificity.

2.5 Microvesicle Generation

2.5.1 Neutrophil Isolation from Peripheral Blood

Blood donations were collected from consenting, healthy individuals with approval from the Barts and the London Research Ethics Committee (QMREC 2014.61). Healthy donor blood (60 mL) was added to 10% v/v sodium citrate (stock concentration of 3.2% w/v) to prevent clotting. The whole blood sample was centrifuged at 120*g* for 20 minutes at room temperature to separate the platelet rich plasma (PRP). PRP was discarded and 10 mL of PBS without calcium chloride or magnesium chloride (PBS^{--}), followed by 8 mL of 6 % w/v Dextran (MW 450,000-600,000, Sigma 31392) were carefully layered upon the blood. Tubes were inverted gently to mix the contents but subsequently avoid neutrophil activation and left for 15 minutes at room temperature to sediment the red blood cells. Following sedimentation, the top layer of leukocytes was collected and gently layered upon 10mL of Histopaque 1077 in a fresh tube. The leukocytes and histopaque were centrifuged at 420*g* for 30 minutes at room temperature to form density layers. The plasma, mononuclear cell and histopaque layers were aspirated and disposed of leaving only the neutrophil and erythrocyte pellet. The pellet was resuspended quickly in 9 mL of ice-cold ultrapure water, before returning the isotonic balance with 1 mL of 10x Hanks Balanced Salt Solution (Sigma H4641). The suspension was made up to 50 mL with PBS^{--} and centrifuged at 300*g* for 10 minutes at room temperature to pellet the neutrophils. Following centrifugation, the supernatant was

aspirated and neutrophils were resuspended in 1 mL of PBS^{--}. Cells were counted using a 1:100 dilution in Turks stain.

2.5.2 Microvesicle Isolation by Stimulation with Tumour Necrosis Factor Alpha

The process of neutrophil isolation and stimulation, and the subsequent microvesicle formation and isolation is illustrated in Figure 14. To generate microvesicle release by the isolated neutrophils, cells were stimulated with tumour necrosis factor alpha (TNFα). Cells were resuspended to a concentration of $2x10^7$ cells/mL and stimulated with 50 ng/mL of human TNFα for 20 minutes at 37°C. Following stimulation, suspensions were centrifuged at 4400*g* for 15 minutes at 4°C to remove cells and large platelets. Supernatants were transferred to fresh tubes and centrifuged at 13,000*g* for 2 minutes at 4°C to remove small platelets and apoptotic bodies. Supernatants were again transferred to fresh tubes and fluorescently labeled using 50 µM of BODIPY FL (Thermo Fisher D2184) or BODIPY TR (Thermo Fisher D6116). The supernatants were then centrifuged at 20,000*g* for 30 minutes at 4°C to pellet the fluorescent microvesicles. The supernatants containing the smaller exosomes were discarded and the microvesicles were resuspended in 70 µL of PBS^{--}. Resuspended fluorescent microvesicles were then ready for use in experiments.

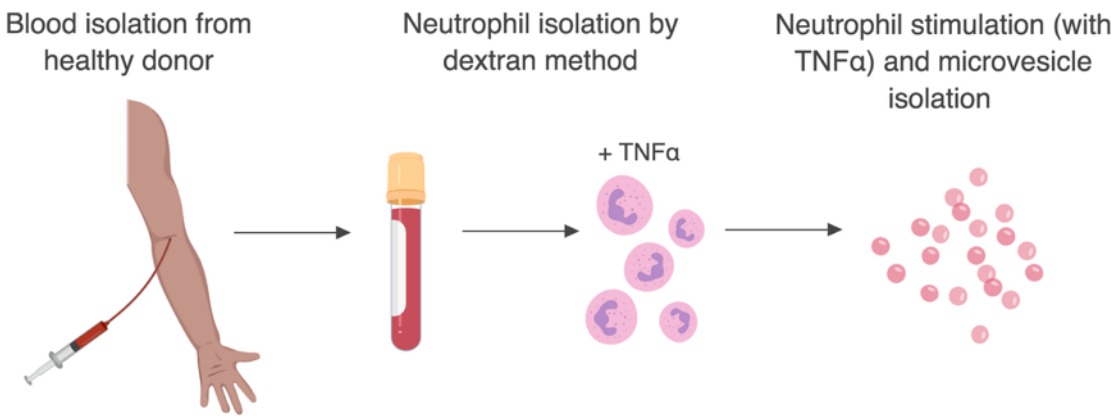

Figure 14. Schematic of microvesicle isolation from healthy donors. Neutrophils are isolated from the whole blood of healthy volunteers and activated with TNFα to stimulate microvesicle shedding. Microvesicles are then purified by differential centrifugation. Image created with Biorender.

2.5.3 Flow Cytometric Analysis of Microvesicles

Microvesicles were fluorescently labeled with BODIPY as previously described. Vesicles were diluted 1:3 in PBS^{--} for flow cytometric analysis. The Imagestream^X Mk II flow cytometer was used for analysis of microvesicles. All samples were acquired on an ImageStream^X MkII imaging cytometer, x60 magnification; with low flow rate/high sensitivity using INSPIRE software. The instrument and software were set up as follows: Channels 1 and 9 for brightfield imaging and channel 6 for side scatter channel, plus the fluorescence channels required. Lasers 488 and 745 were activated for fluorescence and side scatter quantification. To obtain a collection gate, a scatter plot of BODIPY fluorescence intensity was plotted against side scatter intensity. The gate was drawn around the low to mid BODIPY fluorescence intensity but low side scatter population, which is characteristic of fluorescent microvesicles. The high side scatter and low BODIPY fluorescence population confirmed the

presence of speed beads, used as an internal calibrator for the machines image capture. The gated populations were interrogated using the image gallery. Fluorescent microvesicles appear as small, spherical points and can be easily discriminated from cells and speed beads. IDEAS software was used to determine the concentration of the microvesicle population. Raw image files with the entire number of acquired events were opened. A scatter plot was recreated plotting BODIPY intensity against side scatter. The microvesicle gate was re-applied and adjusted as necessary. The objects/mL analysis was performed, which included quantification of all the events recorded and the microvesicle alone population exclusively.

2.6 Fortifying Microvesicles with Anti-Post-Translationally Modified Collagen II Antibodies

Fluorescent microvesicles were quantified as objects/mL as previously described. As illustrated in Figure 15, a 'phospholipid cake' was created by adding 100 µg of 1,2-dioleoyl-*sn*-glycero-3-phospho-L-serine (phospholipid, Avanti 181PS) to a pear-shaped glass flask, and evaporating the chloroform solvent using a nitrogen stream. The result was a layer of dried phospholipid on the bottom of the glass which when resuspended in an aqueous solution forms liposomes.

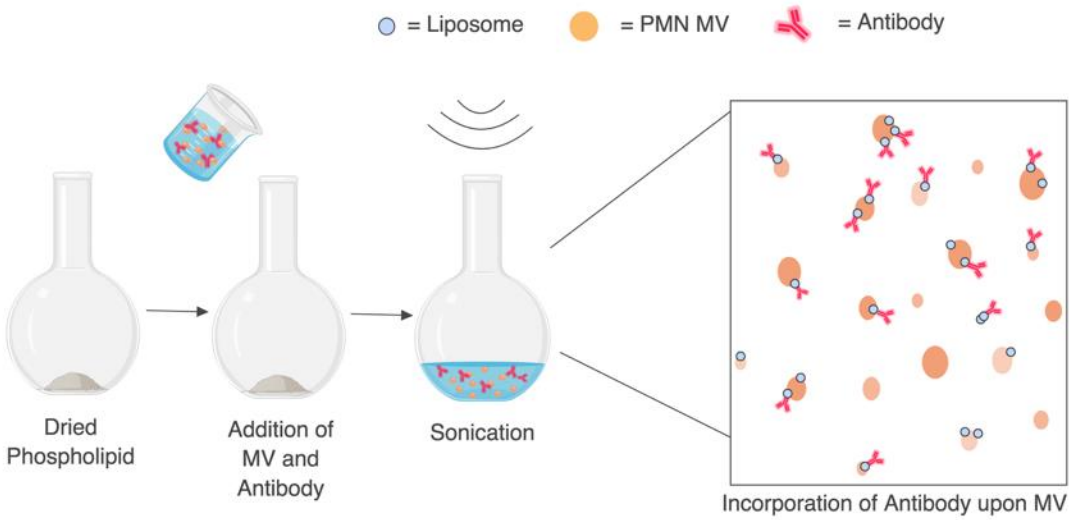

Figure 15. Schematic of the production of enriched vesicles using phosphatidylserine liposome formation. Phospholipid is dried and the antibody/microvesicle cocktail is added. The solution is then sonicated at 3 amplitude microns for 5 minutes to simultaneously create the formation of liposomes which entrap the antibody, but also provide fluidity to the microvesicle membrane allowing the liposomes to incorporate. Image created with Biorender.

A solution of fluorescent anti-ROS-CII scFv antibody and fluorescent MV was prepared, using an in-house optimized protocol of 10 µg of antibody for every $5x10^5$ microvesicles (using 1.5-

$2.5x10^6$ vesicles in a 0.5mL reaction) [139,140]. The MV/antibody solution was added to the phospholipid cake. The solution was sonicated for 5 minutes on a low setting of 3 amplitude microns using a Soniprep 150 ultrasonic disintegrator with an exponential probe. Samples were then appropriately prepared for further experimentation.

2.6.1 Imagestream Analysis

All samples were acquired on an ImageStream^X MkII imaging cytometer, x60 magnification; with low flow rate/high sensitivity using INSPIRE software. The instrument and software were set up as follows: Channels 1 and 9 for brightfield imaging and channel 12 for side scatter channel, plus the fluorescence channels required. Lasers 488 and 745 were activated for fluorescence and side scatter quantification. A compensation matrix was created using fluorescent microvesicles alone and fluorescent antibody incorporated into unlabelled microvesicles. Fluorescent microvesicles were also used as a negative control for antibody incorporation gating. In the IDEAS software, the compensation matrix was applied to all analysis. The MV alone population was gated as previously described. A scatter plot was created using fluorescence intensity of MV against fluorescence intensity of antibody. A Cy5 positive gate was drawn on the MV alone population- of which the Cy5 positivity should be <1%. The Cy5 positive gate was copied and used to assess positivity of antibody incorporation. Experimental samples of MV enriched with antibody were acquired in INSPIRE and analysed in IDEAS software in the same manner as the MV alone population. After gating the positive microvesicle population, a scatter plot was created of fluorescence intensity of vesicles and fluorescence intensity of antibody. The Cy5 positive gate was applied to the

graph to give a percentage positivity of MV that were positive for antibody. This population of antibody positive MV was quantified by the objects/mL analysis.

2.6.2 Enzyme Linked Immunosorbent Assay

Immunosorbent 96-well plates were coated with 100 µL of 10µg/mL collagen II or ROS modified collagen II. Coatings were incubated overnight at 4°C. Following overnight incubation, plates were washed five times with 200 µL of PBS^{--} and blocked with 2.5% powdered milk in PBS^{--}. Plates were blocked for 2 hours at room temperature. During the blocking incubation, the primary antibodies were prepared. For the ELISA to analyse the fortification of MV with antibody, antibody alone, MV alone and antibody positive MV were used as 'primary antibodies'. A phospholipid cake was prepared as previously described. For the ELISA, a concentration of 0.1 mg/mL of antibody was used to give a 10 µg/well input concentration. A solution of MV plus anti-ROS-CII antibody was prepared using 10 µg of antibody for every $5x10^5$ microvesicles. Total volume was adjusted depending on the number of wells. The MV/Antibody solution was added to the phospholipid cake and sonicated as previously described. Following sonication, the solution was transferred to an eppendorf and centrifuged at 20,000*g* for 30 minutes to pellet the MV and remove any unincorporated, free antibody. MV were resuspended in 2.5% Milk in PBS^{--} in the same volume as before the centrifugation step. Antibody enriched MV were added as primary antibody in the ELISA, as well as anti-ROS-CII alone as a positive control and negative control antibody. Following incubation, plates were washed five times with 200 µL of PBS^{--}. Secondary antibody was diluted in 2.5% powdered milk in PBS^{--} (anti-hIgG final concentration 10 µg/mL; anti-His tag

final concentration 2.5 µg/mL) and added to each well. The secondary antibody was incubated for 2 hours at room temperature before five washes with 200 µL of PBS^{--}. The ELISA was then developed using 100 µL of TMB solution (0.1 mg/mL TMB, 0.1 M sodium acetate and 2 µL per 10 mL of 30% Hydrogen Peroxide). The reaction was stopped using 50 µL of 20% Sulfuric Acid and absorbance was read at 450 nm.

2.6.3 Immunofluorescence

Slides were heated for 20 minutes at 60°C. All steps were conducted at room temperature unless stated otherwise. Paraffin wax was removed from the slides by two incubations in Histoclear for 5 minutes. Slides were then dehydrated by two incubations in 100 % Ethanol for 5 minutes. Samples were then rinsed briefly in distilled water and air-dried. Once fully dried, slides were fixed for 5 minutes using 4% Paraformaldehyde (PFA) in PBS. Slides were then washed twice on a shaker for 5 minutes with PBS. Solutions of 0.02 % HCl and 0.02% HCl + 15 mg/mL Pepsin were pre-incubated during the washes to 37°C in a water bath. After washing in PBS, slides were incubated in 0.02% HCl for 15 minutes at 37°C. Following incubation in HCl, slides were transferred to 0.02% HCl + 15 mg/mL pepsin solution and incubated for 45 minutes at 37°C. Slides were then washed briefly using PBS and distilled water and air dried. Tissue was then fixed again by incubating in 4% PFA solution for 5 minutes. Slides were then washed twice on a shaker for 5 minutes with PBS, followed by two incubations in 50 mM ammonium chloride solution for 5 minutes. Circles were drawn carefully around the samples using DAKO hydrophobic pen and non-specific sites were blocked using 2.5% w/v powdered milk in PBS^{--} for 1 hour. During the block, the MV enriched

with antibodies were prepared as described in 2.6. MV and antibody solution was prepared using a final concentration of 10 µg/ml of antibody for every $5x10^5$ microvesicles. Volume was adjusted depending on the number of samples (100 µL per sample was prepared). Following completion of the blocking stage, MV alone, antibody enriched MV or antibody alone were added to the samples and incubated overnight in the dark at 4°C. The following day, slides were washed five times for 10 minutes in PBS^{--}. Following washes the slides were mounted using Fluoroshield with DAPI and coverslips and allowed to dry before storing at 4°C in the dark, prior to imaging on a classic motorised epifluorescence microscope (Olympus, BX61) equipped with a high-definition digital camera (Hamamatsu, Orca-R2). Images were acquired at room temperature using Cell P/Sense software. The acquisition parameters were determined using the positive and negative control slides to achieve the maximum sensitivity and specificity.

2.6.4 *In vivo* Localisation Studies of Antibody Enriched Microvesicles in a Mouse Model of Arthritis

Antigen induced arthritis (AIA) was performed on female, 10-week-old C57BL/6 mice. Mice were housed in groups of five in individually vented cages, maintained at 21 ± 2 °C on a 12-hour light/dark cycle and with food and water provided. All experimental protocols were performed in compliance with the UK Animals (Scientific Procedures) Act 1986 regulations for the handling and use of laboratory animals (Home Office project licence PPL no: 70/8264). Mice were anaesthetized using 2.5% isoflurane. Mice were primed on day 0 with

subcutaneous injection of 100µg of methylated bovine serum albumin (mBSA) in complete Freund's adjuvant (CFA). On day 21, mice were injected intra-articularly with 50 µg of mBSA in saline to stimulate inflammation in the knee joint. Inflammation was stimulated in only one knee, with contralateral knees acting as controls.

On day 22, 24 hours after stimulating inflammation in the right knee joint, mice were administered with fluorescently labelled anti-ROS-CII enriched MV or MV alone (600,000 antibody enriched MV or 600,000 MV alone). Following intravenous administration, mice were biofluorescently imaged by *in vivo* optical imaging at several time points. Fluorescence in the knee joints were analysed by creating Regions of interest (ROI) using Living Image 4.4 software and assessing average fluorescence intensity. At the end-point of the experiment mouse organs were imaged *ex vivo* to assess fluorescence in the stomach, intestines, liver, heart, lungs, kidneys and spleen. Knee joints were also imaged *ex vivo.*

Bioluminescence imaging was performed at several time points 10 minutes following intraperitoneal injection of 100 µL luminol sodium salt 50 mg/mL (Sigma Aldrich). Luminol is a redox sensitive compound that emits blue luminescence (λmax 425 nm) when exposed to reactive oxidants. Mice were imaged 10 minutes after intraperitoneal injection at an exposure time of 5 minutes with high binning and open emission filter. Luminescence in the knee joints were analysed by creating Regions of interest (ROI) using Living Image 4.4 software and assessing average luminescence intensity.

2.6.5 *Ex Vivo* Detection of Antibody Enriched Microvesicles in the Arthritic Joint

At the end-point of the experiments, knees were harvested and snap frozen in Optical Cutting Temperature Compound (OCT, Cellpath) by immersing in pre-cooled isopentane. Knees were stored at -80°C until use. Knee joints were sectioned using an OFT5000 cryostat microtome (Bright Instruments), with specimen and chamber temperature maintained at -20°C. Knee joints were cut into 17µm sections using MX35 premier blades (Thermofisher Scientific), and mounted onto superfrost plus slides (ThermoFisher Scientific). Slides were air dried at room temperature for 30 minutes before mounting using Fluoroshield mounting medium (Sigma, F6182) and analysis by confocal microscopy. Sections were imaged on a Leica SP8 confocal microscope with the use of a 20×water-dipping objective. Images were attained with the use of sequential scanning of different channels at a XY resolution of 1024× 600 with a speed of 700 Hz, zoom factor of 1.28 and line average of 4. Images were analysed with the image processing software IMARIS.

2.7 Fortifying Microvesicles with Anti-Post-Translationally Modified Collagen II Antibodies and Additional Therapeutics

2.7.1 Fortifying Microvesicles with Therapeutic Antibodies

Microvesicles were fortified with therapeutic antibodies in the same manner as was earlier described (Figure 15, section 2.6). The therapeutic antibodies used were 3-11E/vIL-10- 3-11E anti-ROS-CII scFv antibody fused to viral IL-10; and Anti-mTNF- an antibody specific against mouse TNFα. Both antibodies were expressed in house by transient transfection as previously described.

A solution of 3-11E/vIL-10 antibody and fluorescent MV was prepared, using 10 µg of antibody for every $5x10^5$ microvesicles (using $1.5\text{-}2.5x10^6$ vesicles in a 0.5mL reaction). For situations where multiple antibodies were used, 50 picomolar of each antibody were used, to accommodate for the differences in molecular weight due to the differing sizes of antibodies. This equated to 5 µg of 3-11E/vIL-10 and 7.5 µg of anti-mTNF. MV/antibody solution was added to the phospholipid cake and sonicated as previously described.

2.7.2 Imagesteam^X Analysis

Imagestream^X analysis was conducted to assess the antibody incorporation as described in section 2.6.1. The MV alone population was gated as previously described. Single antibody loaded MV were used as fluorescence minus one controls for double positive antibody

gating. A Cy5 positive gate was drawn on the MV enriched with Anti-mTNF. An AF488 positive gate was drawn on the MV enriched with 3-11E/vIL-10. Both gates were copied and applied to the MV enriched with both antibodies analysis to determine double positivity. This population of antibody positive MV was quantified by the objects/mL analysis.

2.7.3 Enzyme Linked Immunosorbent Assay

ELISA analysis was conducted to assess the antibody incorporation as described in section 2.6.2. Immunosorbent 96 well plates were coated with 100 µL of 10 µg/mL of glycated CII or 100 ng/mL of recombinant mouse TNF. A solution of MV plus 3-11E/vIL-10 antibody and MV plus anti-mTNF was prepared using 10 µg of antibody for every 5 x 10^5 microvesicles. A solution of MV combined with both antibodies was prepared using 5 µg of 3-11E/vIL-10 and 7.5 µg of anti-mTNF antibody for every 5 x 10^5 microvesicles. Antibody incorporation was performed as previously described in 2.7.1 and only the microvesicles pelleted down were run on the assay. Antibody enriched MV were added as primary antibody in the ELISA, as well as anti-ROS-CII alone and anti-mTNF alone as controls. Secondary antibody was diluted in 2.5% powdered milk in PBS^{--} (anti-human IgG 1:1000 dilution; anti-mouse IgG 1:1000 dilution) and added to each well. The ELISA was developed and absorbance was read as previously described.

2.7.4 MTT Assay

3-(4,5-Dimethylthiazol-2-Yl)-2,5-Diphenyltetrazolium Bromide (MTT) assay was performed to assess the function of the anti-mTNF antibody in inhibiting TNF dependent cell death. L929 cells were used in the assay which are TNF sensitive. Cells were cultured in DMEM + 10% FBS + 1% penicillin/streptomycin (complete media). Cells were seeded at 50,000 cells/mL in 96 well flat bottom plates for 18 hours. Following the incubation time, media was replaced with complete media plus 1 µg/mL Actinomycin D and 0.45 ng/mL of recombinant mouse or human TNF. Anti-mTNF antibody at two concentrations, MV alone and enriched MV were added to the media and incubated for 24 hours. Following incubation time, MTT was added to each well at a concentration of 500 µg/mL. Plates were incubated for 3 hours at 37 °C. Media was then removed and a solution of 90% isopropanol/10% DMSO was added and incubated for 15 minutes at room temperature. Absorbance was read at 595 nm. MTT assay was repeated over three different L929 passages. Data are presented as % of viability compared to positive control (L929 cells without TNF in culture medium).

2.7.5 Treatment of a Mouse Model of Rheumatoid Arthritis Using Microvesicles Fortified with Therapeutics

Antigen induced arthritis (AIA) was performed on female, 10-week-old C57BL/6 mice as previously described in section 2.2.2. On day 22, 24 hours after stimulating inflammation in the knee joint, mice were administered treatments intravenously. Mice treated with MV enriched with therapeutics were administered 600,000 antibody-positive MV. For mice being

treated with MV enriched with multiple therapeutics, 600,000 MV positive for both antibodies were administered. Treatment was administered 24 and 72 hours after stimulation of inflammation in the knee joint. Knees were measured with digital calipers at daily increments from baseline, before the induction of inflammation in the knee. At the end-point of experiment, knee joints were harvested and either snap frozen for confocal imaging/RT-qPCR or fixed in 4% neutral buffered formalin for histological analysis.

2.7.6 Histological Analysis of Knee Joints

Safranin O/fast green staining was conducted as previously described in 2.3.2. Joints were scored 0–4 for disease activity for each of: subsynovial inflammation, synovial lining thickening, cartilage matrix depletion, chondrocyte death, pannus formation, marrow involvement, synovial fluid cells, and bone erosion. The scores are presented as total score out of 36 for each of the two animals assessed.

2.7.7 RT-qPCR Analysis of Knee Joints

2.7.7.1 RNA Extraction

Total RNA was extracted from snap frozen knee joints using Trizol method. Knee joints were placed into reinforced homogenizer tubes (Precellys Lysing Kit for Hard Tissue, MK28) and 1 mL of Trizol was added. Knee joint tissue was homogenized using a Precellys 24 homogenizer (Bertin Technologies) for 2 rounds of 30 seconds, and then centrifuged for 5 minutes at maximum speed. Supernatant was then homogenized using a syringe and 21 G needle and centrifuged for 10 minutes at maximum speed. Supernatants were transferred into new

eppendorfs and made up to 1 mL with Trizol before adding 200 µL of precooled chloroform. Samples were shaken vigorously for 30 seconds and incubated on ice for 1 minute. Samples were then centrifuged for 15 minutes at 10,000*g*. The clear, aqueous layer was transferred to a new eppendorf before adding 500 µL of precooled isopropanol. Samples were shaken vigorously for 30 seconds before incubating on ice for 1 hour. Following incubation, samples were centrifuged for 40 minutes at 20,000*g*. Avoiding the pellet, isopropanol was then removed and 1 mL of precooled 70% ethanol was added. Samples were centrifuged for 5 minutes at 20,000*g*. Ethanol was then removed from the sample and the pellet was air dried on ice. Once the pellet was dried, the pellet was resuspended in 20 µL of RNAse free water. Nanodrop ND-1000 (Nanodrop Technologies) was used to obtain RNA concentration and purity.

2.7.7.2 Removal of Genomic DNA

Genomic DNA contamination was removed using DNase Max Kit (Qiagen) according to the manufacturer's instructions. Briefly, for each sample 1 µL of DNase Max Enzyme, 5 µL of 10x DNase Max Buffer and 29 µL of RNase free water was combined. To this digestion reaction, 15 µL of RNA was added. The digestion reaction was incubated for 20 minutes at 37 °C. Following incubation, 5 µL of DNase Max Removal Resin was added and incubated for 10 minutes at room temperature with regular inverting. The sample was centrifuged at 13,000 *g* for 1 minute to pellet the resin. The supernatant was then transferred to a new eppendorf, analysed by Nanodrop ND-1000 to assess purity following DNA removal and then stored at -80 °C until further use.

2.7.7.3 cDNA Synthesis

cDNA was produced from RNA using a high capacity cDNA reverse transcription kit (Applied Biosystems) according to the manufacturer's instructions. Briefly, a 2x master mix was firstly prepared by combining 2 µL of 10X RT Buffer, 0.8 µL of 25X dNTP Mix, 2 µL 10X RT Random Primers, 1 µL Multiscribe Reverse Transcriptase and 4.2 µL of nuclease free H_2O for each sample. RNA was diluted to a concentration of 1 µg in 10 µL of nuclease free H_2O and added to the 2X master mix in an individual 0.2 mL PCR tube. Reverse transcription was performed in a thermal cycler under the following conditions: Step 1- 10 minutes at 25 °C; Step 2- 120 minutes at 37 °C; Step 3- 5 minutes at 85 °C and then held at 4 °C. cDNA was stored at -20 °C until use.

2.7.7.4 RT-qPCR

For each reaction, a total volume of 10 µl was used, consisting of 1 µl of cDNA, 5 µl of 2X Power SYBR Green Mastermix (Applied Biosystems, Inc.), 3 µl of dH2O, and 1 µl of gene-specific primer. Primers were commercially available (Qiagen) and the following were used to probe specific mRNA targets: *Rpl32*, QT00131992; *Col2a1*, QT01055523; *Sox9*, QT00163765; *Acan*, AT00175364; *Il10*, QT00106169; *Il1β*, QT01048355; *Il4*, QT00160678; *Il6*, QT00098875; *Adamts5*, QT00131376; *Fpr2*, QT00171514; *Mmp13*, QT00111104; *Tnf*, QT00104006. Real-time PCR was carried out with the following amplification settings: 95°C for 15 min; 35 cycles of 94°C for 15 s, 55°C for 30 s, and 72°C for 30 s, followed by melt curve analysis, using the ABI Prism 7900 Real-time PCR system (Applied Biosystems Inc.). Data are expressed as

relative units calculated by $2^{-\Delta\Delta CT}$ by normalization relative to RPL32 and to fold change over knee joints from naïve control samples. Negative controls were also run and included cDNA without primer and RNA reverse transcribed in the absence of reverse transcriptase.

2.8 Statistical Analysis

Statistical analysis was performed using Graphpad Prism 7 software. Data are expressed as mean ± standard error of mean (SEM), unless indicated otherwise. A P value of <0.05 was considered significant to reject the null hypothesis. Two-way ANOVA was used in circumstances where two or more groups existed with two variables (e.g. time and treatment) with Bonferroni post-hoc test. One way ANOVA was used in circumstances where three or more groups were being tested with one variable. For RT-qPCR analysis, Kruskal Wallis test with Dunn's multiple comparison post-test was performed to compare three or more groups in a non-parametric fashion.

2.9 Biorender Software

All original schematics and cartoons used herein were created with Biorender (https://biorender.io/).

Chapter 3: Results

3.1 Validation of Anti-ROS-CII *in Vitro*

The antibodies used herein were previously raised from a scFv phage display human library by the Nissim Lab. Antibody phage display is a technique based on the genetic engineering of bacteriophages with repeated rounds of antigen guided selection to allow in vitro selection of antibodies. It is a powerful technique that is responsible for the production of some of the most potent and widely used medicines worldwide.

For the antibodies used within this thesis, native CII and ROS-CII were the antigens used for selection. For ROS-CII antibody selection, 3 rounds of subtractive selection performed using native CII for subtraction. The result was a panel of antibodies with varying specificities to CII and ROS-CII [118]. The antibodies raised by phage display were scFv format, with subsequent subcloning performed to produce full IgG versions. The Nissim lab selected antibody candidates based on their binding specificity and affinity, with 1-11E antibody being a primary candidate for targeting ROS-CII. As aforementioned, the 1-11E antibody was found to undergo glycosylation during production, inhibiting its binding potential. Therefore, alternative antibody candidates were selected, and hence 3-11E was chosen for future studies and is the candidate primarily used herein.

Antibody Name	Binding Specificity	Generation	Format	Reference
1-11E	ROS-CII	scFv Phage Library[142]	scFv, IgG and scFv-vIL-10 fusion	[39,115,118]
3-11E	ROS-CII	scFv Phage Library[142]	scFv, IgG and scFv-vIL-10 fusion	n/a
6-11D	CII & ROS-CII	scFv Phage Library[142]	scFv	n/a
C7	HEL	scFv Phage Library[142]	scFv, IgG and scFv-vIL-10 fusion	[39,115,118]

Table 1. Description of binding specificity and format of 1-11E, 3-11E, 6-11D and C7 antibodies.

3.1.1 Electrophoretic Analysis of Antibodies after Purification

Following the antibody production, either by bacterial expression or transient transfection in mammalian cells, protein was purified by either protein A or Ni-NTA column. To evaluate the purification process, an SDS-PAGE with coomassie blue staining was performed to visualize protein.

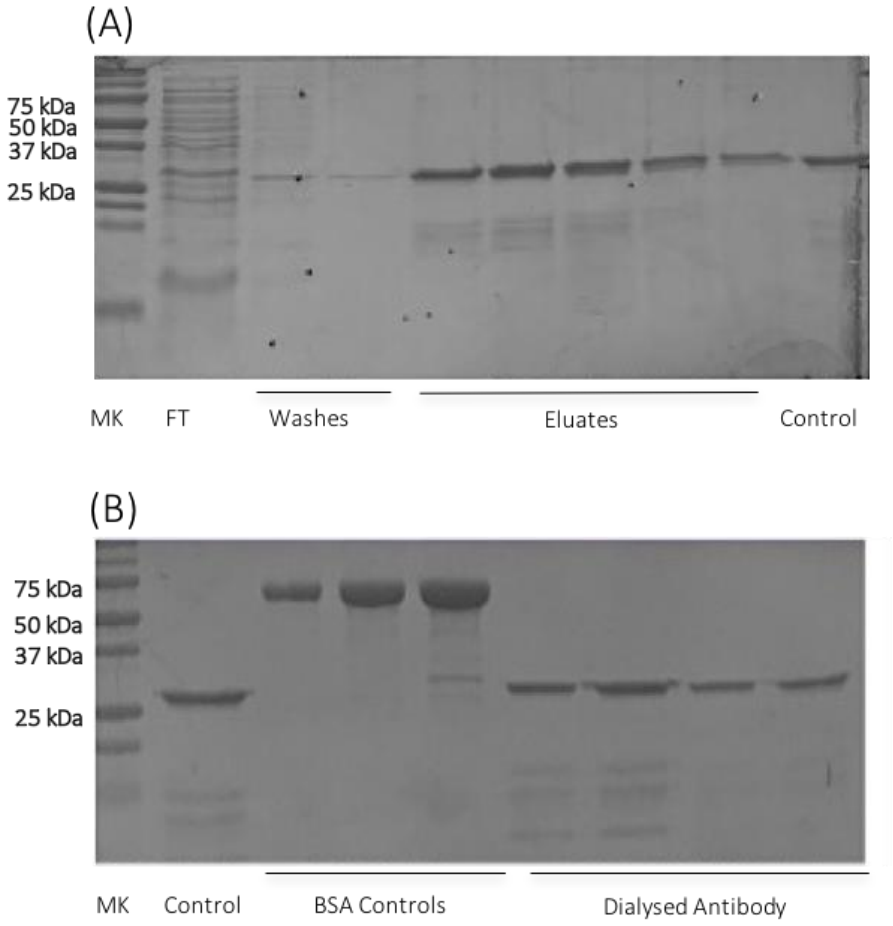

Figure 16. SDS PAGE analysis of antibody following purification dialysis. (A) 12% polyacrylamide gel of purified scFv (25 kDa). Minimal protein of interest is observed in the flow through and washes, with an abundance of protein visible in the eluates. (B) Following dialysis, a clean band of protein at 25 kDa is visible. MK, molecular weight marker; Control; scFv antibody; FT, flow through; BSA, bovine serum albumin.

Figure 16(A) shows a representative SDS-PAGE following the purification of an anti-ROS-CII scFv. A protein ladder depicting a variety of weights in kDa confirms the expected molecular weight of the protein. The flow through from the purification shows an abundance of protein at a variety of molecular weights, but no large amount at the 25 kDa range. Furthermore, there is little protein at the 25 kDa weight in the lanes containing the washes. The purification eluates, however, contain a visibly larger amount of protein at the 25 kDa range,

indicating the production and purification was successful. The eluted protein is the same molecular weight as the scFv control, suggesting that it is a scFv antibody. The standard yield from a scFv production was around 300 µg/mL.

Following the purification, antibodies must be dialysed into a phosphate buffer solution, as the purification process uses strongly acidic buffers to elute the protein. Following dialysis, an SDS-PAGE is performed once more to ensure protein isn't lost during the process. Figure 16(B) shows a typical SDS-PAGE following the dialysis of the antibody into a neutral buffer. As well as a scFv control, BSA concentration controls are included. The dialysed antibody shows as a strong band at 25 kDa, similarly to the SDS-PAGE performed after purification. This is indicative that no protein was lost during the dialysis process.

3.1.2 Electrophoretic Analysis of *in vitro* Modifications of Collagen II

The antibodies used in this thesis were raised from phage display library using *in vitro* modified CII as an antigen. ELISA uses the in vitro modifications to test the binding of produced antibodies. The coating step of the ELISA uses the native and ROS-CII as the antigen, therefore before antibody binding can be checked the *in vitro* modifications must be performed. Figure 17 shows a representative SDS page of the CII modifications. Glycated CII (Gly CII) and chlorinated CII (HOCl CII) are used throughout this thesis as the two post-translational modifications as they have previously found to be the most reactive to RA patient's sera [107].

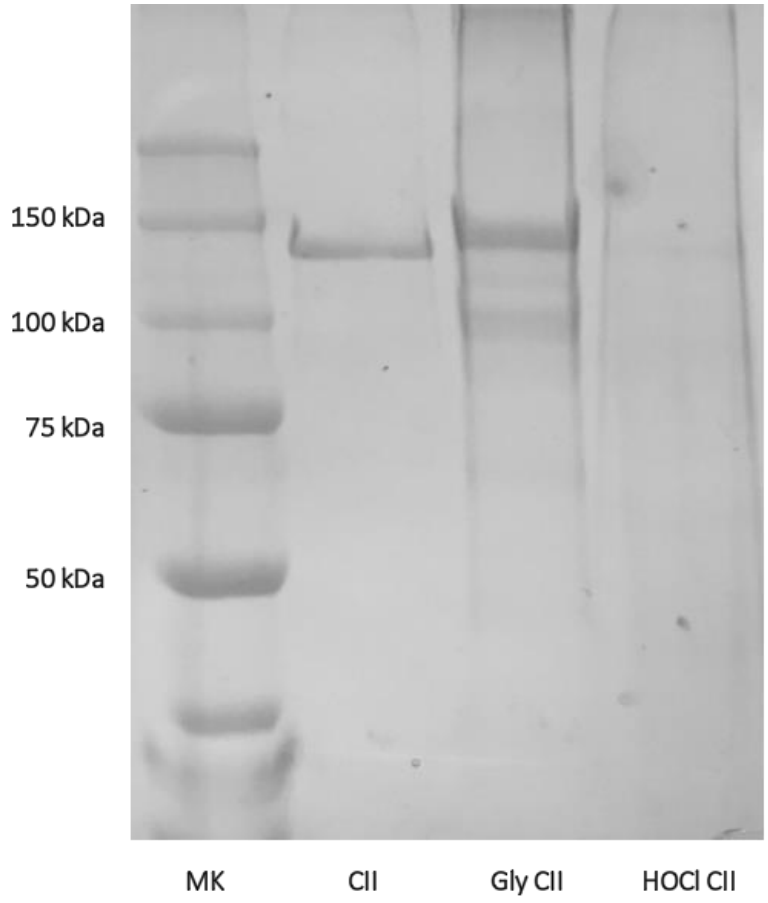

Figure 17. SDS-PAGE analysis of collagen II following in vitro mimicking of ROS modification. CII is observed in its native state, with a molecular weight of 141 kDa. Gly CII can be seen to have a larger molecular weight than CII, representing the addition of sugar molecules. HOCl CII almost completely loses the native CII band and appears a smear of protein due to fragmentation. MK, molecular weight marker; CII, native collagen II; Gly CII, native collagen II modified by non-enzymatic glycation; HOCl CII, native collagen II modified by chlorination.

The molecular weight of native CII is 141 kDa, which is observed in the SDS page as a single band. Gly CII appears as a slightly larger molecular weight, with additional smearing of the protein. This is due to the addition of sugar molecules, resulting in a shift in the position of the CII α-chain band to a region of slightly higher molecular mass, as well as fragmentation to bands in the electrophoretic region of 50–150 kDa. The degradation of CII caused by chlorination from HOCl is observed in lane 4. HOCl CII almost completely loses the 141 kDa

band and appears as a smear of protein. The modifications shown in Figure 17 are as previous data would suggest.

3.1.3 Antibody Binding to Target

Once the antibodies had been produced, purified and dialysed into a neutral pH buffer, their binding capacities were checked by ELISA. The unique quality of an antibody is its binding specificity, therefore assessing that the antibody has retained its specific binding qualities throughout the production and purification is paramount. The graphs below show an ELISA of the correct binding specificities from three scFv antibodies produced as part of the studies.

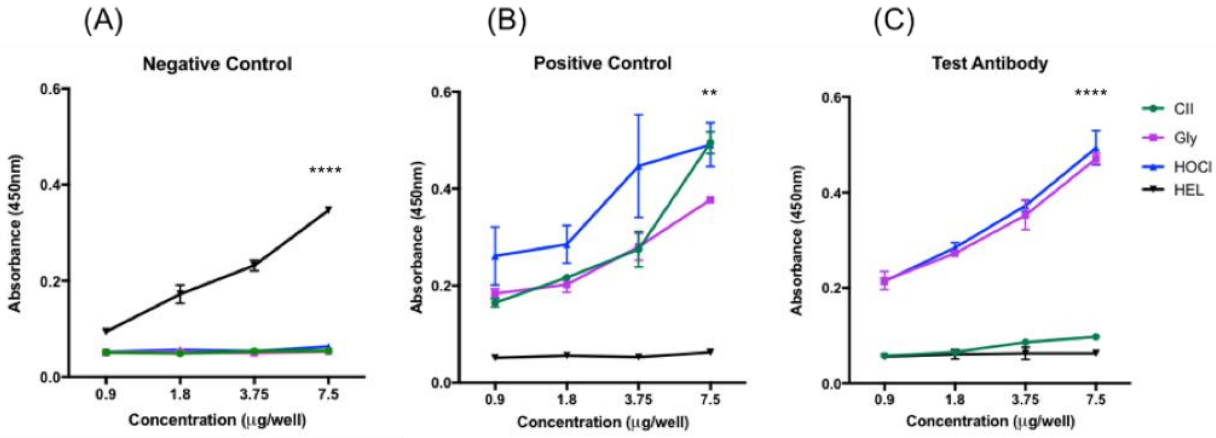

Figure 18. ELISA to assess binding of produced antibodies. (A) ELISA of negative control antibody 'C7', specific to Hen Egg Lysozyme (HEL). The antibody showed no binding to native collagen (CII), glycated collagen II (Gly) or HOCl modified collagen II (HOCl). Binding of negative control antibody 'C7' to HEL is statistically significantly greater than its binding to collagen II types. (B) ELISA of positive control antibody '6-11D', specific to both native and ROS-modified CII. 6-11D showed strong binding to all collagen types, which was statistically significantly greater than binding to negative control HEL. (C) ELISA of anti-ROS-CII antibody '3-11E', specific to ROS modified CII. 3-11E showed specific binding to Gly and HOCl CII, but no binding to native CII or HEL. Binding to both Gly CII and HOCl CII is statistically significantly greater than binding to both CII and HEL. Two-way ANOVA was performed with Bonferroni multiple comparisons to compare overall column effect between antigen types. ** P ≤0.01; **** P ≤0.0001. CII, native collagen II; Gly CII, native collagen II modified by non-enzymatic glycation; HOCl CII, native collagen II modified by chlorination.

Figure 18(A) shows the binding capacity of our negative control antibody, namely C7, to both native and ROS-modified CII. The C7 scFv shows no specific binding to either native CII or ROS-modified CII, even at high concentrations. C7 is specific to Hen Egg Lysozyme, and a concentration dependent increase in binding was observed. Figure 18(B) shows the binding capacity of a positive control antibody, namely 6-11D. 6-11D scFv is specific to both native CII and ROS modified CII, and as Figure 18(B) shows, strong binding to all collagen types was observed in a concentration-dependent manner. Figure 18(C) demonstrates the binding of one of the anti-ROS-CII antibodies, namely 3-11E. 3-11E scFv shows strong, specific binding to both modified forms of CII in a concentration dependent manner, but no binding to native CII even at high concentrations.

3.1.4 Antibody Binding in Tissue from a Rheumatoid Arthritis Mouse Model

To further assess the specificity of the anti-ROS-CII antibody, 3-11E, immunofluorescence was conducted using tissue from arthritic mice. In this instance, sections from mice with AIA were used.

Figure 19 shows representative images obtained following immunofluorescence staining. In healthy mouse tissue, there is minimal staining with either 3-11E scFv or C7 scFv. The structure of the cartilage and bone is identifiable by the DAPI stain, and no staining of 3-11E scFv is identifiable in either tissue. Furthermore, the 3-11E scFv stain is comparable to the C7 negative control, confirming that our anti-ROS-CII antibody does not bind to healthy cartilage. In AIA knee tissue, there is strong, pericellular staining within the cartilage by 3-11E scFv. The staining of 3-11E is diffused throughout the cartilage and focused around the chondrocytes, which is not observed in the staining of healthy tissue. Furthermore, the 3-11E scFv staining in arthritic knees is exclusive to the cartilage, with no staining present in the bone tissue. The negative control antibody also showed no binding in the AIA tissue, confirming that the 3-11E scFv binding is specific to damaged cartilage.

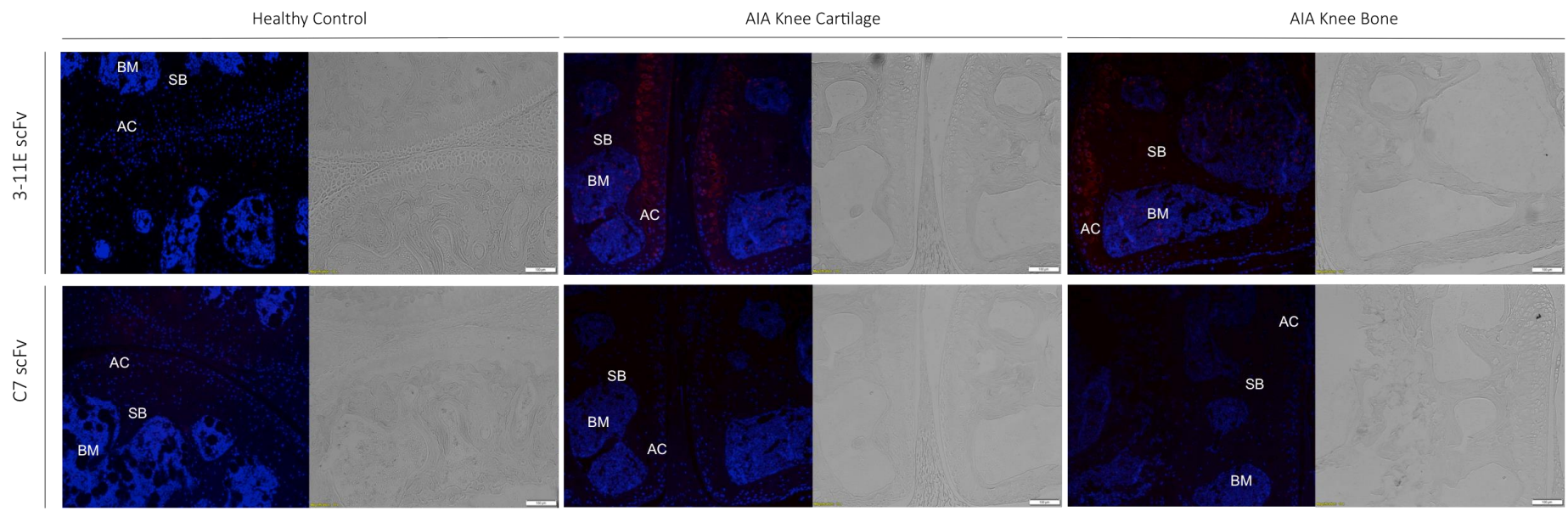

Figure 19. Immunofluorescence staining of AIA knee tissue using anti-ROS-CII fluorescently labelled scFv and fluorescently labelled negative control scFv antibody. Healthy mice knee sections are used as additional controls. Blue = DAPI stain; Red= Cy5.5 labelled antibody. AC = articular cartilage; SB = subchondral bone; BM = bone marrow. Representative images of 3 samples per group.

3.1.5 Antibody Binding in Tissue from an Osteoarthritis Mouse Model

After observing positive, specific binding in AIA tissue, immunofluorescence was repeated in tissue from mice subjected to DMM surgery. Figure 20 shows the representative images of the staining. As previously observed with the AIA immunofluorescence, there is no specific binding of 3-11E scFv or C7 scFv in healthy mouse cartilage.

The DMM tissue used for the immunofluorescence is from mice 8 weeks or 12 weeks post-surgery. In the 8 weeks post-surgery tissue, there is strong staining by 3-11E scFv in the cartilage. Similarly, to binding in the AIA tissue, the staining appears to be around the chondrocytes in the cartilage. There is no evident binding to the tissue of the bone, and the point where the tide mark between cartilage and bone exists is clear due to the specific binding of 3-11E scFv. The C7 scFv negative control shows no specific binding in the 8 weeks post-surgery tissue.

In the tissue taken from 12 weeks post-surgery mice, 3-11E scFv also shows strong binding specific to the cartilage. There is no binding observed in the bone tissue. C7 scFv showed no specific binding in the 12 weeks post-surgery tissue.

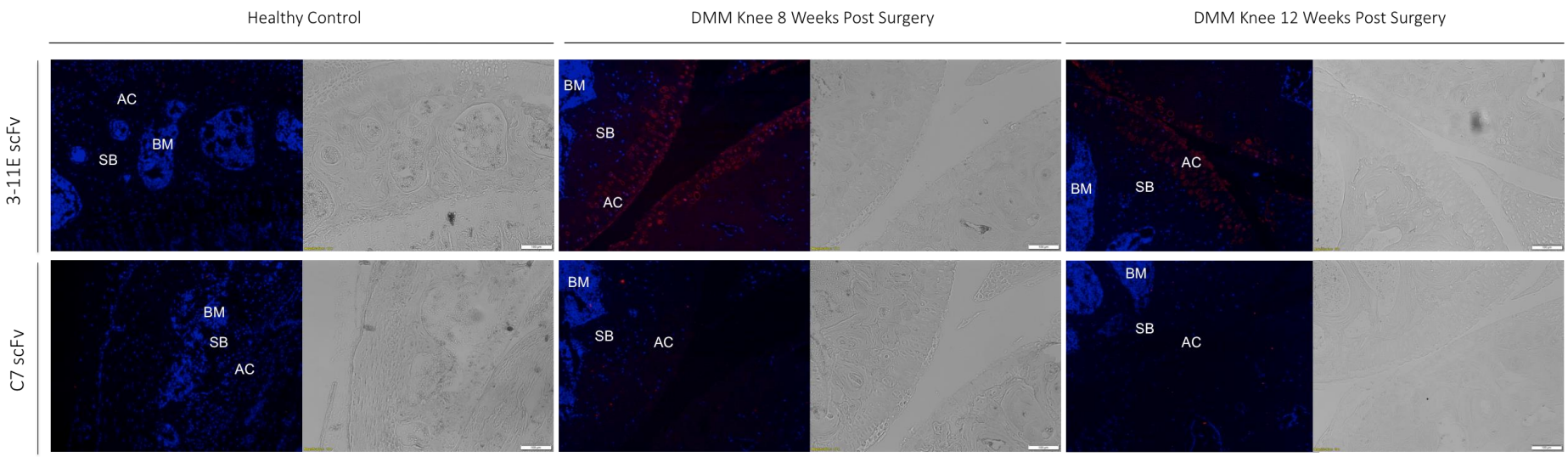

Figure 20. Immunofluorescence staining of DMM knee tissue using anti-ROS-CII fluorescently labelled scFv and fluorescently labelled negative control scFv antibody. Healthy mice knee sections are used as additional controls. Blue = DAPI stain; Red= Cy5.5 labelled antibody. AC = articular cartilage; SB = subchondral bone; BM = bone marrow. Representative images of 3 samples per group.

3.2 Validation of Anti-ROS-CII *In Vivo*

3.2.1 *In vivo* Imaging System Analysis Shows Localisation of Antibodies in Antigen Induced Arthritis Mouse Model

To analyse the localisation of anti-ROS-CII antibodies exclusively to the arthritic joint, optical imaging was utilised to track the fluorescence of the labelled scFv after intravenous administration. An antigen induced arthritis mouse model was used due to the ability to induce inflammation in the right knee, with the contralateral knee acting as an internal control. Figure 21 shows the results of the optical imaging following intravenous administration of scFv antibodies. The 1-11E and 3-11E candidates were used for optical imaging to assess the comparative localisation of the already established 1-11E with the new 3-11E candidate. As described in Table 1, both 1-11E and 3-11E are specific to ROS-CII. C7 is specific to HEL and was used as a negative control in these experiments.

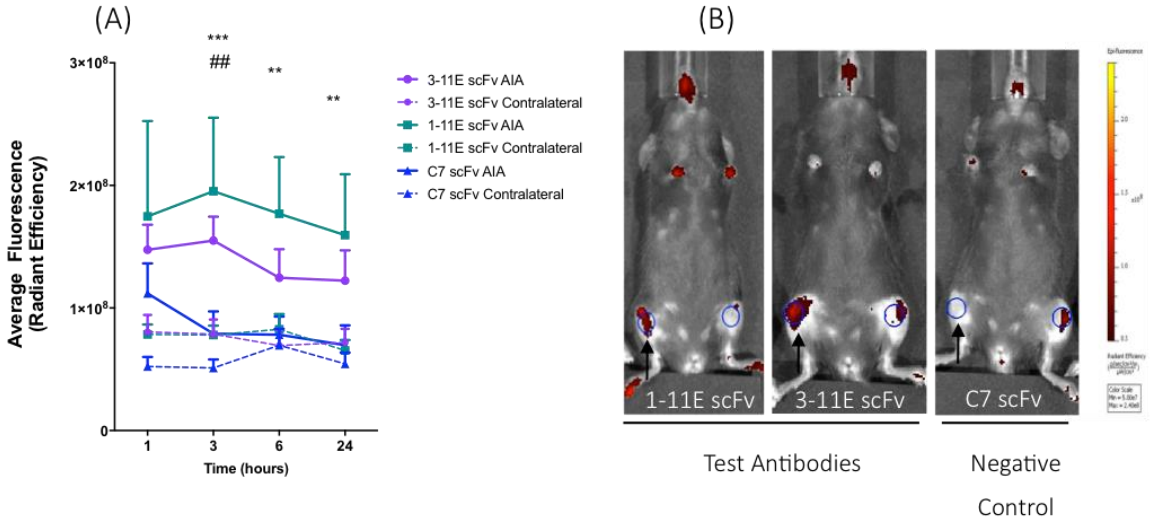

Figure 21. Localisation of anti-ROS-CII antibodies (1-11E scFv, 3-11E scFv) and negative control antibody (C7 scFv) in an antigen induced arthritis mouse model. Fluorescence is calculated using region of interests (blue circles) and plotted as radiant efficiency (A). Representative images from time point 3 of fluorescent localisation of injected antibodies. Arthritis is present exclusively in the right knee as indicated with a black arrow (B) n = 6-8 mice per group. Two-way ANOVA was performed with Tukey multiple comparisons to compare differences in treatment groups at each time point. * denotes statistical significance between 1-11E scFv and C7 scFv; # denotes statistical significance between 3-11E scFv and C7 scFv. ** P ≤0.01; *** P ≤0.001.

Figure 21(A) depicts the fluorescence present in the right knee of AIA mice injected intravenously with scFv. Identical regions of interest were drawn on each knee of mice (depicted as blue circles in Figure 21(B)) to give a quantitative measure of fluorescence. Figure 21(B) shows IVIS images of three mice 2 hours post injection with 1-11E, 3-11E and C7 scFv. For 3-11E and 1-11E scFv there is accumulation of scFv in the arthritic knee, but not the contralateral. The C7 scFv control shows no specific localisation in the arthritic knee. The localisation of the anti-ROS-CII was strong in the arthritic knees, with peak localisation at the 3-hour time point, which coincides with the half-life of the scFv.

Following confirmation of the scFv localisation, optical imaging was performed using the IgG format of each antibody. The IgG format was produced from the scFv clones and is a full-length antibody, with a larger molecular weight and extended half-life. The beneficial

use of an scFv or IgG would vary depending on the nature of an experiment. The IgG format is beneficial as it contains the Fc portion, which has been found to interact with the neonatal Fc receptor, causing the IgG to be recycled and thus having an extended half-life [143], whereas the smaller scFv format has found to have greater penetrative characteristics than the full size antibody [144]. It is important to characterise both formats *in vivo* to assess these abilities and determine which is best used for future studies.

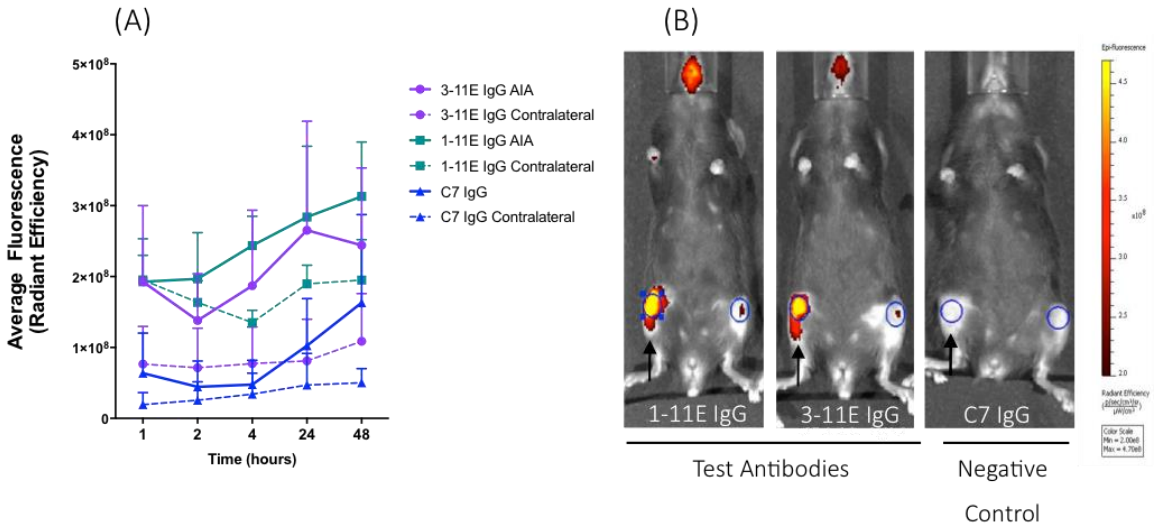

Figure 22. Localisation of anti-ROS-CII antibodies (1-11E IgG, 3-11E IgG) and negative control antibody (C7 IgG) in an antigen induced arthritis mouse model. Fluorescence is calculated using region of interests (blue circles) and plotted as radiant efficiency (A). Representative images from time point 24 of fluorescent localisation of injected antibodies. Arthritis is present exclusively in the right knee as indicated with a black arrow (B). n=3 mice per group. Two-way ANOVA was performed with Bonferroni multiple comparisons to compare differences in treatment groups at each time point (no statistical significance).

Figure 22(B) shows IVIS images of 3 mice 48 hours post injection with 1-11E, 3-11E and C7 IgG. 1-11E and 3-11E show clear localisation in the arthritic knee, however at the 48-hour time point there is an observation of the C7 IgG control in the arthritic knee. From the plot in Figure 22(A), it is evident that the peak of fluorescence has not been reached. The half-life of IgG is around 100 hours, therefore the presence of C7 IgG in the arthritic

knee at 48 hours is likely to be non-specific and due to the high level of antibody in circulation. The low levels of C7 IgG fluorescence at every previous time point and in the contralateral knee is also indicative of this, particularly when comparing to 1-11E and 3-11E IgG where there is a steady increase over time.

Interestingly, the localisation of 3-11E IgG appears more specific than 1-11E IgG. Mice treated with 1-11E IgG showed high fluorescence in the contralateral knee throughout the time course, whereas mice treated with 3-11E IgG had high fluorescence in the AIA knee but very little in the contralateral. This high specificity *in vivo* is further indication that 3-11E makes a good alternative candidate to 1-11E.

The optical imaging performed in the AIA model confirmed the localisation previously observed with the 1-11E antibody [118]. Furthermore, the 3-11E-candidate antibody has shown similar localisation patterns to 1-11E *in vivo.* Together with the *in vitro* data, this validates the use of 3-11E for targeting the arthritic joint.

3.2.2 Targeting of vIL-10 to the Arthritic Joint using Antibodies to Post-Translationally Modified Collagen II

Antibodies against ROS-CII were raised by phage display and fused to vIL-10 via a MMP cleavable linker by previous members of the Nissim Lab. To confirm the localisation of the fusion antibody before use for therapy in future experiments, a study in mice with AIA was performed. The aim of the study was to confirm that the produced anti-ROS-CII scFv fused to vIL-10 could localize to the joint in the same manner that was observed with the scFv and IgG protein alone, as was observed in Figure 21 and Figure 22.

Figure 23 shows the results of the optical imaging localisation study. The quantification of fluorescence in Figure 23(A) shows 3-11E/vIL-10 peak fluorescence at 72 hours post injection, which coincides with the half-life of the protein. The C7/vIL-10 shows no specific localisation in the arthritic knee. Figure 23(B) shows representative images of the optical imaging process 72 hours post injection. The fluorescence of 3-11E/vIL-10 is predominantly in the arthritic knee, with little fluorescence in the contralateral. C7/vIL-10 showed little fluorescence in the arthritic knee, with one mouse showing higher fluorescence as seen in Figure 23(B). Overall, however, the fluorescence of C7/vIL-10 was non-specific and antibody levels were low in the arthritic and contralateral knees.

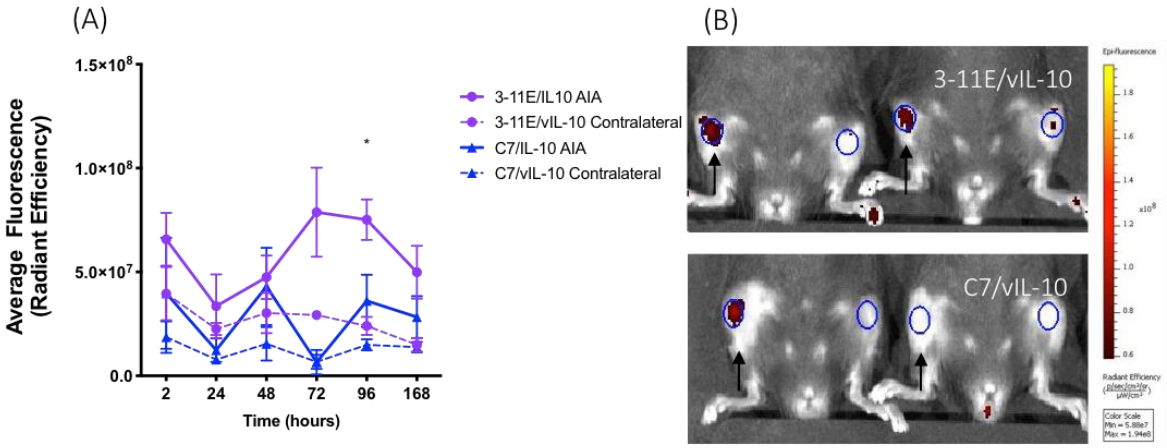

Figure 23. Localisation of anti-ROS-CII antibody fused with vIL-10 (3-11E/vIL-10) and negative control antibody fused to vIL-10 (C7/vIL-10) in an antigen induced arthritis mouse model. Fluorescence is calculated using region of interests (blue circles) and plotted as radiant efficiency (A). Representative images from time point 72 of fluorescent localisation of injected antibodies. Arthritis is present exclusively in the right knee as indicated with a black arrow (B). n=5 mice per group. Two-way ANOVA was performed with Bonferroni multiple comparisons to compare differences in treatment groups at each time point. Statistical significance was observed at 96 hours between 3-11E/vIL-10 AIA knee fluorescence with 3-11E/vIL-10 contralateral knee fluorescence and C7/vIL-10 AIA and contralateral knee fluorescence.* P ≤0.05.

3.2.3 Arthritic Knees Treated with Antibodies to Post-Translationally Modified Collagen II Show Stronger Safranin O Staining and Fewer Cellular Infiltrates

Following the localisation study, knee joints were harvested to assess the effect of the vIL-10 fused to the antibodies on the knee histology. Mice were injected with 3-11E/vIL-10 on day 1 post arthritis induction, with euthanisation and harvesting of knee joints occurring on day 7. Both arthritic and non-arthritic knees were stained with safranin O (to stain proteoglycans) and hematoxylin and eosin (H&E, to stain basophilic and acidophilic structures). Staining was also conducted on healthy control mouse knees. As shown in Figure 24, the c7/vIL-10 treated mice show a loss of safranin O stain in the AIA knee. There are also many cellular infiltrates observed in the joint space in the AIA knee. The contralateral knee of the C7/vIL-10 treated mice shows a stronger safranin O stain, less visible structural damage and few cellular infiltrates. The 3-11E/vIL-10 treated mice show strong safranin O stain in both the AIA knee and contralateral knee. There is evidence of cellular infiltrates in the H&E staining of the 3-11E/vIL-10 mice, but much fewer than the C7/vIL-10 treated mice. The 3-11E contralateral knee shows strong safranin O stain with minimal damage and infiltration.

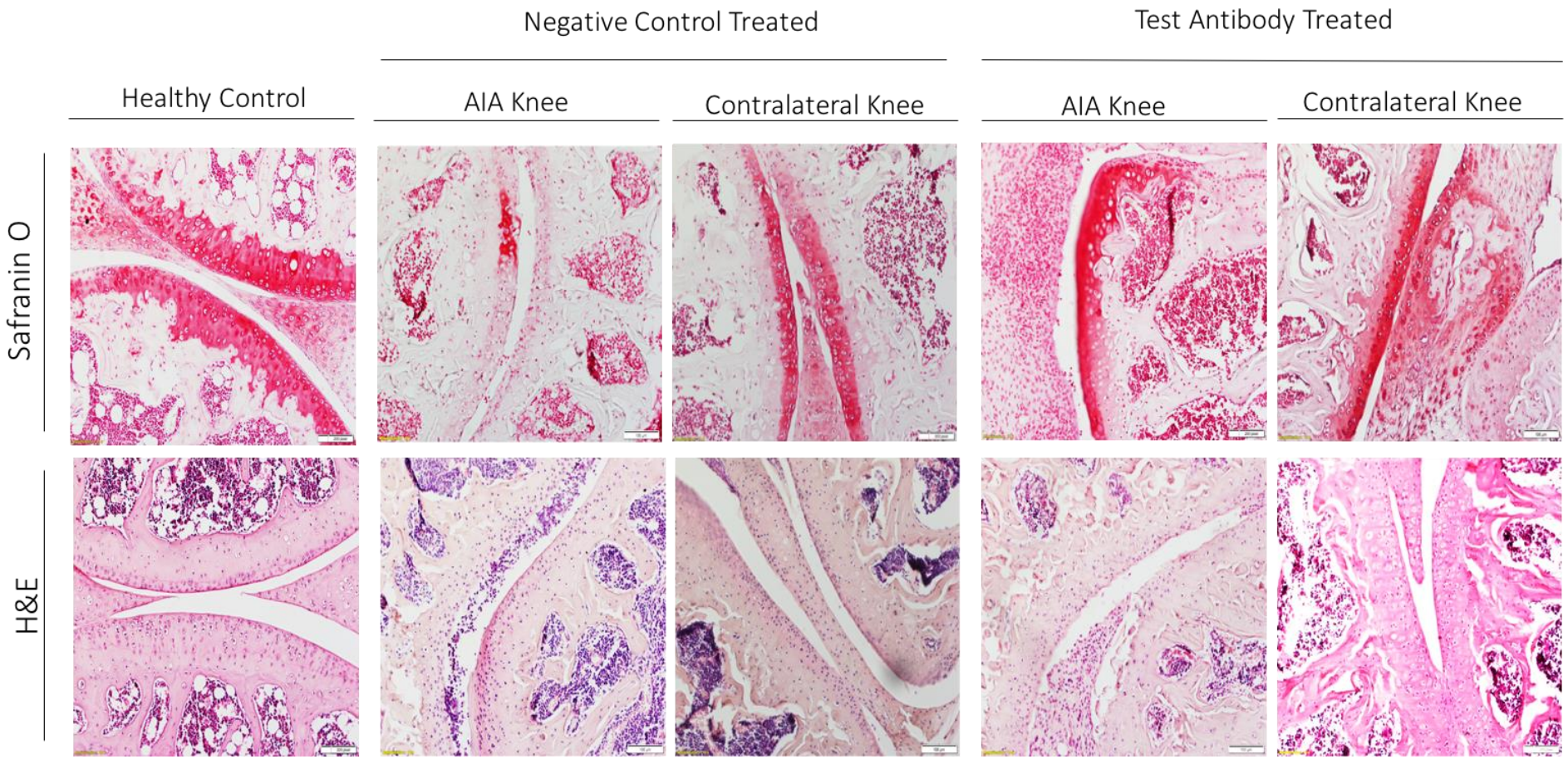

Figure 24. Representative images of histological staining of knees from mice treated with anti-ROS-CII antibody fused with vIL-10 (3-11E/vIL-10) and negative control antibody fused to vIL-10 (C7/vIL-10). Safranin O and Hematoxylin and Eosin (H&E) staining of both AIA knee and contralateral knee of arthritic mice treated with either anti-ROS-CII fused to vIL-10 or negative antibody fused to IL-10. Healthy mice knee sections are used as controls. Images representative of 5 mice per group.

3.2.4 *In vivo* Imaging System Analysis Shows Localisation of Antibodies in Destabilisation of the Medial Meniscus Osteoarthritis Mouse Model

The previous experiments have confirmed that anti-ROS-CII localize in the arthritic joint in a mouse model of RA. Experiments were also conducted using a mouse model of osteoarthritis to determine whether the same localisation occurs. These experiments were conducted primarily for the validation of the new anti-ROS-CII candidate in an OA model for means of future work outside of this thesis. The OA model used was destabilisation of the medial meniscus (DMM), a surgical model in which the medial meniscus in one knee joint is severed, causing mechanically induced osteoarthritis.

Figure 25 depicts the results following intra-articular administration of anti-ROS-CII 3-11E scFv and positive control 6-11D scFv (which binds to both unmodified and modified CII) at 4 weeks post-surgery. As aforementioned, regions of interest were generated to quantify fluorescence, which is depicted Figure 25(A). 6-11D shows strong retention in both DMM and contralateral knees, which is mostly cleared by 128 hours. 3-11E showed strong retention in the DMM knee, similarly to the levels observed for 6-11D. However, 3-11E was not retained in the contralateral knee, observed from the first time point of 2 hours. The ratio of fluorescence in the operated knee and contralateral knee is depicted in Figure 25(B). 6-11D has a low ratio of around 1, representing the equal fluorescence in both the arthritic and non-arthritic knees. 3-11E has a higher ratio, peaking at 54 hours at 7, indicating the greater fluorescence observed in the DMM knee. Figure 25(C) and (D) are images from the optical imaging process of mice 4 hours post injection with 3-11E

scFv and 6-11D scFv, respectively. Mice injected with 3-11E scFv retain antibody in the DMM knee, but minimal fluorescence is observed in the contralateral. Mice injected with 6-11D, however, have strong fluorescence in both the DMM and contralateral knees.

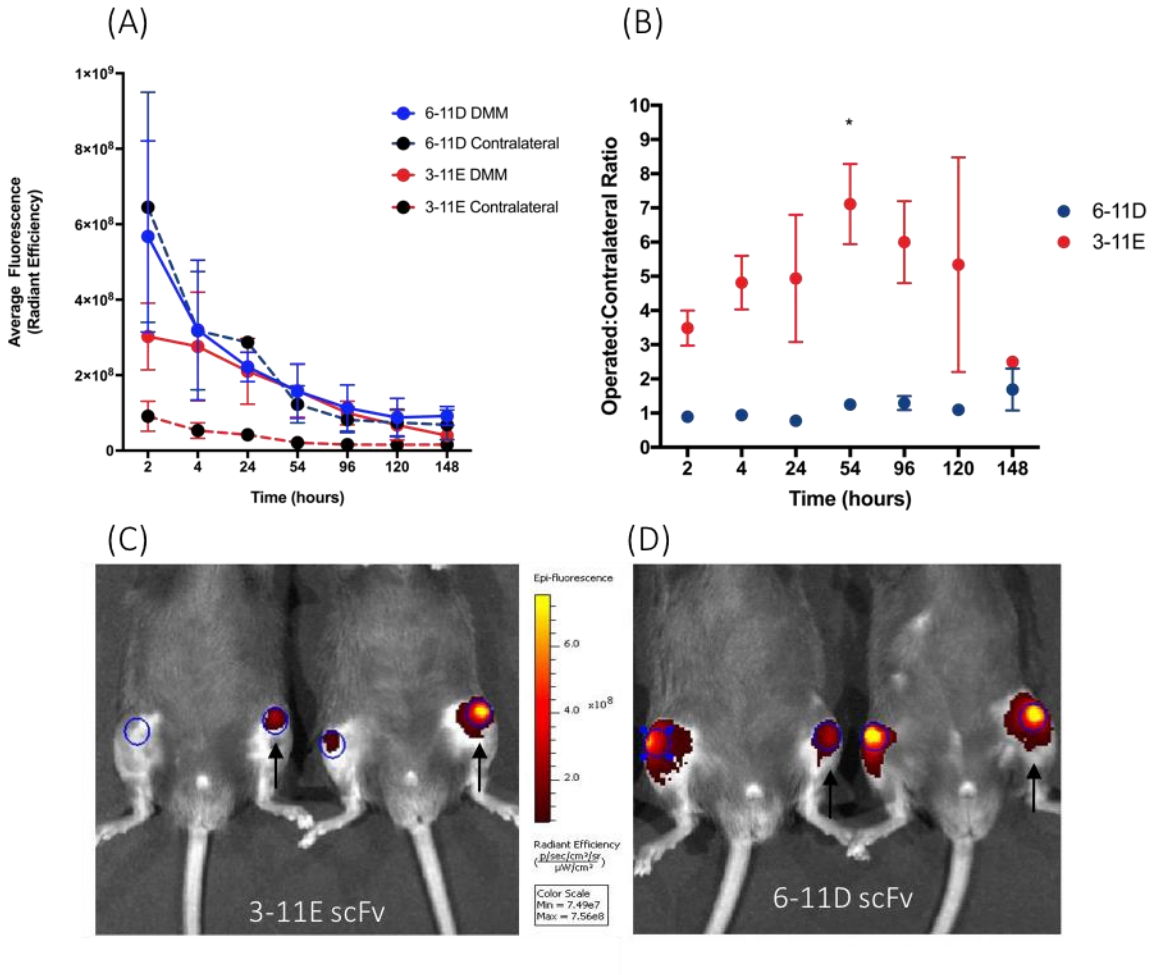

Figure 25. Retention of anti-ROS-CII antibody (3-11E scFv) and positive control antibody (6-11D scFv) in a destabilisation of the medial meniscus osteoarthritis model 4 weeks post-surgery. (A) Knee fluorescence is calculated using region of interests (blue circles) and plotted as radiant efficiency. (B) Ratio of fluorescence in operated versus contralateral knee. Arthritis is present exclusively in the left knee as indicated with a black arrow (C and D). Representative images from time point 54 of fluorescent localisation of injected antibodies. n = 3 mice per group. Two-way ANOVA was performed with Bonferroni multiple comparisons to compare differences in treatment groups at each time point. * P ≤0.05.

The same experiment was repeated at 8 weeks post-surgery and is shown Figure 26. 6-11D shows retention in both the DMM knee and contralateral, however the first time-point shows a weaker retention of 6-11D in the DMM knee compared to the

contralateral. 3-11E scFv continues to show strong retention in the DMM knee, but not in the contralateral. Similarly, to the 4-week time point, by 128 hours most of the antibody has been cleared from the joint. The ratio between the operated and contralateral knees is low for the 6-11D control, staying around 1. The ratio for the 3-11E scFv is greater, peaking at the 4-hour time point at a value of 3. The ratio observed for 3-11E scFv in the 4-week experiment was larger and peaked later than the 8-week experiment. Figure 26(C) and (D) are images from the optical imaging process of mice 24 hours post injection with 3-11E scFv and 6-11D scFv, respectively. Mice injected with 3-11E scFv retain antibody in the DMM knee, but minimal fluorescence is observed in the contralateral. Mice injected with 6-11D, however, have equal fluorescence in both the DMM and contralateral knees.

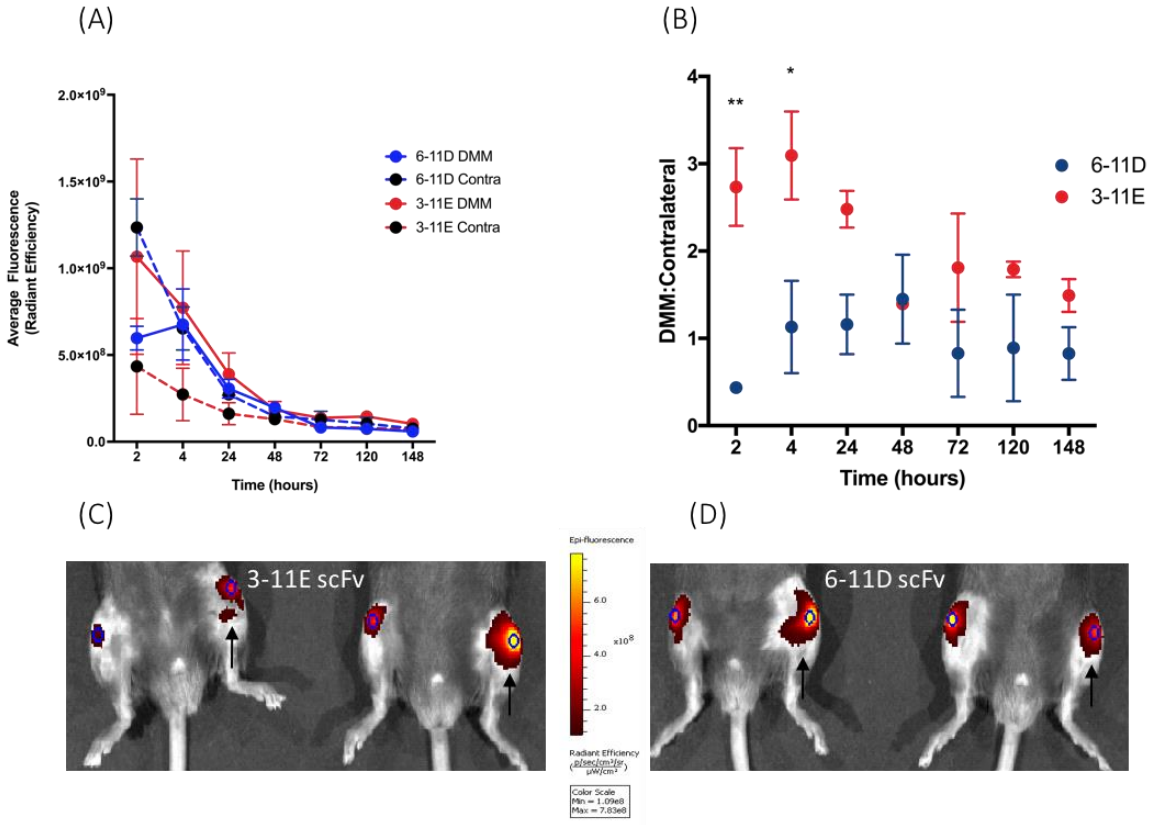

Figure 26. Retention of anti-ROS-CII antibody (3-11E scFv) and positive control antibody (6-11D scFv) in a destabilization of the medial meniscus osteoarthritis model 8 weeks post-surgery. (A) Knee fluorescence is calculated using region of interests (blue circles) and plotted as radiant efficiency. (B) Ratio of fluorescence in operated versus contralateral knee. Arthritis is present exclusively in the left knee as indicated with a black arrow (C and D). Representative images from time point 4 of fluorescent localisation of injected antibodies. n=3 mice per group. Two-way ANOVA was performed with Bonferroni multiple comparisons to compare differences in treatment groups at each time point. * P ≤0.05; ** P ≤0.01.

The work in this thesis thus far has demonstrated the ability of the 3-11E antibody candidate to target the arthritic joint in both RA and OA murine models. The 3-11E antibody is sufficient for use in future studies in place of the 1-11E antibody, which cannot be expressed efficiently due to problems associated with glycosylation of the binding site. The anti-ROS-CII antibodies have previously shown to target drugs to the joint, but in the following chapters the antibodies will be utilized to target a biological scaffold to the joint for the first time. The biological scaffold used will be microvesicles derived from neutrophils.

3.3 Fortifying Neutrophil Derived Microvesicles with Anti-ROS-CII

Microvesicles (MV) derived from neutrophils (PMN) have been previously shown to exert anti-inflammatory, pro-resolving and penetrative mechanisms in arthritic cartilage. Efficacy of MV has only been demonstrated by local administration in the arthritic knee, with systemic administration having no effect on clinical scoring [136,141]. To overcome this, MV have been enriched with anti-ROS-CII antibodies to localise and retain them to the arthritic joint, where they can exert their beneficial effects. As will be shown in this chapter, MV have been isolated from healthy donor neutrophils and characterised *in vitro*. MV have then been enriched with antibodies using aqueous energy dissemination; a technique that has previously been utilised to enrich MV with additional pro-resolving mediators and proteins.

3.3.1 Microvesicle Generation Analysis by Flow Cytometry and Nanoparticle Tracking

To confirm the purity of isolated microvesicles from PMN, characterization by flow cytometry and nanoparticle tracking analysis was performed. The Imagestream^X (IS^x) analyser was used for MV analysis due to its high sensitivity and part high-resolution microscope, allowing you to observe all the events passing through. Furthermore, the IS^x can calculate concentration of MV without the use of calibration beads.

Figure 27 shows flow cytometric plots and microscopic images obtained from IS^x analysis of isolated PMN MV labelled with BODIPY FL, which is a non-specific membrane stain. Figure 27(A) shows the isolated MV population (blue) plotted as side scatter against the fluorescence of BODIPY. The MV population show low side scatter and high fluorescence intensity. The population circled in red represent the speed beads that run through the IS^x for calibration of the flow of the sample and the focus of the microscope. The population circled in yellow represents background noise of the machine. Figure 27(B) represents the gated MV population, plotted as MV fluorescence against Cy5 fluorescence. The MV stained with BODIPY FL show negligible Cy5 fluorescence, which was important to determine before moving onto fortifying with antibody. Figure 27(C) is a representative microscopic image from the IS^x analysis of the gated MV population. The microscope on the IS^x allows for visual confirmation of correct MV gating. Figure 27(C) shows the expected visualization of the population following a successful isolation of MV. The MV are barely visible on the brightfield channels, represented as CH01 and CH09 in the figure. The BODIPY fluorescence, shown in CH02 on the figure, shows a bright green, round, small MV. The Cy5 fluorescence, observed in CH09 is negative. The side scatter of the MV, shown in CH12 is low and almost non-detectable.

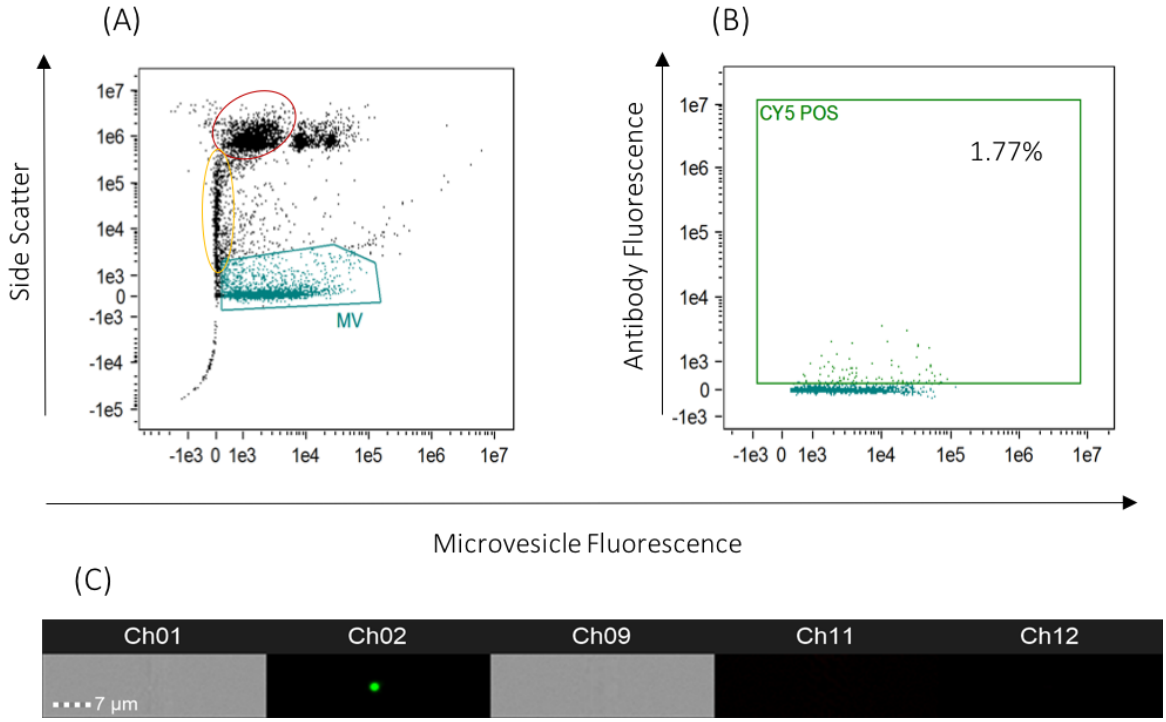

Figure 27. Imagestream^x analysis of polymorphonuclear neutrophil derived microvesicles stained with BODIPY. (A) Vesicle gating (blue) using side scatter and BODIPY fluorescence. Red circle represents speed beads used to calibrate the machine and yellow circle represents noise from the machine. (B) Cy5 positivity of MV. Gating of cy5 positivity is conducted for future experiments of fortifying MV with antibody. (C) Representative microscopic image of a gated MV obtained from the Imagestream^x during analysis.

Isolated MV were also run on the Nanosight nanoparticle tracker to confirm size and concentration. Figure 28(A) is a plot representing the different sizes within the population and the concentrations at which they arise. From this representative plot, we can see most of the population is around 116 nm, with additional vesicles at 167nm, 235nm, 312nm and 596nm. The background of the plot shows an image taken from the nanoparticle analysis, with each particle being tracked individually by a red dot. Figure 28(B) shows a scatter plot of every particle passed through the analyser. As evident from the plot, the population diameter is most abundant from the 50-250nm range, with the largest event sizing at around 600nm. Figure 28(C) represents a cumulative plot of the percentile of the population plotted against the size in nm. From the plot, we can confirm

that 100% of our population is 600nm or less. Furthermore, we can confirm that a very small proportion of the population is less than 100nm.

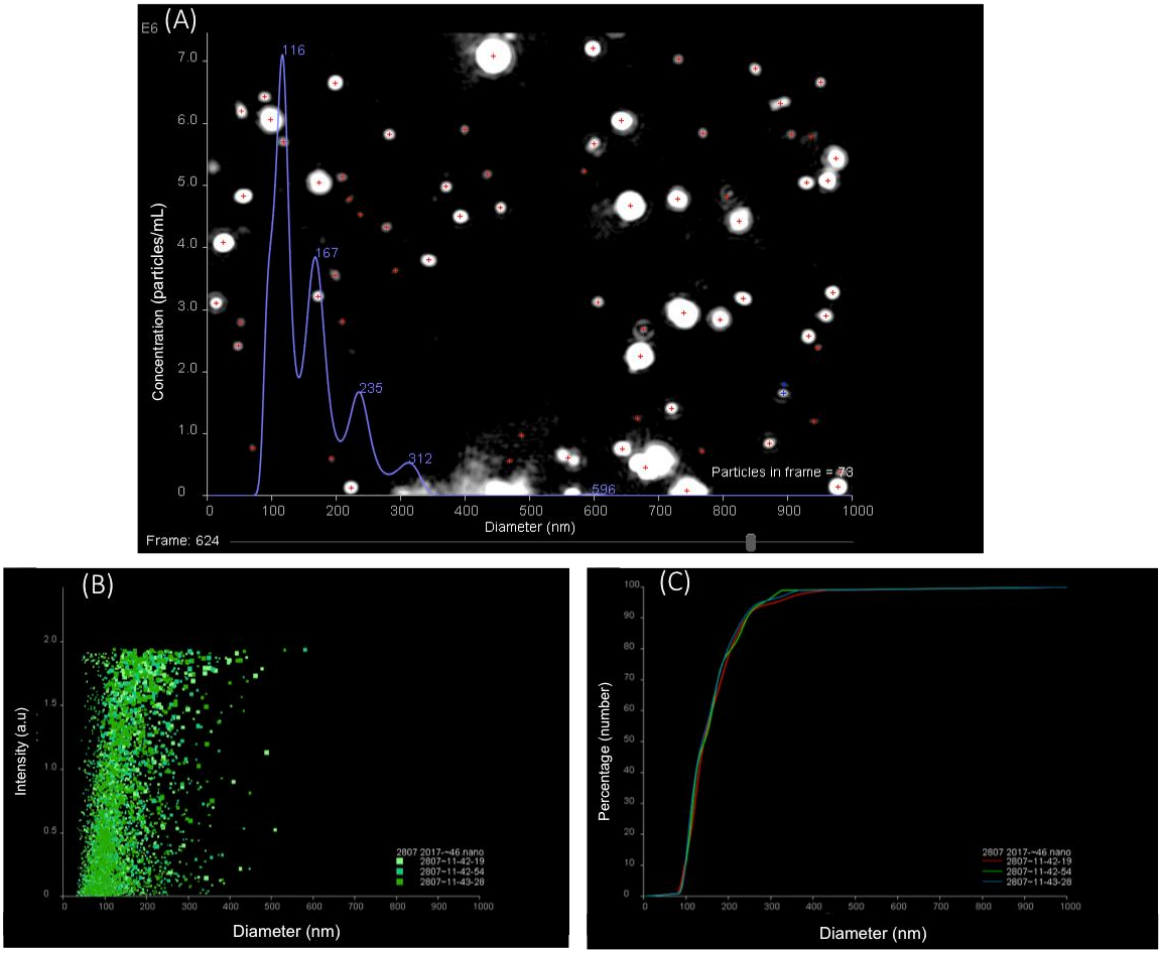

Figure 28. Nanoparticle Tracker analysis of isolated microvesicles. (A) Plot showing the distribution of size in nm against concentration of the isolated sample. (B) Scatter plot showing the size and intensity of all events run through the analyser. (C) Cumulative plot showing the percentile of the population and size in nm.

3.3.2 Double Positive Events for Microvesicle and Antibody Following Aqueous Energy Dissemination

To attempt to present anti-ROS-CII antibodies upon the surface of PMN MV, aqueous energy dissemination was performed in the presence of liposome forming phospholipid.

This technique has been used previously to enrich microvesicles with protein and lipid mediators, but never attempted with antibodies [139,140]. Aqueous energy dissemination uses sonication to form small, nano-sized liposomes. These nano-sized liposomes entrap the antibody upon formation. Simultaneously, the energy provided from the sonication causes fluidity of the microvesicle membrane, allowing liposomes (with antibody entrapped) to incorporate and fuse with the membrane.

A comparison study was first performed to assess the optimal conditions for enrichment and to assess whether sonication is necessary to have the desired effect. Figure 29 depicts a representative replicate of MV resuspended (A and C) or vortexed (B and D) with phospholipid and anti-ROS-CII scFv. MV manually resuspended in phospholipid with anti-ROS-CII shows incorporation of antibody on 48% of the population (Figure 29(A)). As seen in Figure 29(C), the double positive population are visible on the brightfield microscope (CH01 and CH09), have strong BODIPY fluorescence (CH02), show positive antibody fluorescence (CH11) and have a visible side scatter (CH12). MV that were vortexed in phospholipid with anti-ROS-CII shows incorporation of antibody on 5.6% of the population, lower than that of the manually resuspended (Figure 29(B)). The events of the double positive population, seen in Figure 29(D), are like that of the manually resuspended. They are visible by brightfield (CH01 and CH09), show fluorescence of MV and antibody (CH02 and CH09, respectively) but have a larger side scatter (CH12).

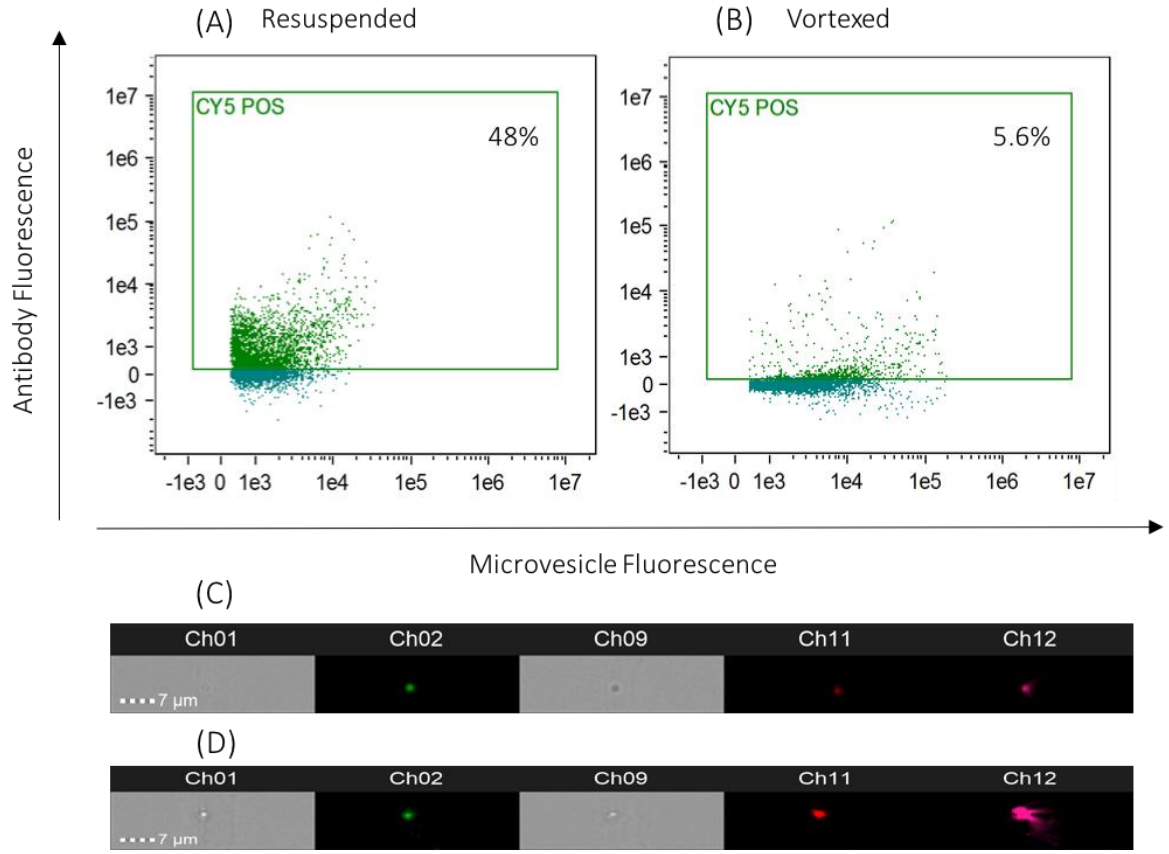

Figure 29. Imagestream^x analysis of polymorphonuclear neutrophil derived microvesicles enriched with anti-ROS-CII. (A) MV were incubated with anti-ROS-CII and liposome forming phospholipid and resuspended with a pipette for 5 minutes. (B) MV were incubated with anti-ROS-CII and liposome forming phospholipid and vortexed for 5 minutes. (C) Representative microscopic image of resuspended MV plus anti-ROS-CII. (D) Representative microscopic image of vortexed MV plus anti-ROS-CII. Ch01 & Ch09: brightfield; Ch02: MV fluorescence; Ch11: antibody fluorescence; Ch12: side scatter. n = 4 replicates.

A representative replicate of MV sonicated in phospholipid with anti-ROS-CII scFv are shown in Figure 30. Three sonication conditions were used: (i) 5 minutes' sonication at 1 amplitude micron (Figure 30(A)); (ii) 5 minutes' sonication at 3 amplitude microns (Figure 30(B)) and (iii) 10 minutes' sonication at 3 amplitude microns (Figure 30(C)). The first condition resulted in an incorporation of 20%, the second an incorporation of 68% and the third 38%. From the microscopic images, there are differences observed between the conditions. The first condition shows a less rounded fluorescence of the vesicle (CH02, Figure 30(D)) and a large side scatter (CH12, Figure 30(D)). The second condition showed a larger size as seen in the vesicle fluorescence (CH02) and antibody fluorescence (CH11)

of Figure 30(E). The side scatter of the second condition is reduced compared to the first, and the shape of the vesicle is rounder. The third condition results in what looks more like a regular vesicle (CH02, Figure 30(F)), with the exception that it is also positive for the antibody fluorescence (CH11, Figure 30(F)). The side scatter is significantly reduced also, resembling that of the vesicle alone population (CH12, Figure 30(F)).

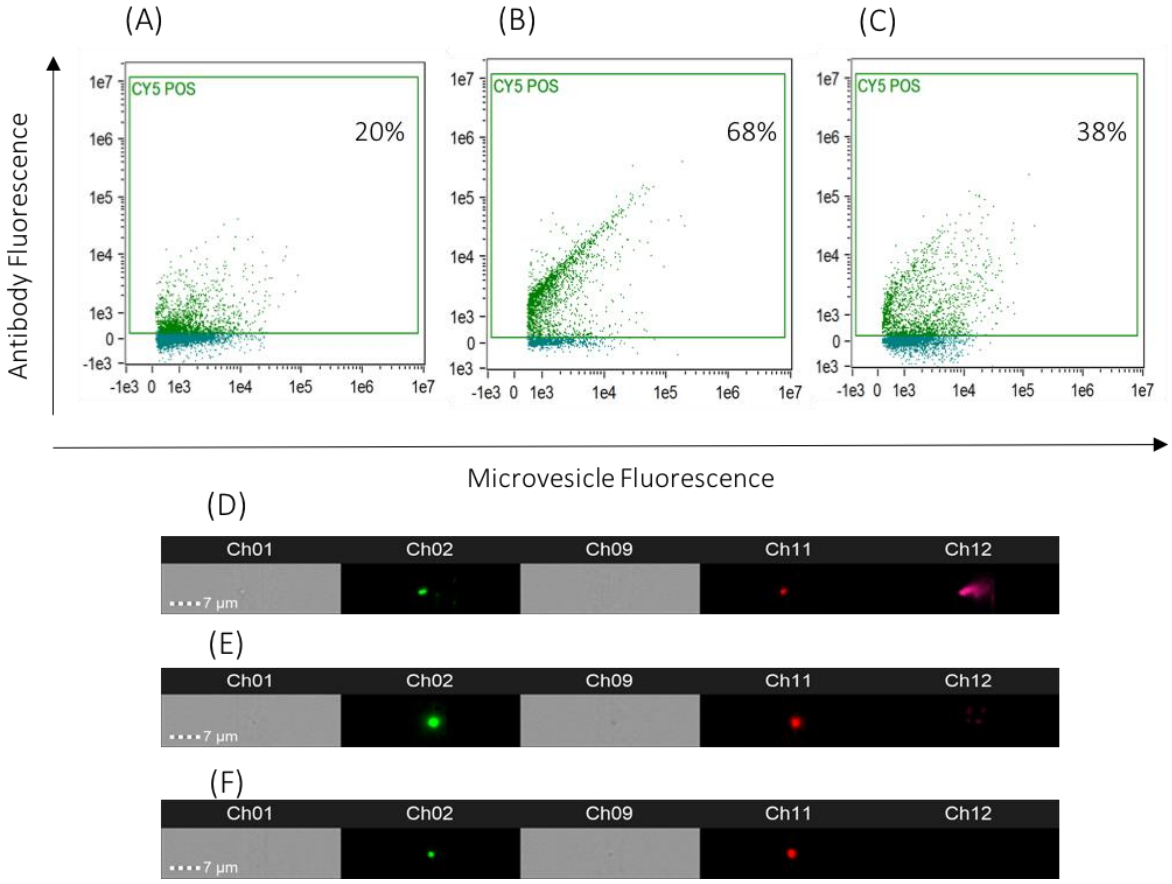

Figure 30. Imagestream^x analysis of polymorphonuclear neutrophil derived microvesicles enriched with anti-ROS-CII. (A) MV were incubated with anti-ROS-CII and liposome forming phospholipid and sonicated for 5 minutes at 1 amplitude microns. (B) MV were incubated with anti-ROS-CII and liposome forming phospholipid and sonicated for 5 minutes at 3 amplitude microns. (C) MV were incubated with anti-ROS-CII and liposome forming phospholipid and sonicated for 10 minutes at 3 amplitude microns. (D) Representative microscopic image of MV plus anti-ROS-CII sonicated for 5 minutes at 1 amplitude micron. (E) Representative microscopic image of MV plus anti-ROS-CII sonicated for 5 minutes at 3 amplitude microns. (F) Representative microscopic image of MV plus anti-ROS-CII sonicated for 10 minutes at 3 amplitude microns. Ch01 & Ch09: brightfield; Ch02: MV fluorescence; Ch11: antibody fluorescence; Ch12: side scatter. n = 4 replicates.

3.4 Antibodies Incorporated onto Microvesicles Can Still Bind to Its Target

3.4.1 Enzyme Linked Immunosorbent Assay

Analysis of incorporation by IS^x showed double positive events, indicating that incorporation was successful. The percentage of incorporation varied under the differing conditions. The successful incorporation of anti-ROS-CII upon PMN MV is redundant if the antibody does not retain its binding properties. To assess whether the antibody is still functional, an ELISA was conducted using the MV fortified with anti-ROS-CII. The ELISA antigen was the same as when testing the production of the antibody. Before testing by ELISA, the MV incorporated with anti-ROS-CII (all conditions) were pelleted at 20,000*g* for 30 minutes to remove any unbound, free anti-ROS-CII. The pellet was resuspended in the same volume of PBS^{--} and both the resuspended pellet and supernatant was tested on ELISA to determine the activity of the antibody. In the glycated ELISA (Figure 31(A)), the resuspended condition showed activity in the resuspended pellet (R Pellet), with less reactivity in the supernatant (R Sup). The vortexed condition showed very similar reactivity (V Pellet and V Sup). Of the sonication conditions, sonication one showed nearly equal reactivity between the pellet and supernatant (S1 Pellet and S1 Sup), similarly to sonication condition 2 (S2 Pellet and S2 Sup). Sonication condition number three showed very low activity in the pellet (S3 Pellet), with more activity in the supernatant (S3 Sup). The activity of sonication condition 3 overall, however, was much lower than all other conditions.

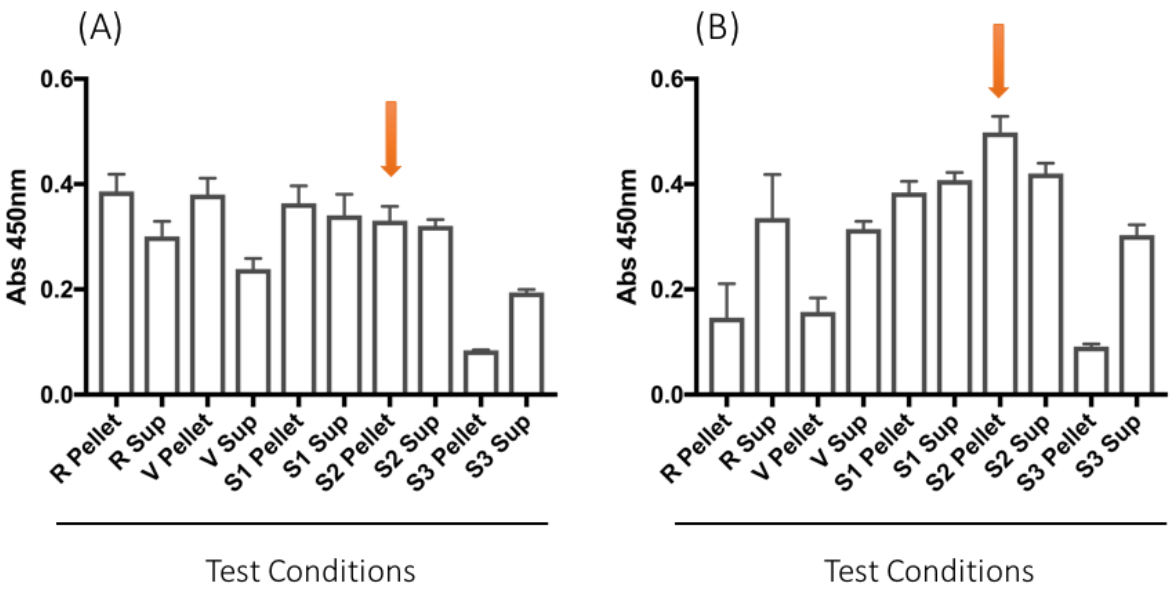

Figure 31. ELISA of microvesicles fortified with anti-ROS-CII. (A) ELISA using glycated CII as antigen. (B) ELISA using HOCl modified CII as antigen. Microvesicles were pelleted to remove free antibody. Both the resuspended pellet and supernatant of each condition was tested by ELISA. Based on the flow cytometric incorporation data and the antibody activity on the MV data, sonication condition 2 was decided to be the best for enriching MV with anti-ROS-CII (indicated with red arrows). R, resuspended condition; V, vortexed condition; S1, sonication condition 1; S2, sonication condition 2; S3, sonication condition 3; Pellet, Resuspended MV pellet; Sup, supernatant. n = 3 replicates.

Figure 31(B) represents the same samples run using the HOCl CII as the antigen in the ELISA. Interestingly, the activity differs slightly than the Glycated CII ELISA. Resuspension and vortexing conditions have much more activity in the supernatant than in the pellet. Sonication condition 1 has equal activity between the pellet and supernatant, like the Glycated CII ELISA. Sonication condition 2 showed greater activity in the pellet than in the supernatant. Similarly, to the Glycated CII ELISA, sonication condition 3 has very low antibody activity in the pellet, with more in the supernatant. Also, similarly, the sonication condition 3 has an overall lower activity than the other conditions.

Based on the flow cytometric incorporation data and the antibody activity on the MV data, sonication condition 2 was decided to be the best for enriching MV with anti-ROS-

CII (indicated with red arrows in Figure 31). Sonication condition 2 saw the greatest percentage of incorporation, ranging throughout repeated experiments from 60-80%. Furthermore, the antibody activity on MV that have been incorporated through sonication condition 2 showed stronger activity than the supernatants and all other conditions. This confirms the incorporation data and that sonication condition 2 is the best option. Sonication condition 2 will be used throughout for antibody incorporation onto MV.

3.4.2 Immunofluorescence

To try and visualize the incorporation of anti-ROS-CII on MV, as well as confirm the ability of enriched MV to bind to arthritic tissue, immunofluorescence was conducted using the MV enriched with anti-ROS-CII as a primary antibody. The immunofluorescence was conducted on two types of arthritic tissue as previously described: AIA and DMM mouse model tissue.

Figure 32 shows the immunofluorescence on AIA tissue. In the 3-11E scFv control we see strong pericellular staining, characteristic of the anti-ROS-CII antibody. Using the MV alone as a 'primary antibody' does not result in strong staining, although MV are detectable in the cartilage, as shown by white arrows. The 3-11E/Microvesicles showed much stronger MV staining within the cartilage. Interestingly, however, there is little co-localisation of antibody and MV visible in the slide. The amount of antibody used in the MV preparation is lower than the antibody alone control, so a reduced fluorescence of antibody compared to control is expected. The lack of co-localisation may be due to the separation of MV from anti-ROS-CII after retention in the mouse tissue, although this wasn't further investigated. Slides stained using C7/Microvesicle as a 'primary antibody' showed little fluorescence of either antibody or MV, indicating that the retention of MV observed in the 3-11E/MV treated sample is due to the specificity of 3-11E to ROS-CII.

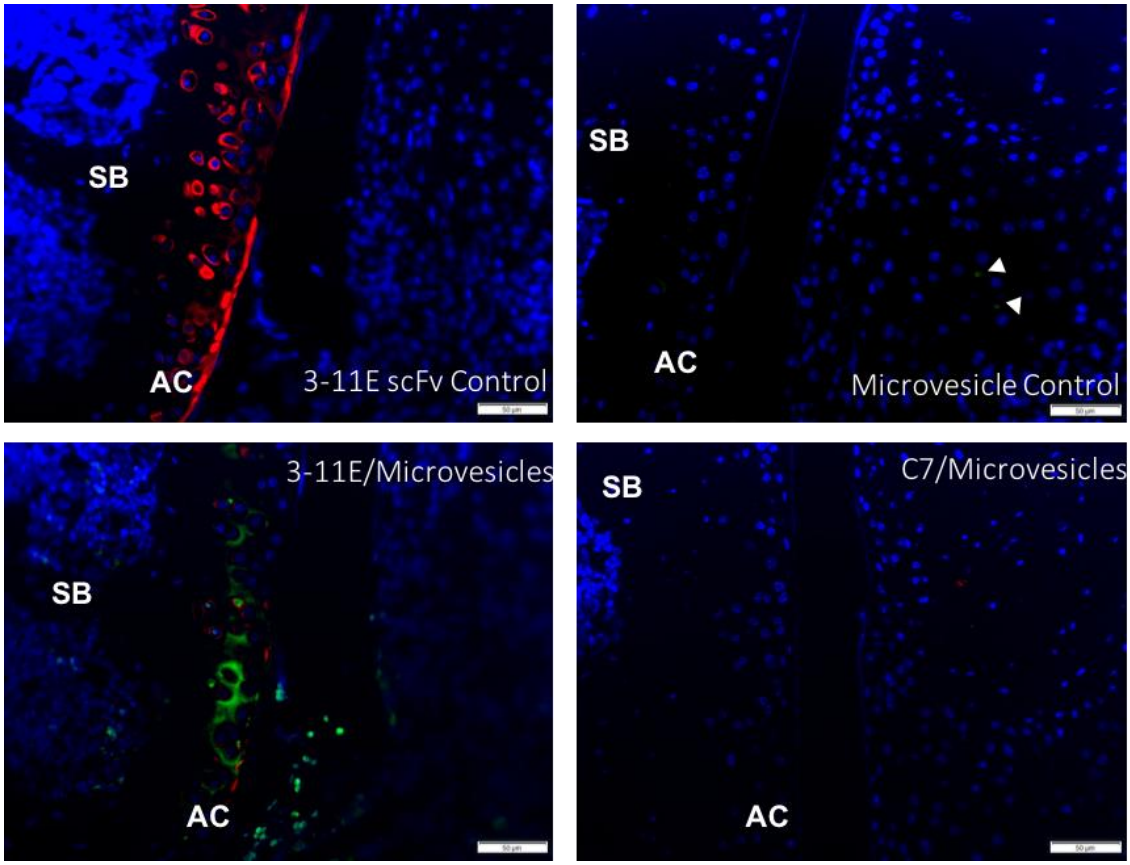

Figure 32. Immunofluorescence staining using microvesicles enriched with antibodies on rheumatoid arthritis mouse model tissue. Sections were cut from paraffin embedded AIA knees and were immunofluorescently stained using scFv antibody alone, microvesicle alone or scFv enriched microvesicles. Blue= DAPI stain, Red= Cy5.5 labelled antibody, Green= BODIPY labelled microvesicles. AC = articular cartilage; SB = subchondral bone. Data representative of 3 samples per group.

The immunofluorescence using DMM tissue showed similar results to the AIA tissue, as seen in Figure 33. The 3-11E scFv control showed a strong staining specifically to the cartilage, as expected. The MV alone slide showed the presence of some staining in the cartilage, as shown by white arrow heads. The 3-11E/Microvesicles treated slide showed greater green MV fluorescence in the cartilage, with the antibody stain also detectable still. Once again, there is little co-localisation observed. The negative control C7/Microvesicles showed little fluorescence of either antibody or MV.

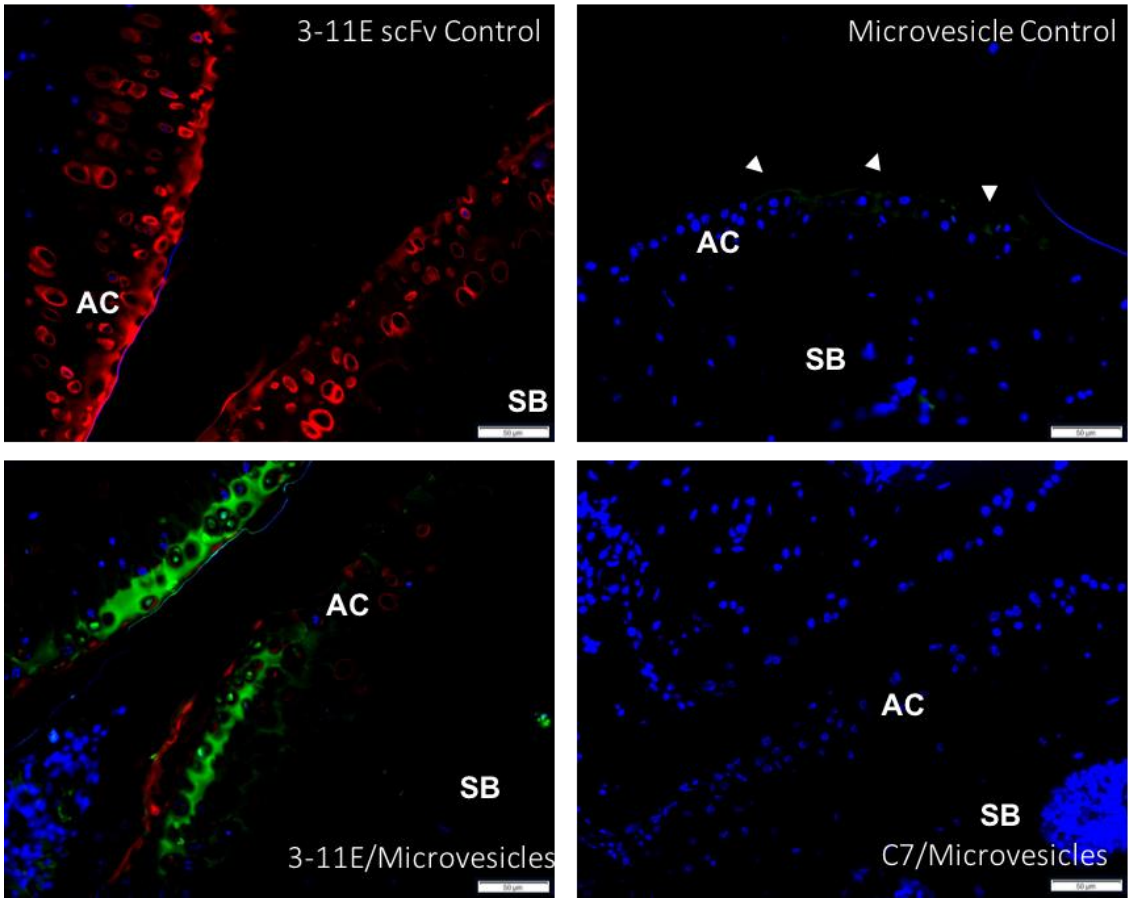

Figure 33. Immunofluorescence staining using microvesicles enriched with antibodies on osteoarthritis mouse model tissue. Sections were cut from paraffin embedded DMM knees and were immunofluorescently stained using scFv antibody alone, microvesicle alone or scFv enriched microvesicles. Blue= DAPI stain, Red= Cy5.5 labelled antibody, Green= BODIPY labelled microvesicles. AC = articular cartilage; SB = subchondral bone.

The immunofluorescence alongside the flow cytometry and ELISA data (Figure 31, Figure 32 and Figure 33) indicated that anti-ROS-CII can be used to retain MV to arthritic tissue. Following validation of reactivity *in vitro*, we attempted to systemically deliver MV into arthritic mice.

3.5 Microvesicles Fortified with Anti-Post-Translationally Modified Collagen II Antibodies Localise in Arthritic Joints

Before imaging commenced using the MV enriched with anti-ROS-CII, tweaks had to be adapted for use in the *in vivo* imaging system (IVIS) used for experiments. BODIPY FL is a fluorophore used under a 488nm laser, with a maximum excitation of 503nm and maximum emission of 512nm. When imaging mice by optical imaging, it is important to use fluorophores as near infrared as possible to avoid problems with autofluorescence. Fluorophores under the 488nm laser would result in a great amount of autofluorescence, so a switch from BODIPY FL to BODIPY Texas Red was necessary. The excitation and emission of BODIPY Texas Red is 580nm and 620nm, respectively.

Because the spectrum of Texas Red is close to Cy5.5 (excitation and emission 660nm and 710nm, respectively), a simple experiment was set up to ensure there was no spill over between the fluorophores. Figure 34 shows the results of the experiment, in which serial dilutions of MV and antibody were imaged in eppendorfs until saturation to assess whether a spill-over would occur. Figure 34(A) shows the imaging under the Texas Red scan. The image on the left shows the fluorescence of MV in serial dilution (MV1 being fully concentrated down to MV4 at a lower concentration). The high 10 second scan saturated the MV1 eppendorf. No fluorescence was observed for any of the antibody eppendorfs. The graph shows the quantified fluorescence, obtained by drawing regions of interest. Figure 34(B) depicts the imaging under the Cy5.5 scan. The image shows the strong fluorescence of the 3-11E scFv antibody in serial dilution (scFv1 fully concentrated down to scFv4 at lower concentration). A 10 second scan was performed which saturated

the scFv1 eppendorf, and again no fluorescence spill over was detected as seen in the MV eppendorfs. The graph depicts the quantified fluorescence, and is a mirror image of the graph in Figure 34(A).

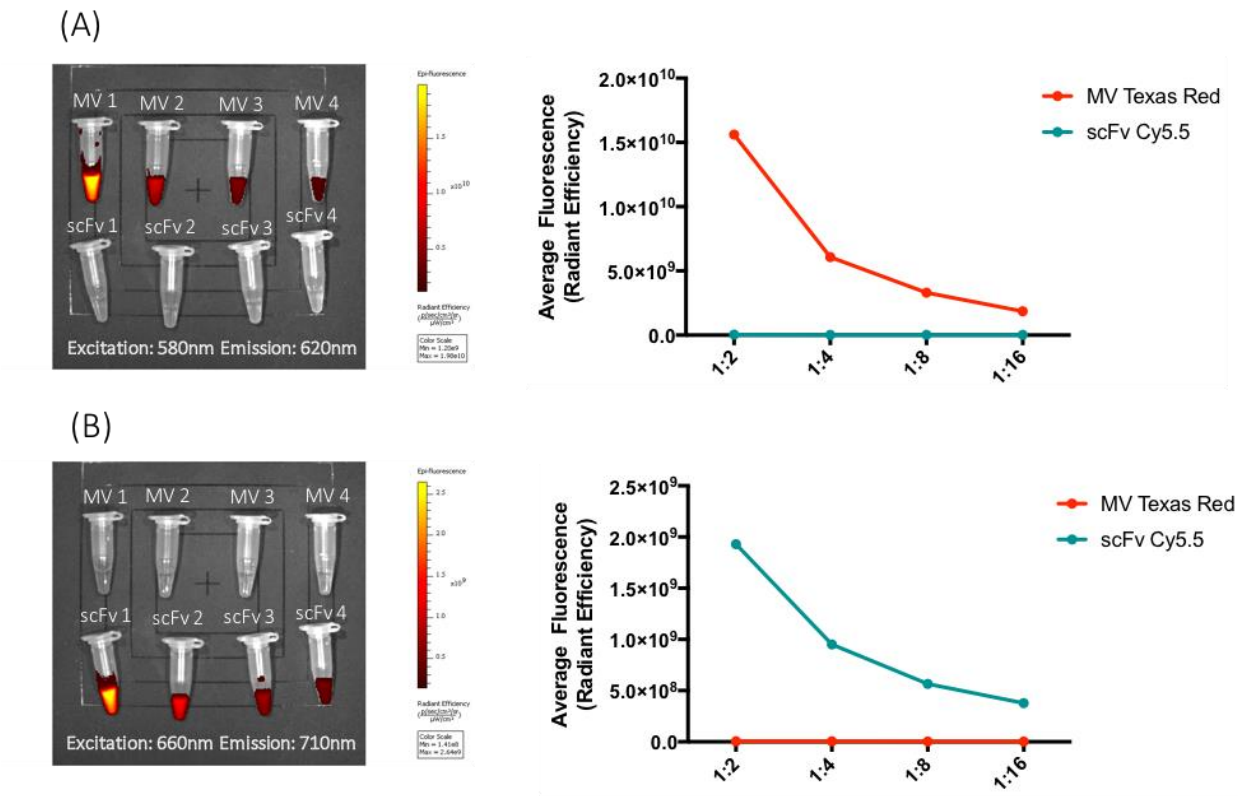

Figure 34. In vivo imaging system scans of serial dilutions of microvesicles stained with Texas Red BODIPY and antibody stained with Cy5.5. Both microvesicles and antibody were imaged under the Texas Red scan at serial dilutions of 1:2, 1:4, 1:8 and 1:16. (excitation 580nm, emission 620nm, panel A) and Cy5.5 scan (excitation 660nm, emission 710nm, panel B) to determine spill-over of fluorophores.

3.5.1 *In Vivo* Imaging System Analysis of Localisation of Microvesicles Enriched with Anti-ROS-CII in Antigen Induced Arthritis

After confirming the absence of spill over between Texas Red and Cy5.5 fluorophores, the microvesicles enriched with anti-ROS-CII were administered intravenously and tracked in AIA mice. All *in vivo* work conducted from this point were conducted in the inflammatory arthritis model antigen induced arthritis. Mice were imaged by IVIS, scanned under both the Texas Red and Cy5.5 settings.

Figure 35 shows the results of the *in vivo* localisation study of MV fortified with 3-11E scFv or C7 scFv (negative control antibody). Mice were injected intravenously 24 hours (day 1) after inducing arthritis. (A) and (B) are graphs representing the Texas Red scans, whereas (C) and (D) represent the Cy5.5 scans. Figure 35(A) shows the vesicle fluorescence of 3-11E/MV and C7/MV in the AIA and contralateral knees of mice. Mice injected with 3-11E/MV show more fluorescence in the AIA knee, peaking at 18 hours post injection. The contralateral knee of both 3-11E/MV and C7/MV show low MV fluorescence. The C7/MV injected mice have a slightly higher fluorescence in the AIA knee than the contralateral, but with no specific peak. Mice injected with MV alone show high fluorescence in the arthritic knee in the first time point, which is quickly diminished over the time course of the experiment. Figure 35(B) is a representation of the ratio between the vesicle fluorescence in the AIA knee and fluorescence in the contralateral knee. At 3 hours post injection, there is little difference between the mice injected with 3-11E/MV and C7/MV, but at the 18-hour time point there is an increase in the ratio in mice injected with 3-11E/MV, of around 3.5. This indicates there is a localisation of 3-

11E/MV in the arthritic knees of mice. The C7/MV group ratio decreases at the 18-hour time point to 1, where it remains for the continuation of the time points. Figure 35(C) represents the antibody fluorescence of 3-11E/MV and C7/MV in the AIA and contralateral knees of mice. Like the vesicle fluorescence, the contralateral knees show little fluorescence at every time point. The C7/MV fluorescence in the AIA knee is lower than the vesicle fluorescence and closer to that of the contralateral knees. The 3-11E/MV fluorescence in the AIA knee peaks at 18 hours. Figure 35(D) represents the ratio of the antibody fluorescence in the AIA knee and contralateral knee in mice injected with 3-11E/MV or C7/MV. The C7/MV antibody fluorescence stays low, at a value of 1 at each time point, indicating there is no accumulation of C7/MV in either joint. The 3-11E/MV ratio peaks at 18 hours at a value of just over 3, indicating there is a localisation of 3-11E/MV in the arthritic knee.

The *in vivo* localization data indicates that MV go to the inflamed joint after intravenous administration, however the MV do not stay at the inflamed site for long, as seen by the clearance after the 3 hour time point. The 3-11E enriched MV also go to the inflamed site after administration, but are able to be retained in the joint for longer, as observed with the peak of MV fluorescence at the 18-hour time-point and high fluorescence at the end-point of experiment. As this effect isn't observed in the healthy contralateral knee, nor in the arthritic knees of mice treated with non-specific antibody enriched MV (C7/MV), we can attribute that the retention of MV in the arthritic joint is due to the enrichment with 3-11E.

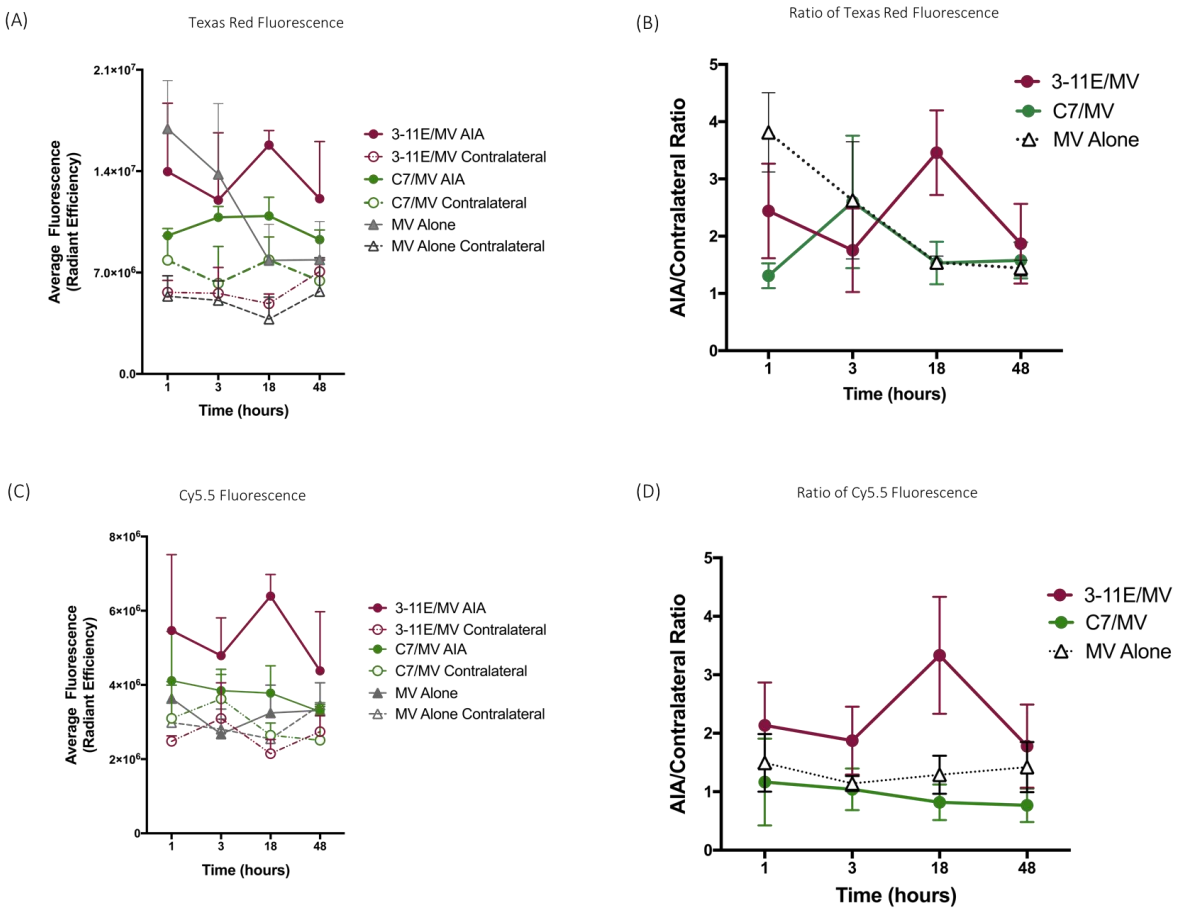

Figure 35. Localisation of microvesicles enriched with anti-ROS-CII antibodies (3-11E/MV) and microvesicles enriched with negative control antibody (C7/MV) in an antigen induced arthritis mouse model. Mice were injected intravenously with 600,000 fluorescently labelled fortified MV. Arthritis is present exclusively in the right knee and left knee acts as contralateral control. Fluorescence is calculated using region of interests and plotted as radiant efficiency (A and C). (B and D) Ratio of fluorescence in AIA versus contralateral knee. n = 3 or 4 mice per group. Two-way ANOVA was performed with Tukey multiple comparisons to determine significant differences in knee fluorescence between 3-11E/MV and C7/MV treated mice at each time point (no statistically significant difference).

3.5.2 *Ex Vivo* Analysis of Organs and Joints

Following the completion of the *in vivo* localisation study 48 hours post injection, mice were sacrificed, and their organs and joints were imaged *ex vivo* by optical imaging, using the same Texas Red and Cy5.5 scans. *Ex vivo* imaging of knee joints was performed. Images obtained from the ex vivo optical imaging are shown in Figure 36 and Figure 37. Figure 36 shows images obtained of mice injected with either MV alone or 3-11E scFv alone, scanned for both Texas red and Cy5.5. The mice injected with microvesicles alone show no specific fluorescence for Texas red and are completely negative for Cy5.5. Mice injected with 3-11E scFv alone show a strong, specific fluorescence for Cy5.5 in the right arthritic knee, but no fluorescence in the contralateral knee. There is a slight fluorescence of Texas red in the 3-11E scFv alone mice, which should be completely negative.

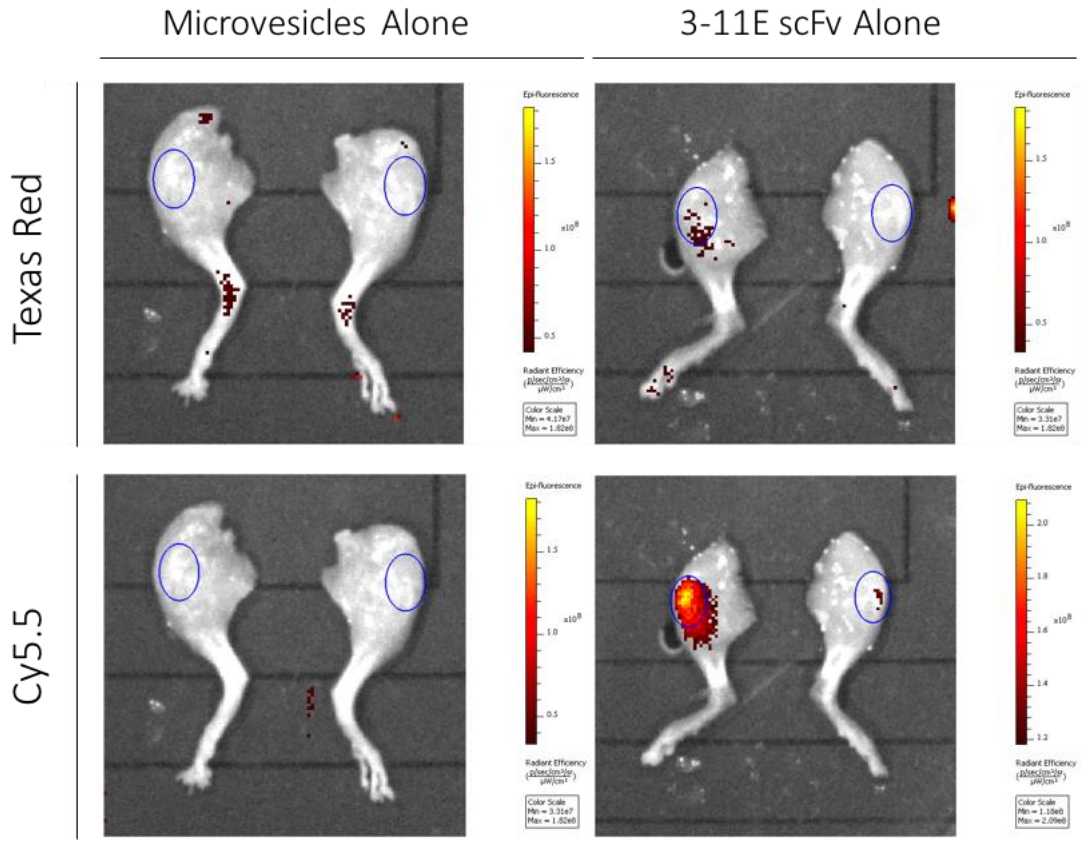

Figure 36. Localisation of anti-ROS-CII, but not microvesicles alone, to arthritic joints. Images of *ex vivo* optical imaging scans of joints of mice injected intravenously with either 600,000 microvesicles or 50 µg of anti-ROS-CII. AIA mice were sacrificed 48 hours post treatment injection and hind legs were imaged ex vivo. Right knee joint (left hand in image) is arthritic and left knee joint (right hand in image) is the contralateral control. Top panels: Texas red indicates fluorescence from MV labelled with BODIPY Texas Red. Bottom panels: Cy5.5 indicates fluorescence from conjugated scFv antibody.

Figure 37 depicts images of mice injected with 3-11E/MV or C7/MV, scanned for both Texas red and Cy5.5. Mice injected with 3-11E/MV show a specific AIA knee Texas red fluorescence, with no fluorescence in the contralateral knees. The mice injected with 3-11E/MV also show a specific AIA knee Cy5.5 fluorescence. This fluorescence is lower than the 3-11E scFv alone treated mice due to the differing levels of antibody being administered. The mice administered with 3-11E/MV are receiving significantly lower doses of antibody (around 9.6 µg per 600,000 MV, compared to 50 µg in the antibody alone mice). Mice injected with C7/MV show minimal Texas red fluorescence in either knee, with one mouse showing higher fluorescence in the contralateral knee. However,

the mice injected with C7/MV have no Cy5.5 fluorescence in either the AIA or contralateral knee.

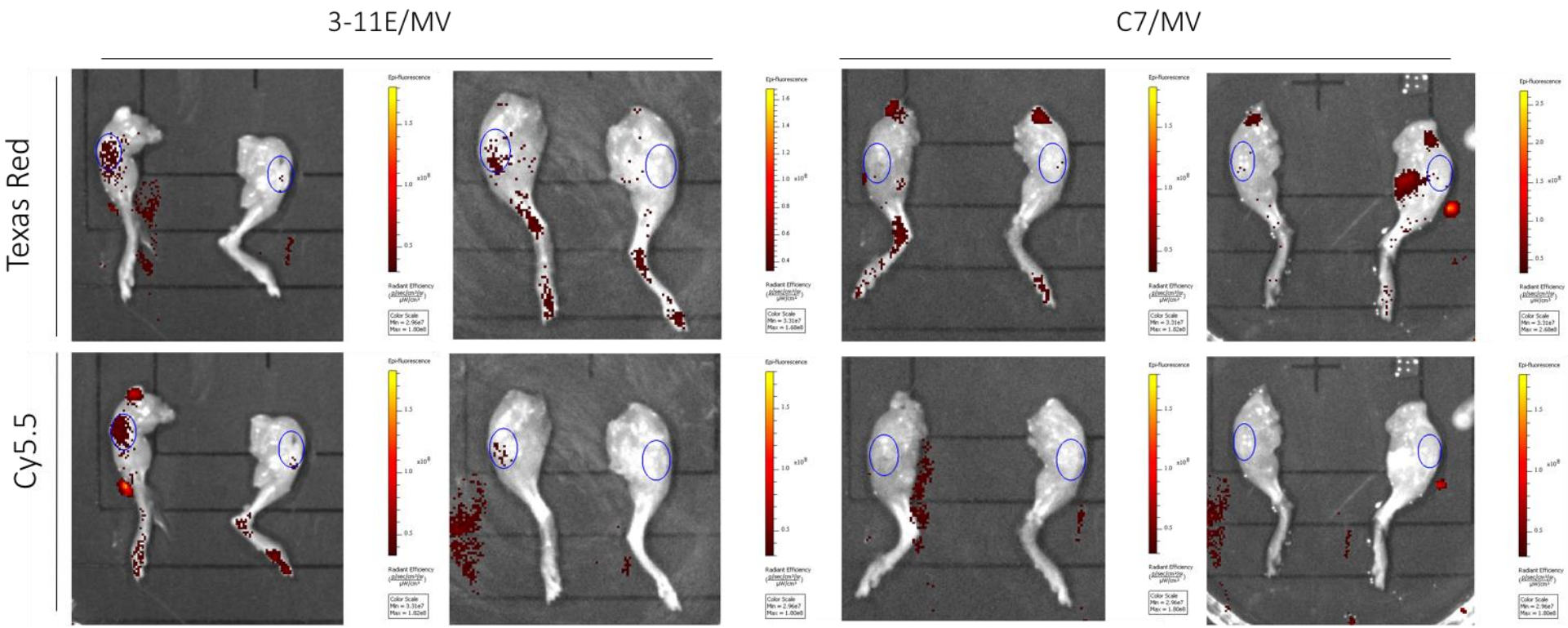

Figure 37. Localisation of microvesicles enriched with anti-ROS-CII, but not microvesicles enriched with anti-HEL, to arthritic joints. Images of ex vivo optical imaging scans of joints of mice injected with either 600,000 microvesicles fortified with anti-ROS-CII or 600,000 microvesicles fortified with negative control antibody. AIA mice were sacrificed 48 hours post treatment injection and hind legs were imaged ex vivo. Top panels: Texas red indicates fluorescence from MV labelled with BODIPY Texas Red. Bottom panels: Cy5.5 indicates fluorescence from conjugated scFv antibody.

The quantification of Texas Red fluorescence of the joints is shown in Figure 38(A), with the Cy5.5 fluorescence of the joints depicted in Figure 38(B). Similarly to the fluorescence of the organs, the 3-11E scFv injected mice act as a negative for the Texas red fluorescence. The mice injected with MV alone show the same Texas red fluorescence as the 3-11E scFv injected mice, therefore there are no vesicles present in either knee joint of mice injected with MV alone. The mice injected with the 3-11E/MV show the highest fluorescence in the AIA knee. The contralateral knee is lower and close to that of the 3-11E scFv alone injected mice. The higher fluorescence in the AIA knee of mice injected with 3-11E/MV is indicative of the targeting of the MV to the joint. The mice administered with C7/MV show basal fluorescence in the AIA knee, suggesting that the fluorescence seen in the AIA knee of 3-11E/MV mice is specific.

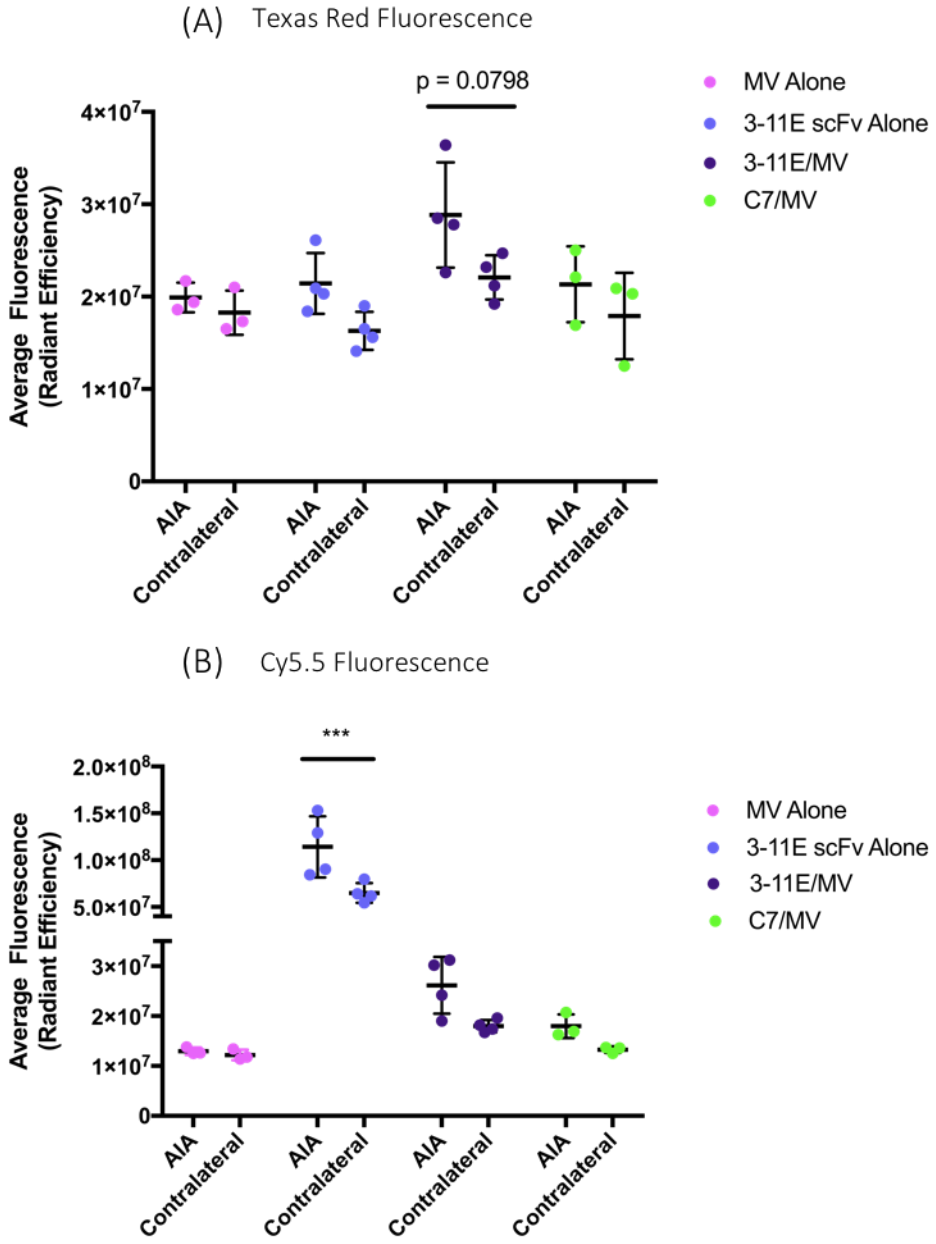

Figure 38. Ex vivo fluorescence measurements of the knee joints of mice injected with microvesicles enriched with anti-ROS-CII antibodies (3-11E/MV) and microvesicles enriched with negative control antibody (C7/MV). Fluorescence is calculated using region of interests and plotted as radiant efficiency. Two-way ANOVA with Bonferroni multiple comparison test was performed to compare differences in localisation between AIA and contralateral knee for each treatment group. **** P ≤0.0001. n = 3-4 mice per group.

Figure 39(A) shows the biodistribution of MV (Texas red) fluorescence in various organs taken 48 hours after injection of either MV alone, 3-11E scFv alone, 3-11E/MV or C7/MV. Mice injected with 3-11E scFv alone act as a negative control for the Texas red fluorescence (as they are labelled with only Cy5.5). Compared to the 3-11E scFv alone, 3-11E/MV and C7/MV mice do not show retention of vesicles in any organ. Figure 39(B) shows the biodistribution of Cy5.5 (scFv) fluorescence of mice administered either MV alone, 3-11E scFv alone, 3-11E/MV or C7/MV. Mice injected with MV alone act as a negative control for the Cy5.5 fluorescence (as they are labelled with only Texas Red). The 3-11E scFv alone mice show strong fluorescence in the liver and some fluorescence in the kidney, but minimal fluorescence in the heart, lungs and spleen. The 3-11E/MV and C7/MV group show minimal fluorescence in all organs, indicating there is no accumulation present in the organs 48 hours post injection.

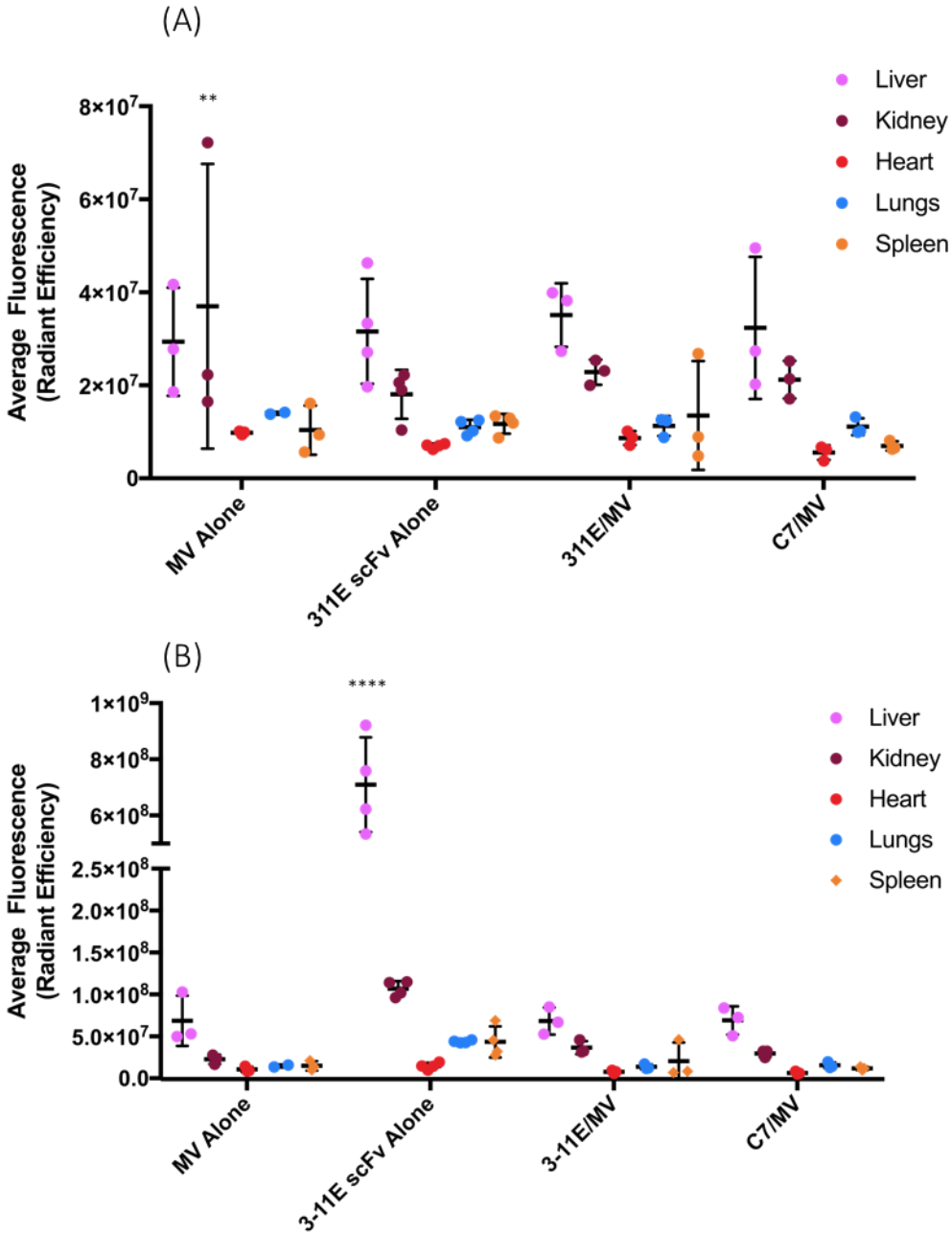

Figure 39. Ex vivo fluorescence of organs of mice injected with microvesicles enriched with anti-ROS-CII antibodies (3-11E/MV) and microvesicles enriched with negative control antibody (C7/MV). Fluorescence is calculated using region of interests and plotted as radiant efficiency. n = 3 or 4 mice per group. Two-way ANOVA with Bonferroni multiple comparison test was performed to compare differences in localisation between each treatment group for each organ. ** P ≤0.01; **** P ≤0.0001.

3.6 Fortifying Microvesicles with Antibodies Fused to Therapeutics Reduces Inflammation in Arthritic Mice

Although localisation in the arthritic knee was observed in mice treated with 3-11E/MV, there was no difference in the clinical knee swelling between mice treated with MV alone and mice treated with 3-11E/MV. Figure 40 shows the normalized knee swelling of mice treated with MV alone or 3-11E/MV and non-treated control mice. Each mouse had its knee swelling normalized from 0-100%, with baseline levels representing 0% and 100% being knee swelling 24 hours after induction, before treatment administration. The differences in knee swelling between mice treated with MV alone and 3-11E/MV are minimal and not statistically significant ($p > 0.9$ at each time point).

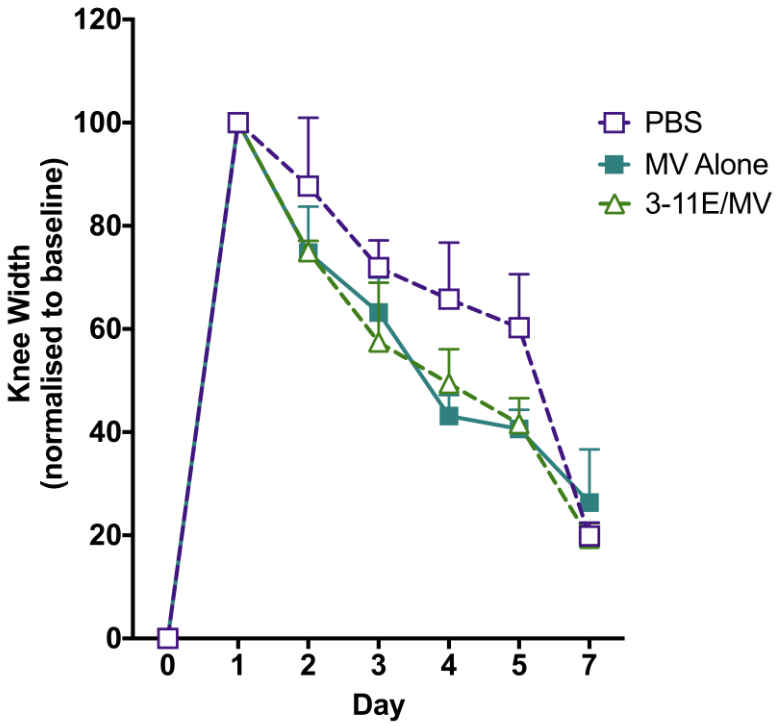

Figure 40. Clinical knee swelling of mice intravenously administered targeted microvesicles. Arthritis was induced on day 0 by intra-articular injection of mBSA, MV, 3-11E/MV or PBS were administered 24 hours post induction. Knee swelling of mice was recorded using digital calipers to assess efficacy of targeting MV to the joint. Although localisation was observed, there was no significant difference in knee swelling between mice administered MV alone or mice administered 3-11E/MV. Data are shown as normalized knee swelling for each individual mouse, with baseline levels representing 0% and 24 hours post induction representing 100%. Two-way ANOVA was performed with Bonferroni multiple comparisons to compare differences in treatment groups at each time point (no statistical significance). n = 3 to 4 mice per group.

After confirming that MV enriched with 3-11E scFv localised to the arthritic joints in mice, a treatment experiment was performed to deliver a therapeutic alongside the MV to improve clinical efficacy. For these experiments, 3-11E scFv fused with vIL-10 (3-11E/vIL-10) was used for MV enrichment. This was previously validated by my group and showed an acceleration in knee reduction when administered intravenously in the antigen induced arthritis mouse model [39].

The AIA model was used for assessment of clinical efficacy as it was the model in which localisation of treatment was confirmed. After arthritis was induced, treatment was

administered on day 1 and 3 post induction. Figure 41 represents the clinical knee oedema following arthritis induction. Figure 41(A) depicts knee swelling of mice injected with anti-ROS-CII antibodies fused with vIL-10 (3-11E/vIL-10) and control non-treated mice. Figure 41(B) depicts knee swelling of mice injected with vesicles fortified antibodies fused with vIL-10 and control non-treated mice (PBS). Mice injected with the 3-11E/vIL-10 antibody showed a reduction in knee swelling after the first treatment on day one. The reduction continues after the second dose of treatment. The mice injected with the negative control antibody fused to vIL-10, namely C7/vIL-10, which is specific against hen egg lysozyme, did not accelerate reduction in knee swelling, and followed a similar pattern to the mice injected with PBS injected mice. Mice treated with microvesicles enriched with 3-11E/vIL-10 show an acceleration in reduction of knee swelling. After the first treatment with 3-11E/vIL-10 MV, swelling was reduced. Mice treated with C7/vIL-10 MV also showed a slight, but non-significant reduction in knee swelling ($p = 0.13$ at day 3 compared to PBS). Figure 41(C) is a direct comparison of mice injected with the 3-11E/vIL-10 fortified microvesicles and 3-11E/vIL-10 alone to assess whether MV add additional benefit. The reduction of swelling in mice treated with 3-11E/vIL-10 MV was marginally greater than the 3-11E/vIL-10 alone group after first treatment at day 1, with 3-11E/vIL-10 MV treated mice being statistically significant from PBS treated mice (3-11E/vIL-10 MV: day 2, $p = 0.0112$; day 3, $p = 0.012$), but 3-11E/vIL-10 treated mice showed no statistical significance. However, both treatment groups are statistically significant from the control non-treated mice after the second administration of treatment (3-11E/vIL-10 MV: day 5, $p = 0.033$ & 3-11E/vIL-10: day 5, $p = 0.0334$). Overall, there aren't great differences in the knee swelling of mice treated with 3-11E/vIL-10 MV

or 3-11E/vIL-10 alone, which indicates that loading the antibody upon the MV doesn't hinder its therapeutic effects.

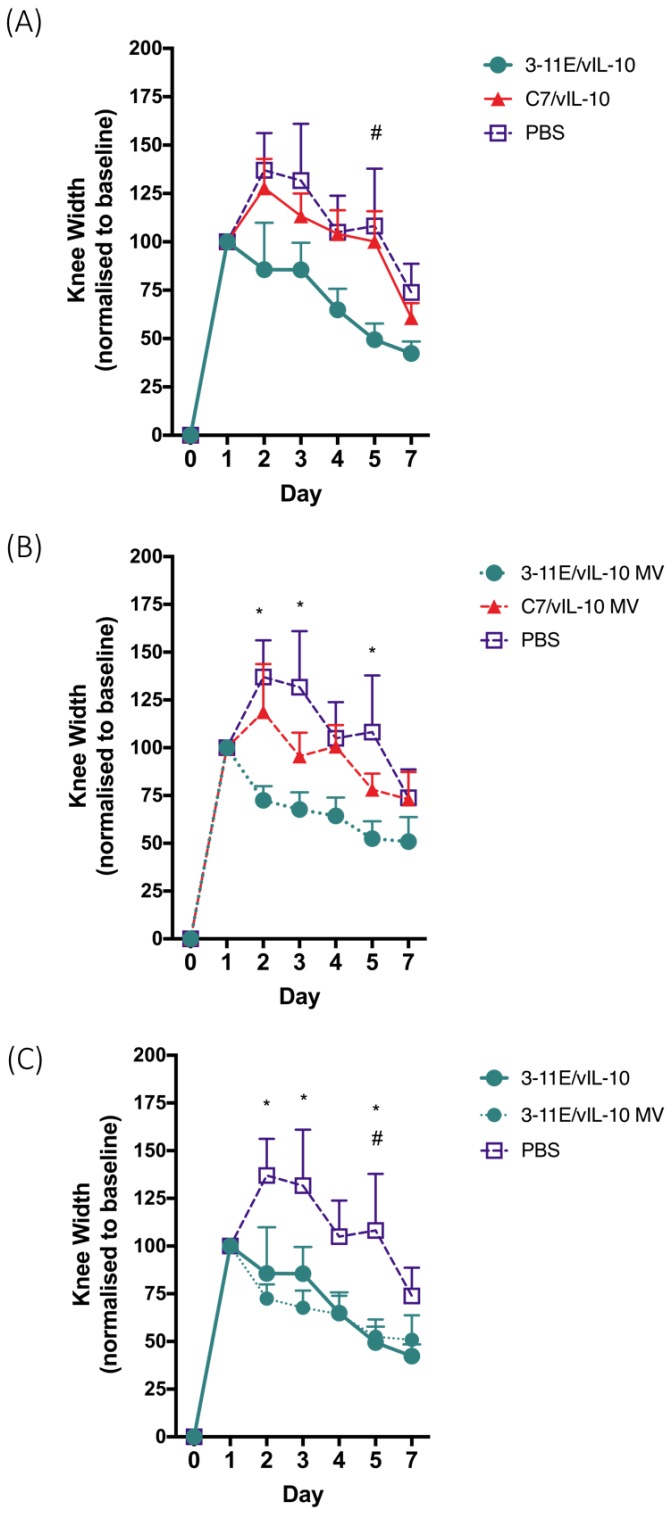

Figure 41. Clinical knee swelling of mice treated with microvesicles fortified with anti-ROS-CII antibody fused with vIL-10. Arthritis was induced on day 0 by intra-articular injection of mBSA, treatment was provided at days 1 and 3. (A) Graph depicting clinical knee scoring of mice treated with 3-11E/vIL-10 antibody, negative control antibody or PBS. (B) Knee scoring of mice treated with MV fortified with 3-11E/vIL-10, MV fortified with negative control antibody or PBS. (C) Graph comparing the efficacy of mice treated with 3-11E/vIL-10 soluble antibody and mice treated with MV enriched with 3-11E/vIL-10. Two-way ANOVA was performed with Bonferroni multiple comparisons to compare differences in treatment groups at each time point. # denotes statistical significance of 3-11E/vIL-10 against PBS injected mice; * denotes statistical significance of 3-11E/vIL-10 MV against PBS injected mice. * $P \leq 0.05$. n = 8 mice per group.

To further confirm the efficacy of fortified MV, luminol bioluminescence imaging was conducted. Luminol is a chemical that emits chemiluminescence when interacting with an oxidizing agent. The chemiluminescence can be detected by an IVIS imaging system to assess the levels of oxidants present in the joint. The imaging works on the basis that the more inflamed the joint, the more oxidants are present. The contralateral knee acts as a control as there is no inflammation present. Figure 42 shows the results from the luminol imaging. Similarly to biofluorescence imaging, regions of interest are drawn (depicted as blue circles) and quantified data are presented as photon flux. The data are presented as fold change over the control knee, which should be negative, for luminol luminescence. Figure 42(A) details the results of mice treated with 3-11E/vIL-10, C7/vIL-10 or PBS. At day 1 post induction, the groups show similar fold change in luminescence, with C7/vIL-10 showing a slightly higher level. By day 3 the PBS and C7/vIL-10 show great increases in the luminescence of the arthritic knee, but the 3-11E/vIL-10 group shows a similar luminescence to the day one level. At day 3, the 3-11E/vIL-10 group is statistically significant from the C7/vIL-10 treated group ($p = 0.0112$). The 3-11E/vIL-10 group remains suppressed at the same level throughout the experiment, and by day 5 the C7/vIL-10 and PBS group starts to reduce. Figure 42(B) demonstrates the fold luminescence of mice treated with 3-11E/vIL-10 MV, C7/vIL-10 MV or PBS. At day 1 post induction, the luminescence present in the inflamed joints is similar between the groups, with 3-11E/vIL-10 MV showing slightly greater luminescence. By day 3 there is a drastic reduction in the mice treated with 3-11E/vIL-10 MV, which continues over day 5 and 7. The mice treated with C7/vIL-10 MV have a similar level between days 1 and 3 which decreases over days 5 and 7, but not to the extent of the 3-11E/vIL-10 treated mice.

Figure 42(C) shows images obtained from the 3 days' post induction optical imaging process.

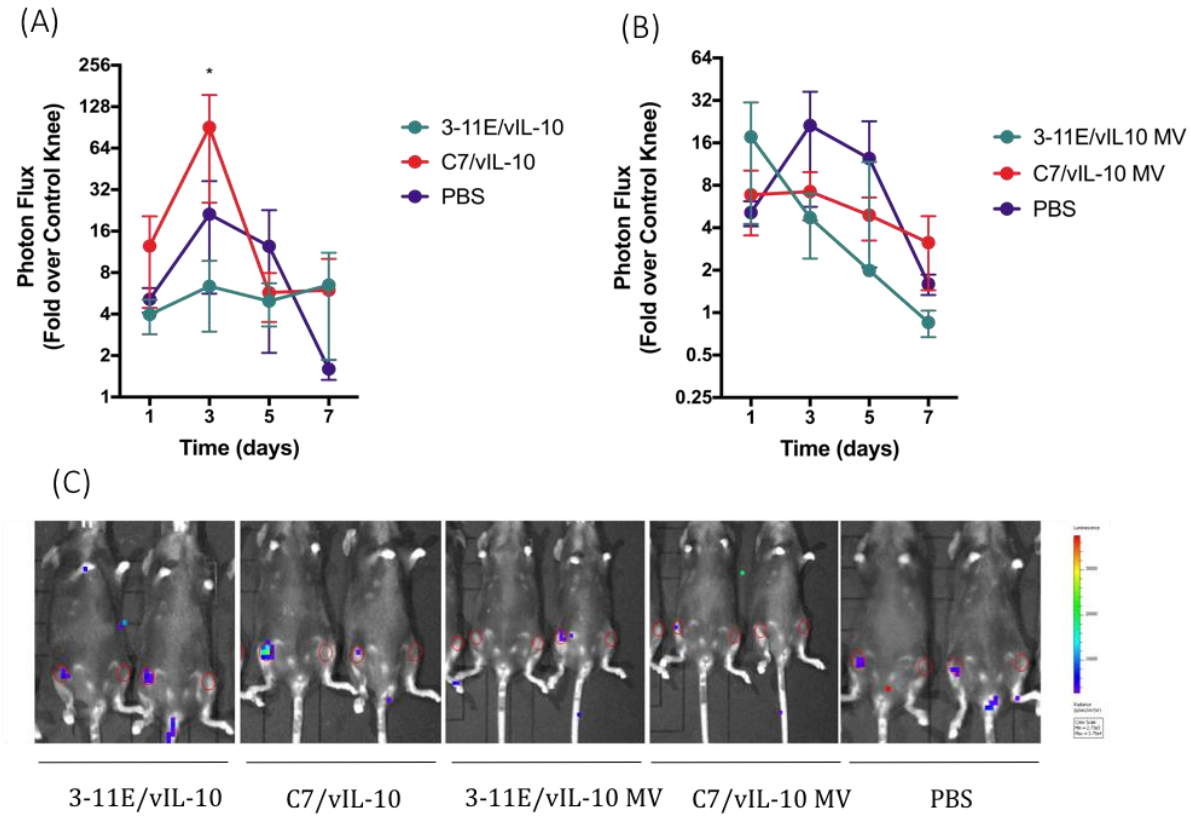

Figure 42. Optical imaging of luminol bioluminescence in knees of mice injected with either antibody alone, antibody enriched microvesicles or PBS control following arthritis induction. Arthritis was induced on day 0 by intra-articular injection of mBSA in the right knee, treatment was provided at days 1 and 3. Two-way ANOVA was performed to determine differences in luminescence between treatment groups at each time point. * P ≤0.05. n = 5 mice per group.

At the end-point of the vIL-10 MV treatment experiment, mouse knees were harvested and snap frozen to probe for the localisation of treatment in the arthritic cartilage. Knees were sectioned and mounted onto microscope slides and imaged by confocal microscopy. The aim of this analysis was to detect the presence of the fluorescent antibody enriched MV treatment (for both the Cy5.5 labelled antibody and BODIPY TR labelled MV). As shown in Figure 43 retention of 3-11E/vIL-10 MV was observed in the arthritic cartilage (Figure 43(A) and (B)). This retention was still detectable at the end-point of experiment

(day 9), 6 days following the second dose of treatment. As shown in Figure 43(C) and Figure 43(D), mice treated with 3-11E/vIL-10 MV showed less localisation in the healthy, contralateral cartilage, with no specific retention observed at the end-point of the experiment. Similarly, mice treated with C7/vIL-10 MV showed no localisation of treatment in either the arthritic cartilage (Figure 43(E) and Figure 43(F)) or the healthy, contralateral cartilage (Figure 43(G) and Figure 43(H)).

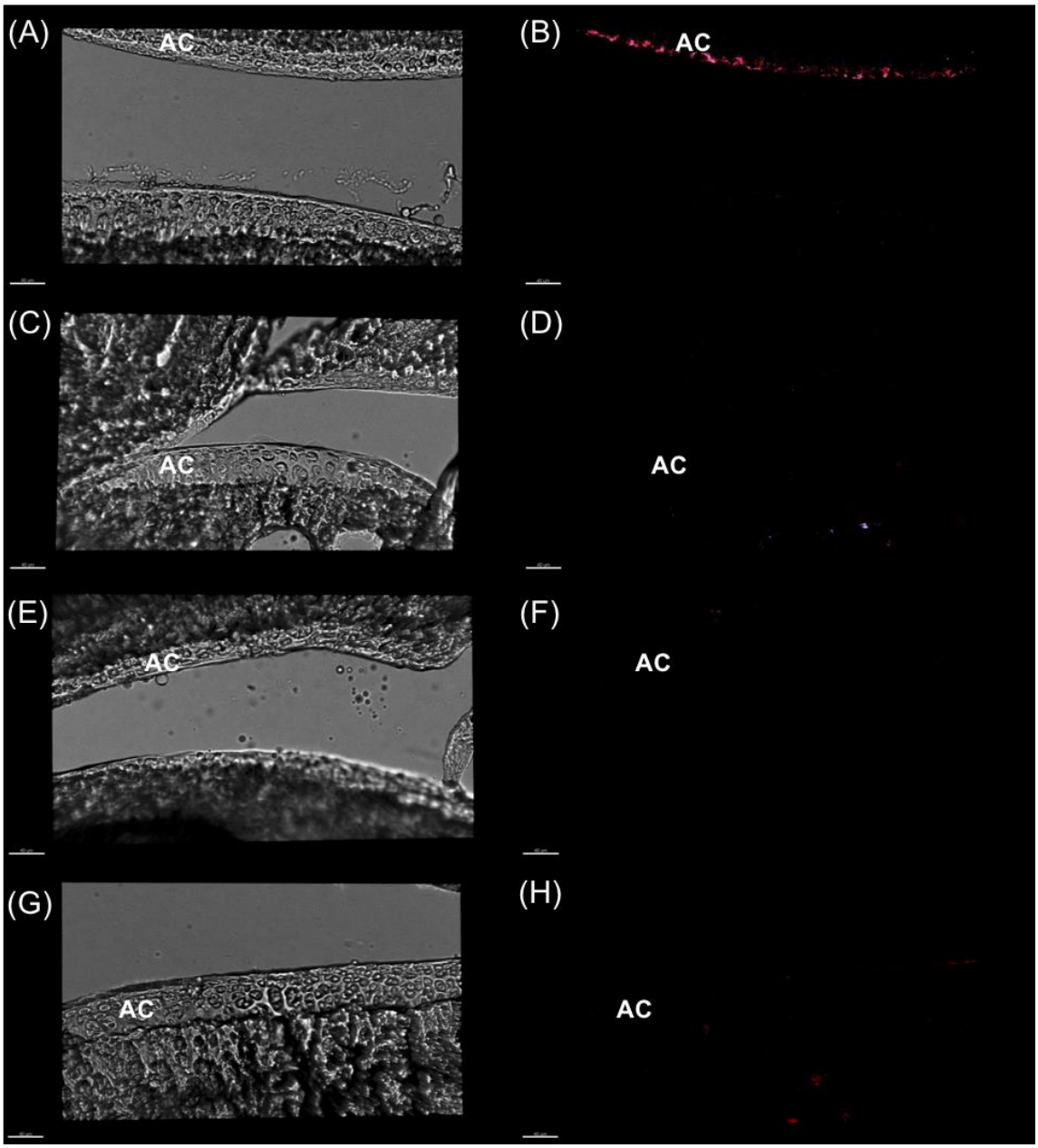

Figure 43. Localisation of microvesicles enriched with anti-ROS-CII antibody fused with vIL-10 in the arthritic joint after intravenous administration. Arthritis was induced on day 0 by intra-articular injection of mBSA in the right knee, treatment was provided at days 1 and 3. At the end-point of experiment (day 7), knees were harvested and snap frozen in OCT medium. Knees were sectioned by cryotomy and probed by confocal microscopy to detect the presence of fluorescent treatment in the arthritic cartilage. Mice treated with 3-11E/vIL-10 MV showed specific localisation of treatment in the superficial layers of the arthritic cartilage (A and B), but not in the healthy contralateral cartilage (C and D). Mice treated with C7/vIL-10 MV showed no localisation in the arthritic knee (E and F), nor in the healthy contralateral cartilage (G and H). n = 3 mice per group. Red = BODIPY TR; Cyan = 3-11E/vIL-10; White = overlay. AC = articular cartilage. n = 3 mice per group.

3.7 Combined Therapeutic Antibodies Can Be Co-Loaded upon Microvesicles

In the previous section, I observed an acceleration in the resolution of inflammation following the administration of MV enriched with 3-11E/vIL-10 antibody compared to control non-treated mice. However, the reduction in swelling between the 3-11E/vIL-10 MV and 3-11E/vIL-10 groups did not differ greatly. The aim of this part of the work was to find out if we can improve efficacy if we targeted MV loaded with multiple therapeutics.

The aim of these experiments was to co-deliver multiple therapeutics which act through different pathways to drive for full resolution of inflammation. Such treatment is difficult to achieve clinically due to the detrimental, immunosuppressive side effects of administering anti-inflammatory drugs. As a proof of concept, the 3-11E enriched MV were used to target vIL-10 and anti-mTNF to the joint. Targeting of the double enriched vesicles to the arthritic joint (through the actions of the 3-11E antibody) was hypothesized to provide the specific localisation of treatment, as had been observed consistently throughout this thesis.

3.7.1 Imagestream Analysis of Microvesicles Enriched with Multiple Antibodies

To first confirm the presence of both antibodies upon the MV, Imagestream flow cytometry (IS^X) analysis was performed as previously described. The MV population were gated upon by their low side scatter and BODIPY TR fluorescence and then assessed for the simultaneous presence of Alexafluor 488 fluorescence (311e/vIL-10 antibody) and Cy5.5 fluorescence (anti-mTNF antibody).

Single antibody loaded MV were used as fluorescence minus one controls for gating, to ensure a true positive selection of the double loaded MV. Figure 44 demonstrates the results of the IS^X analysis for the single antibody loaded MV. Figure 44(A) and Figure 44(B) show the IS^X analysis for MV loaded with anti-mTNF and 3-11E/vIL-10, respectively. Both enriched MV show no double positive population, and only positive fluorescence for the specific loaded antibody. Figure 44(C) shows a representative example of an anti-mTNF positive MV, with Ch01 and Ch09 showing brightfield images, Ch04 showing MV positivity, Ch11 showing anti-mTNF fluorescence and Ch12 showing side scatter. Figure 44(D) shows a representative example of an 3-11E/vIL-10 positive MV, with Ch01 and Ch09 shows brightfield images, Ch02 showing 3-11E/vIL-10 fluorescence, Ch04 showing MV positivity and Ch12 showing side scatter.

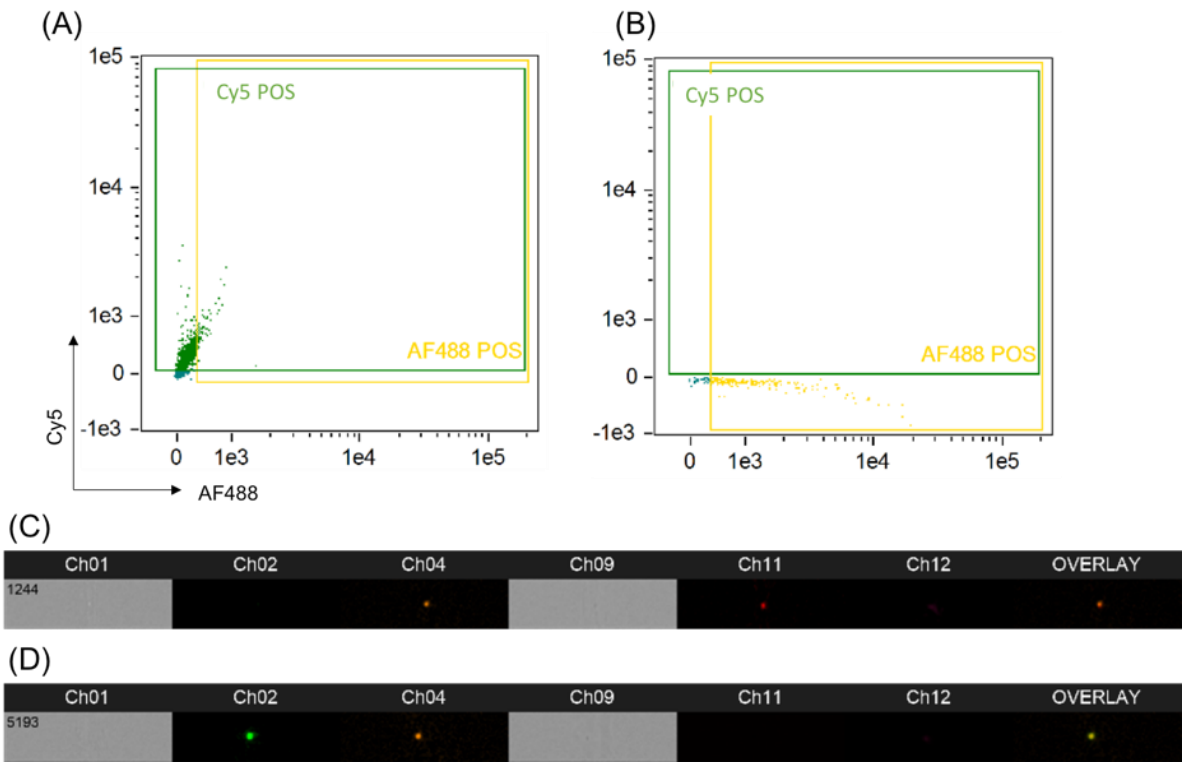

Figure 44. Imagestream^x analysis of polymorphonuclear neutrophil derived microvesicles enrichment with anti-ROS-CII or anti-mTNF. MV were incubated with 3-11E/vIL-10 or anti-mTNF and dried liposome forming phospholipid and sonicated for 5 minutes at 3 amplitude microns. (A) Imagestream analysis of MV enriched with anti-mTNF (B) Imagestream analysis of MV enriched with anti-ROS-CII (C) Representative microscopic image of MV plus anti-mTNF. (D) Representative microscopic image of MV plus anti-ROS-CII. Ch01 & Ch09; brightfield images, Ch02; AF488 fluorescence, Ch04; BODIPY TR fluorescence, Ch11; Cy5 fluorescence, Ch12; side scatter. n = 4 replicates.

Figure 45 shows IS^X analysis of MV fortified with both 3-11E/vIL-10 and anti-mTNF antibodies. The dotplot in Figure 45 shows the MV population positive for both Cy5.5 and Alexafluor 488 fluorescence, with 78% of MV positive for both antibodies (range of 69-84% between replicates). A representative image of the double antibody positive MV is shown in Figure 45(B), with Ch01 and Ch09 indicating brightfield images, Ch04 indicating MV positivity, Ch02 showing 3-11E/vIL-10 fluorescence, Ch11 showing anti-mTNF fluorescence and Ch12 showing side scatter.

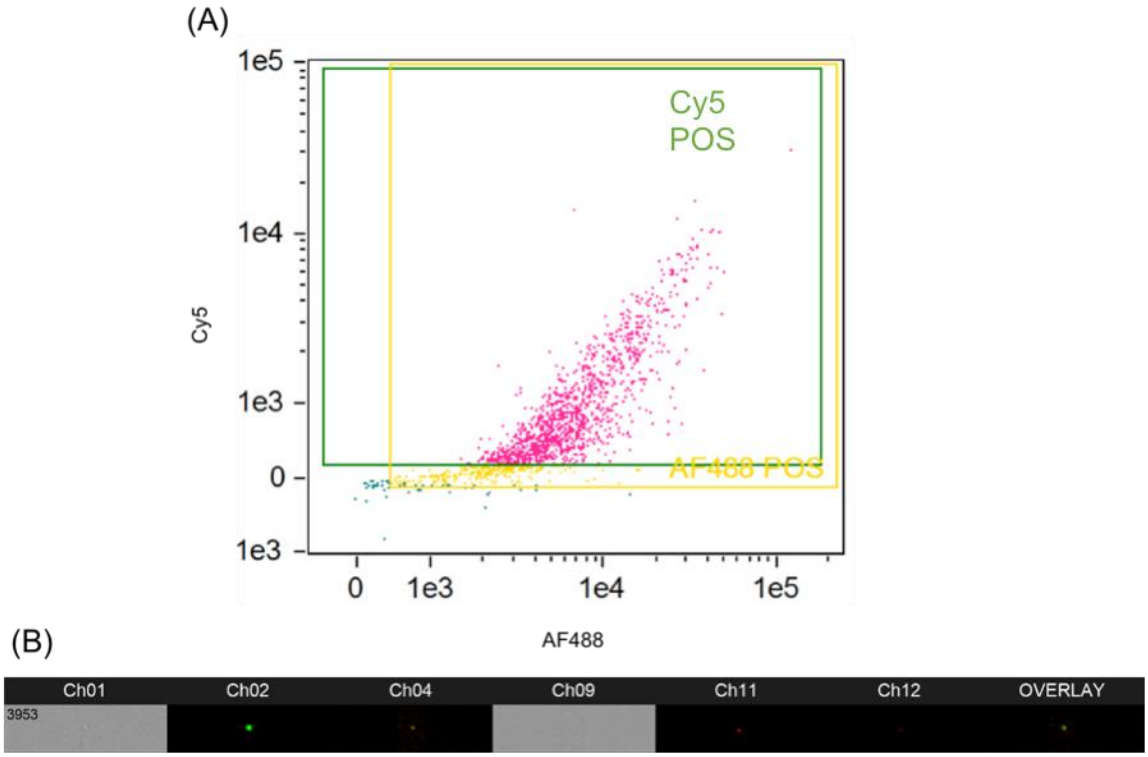

Figure 45. Imagestream^x analysis of polymorphonuclear neutrophil derived microvesicles enriched with anti-ROS-CII and anti-mTNF. (A) Imagestream analysis of MV enriched with anti-mTNF and anti-ROS-CII antibodies, showing 78% of MV positive for both antibodies (B) Representative microscopic image of MV fortified with anti-ROS-CII and anti-mTNF. Ch01 & Ch09; brightfield images, Ch02; AF488 fluorescence, Ch04; BODIPY TR fluorescence, Ch11; Cy5 fluorescence, Ch12; side scatter. n = 4 replicates.

To give an insight into how the vesicle population is changing after enrichment with antibodies, nanoparticle tracking analysis was conducted to compare the diameter of vesicles, vesicles enriched with a single antibody and vesicles enriched with multiple antibodies. Figure 46 shows a representative NTA analysis, comparing MV alone (Figure 46(A)), MV enriched with single antibody (Figure 46(B)) and MV enriched with multiple antibodies (Figure 46(C)). All three groups show a mean diameter within the MV range, with the MV alone also group showing some smaller vesicles below 100 nm. There is an overall increase in the size of vesicles after enrichment with antibody, however the large standard deviations make these increases not significant. Due to their size being between 100-600 nm, after enrichment with single and multiple antibodies, the vesicles retain an NTA profile that resemble MV and no evidence of aggregates or MV debris was observed.

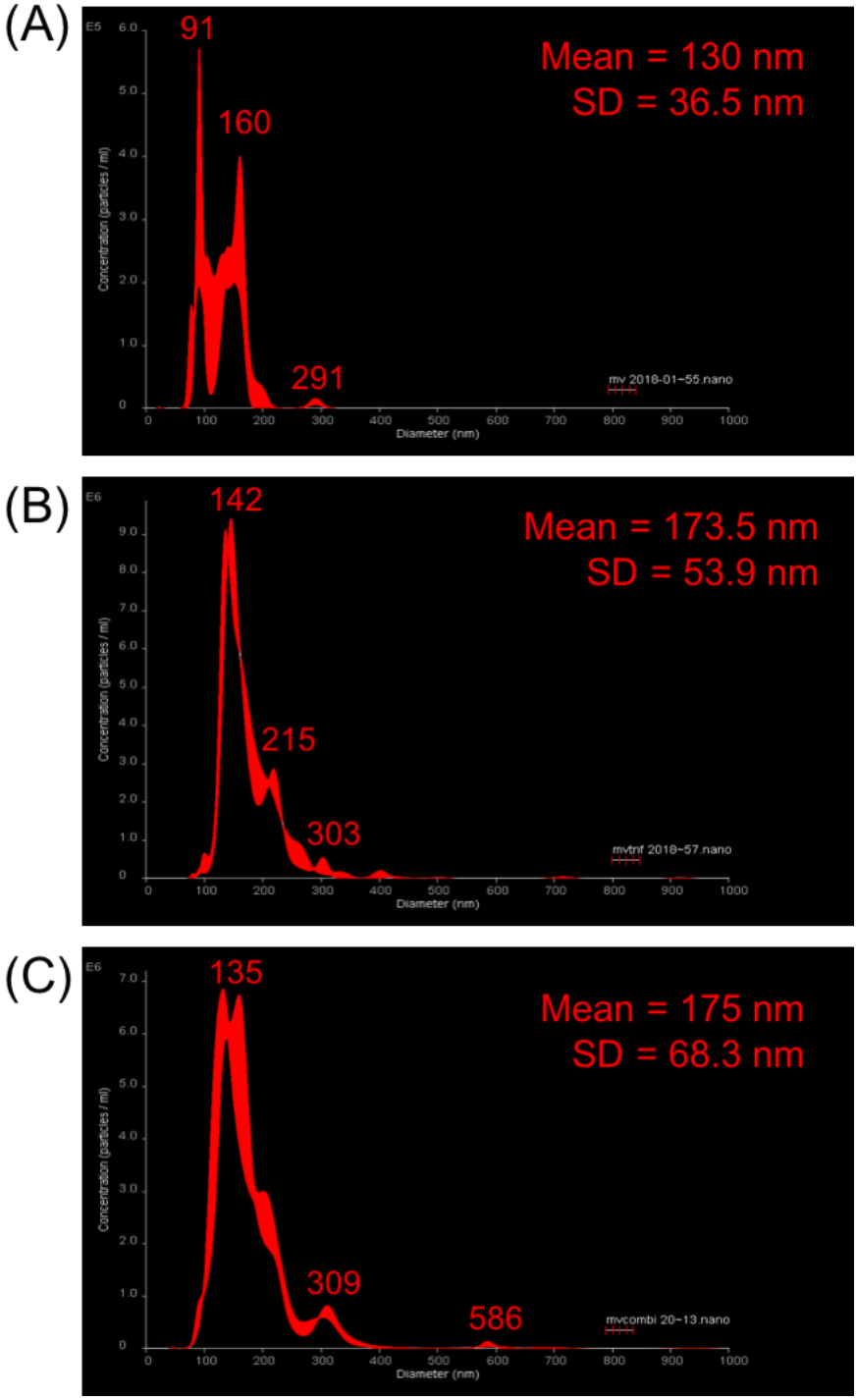

Figure 46. Representative nanoparticle tracking analysis comparing microvesicles alone and microvesicles enriched with antibodies. (A) NTA analysis of PMN derived MV from healthy donors without any enrichment. (B) NTA anaysis of PMN MV enriched with a single antibody. (C) NTA analysis of PMN MV enriched with multiple antibodies. n = 4 replicates.

3.7.2 Microvesicles Enriched with Two Antibodies Can Bind Specifically to Two Targets

3.7.3 Enzyme Linked Immunosorbent Assay

Following confirmation that both antibodies were present upon the MV, analysis was performed to confirm the antibodies can still bind to their targets after incorporation on MV. ELISA were performed to determine the binding of double antibody enriched MV to recombinant mTNF and glycated CII (as an example of ROS-CII). Figure 47 shows the results of the ELISA to check binding specificity. For all test conditions, after incorporation upon MV the samples were centrifuged at 20,000 *g* to pellet the MV population for testing on the ELISA. Single antibody and MV enriched with single antibody were used as positive controls for binding. Enriched antibodies were checked by Imagestream^X before use in ELISA to ensure equal numbers of antibody positive MV were used per group. Both single antibodies and MV enriched with single antibody could bind specifically to either glycated CII or mTNF target, but not to the alternative target. There was a significant difference in the binding of 3-11E/vIL-10 to glycated CII compared to anti-mTNF ($p < 0.0001$) and of anti-mTNF to recombinant mTNF compared to 3-11E/vIL-10 ($p < 0.0001$). However, MV enriched with anti-mTNF and 3-11E/vIL-10 could bind to both the glycated CII and mTNF targets in ELISA. There was no significant difference in the binding of 3-11E/vIL-10 + Anti-mTNF MV to both recombinant mouse TNF and glycated CII when compared to MV enriched with anti-mTNF and MV enriched with 3-11E/vIL-10, respectively ($p > 0.99$ and $p = 0.22$). There was however, a significant difference between

binding of 3-11E/vIL-10 + Anti-mTNF MV to both recombinant mouse TNF and glycated CII when compared to MV enriched with the non-specific antibody (p = 0.0014 compared to 3-11E/vIL-10 MV binding to mTNF; and p = 0.0005 compared to anti-mTNF MV binding to glycated CII).

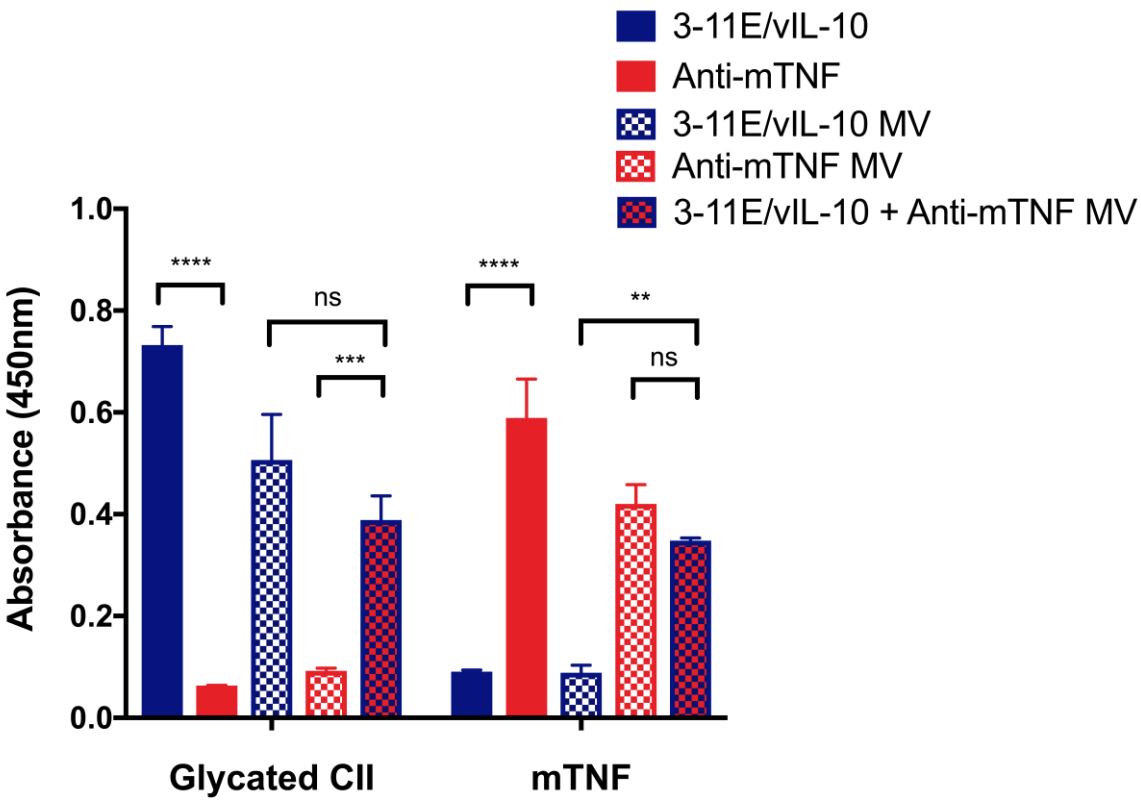

Figure 47. Binding capacity of microvesicles enriched with multiple therapeutic antibodies. ELISA was coated with recombinant mTNF or glycated CII to test the specificity of the antibodies after incorporation. MV enriched with either 3-11E/vIL-10, anti-mTNF or a combination of both antibodies as previously described. Enriched MV were used as the primary incubation to test the binding specificities after incorporation. Two-way ANOVA with Bonferroni post-test was performed to determine statistical significance. ** P ≤0.01; *** P ≤0.001; **** P ≤0.0001; ns = not significant. n = 3 replicates.

3.7.4 MTT Cell Cytotoxicity Assay

Although ELISA analysis confirmed the ability of both 3-11E/vIL-10 and anti-mTNF to bind specifically to target after incorporation upon MV, an MTT assay was performed to test the physiological functionality of the anti-mTNF to inhibit TNF dependent cell death using L929 cells, which are TNF cytotoxic. Figure 48 shows the results of the MTT assay, displayed as the average percentage of viability (compared to positive viability control-cells without TNF in culture medium), which was performed over three cell passages. The L929 cell death can be inhibited by the addition of anti-mTNF antibody to the cell culture in a concentration dependent manner, as shown in Figure 48. MV enriched with anti-mTNF are also able to inhibit cell death to similar abilities as the anti-mTNF antibody treated cells. Furthermore, MV enriched with both anti-mTNF and 3-11E/vIL-10 antibodies are also able to inhibit cell death to the same extent as cells treated with 10 mM of anti-mTNF alone. The inhibition of death in cells treated with Anti-mTNF MV and 3-11E/vIL-10 + Anti-mTNF MV was not statistically significant from cells treated with the highest dose of anti-mTNF antibody alone ($p = 0.3192$ and $p = 0.06$, respectively). L929 cells treated with MV alone are unable to inhibit cell death, with around 90% of cell cytotoxicity after treatment with MV. Similarly, when treating L929 cells with human TNF, cell death cannot be inhibited after treatment with anti-mTNF or MV enriched with anti-mTNF. These differences were statistically significant from cells in the presence of mTNF treated with anti-mTNF MV and 3-11E/vIL-10 + Anti-mTNF MV. This indicates the specificity of anti-mTNF to mTNF and not TNF derived from other species.

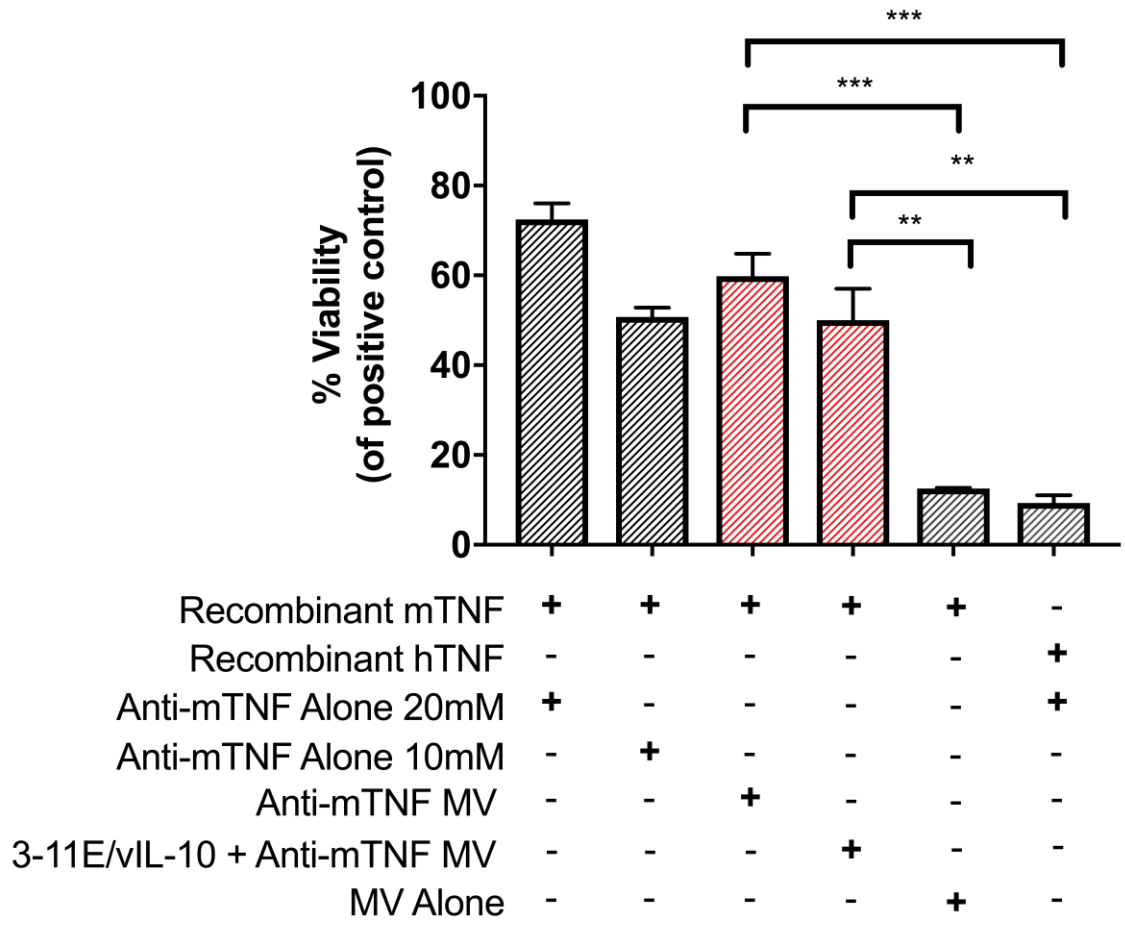

Figure 48. Anti-mTNF can still inhibit TNF dependent cell death after enrichment on microvesicles. MTT assay was performed to assess the ability of anti-mTNF to inhibit cell death. L929 cells were cultured in the presence of recombinant mouse TNF or human TNF and treated with either anti-mTNF alone, anti-mTNF MV, anti-mTNF + 3-11e/vIL-10 MV or MV alone. MV enriched with anti-mTNF or anti-mTNF + 3-11E/vIL-10 could inhibit TNF dependent cell death, unlike MV alone. One way ANOVA with Bonferroni post-test was performed to determine statistical significance. ** P ≤0.01; *** P ≤0.001. n = 3 replicates at different passage numbers.

3.8 Microvesicles Enriched with Multiple Therapeutic Antibodies Promotes the Resolution of Inflammation in Arthritic Mice

3.8.1 Clinical Scoring

After the *in vitro* confirmations regarding the incorporation of anti-mTNF upon MV and the ability of the anti-mTNF to bind to to mTNF after incorporation upon MV, *in vivo* proof of concept studies were performed to test whether the MV enriched with multiple therapies (vIL-10 and anti-mTNF), had an enhanced efficacy compared to the 3-11E/vIL-10 MV mono therapy. As with the previous localisation and treatment experiments, the *in vivo* studies were performed in the AIA mouse model. Arthritis was induced by intra-articular injection in the right knee on day 0, with treatment administered intravenously on days 1 and 3. Knee widths were measured at daily time points using digital calipers.

Figure 49 shows the clinical knee scoring of mice treated with MV alone, 3-11E/vIL-10 MV, 3-11E/vIL-10 + Anti-mTNF MV and control vehicle (PBS) treated mice. Knee scoring for each individual animal was normalized, with 0% representing baseline knee measurements before disease induction and 100% representing knee measurements of each mouse 24 hours after stimulation of inflammation. Mice injected with PBS show an exacerbated inflammation, peaking at day 2, which does not return to baseline levels and ended at 27% normalized value. Mice treated with MV alone showed better clinical scoring than PBS throughout the experiment, which was statistically significant at day 5 ($p = 0.038$). MV alone treated mice had a normalized knee score of 28% at the end-point of experiment. Mice treated with 3-11E/vIL-10 MV showed a greater reduction in knee

swelling, as expected based on the previous experiments. Normalised knee width values for mice treated with 3-11E/vIL-10 MV were reduced to 17% on average at the end-point of experiment. Strikingly, mice treated with 3-11E/vIL-10 + Anti-mTNF MV saw a near complete attenuation of inflammation in the knee joint. The accelerated reduction in knee swelling in 3-11E/vIL-10 + Anti-mTNF MV combination therapy is statistically significant compared to mice treated with MV alone (day 2 $p= 0.001$, day 3 $p= 0.023$), MV loaded with 3-11E/vIL-10 alone (day 2 $p= 0.049$) and non-treated mice (PBS, day 2 $p < 0.0001$, day 3 $p < 0.0001$, day 4 $p < 0.0001$, day 5 $p < 0.0001$, day 7 $p = 0.084$). The normalized knee width of mice treated with 3-11E/vIL-10 + Anti-mTNF MV was 3% at the end-point of experiment.

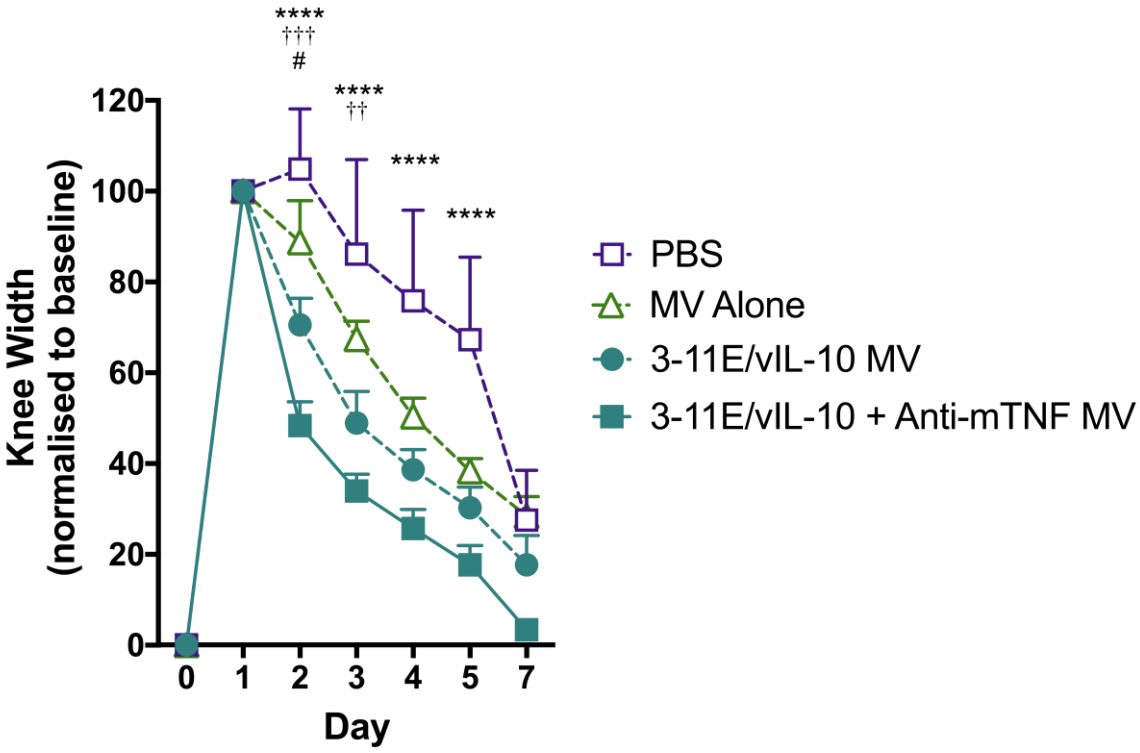

Figure 49. Clinical knee swelling of mice treated with microvesicles enriched with multiple therapeutic antibodies. Arthritis was induced on day 0 by intra-articular injection of mBSA, treatment was provided at days 1 and 3. Knee width was monitored using digital calipers and knee width was normalized to 100% at 24 hours post arthritis induction. Two-way ANOVA with Bonferroni post-test was performed to determine differences in knee swelling across each time point: * denotes statistical significance between 3-11E/vIL-10 + Anti-mTNF MV and PBS; † denotes statistical significance between 3-11E/vIL-10 + Anti-mTNF MV and MV alone; # denotes statistical significance between 3-11E/vIL-10 + Anti-mTNF MV and 3-11E/vIL-10 MV. 3-11E/vIL-10 MV is also statistically significant from PBS treated mice at days 2 ($p = 0.0031$), 3 ($p = 0.001$), 4 ($p = 0.001$) and 5 ($p = 0.0011$). * = $P \leq 0.05$; ** $P \leq 0.01$; *** $P \leq 0.001$; **** $P \leq 0.0001$. n = 6 to 10 mice per group.

A large panel of mice were treated with control antibody or control MV therapies, as shown in Figure 50. C7-vIL-10, 3-11E/vIL-10 and anti-mTNF treated mice were all included to assess the reduction of swelling at similar equivalent doses. As expected from previous experiments, 3-11E/vIL-10 reduces knee swelling most and is statistically significant from PBS treated mice. C7/vIL-10, the untargeted equivalent, is unable to reduce knee swelling to the same extent. Mice treated with anti-mTNF saw a modest reduction of knee swelling, but not to the extent observed with 3-11E/vIL-10. This is explained by the low

dose of anti-mTNF used in this study compared to other published work showing efficacy *in vivo*.

Figure 50 panel B shows the knee swelling data for mice treated with the MV control therapies. As a control for the combined therapy approach, a non-targeted alternative was used. C7/vIL-10 + Anti-mTNF was loaded upon MV to show that the amelioration in inflammation observed in the 3-11E/vIL-10 + Anti-mTNF MV is due to the specific localisation of the therapy. The C7/vIL-10 + Anti-mTNF MV therapy was unable to reduce knee swelling at the rate of the 3-11E/vIL-10 + Anti-mTNF treatment, and statistical significance between these two groups was observed at day 2 ($p = 0.0058$). C7/vIL-10 + Anti-mTNF MV did show statistical significance from PBS treated mice at day 3 ($p = 0.0181$), which indicates that administering the combined treatment of vIL-10 and anti-mTNF upon MV has significant efficacy even without targeting. Single therapy of Anti-mTNF MV showed no greater efficacy than MV alone.

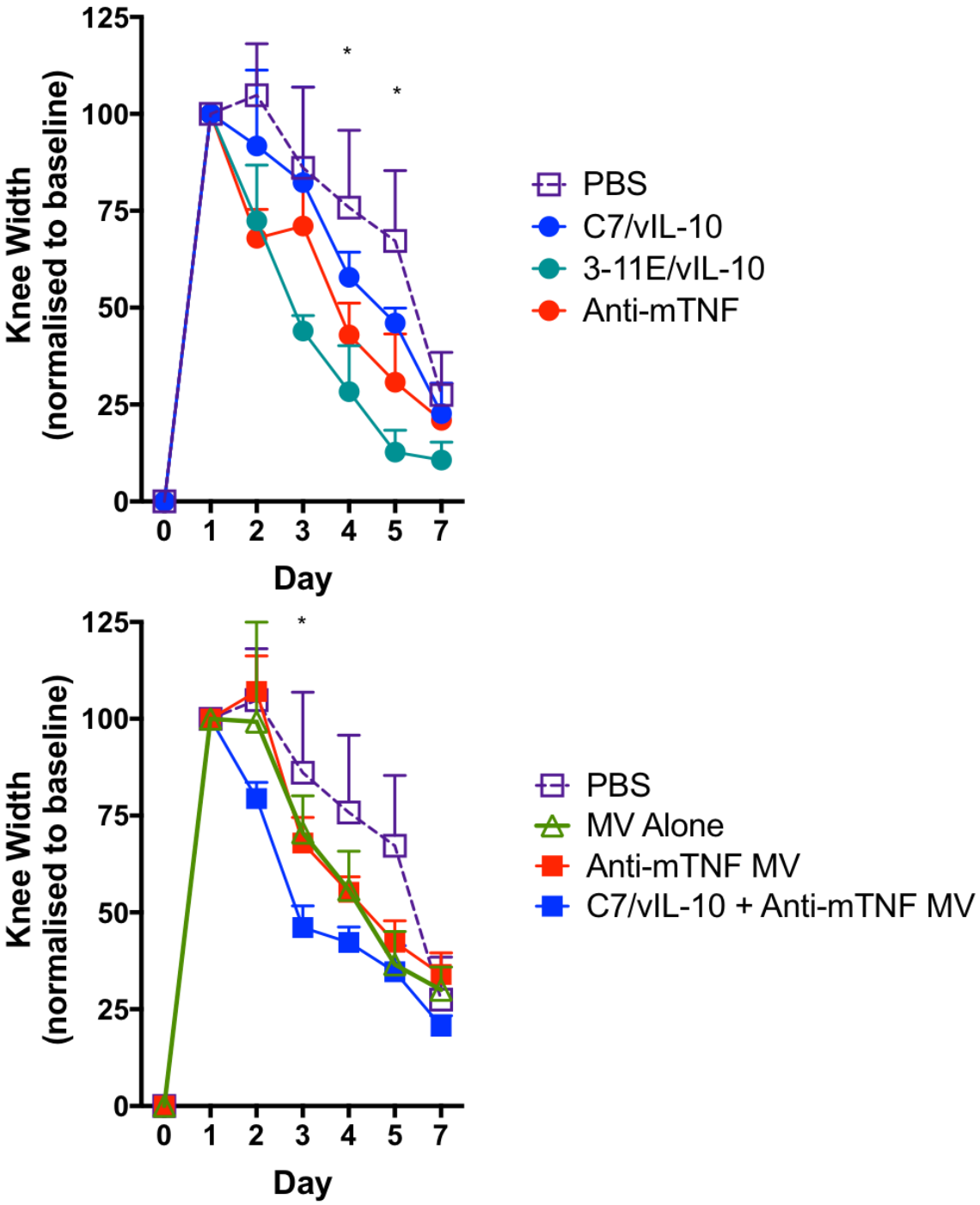

Figure 50. Clinical knee swelling of mice treated with antibody and microvesicle controls. Arthritis was induced on day 0 by intra-articular injection of mBSA, treatment was provided at days 1 and 3. Knee width was monitored using digital calipers and knee width was normalized to 100% at 24 hours post arthritis induction. (A) Knee swelling data of mice treated with PBS, C7/vIL-10, 3-11E/vIL-10 or Anti-mTNF controls. * denotes statistical significance between 3-11E/vIL-10 treated mice and PBS treated mice at days 4 ($p = 0.0362$) and 5 ($p = 0.0104$. No statistical significance observed between any other treatment groups). (B) Knee swelling data of mice treated with PBS, MV alone, Anti-TNF MV or C7-vIL-10 + Anti-mTNF MV. * denotes statistical significance between C7-vIL-10 + Anti-mTNF MV treated mice and PBS treated mice at day 3 ($p = 0.0181$. no statistical significance observed between any other treatment groups). Two-way ANOVA with Bonferroni post-test was performed to determine differences in knee swelling across each time point. * = $P \leq 0.05$. n = 5 to 6 mice per group.

3.8.2 Histological Analysis

At the end-point of the combined antibody MV treatment experiment, three mouse knees per group were harvested and snap frozen. Knees were sectioned and mounted onto microscope slides and imaged by confocal microscopy. The aim of this analysis was to confirm the localisation that was shown in the previous treatment experiment. As shown in Figure 51, control PBS treated mice show no fluorescence in the arthritic knee joint. Mice treated with MV alone show some vesicle fluorescence in the arthritic joint, mainly located within the bone marrow and small amounts detected in the superficial layers of the cartilage. Confirming what was observed in the previous treatment experiment, mice treated with 3-11E/vIL-10 MV show a high retention of MV fluorescence in the arthritic cartilage at the end-point of the experiment. Unexpectedly, the mice treated with 3-11E/vIL-10 + Anti-mTNF MV showed extremely little MV fluorescence in the arthritic knee joints at the end-point of the experiment. This was the case for all three mice in the 3-11E/vIL-10 + Anti-mTNF MV confocal analysis. This unexpected clearance of MV was likely linked to the clearance of oedema observed in the clinical knee swelling of 3-11E/vIL-10 + Anti-mTNF MV treated mice.

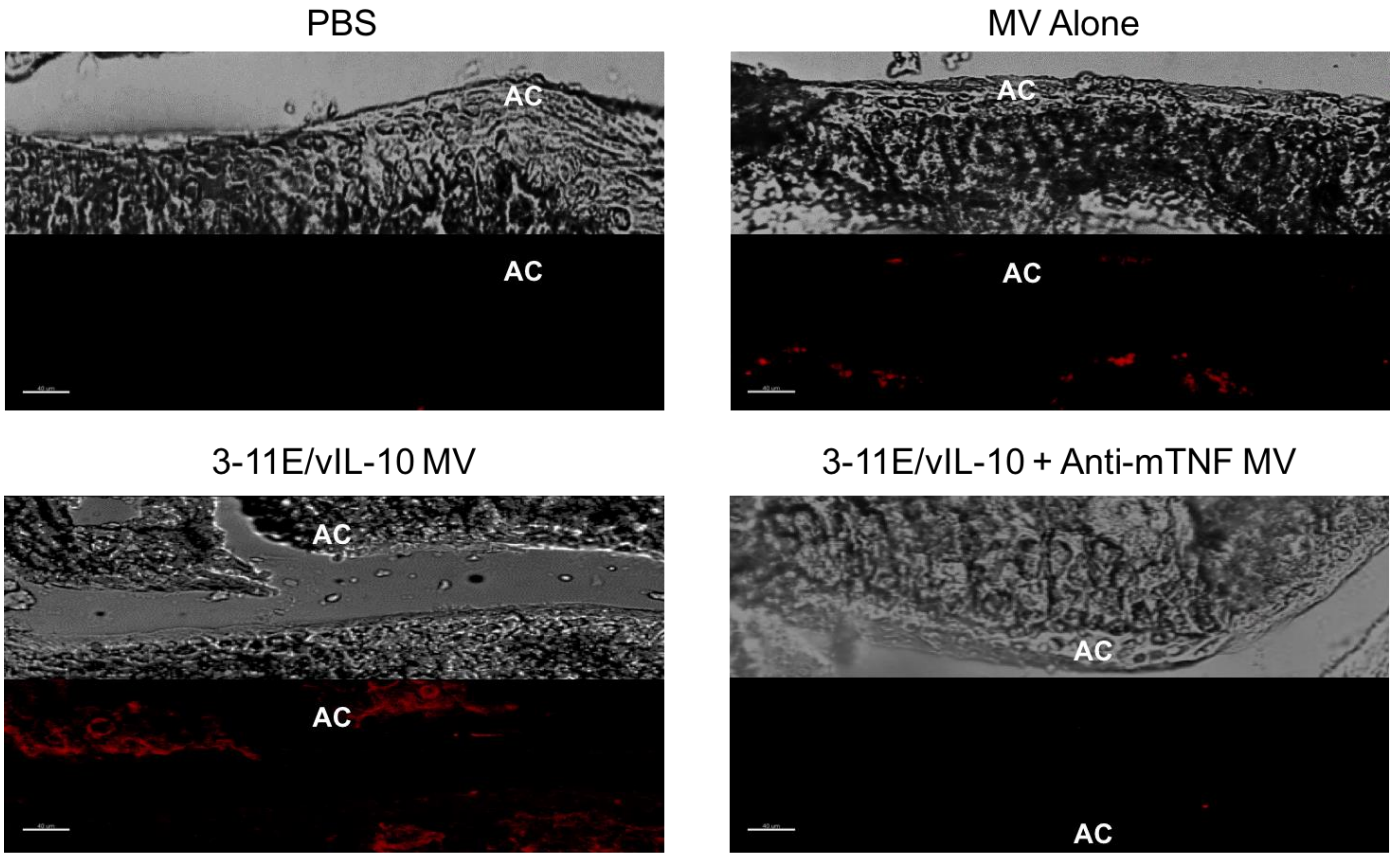

Figure 51. Localisation of microvesicles alone, anti-ROS-CII fused to vIL10 enriched microvesicles (3-11E/vIL-10 MV) and anti-ROS-CII fused to vIL10 + Anti-mTNF enriched microvesicles (3-11E/vIL-10 + Anti-mTNF MV) in the arthritic joint after intravenous administration. At the end-point of experiment (day 7), knees were harvested and snap frozen in OCT medium. Knees were sectioned by cryotomy and probed by confocal microscopy to detect the presence of fluorescent treatment in the arthritic cartilage. As observed previously, mice treated with 3-11E/vIL-10 MV showed specific localisation of treatment in the arthritic cartilage. Unexpectedly, mice treated with 3-11E/vIL-10 + Anti-mTNF MV showed no fluorescence retention in the arthritic knee. AC = articular cartilage. n = 3 mice per group.

Histological staining was also performed to assess cartilage damage and inflammation within the joint. Knees were harvested, formalin fixed and decalcified before paraffin embedding and sectioning. Knee sections were stained with safranin O to assess cartilage damage. Naïve mice showed strong safranin O staining in all layers of the cartilage. PBS injected mice shows visual loss of safranin O staining, throughout all layers of some areas of the cartilage. MV alone treated mice showed some loss of proteoglycans in the cartilage, but overall showed a healthier phenotype, similar to naïve mice . 3-11E/vIL-10 MV and 3-11E/vIL-10 + Anti-mTNF MV treated mice showed strong staining of cartilage but surprisingly had more inflammation present compared to MV alone treated mice, although less than the PBS treated controls.

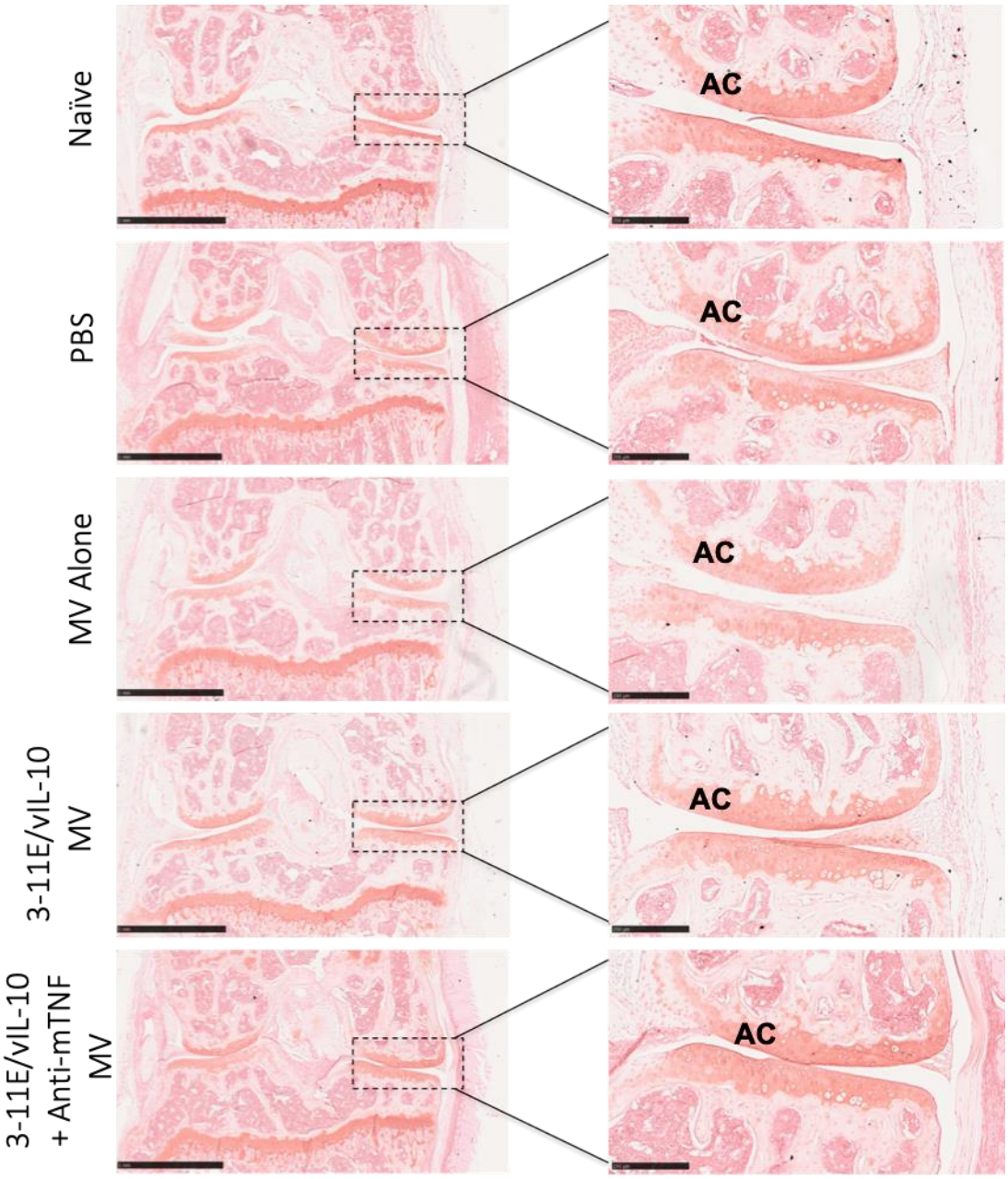

Figure 52. Safranin O staining of treated arthritic mouse knees. Mouse knees were fixed and decalcified before sectioning and staining with safranin O to assess cartilage integrity. Representative images of each group are shown. AC = articular cartilage. n = 5 mice per group.

Stained knee joints were given a value of 0–5 for inflammatory score: 0- normal; 1- acute synovitis; 2- marrow reaction; 3- bone erosion; 4- expanded synovial granulation (severe thickening); 5- loss of cartilage (as a result of structural collapse) and ankyloses.. As expected, PBS mice showed the highest inflammatory grade. Surprisingly, MV alone mice scored the best on average, followed by the 3-11E/vIL-10 MV and 3-11E/vIL-10 + Anti-mTNF mice. This trend is the opposite to the clinical knee swelling, but is likely the difference between acute oedema observed in the swelling and cellular changes observed in the histology. From these observations, the loaded MV are most efficacious to eliminate the initial inflammation in the joint, whereas these additional treatments have less of an effect on the infiltrate compared to MV alone. All treatment groups see an improvement compared to PBS control mice, however, in line with the clinical knee measurements..

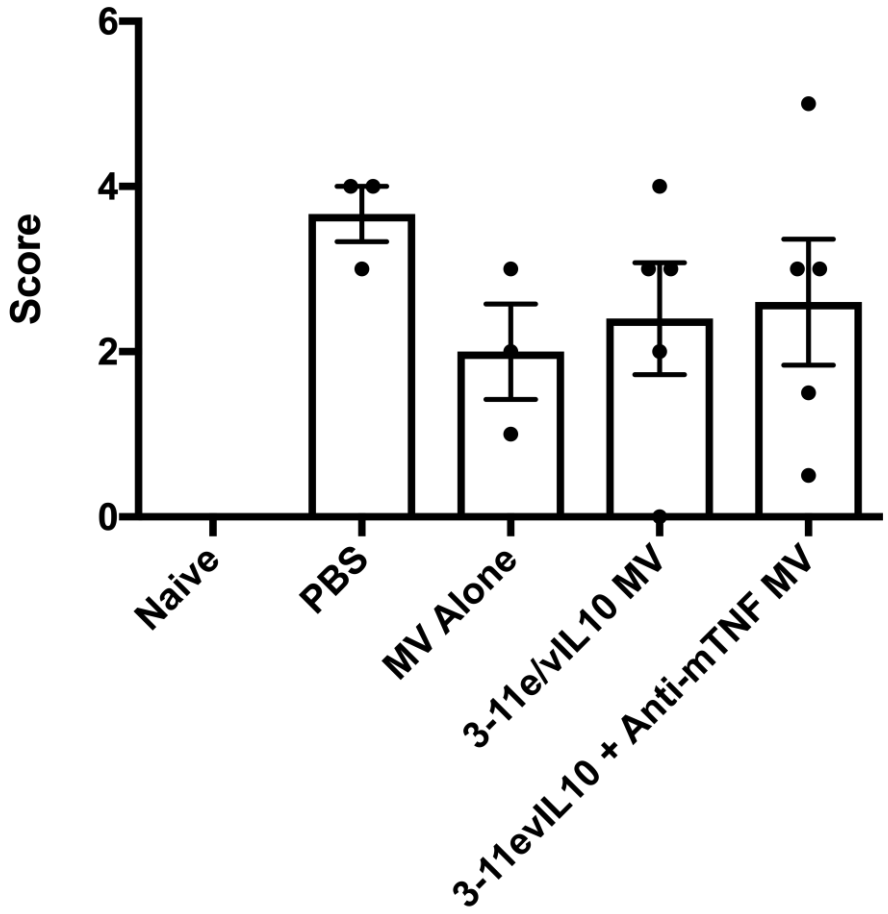

Figure 53. Histological arthritis scores of antigen induced arthritic stifle joints. Joints were scored 0-5 based on the degree of inflammation within the joint. Mice were treated intravenously with either PBS, MV Alone, 3-11E/vIL-10 MV or 3-11E/vIL-10 + Anti-mTNF MV. One-way ANOVA with Dunn's multiple comparisons test was performed to determine differences in inflammatory score. No statistical significance was observed.

3.8.3 RT-qPCR of Knee Joints

As aforementioned, arthritic knee joints were harvested and snap frozen immediately. Knee joints were thawed and excess muscle and bone was removed before RNA was extracted by trizol method. RNA was reverse transcribed into cDNA and analysed by RT-qPCR to look at the expression of a panel of chondroprotective and chondrodestructive genes within the knee joint. Figure 54 shows the expression of chondroprotective genes within the knee joints of treated mice. Gene expression was calculated as $2^{-\Delta\Delta Ct}$ relative to housekeeping gene RPL32. Relative gene expression is shown over naïve mice expression. Overall, the chondrodestructive panel showed larger variation in gene expression between treatment groups than the chondroprotective panel. Figure 54 shows the expression of chondroprotective genes in mice treated with PBS, MV alone, 3-11E/vIL-10 MV or 3-11E/vIL-10 + anti-mTNF MV. PBS treated mice do not see large reductions in the expression of chondroprotective genes, with only aggrecan and SOX9 largely downregulated. In these two genes, the treatment groups all saw an increase of expression, albeit not statistically significant.

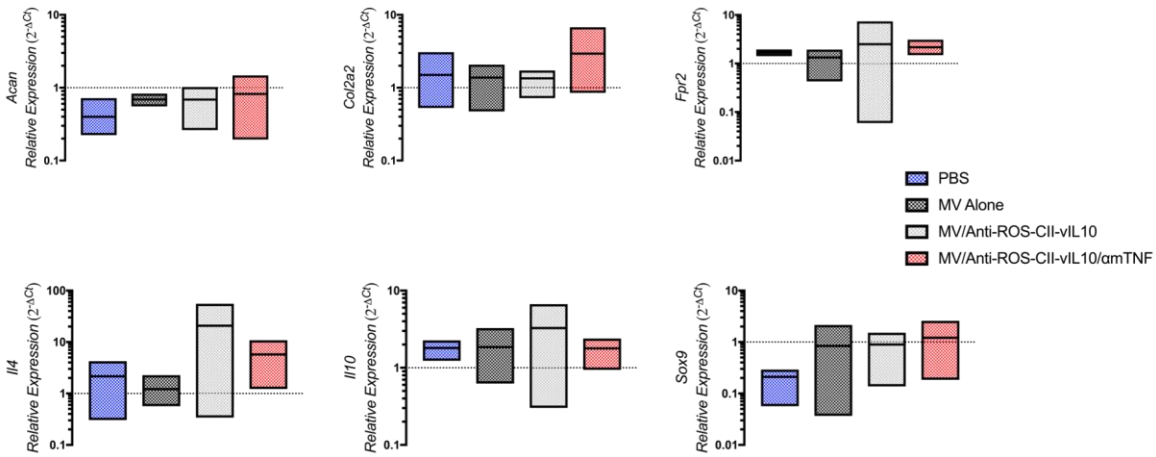

Figure 54. RT-qPCR analysis of local chondroprotective gene expression in treated mice. RNA was extracted from whole knee joints and reverse transcribed into cDNA. RT-qPCR was performed to assess local gene expression of a panel of chondroprotective genes. Data shown are $2^{-\Delta\Delta}$CT with knee joints from naive mice as calibrator and RPL32 as housekeeping gene. Data are expressed as min to max floating bars with line at mean. Kruskal Wallis test with Dunn's multiple comparison post-test conducted to test significance (no significant difference). n = 3 mice per group.

Figure 55 shows the expression of chondrodestructive genes within the knee joints of treated mice. The chondrodestructive panel saw greater variation of gene expression over naïve mice. PBS mice had the most upregulation of all the genes assessed in the panel, with a general downward trend for mice treated with MV alone, 3-11E/vIL-10 MV or 3-11E/vIL-10 + anti-mTNF MV. ADAMTS5 is the only exception to this, remaining highly upregulated in all treatment groups. Mice treated with 3-11E/vIL-10 MV or the combined treatment of 3-11E/vIL-10 + anti-mTNF MV overall saw the most reduction in expression compared to PBS treated mice, coming closely down to naïve levels. These differences were not statistically significant from PBS treated mice, however.

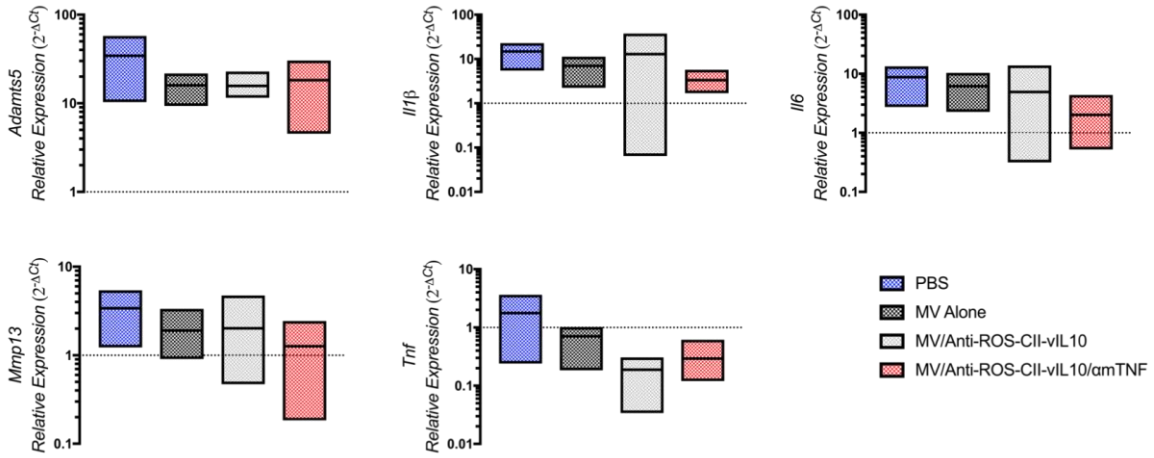

Figure 55. RT-qPCR analysis of local chondrodestructive gene expression in treated mice. RNA was extracted from whole knee joints and reverse transcribed into cDNA. RT-qPCR was performed to assess local gene expression of a panel of chondrodestructive genes. Data shown are $2^{-\Delta\Delta}$CT with knee joints from naïve mice as calibrator and RPL32 as housekeeping gene. Data expressed as min to max floating bars with line at mean. Kruskal Wallis test with Dunn's multiple comparison post-test conducted to test significance (no significant difference). n = 3 mice per group.

Figure 56 shows a heat map summary of average gene expression profiles for visual clarification and comparison. The left panel represents the genes in the chondrodestructive gene panel, with the right panel the chondroprotective cluster of genes. Notably, the MV alone, 3-11E/vIL-10 MV and 3-11E/vIL-10 + Anti-mTNF MV treated mice have gene expression more similar to naïve mice than the PBS treated mice.

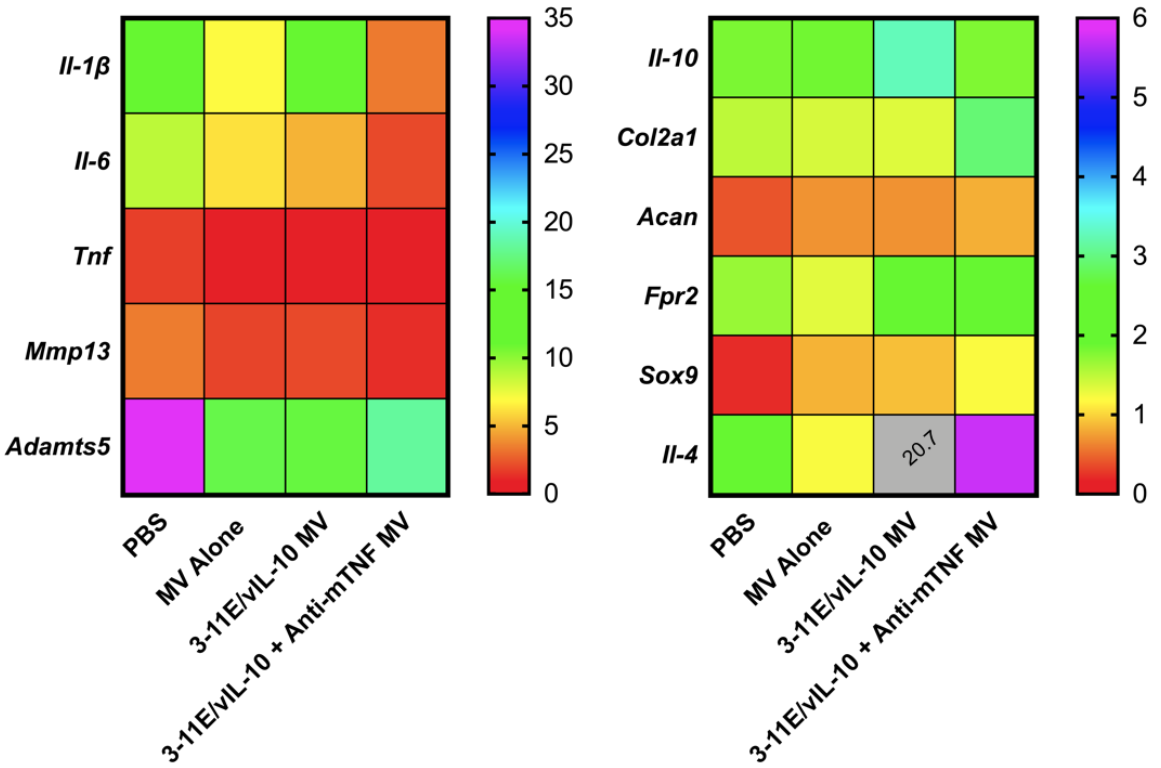

Figure 56. Heat map summary of average local gene expression in treated mice. Data shown are $2^{-\Delta\Delta}$CT with knee joints from naive mice as calibrator and RPL32 as housekeeping gene. Chondrodesctructive genes are shown in the left panel, with chondroprotective genes in the right panel. The range of gene regulation for chondrodestructive genes was vast, from 0-35, whereas chondroprotective gene regulation ranged only from 0-6. n = 3 mice per group.

Chapter 4: Discussion of Results

EV have been extensively explored in recent years as therapeutic vectors. EV can be utilised as a scaffold for novel nanomedicines due to the ease of incorporation of drugs, and have been utilised in a variety of disorders, with many used for delivering RNA based therapies [145,146]. PMN MV have been previously enriched with pro-resolving proteins and mediators, to facilitate trafficking of mediators with minimal dilution and/or inactivation [139,140]. Loading with additional therapies has enhanced the innate anti-inflammatory effect observed by PMN MV. The potential of PMN MV for inflammatory arthritis treatment was further propelled following the observations of cartilage penetration and protection [136]. The pro-resolving and anti-inflammatory properties of neutrophil MV in the context of arthritis are now well described, making them an attractive candidate as a biological scaffold. Nevertheless, studies have been limited by the need for local administration to observe the desired effects [136,147]. Existing therapies for RA, such as anti-TNF therapy combined with methotrexate, can counteract chronic inflammation and reduce symptoms [148], but no current therapy is able to actively protect cartilage from further degradation.

The utilization of anti-ROS-CII antibodies provide a means to delivering tailored therapies directly to the site of the body that needs it. Previous studies have shown anti-ROS-CII fused with anti-inflammatory cytokines localise and reduce inflammation in an arthritis mouse model [39]. This innovative antibody technology helps to address the unmet need of RA treatment to improve therapies by reducing side effects and non-response. For the

first time, we have enriched MV with an antibody as means of specific delivery of MV to the diseased tissue.

This thesis aimed to challenge this current state of treatment and make a progressive step towards: i) producing an effective treatment of systemically injected MV; (ii) targeting MV biological scaffolds loaded with therapies to the arthritic cartilage; (iii) developing a new combined therapy using traditionally used anti-inflammatory therapies alongside PMN MV.

This thesis aimed to test the possibility of targeting PMN MV using antibodies to ROS modified CII and assess the ability to resolve ongoing inflammation. The potency has been evaluated both with and without additional anti-inflammatory therapeutics.

4.1 Anti-ROS-CII Antibodies Localise Specifically in the Arthritic Joint

The first part of my project was to validate a new anti-ROS-CII candidate and its reliability for targeting to the arthritic joint. Initial experiments were centered on the production and validation of anti-ROS-CII *in vitro.* The main candidate used in this thesis, 3-11E scFv, has not been characterised and validated previously, whereas, the candidate 1-11E had been utilized in previous experiments and thus published material is available [39,115,118]. As previously explained, the 3-11E scFv candidate has been utilised in this thesis due to the problems arising during the 1-11E scFv candidate production. The 1-11E candidate undergoes glycosylation of the binding site during production, which can be inhibited by treating the cells with tunicamycin, but subsequently results in a low yield. Thus, the 3-11E scFv candidate was explored in this thesis as an appropriate alternative to target the arthritic joint.

The expected and observed *in vitro* findings were similar to that of the established 1-11E antibody. The molecular weight of the produced antibody was standard for a scFv (Figure 16) and the binding of the antibody was strong to the ROS modified CII, but minimal to the native CII (Figure 18). The characteristics of the 3-11E antibody appears very similar to that of the 1-11E candidate *in vitro* [39,118] . Immunofluorescence using the 3-11E antibody also shows similar patterns to that of the 1-11E antibody, binding strongly in RA mouse tissue around the chondrocytes in a pericellular fashion (Figure 19) [39]. Following validation of the 3-11E antibody *in vitro*, localisation studies were performed *in vivo*. For the initial *in vivo* experiments, 1-11E was included as a comparative control, as well as the

C7 negative antibody. The 3-11E showed strong localisation in the arthritic joint following systemic administration. Mice injected with scFv antibodies showed similar localisation of 1-11E and 3-11E, although 1-11E was slightly higher (Figure 21). The C7 scFv injected mice showed no specific localisation in the arthritic joint.

Similarly, for the mice injected with IgG antibodies, 3-11E and 1-11E showed strong localisation in the arthritic knee, with no localisation in the contralateral control knees (Figure 22). The difference between 3-11E and 1-11E in the IgG injected mice was lower than the scFv injected mice. The standard error is high in the IgG injected mice, but an n of 3 mice per group is likely responsible for that error. The behavior of the 1-11E antibody was similar to that observed in previous published data, which both confirmed the previous publications and that the optical imaging system is running efficiently [39,118]. The observation of the 3-11E localisation being like the 1-11E antibody certifies that the new candidate behaves similarly to the 1-11E candidate, and that using the 3-11E candidate for targeting the joint is viable.

After the validation of the 3-11E antibody in an inflammatory arthritic model, the *in vivo* localisation of the antibody in an OA model was evaluated. As OA is considered less inflammatory than RA [50], the antibodies were administered by intra-articular injection as opposed to intravenous administration. The lack of vascularization in the knee in OA, which is often not the case in models of RA due to *de novo* blood vessel formation [149], meant the scFv (with a short half-life) may not reach the joint well in an OA model [150]. To overcome this, intra-articular injection and the retention of the antibody in the joint was assessed to determine if the 3-11E candidate binds to osteoarthritic cartilage.

The experiment used the 6-11D antibody as a positive control, which binds to both healthy and ROS modified cartilage. As expected, the retention of the 6-11D antibody is high in both the arthritic and contralateral knees of mice at 4 weeks and 8 weeks post-surgery (Figure 25 and Figure 26). The 3-11E antibody was retained exclusively in the arthritic knee of mice at both 4 weeks and 8 weeks post-surgery. The antibody injected into the contralateral knees was cleared quickly, indicating that 3-11E binds to osteoarthritic cartilage as well as rheumatic cartilage. The 1-11E candidate was previously shown to bind to arthritic cartilage in the mouse model of DMM, so the retention of 3-11E scFv in the DMM model is not surprising [115]. As the previous experiments comparing the 1-11E and 3-11E localisation in the AIA model showed similar behavior of the two candidates, the same is likely for localisation in OA tissue.

The ratio of 3-11E fluorescence observed in the arthritic and contralateral knees was lower at 8 weeks post-surgery than 4 weeks post-surgery. Additionally, the binding of 3-11E antibody to OA tissue by immunofluorescence appears slightly dampened in later time points (Figure 20). This may be due to the cumulative degradation of cartilage throughout the model. DMM is a progressive model resulting in degenerative cartilage loss over time [151]. It is possible that as cartilage damage becomes extensive, the ROS modified CII epitopes become destroyed, hence antibody binding would decrease. The molecular changes to the cartilage in the earlier stages of disease likely results in stronger binding than in the later stages of disease, where overt cartilage damage is evident. In terms of translation into patient strategies, I envisage that the 3-11E antibody can be utilized for early OA detection, when molecular changes are occurring in the cartilage, but

overt damage is not necessarily observed. The 3-11E antibody could potentially be used translationally as an imaging tool in humans as an immunoconjugate for SPECT or PET imaging, such as is currently used in oncologic imaging [152].

To assess the ability of the 3-11E antibody to target a therapeutic agent to the arthritic joint, a localisation study using 3-11E fused to vIL-10 was conducted. A similar study was conducted previously using the 1-11E antibody, and found that localisation in the joint resulted in the cleavage of the matrix metalloprotease (MMP) linker fusing the antibody to the vIL-10 [39]. Whilst in a fused form, the vIL-10 is latent, and thus cannot exert its anti-inflammatory effects. The antibody must localise in the inflammatory microenvironment (rich in MMP) for the cleavage to occur and for the vIL-10 to manifest. The localisation study conducted in an AIA mouse model found that the 3-11E/vIL-10 antibody still localizes successfully in the arthritic joint. Furthermore, the immunohistochemistry analysis showed the effects of the therapeutic vIL-10, with fewer cellular infiltrates and a greater safranin O staining in the arthritic joint of mice treated with 3-11E/vIL-10. This effect was not observed in mice injected with C7/vIL-10- vIL-10 fused to a negative antibody which did not localise and hence cleave the MMP linker. This is further validation of the antibody targeting strategy and hence reinforcing the observation that the 3-11E antibody behaves similarly to the 1-11E counterpart.

4.2 Aqueous Energy Dissemination Results in Positive Incorporation of Anti-ROS-CII upon Microvesicles

Having validated the 3-11E antibody *in vitro* and *in vivo*, the focus of the project shifted into the aim of targeting of MV to the arthritic joint. As aforementioned, the 3-11E antibody was used throughout the continuation of the studies of this thesis.

The generation of MV from PMN was first performed according to established techniques of our laboratory. Analysis of the MV generated from activated PMN was conducted by two methods; flow cytometry and nanoparticle tracking. The analysis conducted by IS^x is beneficial as it allows visual observation of the sample to ensure you have a relatively pure MV population [136]. The method of generating MV is robust, as IS^x analysis is reproducible throughout different MV productions. Furthermore, the nanoparticle tracking analysis allows for identification of the purity of the MV population based on size. The MV produced are rarely less than 100nm or greater than 1000nm, suggesting that, by the official nomenclature of extracellular vesicles, the population are primarily 'microvesicles', as opposed to exosomes. Studies previously conducted by Norling *et al* and Dalli *et al* utilized a technique termed as aqueous energy dissemination [139,140]. This technique involves using liposome forming phospholipid to enrich MV with proteins or lipids. Liposomes are formed when the phospholipid is exposed to an aqueous solution, and the size of the liposomes can be altered by techniques such as sonication. In the previous studies, MV have been successfully enriched with pro-resolving proteins in the context of peritonitis and sepsis. This enrichment technique showed efficacy *in vivo* in

both studies, and provides an opportunity to simply, cheaply and effectively incorporate antibodies upon MV to target them to the arthritic joint.

The initial studies followed protocols adapted from the aforementioned papers [139,140]. A range of conditions were used to determine the optimum for incorporation of the antibody. Sonication is known to be needed to produce liposomes of nanometer size range, which would be best to incorporate the antibody without completely masking the MV [139]. Nonetheless, the conditions of manual resuspension and vortexing were also included for comparison. The flow cytometric analysis of incorporation determined double positive events, i.e. BODIPY stained vesicles that were positive for Cy5 antibody. The manual resuspension showed double positive events which have a larger side scatter than vesicles alone. They were also visually observed on the brightfield channels of the IS^{x}, unlike MV, indicating they are of larger size. The vortexing condition showed a low incorporation, although throughout repeats of the experiment this was variable and did increase. The size of these vesicles also appears larger due to the scatter and brightfield observations. The sonication conditions appear to show reduced size of MV as the intensity and time of sonication increases. The best incorporation was observed consistently in the sonication condition of 3 amplitude microns for 5 minutes. The range of double positive events throughout repeats was from 50-75%. The microscopic images from the IS^{x} analysis show the third sonication condition to produce what looks most like an MV before treatment but are also positive for the antibody.

To properly analyse size, nanoparticle-tracking analysis was conducted to determine the changes to the MV throughout each condition. After enrichment with antibodies, the MV

retained their characteristic size with just a small increase in average diameter. This increase was not statistically significant due to the attributions of the standard deviation. Previous studies utilizing aqueous energy dissemination observed a decrease in diameter following enrichment of protein, which was not observed in these studies [139]. The previous analysis was conducted using electron microscopy, whereas herein NTA was used. This is likely why differences are observed between studies, particularly as there is evidence to suggest the sensitivity of NTA for sizing is lower. Electron microscopy has a detection limit as low as 1 nm, whereas NTA has a higher detection limit of around 50-70 nm [153]. Nonetheless, the NTA analysis did confirm that the population of MV was not dramatically altered in diameter following incorporation with the antibodies.

After confirming by flow cytometry that the MV are positive for the antibody fluorescence after aqueous energy dissemination, it was important to determine whether the functions of the antibody were withheld throughout the process. The incorporation of anti-ROS-CII is futile if the binding capabilities are masked or destroyed. To check the binding of the antibody was still active, the established ELISA used to check the production of antibodies was slightly modified for checking the enriched MV. Native CII and ROS modified CII were used as the antigenic coating, with the enriched MV used as primary antibody (with MV alone and 3-11E alone as negative and positive controls, respectively). Importantly, enriched MV were pelleted at 20,000 *g* to remove the supernatant and any unbound antibody. Both the resuspended pellet and supernatant were run to determine how much antibody was incorporated as well as if the antibody binding site was still active. Sonication condition 2, which produced the most double positive events, showed positive binding of the enriched MV to ROS modified CII. There

was slightly more antibody activity in the resuspended pellet than in the supernatant, which represents the flow cytometry data nicely. Sonication condition 3 had a reduced antibody binding in both the resuspended pellet and the supernatant. It is likely that the prolonged and intense sonication has damaged the antibody-binding site somehow, due to the lack of binding in both the pellet and supernatant. Based on the microscopic images taken from the IS^x, the microvesicles still seem to be intact in all sonication conditions. It is known that the sonication of a range of proteins can induce the formation of aggregates that resemble amyloid [154]. It is likely that the antibodies are undergoing such a process, either masking or denaturing the binding site. The second sonication condition proved optimum, with the greatest incorporation and highest antibody activity of the enriched MV. This condition was used throughout the continuation of enrichment experiments.

The enriched MV were tested by immunofluorescence on AIA and DMM mouse tissue to certify the antibody binding but also to try and show the presence of both antibody and MV. For the first time, MV alone was used in immunofluorescence to assess their binding to arthritic cartilage tissue *in vitro*. The presence of MV were detected by fluorescence microscopy and are indicated with white arrow heads (Figure 32 and Figure 33). Very few MV were detected but were detected exclusively in cartilage tissue. The enriched MV showed positivity for antibody binding, as well as a huge increase in BODIPY fluorescence, albeit there was not a great amount of co-localisation. The C7 enriched vesicles did not show any antibody or MV fluorescence in the cartilage tissue. Interestingly, greater amounts of MV alone were observed in DMM tissue than AIA tissue, and greater BODIPY fluorescence of enriched MV was also observed in DMM tissue than AIA tissue. The

increase of MV alone in DMM tissue may be due to factors present more in osteoarthritic cartilage, such as a greater expression of FRP2/ALX receptor, which binds AnxA1 [155], or greater expression of phosphatidylserine receptor, which would bind the microvesicle membrane. Literature suggests that the former may be unlikely, as synovial tissue from RA patients has been found to have elevated FPR2 mRNA levels compared to the synovia from patients with OA [156], albeit FPR2 levels specifically within OA cartilage is not well characterised. The high BODIPY fluorescence in the anti-ROS-CII enriched MV is likely due to the binding by the antibody, as opposed to binding of the MV to the cartilage. The large increase of MV fluorescence in the enriched MV compared to the MV alone suggests that the presence of the antibody is responsible. This is promising as it further indicates that MV are being delivered to the cartilage *in vitro* by the enrichment with 3-11E scFv.

4.3 Microvesicles Enriched with Anti-ROS-CII Localise in the Arthritic Joint

In vivo investigations aimed to assess whether the MV enriched with 3-11E scFv localise in the arthritic joint. Not only was it important to show the localisation of the MV enriched with 3-11E scFv in the same manner as was conducted with the antibody validation, it was also important to demonstrate that microvesicles are going to the knee and more specifically into the cartilage.

The starting point of these experiments was to assess the spill over between fluorophores. Optical imaging has rarely been conducted using multiple fluorophores in literature, however it is a perfectly viable option as the technology is built for such experiments. To assess the spill over, a simple experiment was conducted using serial dilution of both fluorescent MV and 3-11E scFv and imaging at full saturation using the IVIS. As observed in Figure 34, there is no spill over between fluorophores observed. Although, in theory, the Texas red and Cy5.5 fluorophores were far enough apart on a spectrum to avoid such an issue, it was important to clarify this experimentally. The Texas Red fluorophore is used at an excitation of 580 nm and an emission of 620 nm. To avoid issues with mouse autofluorescence in optical imaging, it is optimal to use a fluorophore above the 600 nm range [157]. The Texas Red fluorophore sits around the 600 nm range, therefore although it is acceptable to use for imaging purposes a fluorophore nearer infrared would eliminate any trace of possible issues with autofluorescence. By scanning mice pre-treatment to assess autofluorescence levels, this possibility was minimized, however a fluorophore with a higher excitation would still be optimal. The Cy5.5

fluorophore does not have such issues, with an excitation of 660 nm and an emission of 710 nm.

Multiple small-scale experiments were necessary to optimize the imaging process using multiple fluorophores. There are very few studies published utilizing multiple fluorophores in an IVIS system, therefore small-scale localization studies with a low n number were performed to assess localisation specificity and experimental parameters. The experiment shown in Figure 35 was the first larger scale experiment assessing the localisation of enriched MV, both with anti-ROS-CII and negative control antibody. Mice injected with fluorescent MV alone and 3-11E scFv alone were included in the experiment as imaging controls but were not compared to the enrichment groups for *in vivo* localization due to the potential differences in doses. The localisation study looks at the fluorescence of both the MV and the 3-11E scFv to show the presence of both in the arthritic joint. As shown in Figure 35, the MV enriched with 3-11E scFv localized in the arthritic joint exclusively, like what we typically observe with the 3-11E antibody. The Texas Red fluorescence scan shows the localisation of the MV with the antibody. The peak for all fluorescence was observed at 18 hours. The half-life of our scFv antibody is known, and is around 2 hours. The half-life of a MV has not been well characterised. The enrichment process is likely to extend the half-life of both the scFv and the MV, which is why we see a peak at 18 hours. The ratio of the fluorescence between the AIA and contralateral knee for both the Texas Red and Cy5.5 fluorescence also peaks at 18 hours, confirming the peak of localisation for 3-11E enriched MV. The C7 ratio remains low at 1 for the Cy5.5 fluorescence throughout the experiment, but increases slightly at the 3-hour time point for the Texas Red fluorescence. The standard error for this time point is

quite large for the C7 group, and the increase may be down to the limited number of mice. Another possibility may be that the MV injected haven't been fortified with 3-11E scFv, as from the *in vitro* analysis shown in Figure 30, we know that around 70% are fortified with the antibody. As the fluorescence of the C7 isn't high in either the AIA or contralateral knee, the increase in ratio is not of great concern, and does not seem to represent a specific accumulation in the joint.

Organs were imaged *ex vivo* at the end of the experiment to assess whether an accumulation of MV or antibody was present. Small molecule drugs are typically eliminated through the kidney and liver [158], which is what we see from the Cy5.5 fluorescence of mice injected with 3-11E antibody. Interestingly, mice injected with MV alone also showed clearance of the MV through the kidney and liver, depicted by the Texas Red fluorescence. One previous study conducted a similar *ex vivo* analysis and found that extracellular vesicles accumulated in the liver, kidney, brain and intestine 3 hours post injection [159]. Previous studies in literature have also been conducted assessing the macrophage dependent clearance of extracellular vesicles through the liver and spleen. It was shown that when macrophages are depleted using clodronate, clearance of administered extracellular vesicles was much slower [160]. Although our analysis was conducted at the end-point of the experiment- some 72 hours post injection, we can see similarities between the published study and our findings. The organs imaged *ex vivo* did not include the brain in this experiment, which may have seen significant fluorescence 72 hours post injection. Furthermore, the stomach and intestines were imaged but had to be excluded from the analysis due to the chow diet of the mice. Alfalfa in the chow diet is highly fluorescent, and to fluorescently image intestinal organs of the mice an alfalfa free

diet is necessary [161]. Therefore, possible false positive fluorescence of the chow diet in this experiment meant the fluorescence of the intestines and stomach were discarded from analysis.

Overall, the most significant result of the *ex vivo* organ analysis was the presence of the 3-11E scFv antibody in the liver and kidneys. All other groups showed minimal fluorescence for both Texas Red and Cy5.5 fluorescence, suggesting that by 72 hours most of the products had been cleared systemically.

Knee joints were also imaged *ex vivo* to assess the localisation of enriched MV in the arthritic joint. To show that the PMN MV retain their characteristics previously shown in literature [136,141], knees were snap frozen following imaging to be cut and probed for the presence of vesicles within the cartilage. The observations of the localisation of MV as shown in at the end-point of the experiment specifically within the arthritic, and not healthy contralateral cartilage, confirmed the ability of MV to localise in the joint after enrichment with 3-11E. Previous studies have shown that MV penetrate *ex vivo* cartilage in the presence, but not absence, of pro-inflammatory cytokines [136,141], however the localisation observed in the 3-11E enriched MV mice is dependent on the antibody, as no vesicle localisation is observed in the MV alone and negative antibody enriched MV groups. Once localized to the arthritic knee, MV were observed within the arthritic cartilage, indicating that they are retaining their penetrative characteristics previously observed in literature [136,141].

4.4 Enriched Microvesicles Can Be Fortified with Anti-Inflammatory Therapeutics and Targeted to the Arthritic Joint

To produce a new generation of therapies, we have utilised the anti-ROS antibody for enrichment upon MV. The rationale behind utilising the MV as a biological scaffold to carry the targeted therapeutic antibodies is to co-deliver the chondroprotective MV alongside anti-inflammatory drugs, which thus far has never been attempted in this context. The localisation of 3-11E scFv enriched MV shows, thus far, the successful delivery of MV to the arthritic joint. There was no clinical efficacy observed in administering the targeted MV on their own systemically. This was likely due to the number of vesicles reaching the inflamed joint being lower than what is needed to see clinical efficacy. To enhance the therapeutic efficacy, an experiment attempting to incorporate an anti-inflammatory therapeutic alongside the anti-ROS-CII was performed. In this experiment, 3-11E/vIL-10 fusion protein was used. Previous experiments have shown the ability of vIL-10 fused to anti-ROS-CII candidate (1-11E, via MMP cleavable peptide linker) to reduce inflammation in a mouse model of arthritis [39]. The study showed that vIL-10 was latent in the circulation when it was still fused to 1-11E in the anti-ROS-CII/vIL-10 fusion protein. Once localized in the arthritic joint, where high levels of MMP are present, vIL-10 was cleaved by MMP from the fusion and became active. I utilized the 3-11E/vIL-10 fusion protein for MV enrichment but did not test directly whether the vIL-10 portion would remain latent in surface of the MV, and instead directly measured treatment efficacy of MV loaded with 3-11E/vIL-10 in reducing knee swelling in arthritic mice.

Figure 41 shows a reduction of the knee swelling in AIA mice injected with the above treatments. As previously documented, the anti-ROS-CII fusion with vIL-10 accelerates the reduction in knee swelling greater than in mice treated with vIL-10 fused to a negative control antibody (C7/vIL-10). Similar, and even enhanced, effects were observed in mice treated with MV loaded with 3-11E/vIL-10. Whether the reduction of knee swelling is due to the cleavage of vIL-10 is not known. If the antibody loaded on the MV is working in a similar manner to the soluble antibody, then it could be that MMP are still able to cleave the latent vIL-10 after incorporation, making the vIL-10 active. However, it may also be that the vIL-10 is not latent in our construct, due to conformational differences of the 3-11E/vIL-10 on MV compared to the 3-11E/vIL-10 antibody in solution. The efficacy of 3-11E/vIL-10 MV in reducing knee swelling suggests that one of the two scenarios is true, as MV enriched with vIL-10 fused to the negative control antibody (C7/vIL-10) did not show efficacy. Previous work characterizing the proteomic profile of neutrophil derived MV discovered that they contain MMP9, but no other MMP. MMP1 and MMP13 were shown to cleave the vIL-10 portion of the antibody, but as MMP9 has more of an important role in cell migration rather than ECM destruction, it it unlikely that the neutrophil MV would cleave the MMP linker on the 3-11E/vIL-10 antibody.

Clinical trials systemically administering recombinant IL-10 as an anti-inflammatory therapeutic have proved unsuccessful for both high dose and low dose, and due to this IL-10 has generally been rejected as a systemic treatment option [162–164]. This implies that a) efficacy is probably due to the targeted treatment and b) vIL-10 is active within the inflamed knee whether following cleavage by MMP if needed, or in the context of loading

upon MV it is not latent. To elucidate which mechanism is occurring with regards to the activity of vIL-10, future *in vitro* bioactivity assays should be performed in the presence and absence of MMP to determine if cleavage is needed to see vIL-10 activity.

Luminescent optical imaging was performed using luminol sodium salt, which produces chemiluminescence once cleaved by reactive oxidants. An inflamed, arthritic knee should emit a high level of luminescence, with a healthy knee producing very little. The luminescence is shown in Figure 42 as the fold change in photon flux in the arthritic knee compared to the healthy contralateral knee. In this way, each mouse has an internal control to normalize the luminescence. The treatment groups using either 3-11E or C7 antibody fused to vIL-10 showed differences akin to that observed in previous studies [39]. The C7/vIL-10 group shows an increase in the luminescence in the arthritic knee from day 1 to day 3, following the treatment administration at day 1 post induction. The increase in luminescence indicates that the inflammation is worsening, and the C7/vIL-10 treated group is like that of the PBS treated group. After 3 days, the inflammation starts to decrease in both the C7/vIL-10 and PBS groups, which is typical of the model. Interestingly, the mice treated with 3-11E/vIL-10 do not have the increase in luminescence between day 1 and 3 post-induction. This is likely due to the suppression by vIL-10 present in the arthritic joint. The level of inflammation in the 3-11E/vIL-10 treated and C7/vIL-10 treated mice does not return to a level of 1, indicating there is still a low level of inflammation at the end of the experiment. This is unexpected, as the PBS treated mice do return to a level of 1 by the end of the experiment, indicating that the levels of reactive oxidants in the arthritic knee is the same as the healthy, contralateral knee. The number of mice used per group was 5, giving statistical power to the experiment, yet the

error bars on the antibody treated groups are still large at the last time point. The 3-11E/vIL-10 MV treated group see a consistent decrease in fold luminescence after the first treatment at 1 day post induction. Interestingly, the C7/vIL-10 group does not show the increase in luminescence as seen in the antibody alone treated mice. Their levels do not decrease to the same degree as the mice treated with 3-11E/vIL-10 MV, but instead stay stagnant at a level of around 6-fold. This may indicate that the presence of vesicles circulating influences the levels of reactive oxidants in the joint. To properly clarify this, a group of mice injected with vesicles alone should also be imaged. In future experiments using luminol imaging, such a group will be included to assess whether the circulation of MV influences the levels of reactive oxidants in the arthritic joint. The luminol method of quantifying inflammation is not perfectly robust, with intraperitoneal injections given at each time point and an identical time needed between injecting and imaging. It is likely there is a degree of human error caused by having to inject each mouse one after the other, which can skew results. Therefore, this data should be taken only as a support of the clinical data.

Overall, the data enriching the MV with 3-11E/vIL-10 showed that we do not lose the function of our therapy once loaded upon the MV. The similar efficacy observed clinically is indicative that our antibody can reduce knee swelling to the same extent when loaded upon MV or administered alone. Furthermore, the reduced amount of antibody loaded on MV compared to the antibody alone control indicates that potentially less drug is needed when loaded upon the MV to achieve the same efficacy. This may be due to the slower release of drug when loaded on the MV, as has previously been observed *in vitro* within other studies utilizing EV for drug delivery [165,166]. This is an important characteristic

given the high expense associated with treating patients with biologics, with over £400 million spent a year by the NHS on Adalimumab alone [167].

4.5 Microvesicles can be enriched with Multiple Therapeutics to Maximize Efficacy

After efficacy was observed using 3-11E/vIL-10 MV to treat antigen induced arthritis, experiments were conducted with the incorporation of an additional anti-inflammatory therapy onto the MV. The efficacy of this combined therapy was compared to the single antibody 3-11E/vIL-10 MV. For the combined therapy, an anti-mTNF antibody was also incorporated onto the MV alongside the 3-11E/vIL-10 antibody. The anti-mTNF antibody used is a monoclonal antibody that can bind to both membrane bound and soluble mouse TNF. The binding of anti-mTNF to TNF inhibits the binding of TNF to TNFR1 and TNFR2, also known as 'death receptors', as observed in Figure 57. A characteristic feature of these receptors is the presence of a death domain- which has been shown to be responsible for the apoptotic function of the receptor. After binding of TNF to a TNF receptor, TRADD (TNFR1-associated death domain protein) interacts with TRAF2 (TNFR-associated factor 2), FADD (Fas-associated protein with death domain) and NIK (NF-κB-inducing kinase) [168,169]. Downstream signalling of these molecules includes caspase 8 and caspase 3 activation- which triggers apoptosis; RIP (receptor interacting protein), p38 and ERK (extracellular signal-regulated kinase) activation- which induces inflammation; and NF-κB activation- which also induces inflammation as well as proteasome degradation [168,169]. As shown in Figure 57, the simultaneous delivery of vIL-10 would result in binding to IL-10R, causing activation of the JAK/STAT pathways. IL-10 binding triggers an intracellular signalling cascade which involves JAK1, Tyk2 and STAT3; STAT3 dimerization and nuclear translocation to induce the expression of target genes [170]. TNF receptor 1 is

expressed in most tissues and is activated by both membrane bound and soluble TNF. TNF receptor 2 is primarily expressed in immune cells and responds to the membrane bound homotrimer form of TNF [171]. IL-10 receptor is expressed on most hematopoietic cells at basal levels but is upregulated upon activation, leading to its inhibitory mechanisms [172]. By utilizing two drugs, one that is an inflammatory blockade and the other a stimulator of anti-inflammatory mechanisms, an enhanced efficacy was observed in Figure 49. This efficacy was greater than the non-targeted control (C7/vIL-10 + Anti-mTNF MV), which suggests the targeting of the therapy is having a great effect. Additional studies using Anti-mTNF and 3-11E/vIL-10 combined, or Anti-mTNF and 3-11E/vIL-10 loaded on a non-specific MV scaffold, such as red blood cell derived MV, are needed to assess the efficacy of the PMN MV in the combination therapy.

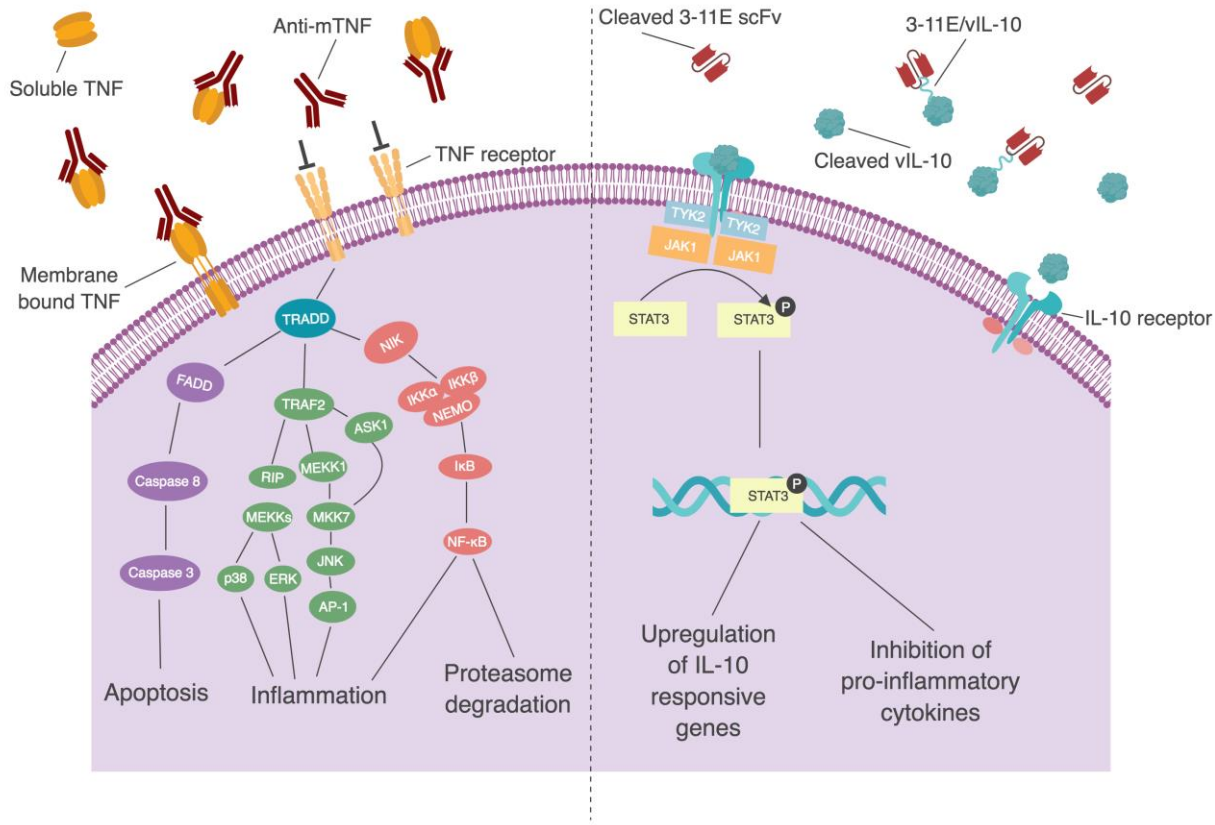

Figure 57. Schematic describing the co-delivery of anti-TNF and anti-ROS-CII fused to vIL-10. Anti-TNF antibody will inhibit soluble and membrane bound TNF, inhibiting activation of the TNF pathway and hence activation, inflammation and apoptosis. Simultaneously, the vIL-10 portion of the 3-11E/vIL-10 is cleaved in the presence of MMP. Once cleaved, the vIL-10 binds to the IL-10 receptor, causing activation of the JAK/STAT pathway and hence the upregulation of anti-inflammatory, IL-10 responsive genes and the inhibition of pro-inflammatory cytokines. Image created with Biorender.

Mice with AIA that were treated with MV loaded with 3-11E/vIL-10 and Anti-mTNF showed a complete amelioration of inflammation in the knee. The clinical scoring of mice treated with 3-11E/vIL-10 + Anti-mTNF MV outperformed the 3-11E/vIL-10 MV treated mice, as well as Anti-mTNF MV, indicating the enhanced efficacy when co-loading two anti-inflammatory therapeutics. This efficacy was only observed when the treatment was targeted using the 3-11E antibody, as mice treated with C7/vIL-10 + Anti-mTNF MV did not result in an amelioration of knee inflammation. The histological analysis did not show as clear a picture as the clinical knee swelling, with inflammatory cells still observed

within the knee joint. The treatment therefore is likely efficacious in reducing oedema but not completely ameliorating the influx of immune cells. The qPCR analysis supported the observations in the histology, with the combined treatment group having improved local gene expression compared to the PBS control mice, but not yet returned to the state of naïve mice. Further studies are needed to elucidate which beneficial effects are due to the targeting using the 3-11E antibody, the presence of MV or the combination of both.

An interesting and unexpected observation was the lack of MV fluorescence detected in 3-11E/vIL-10 + Anti-TNF treated mice at the end-point of experiment, as shown in Figure 51. One could speculate that it is likely related to the amelioration of oedema in these treated mice, and the return of near homeostatic conditions of the knee joint. As previously mentioned, there is limited knowledge regarding the half-life and retention of vesicles after administration in mice. Few studies exist that have explored the pharmacokinetics and pharmacodynamics, however those that have, involve extracellular vesicles administered in healthy mice. To my knowledge, no published pharmacokinetics and pharmacodynamics studies have been performed in arthritic mice. The few studies available in healthy mice have used vesicles derived from dendritic cells, mesenchymal stem cells, HEK293, 4T1, PC3, and MCF-7 cells [159,173,174]. Overall, what has been observed is a quick clearance through the liver after intravenous administration, but with fluorescence still detectable in organs at 48 hours post injection [159,173,174]. Although these studies have used vesicles of different cell origin in different physiological settings, there is a trend towards intravenous administration resulting in a rapid systemic clearance, with retention observed in organs specific for such clearance. These studies cannot be directly

translated to this work due to the vastly different read-outs, however may be indicative that in a non-inflamed, homeostatic state, vesicles are not retained in the body.

Similarly, the mechanism of MV presence within the arthritic joint is not fully understood, but significantly elevated levels of MV have been observed in the blood and synovial fluid of RA patients [136,175,176]. Furthermore, studies confirming the penetration of MV into cartilage *ex vivo* demonstrated that the phenomenon occurs with a higher distribution frequency in the presence of pro-inflammatory cytokines [136]. These previous observations indicate a significant role of neutrophil MV when inflammation is present in the joint. The data observed herein, particularly the data showing that MV go to the inflamed joint after intravenous administration, further supports these previous findings, and indicates that neutrophil MV hold an important mechanistic and therapeutic role in arthritis that is yet to be fully elucidated. It is likely that due to this important mechanism, when inflammation is reduced in the knee joint subsequently PMN MV also are reduced. This could be due to the removal of immune cells within the joint, of which MV have been shown to interact with. For example, it has been shown that macrophages phagocytose PMN MV, causing alternative activation of macrophages and eliciting a pro-resolving effect [147]. The phagocytosis of MV would result in the removal of MV from the joint once the immune cells were cleared. In a similar manner, MV presence within the cartilage is linked to the presence of inflammatory mediators [136]. After the first treatment dose of 3-11E/vIL-10 + Anti-mTNF MV, there was a rapid reduction of swelling from 100% to around 40%. Although inflammation is still present until the end of the experiment, it could be that MV penetration within the cartilage acts through a gradient of inflammatory mediators. By the end-point of the experiment, swelling was reduced to 0.3%- near

baseline levels, which is likely why in all mice treated with 3-11E/vIL-10 + Anti-TNF MV no MV fluorescence could be detected. To confirm these hypotheses, a treatment experiment with mice taken off at additional time points could indicate if the reduction of inflammation coincides with the reduction of MV within the cartilage. Such studies were not feasible due to the time and monetary constraints of this thesis, but in the future, could provide greater insight into the underlying mechanisms of PMN MV during inflammation.

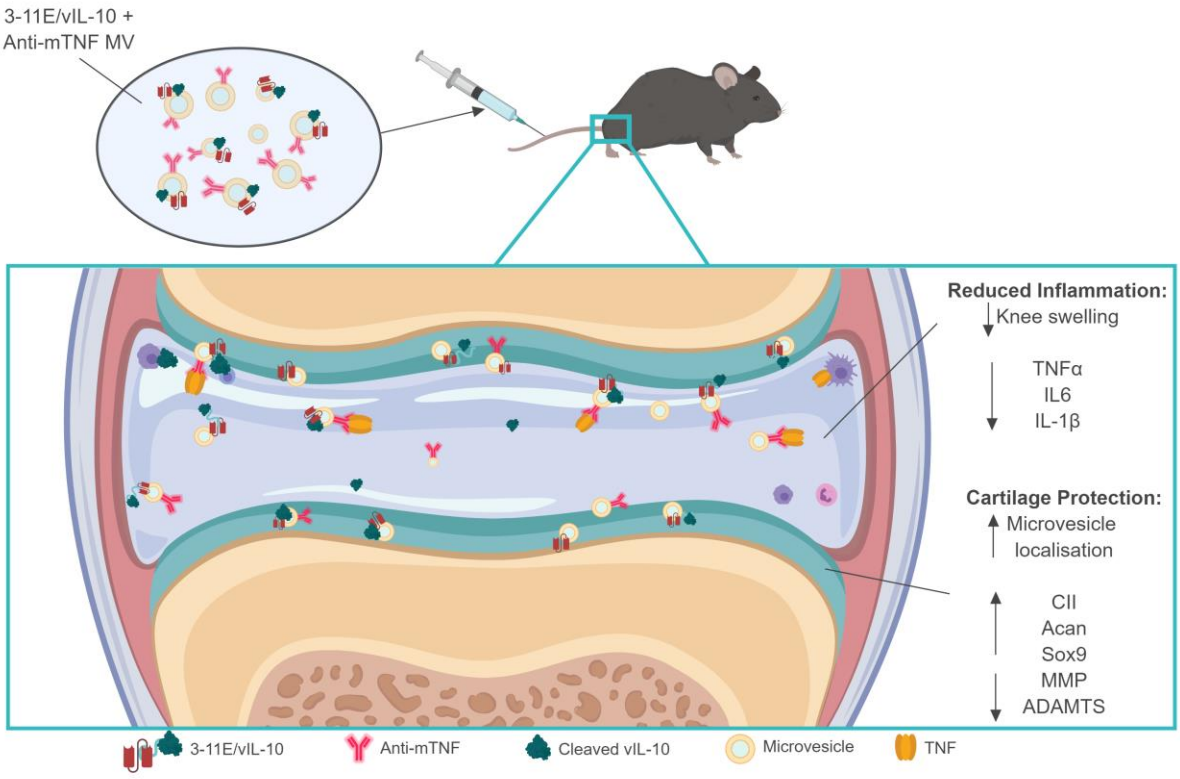

Figure 58. The delivery of vIL-10 and anti-mTNF to the arthritic joint through anti-ROS-CII targeted MV. MV enriched with 3-11E/vIL-10 and anti-mTNF antibody are administered intravenously in arthritic mice. The therapy is localised and retained in the arthritic knee joint by the 3-11E specificity to ROS-CII. The vIL-10 and anti-mTNF are delivered to the arthritic joint where they can elicit their anti-inflammatory actions. Simultaneously, the MV are delivered to the arthritic cartilage where they can exert their chondroprotective effects. Image created with Biorender.

The prime benefit of utilising MV as a biological scaffold is to co-deliver chondroprotective vesicles simultaneously with anti-inflammatory therapies, a remedy which is imperative to halt and potentially reverse disease damage, but is not currently available. Using MV therapeutically could be utilized in an autologous nature. The benefit of using autologous MV are that they are readily available from a small volume of blood, hold beneficial functions and will not result in a negative immune response, which is a potential downfall of using a synthetic scaffold. In this thesis, we have observed simultaneous chondroprotective and anti-inflammatory effects from treatment, but these effects are unlikely to be completely independent of each other, with MV holding anti-inflammatory properties and anti-inflammatory drugs sometimes potentiating chondroprotective effects. For example, although PMN MV have the unique ability to penetrate and protect cartilage, they have also been found to inhibit the release of TNF and IL-6 in macrophages, as well as increase the release of TGF-ß [133,147]. Similarly, studies have indicated that both anti-TNF and IL-10 treatment contributes to inhibiting cartilage destruction, albeit likely indirectly through the removal of cytokines which cause chondrocyte and synovial activation [177,178]. Nonetheless, these studies have shown that the combination of targeted MV with anti-inflammatory therapeutics is able to significantly reduce knee inflammation.

The studies utilising the anti-inflammatory and chondroprotective effects of MV, both herein and previously published in literature, have all used human samples. Although efficacy is seen in mice, using mice MV may allow for clearer stratification of the mechanism and therapeutic potential of MV. Logistically, using mice MV would be difficult due to the low blood volume and hence cell numbers you can obtain. It would

also mean using large numbers of mice to obtain the MV for experiments, which does not comply with the ethical use of animals in research. Furthermore, the characterisation of the protective components of human MV have been translated into mice, as shown by the inefficacy of MV treatment in mice lacking the receptor for annexin a1 [136]. The use of human MV in murine studies can be justified from these viewpoints.

Further studies to decipher the exact efficacious roles of the MV and the loaded therapies would be useful to distinguish the exact benefit of using MV as a scaffold, which hasn't been extensively elucidated herein. Nonetheless, previous studies have utilised the combination of the innate, protective properties of EV alongside the additional benefits of enriching with a drug, however the specific targeting of the therapy through use of an antibody has never previously been attempted but has been successful herein.

Chapter 5: Concluding Remarks and Future Directions

The studies conducted for this thesis have demonstrated the ability of enriched MV to be localized to the joint. The potential of PMN MV as a scaffold for the delivery of anti-inflammatory agents is being tested. The experiment conducted delivering MV with vIL-10 to the joint is efficacious in localisation, and subsequently reducing inflammation, only when targeted using the 3-11E scFv antibody. By enriching the targeted MV with multiple therapeutics, the efficacy can be pushed to fully resolve inflammation in our model. Furthermore, the targeted therapies have shown specific localisation and retention in the arthritic cartilage, as well anti-inflammatory and chondroprotective effects.

This report presents the opportunity of using aqueous energy dissemination for the purposes of enrichment of MV using antibodies. Here, the process has been shown to successfully incorporate whilst also protecting the binding specificity of the antibody. Furthermore, the process has been shown to not hinder the delivery of an anti-inflammatory therapeutic to the inflamed joint. The technique involves no harsh chemistry, is cost effective, efficacious and incredibly flexible. Furthermore, the enrichment using liposomes is likely to extend the half-life of both the antibodies and MV, as partially demonstrated throughout experiments. Nonetheless, the technique would need extensive characterisation to allow the production of consistent batches to meet the regulatory approval of a translational therapeutic.

The mouse model used throughout these studies is a T-cell driven monoarthritis model. Additional treatment studies could also be performed in other murine models of arthritis,

to confirm efficacy in a polyarthritis model with a different aetiology than antigen induced arthritis. Previous studies validating MV chondroprotection have been performed in the K/BxN serum transfer model and G6PI induced arthritis, and this is the first time that protection has been shown in an antigen induced arthritis model. Confirmation in other murine models, including the K/BxN serum transfer model, would be beneficial for confirmation of this proof of concept. Furthermore, additional studies are needed to elucidate the mechanisms of MV presence within the cartilage to fully understand when treatments could be administered and how efficacious cartilage penetration and protection is.

Herein, the technique has been used in a model of inflammatory arthritis for the proof of concept, however it is likely that it can be readily applied to other diseases. An appropriate biological scaffold, as well as a specific antibody for targeting is needed, but can provide an effective way to co-deliver multiple therapeutics specifically to the area of disease..

Bibliography

1. McInnes, I. B. & Schett, G. The Pathogenesis of Rheumatoid Arthritis. *N. Engl. J. Med.* **365,** 2205–2219 (2011).
2. Abramson, S. B. Inflammation in Osteoarthritis. in *Journal of Rheumatology* **31,** 70–76 (2004).
3. Holoshitz, J. The rheumatoid arthritis HLA-DRB1 shared epitope. *Curr Opin Rheumatol* **22,** 293–298 (2010).
4. Auger, I. & Roudier, J. A function for the QKRAA amino acid motif: Mediating binding of DnaJ to DnaK. Implications for the association of rheumatoid arthritis with HLA-DR4. *J. Clin. Invest.* **99,** 1818–1822 (1997).
5. van Vollenhoven, R. F. Sex differences in rheumatoid arthritis: More than meets the eye... *BMC Med.* **7,** (2009).
6. Forslind, K., Hafström, I., Ahlmén, M. & Svensson, B. Sex: A major predictor of remission in early rheumatoid arthritis? *Ann. Rheum. Dis.* **66,** 46–52 (2007).
7. Cutolo, M. *et al.* Synovial fluid estrogens in rheumatoid arthritis. *Autoimmun. Rev.* **3,** 193–8 (2004).
8. Vessey, M. P., Villard-Mackintosh, L. & Yeates, D. Oral contraceptives, cigarette smoking and other factors in relation to arthritis. *Contraception* **35,** 457–464 (1987).
9. Heliovaara, M., Aho, K., Aromaa, A., Knekt, P. & Reunanen, A. Smoking and risk of rheumatoid arthritis. *J. Rheumatol.* **20,** 1830–1835 (1993).
10. Kamphuis, S. *et al.* Tolerogenic immune responses to novel T-cell epitopes from heat-shock protein 60 in juvenile idiopathic arthritis. *Lancet* **366,** 50–56 (2005).
11. D'Aura Swanson, C., Paniagua, R. T., Lindstrom, T. M. & Robinson, W. H. Tyrosine kinases as targets for the treatment of rheumatoid arthritis. *Nat. Rev. Rheumatol.* **5,** 317–24 (2009).
12. McInnes, I. B. & Schett, G. Cytokines in the pathogenesis of rheumatoid arthritis. *Nat. Rev. Immunol.* **7,** 429–442 (2007).
13. Huber, L. C. *et al.* Synovial fibroblasts: key players in rheumatoid arthritis. *Rheumatology (Oxford).* **45,** 669–75 (2006).
14. Waaler, E. on the Occurrence of a Factor in Human Serum Activating the Specific

Agglutination of Sheep Blood Corpuscles. *Acta Pathol. Microbiol. Scand.* **17,** 172–188 (1940).

15. Mewar, D. & Wilson, A. G. Autoantibodies in rheumatoid arthritis: a review. *Biomed. Pharmacother.* **60,** 648–55 (2006).
16. Edwards, J. C., Leigh, R. D. & Cambridge, G. Expression of molecules involved in B lymphocyte survival and differentiation by synovial fibroblasts. *Clin. Exp. Immunol.* **108,** 407–14 (1997).
17. Chaiamnuay, S. & Bridges, S. L. The role of B cells and autoantibodies in rheumatoid arthritis. *Pathophysiology* **12,** 203–16 (2005).
18. Cantaert, T. *et al.* Citrullinated proteins in rheumatoid arthritis: Crucial... but not sufficient! *Arthritis Rheum.* **54,** 3381–3389 (2006).
19. Schellekens, G. A., De Jong, B. A. W., Van Den Hoogen, F. H. J., Van De Putte, L. B. A. & Van Venrooij, W. J. Citrulline is an essential constituent of antigenic determinants recognized by rheumatoid arthritis-specific autoantibodies. *J. Clin. Invest.* **101,** 273–281 (1998).
20. Luban, S. & Li, Z. G. Citrullinated peptide and its relevance to rheumatoid arthritis: An update. *Int. J. Rheum. Dis.* **13,** 284–287 (2010).
21. Asquith, D. L., Miller, A. M., McInnes, I. B. & Liew, F. Y. Animal models of rheumatoid arthritis. *Eur. J. Immunol.* **39,** 2040–4. (2009).
22. Courtenay, J. S., Dallman, M. J., Dayan, A. D., Martin, A. & Mosedale, B. Immunisation against heterologous type II collagen induces arthritis in mice [13]. *Nature* **283,** 666–8 (1980).
23. Stuart, J. M., Tomoda, K., Yoo, T. A. I. J., Townes, A. S. & Kang, A. H. SERUM TRANSFER OF COLLAGEN-INDUCED ARTHRITIS. *J Exp Med.* **158,** 378–92. (1983).
24. Brackertz, D., Mitchell, G. F. & Mackay, I. R. Antigen-induced arthritis in mice. I. Induction of arthritis in various strains of mice. *Arthritis Rheum.* **20,** 841–850 (1977).
25. Van Gaalen, F. A. *et al.* Association of Autoantibodies to Glucose-6-Phosphate Isomerase with Extraarticular Complications in Rheumatoid Arthritis. *Arthritis Rheum.* **50,** 395–9 (2004).
26. Smolen, J. S., Aletaha, D., Koeller, M., Weisman, M. H. & Emery, P. New therapies for treatment of rheumatoid arthritis. *Lancet* **370,** 1861–1874 (2007).

27. Feldmann, M., Brennan, F. & Maini, R. Role of cytokines in rheumatoid arthritis. *Annu. Rev. Immunol.* **14,** 397–440 (1996).
28. Bondeson, J., Feldmann, M. & Maini, R. N. TNF as a therapeutic target. *IMMUNOLOGIST* **8,** 136–140 (2000).
29. Feldmann, M. & Maini, R. N. The role of cytokines in the pathogenesis of rheumatoid arthritis. *Rheumatology* **38,** (1999).
30. Feldmann, M. & Maini, R. N. TNF defined as a therapeutic target for rheumatoid arthritis and other autoimmune diseases. *Nature Medicine* **9,** 1245–1250 (2003).
31. Williams, R. O., Paleolog, E. & Feldmann, M. Cytokine inhibitors in rheumatoid arthritis and other autoimmune diseases. *Current Opinion in Pharmacology* **7,** 412–417 (2007).
32. Scott, D. L., Wolfe, F. & Huizinga, T. W. J. Rheumatoid arthritis. in *The Lancet* **376,** 1094–1108 (2010).
33. Maxwell, L. J. & Singh, J. A. Abatacept for rheumatoid arthritis: a Cochrane systematic review. *J. Rheumatol.* **37,** 234–45 (2010).
34. Weiner, G. J. Rituximab : mechanism of action. **47,** 115–123 (2011).
35. Fleischmann, R. M. *et al.* Tocilizumab inhibits structural joint damage and improves physical function in patients with rheumatoid arthritis and inadequate responses to methotrexate: LITHE study 2-year results. *J. Rheumatol.* **40,** 113–126 (2013).
36. Thomson, T. M. *et al.* Blood-based identification of non-responders to anti-TNF therapy in rheumatoid arthritis. *BMC Med. Genomics* **8,** 26 (2015).
37. Paula, F. S. & Alves, J. D. Non-tumor necrosis factor-based biologic therapies for rheumatoid arthritis: Present, future, and insights into pathogenesis. *Biologics: Targets and Therapy* **8,** (2013).
38. Wijbrandts, C. A. & Tak, P. P. Prediction of Response to Targeted Treatment in Rheumatoid Arthritis. *Mayo Clin. Proc.* **92,** 1129–1143 (2017).
39. Hughes, C. *et al.* Targeting of viral Interleukin-10 with an antibody fragment specific to damaged arthritic cartilage improves its therapeutic potency. *Arthritis Res. Ther.* **16,** R151 (2014).
40. Dixon, W. G. *et al.* Drug-specific risk of tuberculosis in patients with rheumatoid arthritis treated with anti-TNF therapy: results from the British Society for Rheumatology Biologics Register (BSRBR). *Ann. Rheum. Dis.* **69,** 522–8 (2010).

41. Mertens, M. & Singh, J. A. Anakinra for rheumatoid arthritis: a systematic review. *J Rheumatol* **36,** 1118–1125 (2009).
42. Leandro, M. *et al.* Can Synovial Pathobiology integrate with Current Clinical and imaging Prediction Models to Achieve Personalized Health Care in Rheumatoid Arthritis? *Med* **4,** 413389–41 (2017).
43. Jinks, C., Jordan, K. & Croft, P. Osteoarthritis as a public health problem: the impact of developing knee pain on physical function in adults living in the community: (KNEST 3). *Rheumatology (Oxford).* **46,** 877–81 (2007).
44. Sandell, L. J. Etiology of osteoarthritis: genetics and synovial joint development. *Nat. Rev. Rheumatol.* **8,** 77–89 (2012).
45. Spector, T. D., Cicuttini, F., Baker, J., Loughlin, J. & Hart, D. Genetic influences on osteoarthritis in women: a twin study. *Bmj* **312,** 940–943 (1996).
46. Valdes, A. M. & Spector, T. D. Genetics of osteoarthritis. *Rheumatol. Sixth Ed.* **2–2,** 1477–1482 (2014).
47. Murphy, L. *et al.* Lifetime risk of symptomatic knee osteoarthritis. *Arthritis Care Res.* **59,** 1207–1213 (2008).
48. Woolf, A. D. & Pfleger, B. Burden of major muskuloskeletal conditions. *Bull World Heal. Organ* **81,** 646–56 (2003).
49. Glyn-Jones, S. *et al.* Osteoarthritis. in *The Lancet* **386,** 376–387 (2015).
50. Sokolove, J. & Lepus, C. M. Role of inflammation in the pathogenesis of osteoarthritis: latest findings and interpretations. *Ther. Adv. Musculoskelet. Dis.* **5,** 77–94 (2013).
51. Englund, M. & Lohmander, L. S. Risk factors for symptomatic knee osteoarthritis fifteen to twenty-two years after meniscectomy. *Arthritis Rheum.* **50,** 2811–2819 (2004).
52. Vincent, T. L. Targeting mechanotransduction pathways in osteoarthritis: A focus on the pericellular matrix. *Current Opinion in Pharmacology* **13,** 449–454 (2013).
53. Henrotin, Y., Kurz, B. & Aigner, T. Oxygen and reactive oxygen species in cartilage degradation: Friends or foes? *Osteoarthritis and Cartilage* **13,** 643–654 (2005).
54. Scanzello, C. R. & Goldring, S. R. The role of synovitis in osteoarthritis pathogenesis. *Bone* **51,** 249–257 (2012).
55. Ludwig, T. E., Mcallister, J. R., Lun, V., Wiley, J. P. & Schmidt, T. A. Diminished

Cartilage-Lubricating Ability of Human Osteoarthritic Synovial Fluid Deficient in Proteoglycan 4 Restoration Through Proteoglycan 4 Supplementation. **64,** 3963–3971 (2012).

56. Roemer, F. W. *et al.* Presence of MRI-detected joint effusion and synovitis increases the risk of cartilage loss in knees without osteoarthritis at 30-month follow-up: the MOST study. *Ann. Rheum. Dis.* **70,** 1804–9 (2011).
57. Zhang, W., Ouyang, H., Dass, C. R. & Xu, J. Current research on pharmacologic and regenerative therapies for osteoarthritis. *Bone Res* **4,** 15040 (2016).
58. Christensen, R., Astrup, A. & Bliddal, H. Weight loss: the treatment of choice for knee osteoarthritis? A randomized trial. *Osteoarthr. Cartil.* **13,** 20–27 (2005).
59. Roddy, E., Zhang, W., Doherty, M. & Roddy, E. Aerobic walking or strengthening exercise for osteoarthritis of the knee? A systematic review. *Ann Rheum Dis* **64,** 544–548 (2005).
60. Laupattarakasem, W., Laopaiboon, M., Laupattarakasem, P. & Sumananont, C. Arthroscopic debridement for knee osteoarthritis. *Cochrane Database Syst. Rev.* **23,** CD005118 (2008).
61. Grayson, C. W. & Decker, R. C. Total Joint Arthroplasty for Persons With Osteoarthritis. *PM R* **4,** (2012).
62. Pirmohamed, M. *et al.* Adverse drug reactions as cause of admission to hospital: prospective analysis of 18,820 patients. *Br. Med. J.* **329,** 15–19 (2004).
63. Wright, E. A., Katz, J. N., Abrams, S., Solomon, D. H. & Losina, E. Trends in prescription of opioids from 2003-2009 in persons with knee osteoarthritis. *Arthritis Care Res.* **66,** 1489–1495 (2014).
64. Chappell, A. S. *et al.* Duloxetine, a centrally acting analgesic, in the treatment of patients with osteoarthritis knee pain: A 13-week, randomized, placebo-controlled trial. *Pain* **146,** 253–260 (2009).
65. Lohmander, L. S. *et al.* Intraarticular sprifermin (recombinant human fibroblast growth factor 18) in knee osteoarthritis: a randomized, double-blind, placebo-controlled trial. *Arthritis Rheumatol. (Hoboken, N.J.)* **66,** 1820–31 (2014).
66. Goldring, M. B. & Marcu, K. B. Cartilage homeostasis in health and rheumatic diseases. *Arthritis Res. Ther.* **11,** 224 (2009).
67. Akkiraju, H. & Nohe, A. Role of Chondrocytes in Cartilage Formation, Progression of

Osteoarthritis and Cartilage Regeneration. *J. Dev. Biol.* **3,** 177–192 (2015).

68. Pathria, M. N., Chung, C. B. & Resnick, D. L. Acute and Stress-related Injuries of Bone and Cartilage: Pertinent Anatomy, Basic Biomechanics, and Imaging Perspective. *Radiology* **280,** 21–38 (2016).
69. Poole, A. R. *et al.* Composition and structure of articular cartilage: a template for tissue repair. *Clin. Orthop. Relat. Res.* **1,** S26–S33 (2001).
70. Sophia Fox, A. J., Bedi, A. & Rodeo, S. A. The basic science of articular cartilage: Structure, composition, and function. *Sports Health* **1,** 461–468 (2009).
71. Torzilli, P. A., Grigiene, R., Borrelli, J. & Helfet, D. L. Effect of Impact Load on Articular Cartilage: Cell Metabolism and Viability, and Matrix Water Content. *J. Biomech. Eng.* **121,** 433 (1999).
72. Rannou, F., François, M., Corvol, M. T. & Berenbaum, F. Cartilage breakdown in rheumatoid arthritis. *Joint Bone Spine* **73,** 29–36 (2006).
73. Sherwood, J. *et al.* A homeostatic function of CXCR2 signalling in articular cartilage. *Ann. Rheum. Dis.* **74,** 2207–2215 (2015).
74. Naranda, J., Gradišnik, L., Gorenjak, M., Vogrin, M. & Maver, U. Isolation and characterization of human articular chondrocytes from surgical waste after total knee arthroplasty (TKA). *PeerJ* **5,** e3079 (2017).
75. Pap, T. & Korb-Pap, A. Cartilage damage in osteoarthritis and rheumatoid arthritis—two unequal siblings. *Nat. Rev. Rheumatol.* **11,** 606–615 (2015).
76. Wojdasiewicz, P. *et al.* The Role of Inflammatory and Anti-Inflammatory Cytokines in the Pathogenesis of Osteoarthritis, The Role of Inflammatory and Anti-Inflammatory Cytokines in the Pathogenesis of Osteoarthritis. *Mediat. Inflammation, Mediat. Inflamm.* **2014,** e561459 (2014).
77. López-Armada, M. J. *et al.* Cytokines, tumor necrosis factor-α and interleukin-1β, differentially regulate apoptosis in osteoarthritis cultured human chondrocytes. *Osteoarthr. Cartil.* **14,** 660–669 (2006).
78. Koshy, P. J. T. *et al.* The modulation of matrix metalloproteinase and ADAM gene expression in human chondrocytes by interleukin-1 and oncostatin M: A time-course study using real-time quantitative reverse transcription-polymerase chain reaction. *Arthritis Rheum.* **46,** 961–967 (2002).
79. Hadjidakis DJ & Androulakis II. Bone Remodeling. *Ann. N. Y. Acad. Sci.* **1092,** 385–

396 (2006).

80. Diarra, D. *et al.* Dickkopf-1 is a master regulator of joint remodeling. *Nat. Med.* **13,** 156–163 (2007).

81. Scott, D. L. Radiological Progression in Established Rheumatoid Arthritis. in *Journal of Rheumatology* **31,** 55–65 (2004).

82. Wu, W. *et al.* Sites of collagenase cleavage and denaturation of type II collagen in aging and osteoarthritic articular cartilage and their relationship to the distribution of matrix metalloproteinase 1 and matrix metalloproteinase 13. *Arthritis Rheum.* **46,** 2087–2094 (2002).

83. Mengshol, J. A., Vincenti, M. P., Coon, C. I., Barchowsky, A. & Brinckerhoff, C. E. Interleukin-1 induction of collagenase 3 (matrix metalloproteinase 13) gene expression in chondrocytes requires p38, c-Jun N-terminal kinase, and nuclear factor κB: Differential regulation of collagenase 1 and collagenase 3. *Arthritis Rheum.* **43,** 801–811 (2000).

84. Mort, J. S., Magny, M. C. & Lee, E. R. Cathepsin B: an alternative protease for the generation of an aggrecan 'metalloproteinase' cleavage neoepitope. *Biochem. J.* **335 (Pt 3,** 491–494 (1998).

85. Stanton, H. *et al.* ADAMTS5 is the major aggrecanase in mouse cartilage in vivo and in vitro. *Nature* **434,** 648–652 (2005).

86. Glasson, S. S. *et al.* Deletion of active ADAMTS5 prevents cartilage degradation in a murine model of osteoarthritis. *Nature* **434,** 644–648 (2005).

87. Doyle, H. A. & Mamula, M. J. Post-translational protein modifications in antigen recognition and autoimmunity. *Trends in Immunology* **22,** 443–449 (2001).

88. Hogquist, K. A., Baldwin, T. A. & Jameson, S. C. Central tolerance: Learning self-control in the thymus. *Nature Reviews Immunology* **5,** 772–782 (2005).

89. Schwartz, R. H. Acquisition of immunologic self-tolerance. *Cell* **57,** 1073–1081 (1989).

90. Sykes, M. & Sachs, D. H. Bone marrow transplantation as a means of inducing tolerance. *Semin. Immunol.* **2,** 401–417 (1990).

91. Eggleton, P., Nissim, A., Ryan, B. J., Whiteman, M. & Winyard, P. G. Detection and isolation of human serum autoantibodies that recognize oxidatively modified autoantigens. *Free Radic. Biol. Med.* **57,** 79–91 (2013).

92. Strollo, R. *et al.* Autoantibodies to posttranslationally modified type II collagen as potential biomarkers for rheumatoid arthritis. *Arthritis Rheum.* **65,** 1702–1712 (2013).
93. Burska, A. N. *et al.* Autoantibodies to posttranslational modifications in rheumatoid arthritis. *Mediators Inflamm.* **2014,** (2014).
94. Strollo, R. *et al.* Antibodies to post-translationally modified insulin as a novel biomarker for prediction of type 1 diabetes in children. *Diabetologia* **60,** 1467–1474 (2017).
95. Afonso, V., Champy, R., Mitrovic, D., Collin, P. & Lomri, A. Reactive oxygen species and superoxide dismutases: Role in joint diseases. *Joint Bone Spine* **74,** 324–329 (2007).
96. Aruoma, O. I. Free radicals, oxidative stress, and antioxidants in human health and disease. *J. Am. Oil Chem. Soc.* **75,** 199–212 (1998).
97. Turrens, J. F. Mitochondrial formation of reactive oxygen species. *J. Physiol.* **552,** 335–344 (2003).
98. Bansal, S. *et al.* Advanced glycation end products enhance reactive oxygen and nitrogen species generation in neutrophils in vitro. *Mol Cell Biochem* **361,** 289–296 (2012).
99. Mittal, M., Siddiqui, M. R., Tran, K., Reddy, S. P. & Malik, A. B. Reactive Oxygen Species in Inflammation and Tissue Injury. *Antioxid. Redox Signal.* **20,** 1126–1167 (2014).
100. Fialkow, L., Wang, Y. & Downey, G. P. Reactive oxygen and nitrogen species as signaling molecules regulating neutrophil function. *Free Radical Biology and Medicine* **42,** 153–164 (2007).
101. Miyata, T. *et al.* Increased pentosidine, an advanced glycation end product, in plasma and synovial fluid from patients with rheumatoid arthritis and its relation with inflammatory markers. *Biochem. Biophys. Res. Commun.* **244,** 45–9 (1998).
102. Sharma, S. D., Pandey, B. N., Mishra, K. P. & Sivakami, S. Amadori product and age formation during nonenzymatic glycosylation of bovine serum albumin in vitro. *J. Biochem. Mol. Biol. Biophys.* **6,** 233–242 (2002).
103. Wright, H. L., Moots, R. J. & Edwards, S. W. The multifactorial role of neutrophils in rheumatoid arthritis. *Nature Reviews Rheumatology* **10,** 593–601 (2014).

104. Wright, H., Moots, R., Bucknall, R. & Edwards, S. Neutrophil function in inflammation and inflammatory diseases. *Rheumatology (Oxford).* **49,** 1618–31 (2010).
105. Korhonen, R., Lahti, A., Kankaanranta, H. & Moilanen, E. Nitric Oxide Production and Signaling in Inflammation. *Curr. Drug Targets -Inflammation Allergy* **4,** 471–479 (2005).
106. Auten, R. L. & Davis, J. M. Oxygen toxicity and reactive oxygen species: The devil is in the details. *Pediatric Research* **66,** 121–127 (2009).
107. Strollo, R. *et al.* Autoantibodies to posttranslationally modified type II collagen as potential biomarkers for rheumatoid arthritis. *Arthritis Rheum.* **65,** 1702–1712 (2013).
108. Nissim, A. *et al.* Generation of neoantigenic epitopes after posttranslational modification of type II collagen by factors present within the inflamed joint. *Arthritis Rheum.* **52,** 3829–3838 (2005).
109. Ryan, B. J., Nissim, A. & Winyard, P. G. Oxidative post-translational modifications and their involvement in the pathogenesis of autoimmune diseases. *Redox Biol.* **2,** 715–724 (2014).
110. Mackay, I. & Burnet, F. *Autoimmune diseases : pathogenesis, chemistry and therapy*. (Springfield: Charles C. Thomas, 1964).
111. Greenbury, C. L. & Skingle, J. Anti-cartilage antibody. *J. Clin. Pathol.* **32,** 826–31 (1979).
112. Mullazehi, M., Wick, M. C., Klareskog, L., van Vollenhoven, R. & Rönnelid, J. Anti-type II collagen antibodies are associated with early radiographic destruction in rheumatoid arthritis. *Arthritis Res. Ther.* **14,** R100 (2012).
113. Stuart, J. M., Townes, A. S. & Kang, A. H. Collagen autoimmune arthritis. *Annu. Rev. Immunol.* **2,** 199–218 (1984).
114. Trentham, D. E., Townes, A. S. & Kang, A. H. Autoimmunity to type II collagen an experimental model of arthritis. *J. Exp. Med.* **146,** 857–68 (1977).
115. Lim, N. H., Vincent, T. L. & Nissim, A. In vivo optical imaging of early osteoarthritis using an antibody specific to damaged arthritic cartilage. *Arthritis Res. Ther.* **17,** 376 (2015).
116. Sakata, M. *et al.* Autoantibodies to osteopontin in patients with osteoarthritis and

rheumatoid arthritis. *J. Rheumatol.* **28,** 1492–5 (2001).

117. Du, H. *et al.* The prevalence of autoantibodies against cartilage intermediate layer protein, YKL-39, osteopontin, and cyclic citrullinated peptide in patients with early-stage knee osteoarthritis: Evidence of a variety of autoimmune processes. *Rheumatol. Int.* **26,** 35–41 (2005).
118. Hughes, C. *et al.* Human single-chain variable fragment that specifically targets arthritic cartilage. *Arthritis Rheum.* **62,** 1007–1016 (2010).
119. Raposo, G. & Stoorvogel, W. Extracellular vesicles: Exosomes, microvesicles, and friends. *J. Cell Biol.* **200,** 373–383 (2013).
120. György, B. *et al.* Membrane vesicles, current state-of-the-art: Emerging role of extracellular vesicles. *Cellular and Molecular Life Sciences* **68,** 2667–2688 (2011).
121. Harding, C., Heuser, J. & Stahl, P. Endocytosis and intracellular processing of transferrin and colloidal gold-transferrin in rat reticulocytes: demonstration of a pathway for receptor shedding. *Eur. J. Cell Biol.* **35,** 256–63 (1984).
122. Cocucci, E., Racchetti, G. & Meldolesi, J. Shedding microvesicles: artefacts no more. *Trends in Cell Biology* **19,** 43–51 (2009).
123. Andriantsitohaina, R., Gaceb, A., Vergori, L. & Mart??nez, M. C. Microparticles as Regulators of Cardiovascular Inflammation. *Trends in Cardiovascular Medicine* **22,** 88–92 (2012).
124. Inal, J. M. *et al.* Microvesicles in health and disease. *Archivum Immunologiae et Therapiae Experimentalis* **60,** 107–121 (2012).
125. Miyoshi, H. *et al.* Calpain activation in plasma membrane bleb formation during tert-butyl hydroperoxide-induced rat hepatocyte injury. *Gastroenterology* **110,** 1897–1904 (1996).
126. Chieregatti, E. & Meldolesi, J. Opinion: Regulated exocytosis: new organelles for non-secretory purposes. *Nat. Rev. Mol. Cell Biol.* **6,** 181–187 (2005).
127. MacKenzie, A. *et al.* Rapid secretion of interleukin-1β by microvesicle shedding. *Immunity* **15,** 825–835 (2001).
128. Lösche, W., Scholz, T., Temmler, U., Oberle, V. & Claus, R. a. Platelet-derived microvesicles transfer tissue factor to monocytes but not to neutrophils. *Platelets* **15,** 109–115 (2004).
129. Gasser, O. & Schifferli, J. A. Activated polymorphonuclear neutrophils disseminate

anti-inflammatory microparticles by ectocytosis. *Blood* **104,** 2543–2548 (2004).

130. Distler, J. H. W. *et al.* Microparticles as regulators of inflammation: Novel players of cellular crosstalk in the rheumatic diseases. *Arthritis Rheum.* **52,** 3337–3348 (2005).
131. Mesri, M. & Altieri, D. C. Endothelial cell activation by leukocyte microparticles. *J. Immunol.* **161,** 4382–4387 (1998).
132. Henson, P. M. *et al.* Interaction between Phosphatidylserine and the Phosphatidylserine Receptor Inhibits Immune Responses In Vivo. *J Immunol.* **174,** 1393–1404 (2017).
133. Eken, C. *et al.* Ectosomes released by polymorphonuclear neutrophils induce a MerTK-dependent anti-inflammatory pathway in macrophages. *J. Biol. Chem.* **285,** 39914–39921 (2010).
134. Dalli, J. *et al.* Annexin 1 mediates the rapid anti-inflammatory effects of neutrophil-derived microparticles. *Blood* **112,** 2512–2519 (2008).
135. Sugimoto, M. A., Vago, J. P., Teixeira, M. M. & Sousa, L. P. Annexin A1 and the Resolution of Inflammation: Modulation of Neutrophil Recruitment, Apoptosis, and Clearance. *Journal of Immunology Research* **2016,** (2016).
136. Headland, S. E. *et al.* Neutrophil-derived microvesicles enter cartilage and protect the joint in inflammatory arthritis. *Sci. Transl. Med.* **7,** 315ra190 (2015).
137. EL Andaloussi, S., Mäger, I., Breakefield, X. O. & Wood, M. J. A. Extracellular vesicles: biology and emerging therapeutic opportunities. *Nat. Rev. Drug Discov.* **12,** 347–357 (2013).
138. Zitvogel, L. *et al.* Eradication of established murine tumors using a novel cell-free vaccine: dendritic cell derived exosomes. *Nat. Med.* **4,** 594–600 (1998).
139. Norling, L. V *et al.* Cutting Edge: Humanized Nano-Proresolving Medicines Mimic Inflammation-Resolution and Enhance Wound Healing. *J. Immunol.* **186,** 5543–5547 (2011).
140. Dalli, J. *et al.* Microparticle alpha-2-macroglobulin enhances pro-resolving responses and promotes survival in sepsis. *EMBO Mol. Med.* **6,** 27–42 (2014).
141. Headland, S. E. The role of neutrophil microparticles in rheumatoid arthritis. (Queen Mary University of London, 2014).
142. De Wildt, R. M. T., Mundy, C. R., Gorick, B. D. & Tomlinson, I. M. Antibody arrays

for high-throughput screening of antibody-antigen interactions. *Nat. Biotechnol.* **18,** 989–94. (2000).

143. Roopenian, D. C. & Akilesh, S. FcRn: The neonatal Fc receptor comes of age. *Nat. Rev. Immunol.* **7,** 715–725 (2007).
144. Nelson, A. L. Antibody fragments: Hope and hype. *MAbs* **2,** 77–8 (2010).
145. Usman, W. M. *et al.* Efficient RNA drug delivery using red blood cell extracellular vesicles. *Nat. Commun.* **9,** 2359 (2018).
146. Kojima, R. *et al.* Designer exosomes produced by implanted cells intracerebrally deliver therapeutic cargo for Parkinson's disease treatment. *Nat. Commun.* **9,** 1305 (2018).
147. Rhys, H. I. *et al.* Neutrophil Microvesicles from Healthy Control and Rheumatoid Arthritis Patients Prevent the Inflammatory Activation of Macrophages. *EBioMedicine* **29,** 60–69 (2018).
148. Weinblatt ME, Keystone EC, Furst DE, Moreland LW, Weisman MH, Birbara CA, et al. Adalimumab, a fully human anti-tumor necrosis factor alpha monoclonal antibody, for the treatment of rheumatoid arthritis in patients taking concomitant methotrexate: the ARMADA trial. *Arthritis Rheum* **48,** 35–45 (2003).
149. Szekanecz, Z., Besenyei, T., Szentpétery, Á. & Koch, A. E. Angiogenesis and vasculogenesis in rheumatoid arthritis. *Current Opinion in Rheumatology* **22,** 299–306 (2010).
150. Brenchley, P. E. Antagonising angiogenesis in rheumatoid arthritis. *Ann. Rheum. Dis.* **60 Suppl 3,** iii71-4 (2001).
151. Iijima, H. *et al.* Destabilization of the medial meniscus leads to subchondral bone defects and site-specific cartilage degeneration in an experimental rat model. *Osteoarthr. Cartil.* **22,** 1036–1043 (2014).
152. Kaur, S. *et al.* Recent trends in antibody-based oncologic imaging. *Cancer Lett.* **315,** 97–111 (2012).
153. van der Pol, E. *et al.* Particle size distribution of exosomes and microvesicles determined by transmission electron microscopy, flow cytometry, nanoparticle tracking analysis, and resistive pulse sensing. *J. Thromb. Haemost.* **12,** 1182–1192 (2014).
154. Stathopulos, P. B. *et al.* Sonication of proteins causes formation of aggregates that

resemble amyloid. *Protein Sci.* **13,** 3017–3027 (2008).

155. Bena, S., Brancaleone, V., Wang, J. M., Perretti, M. & Flower, R. J. Annexin A1 interaction with the FPR2/ALX receptor: identification of distinct domains and downstream associated signaling. *J. Biol. Chem.* **287,** 24690–7 (2012).
156. Perretti, M., Cooper, D., Dalli, J. & Norling, L. V. Immune resolution mechanisms in inflammatory arthritis. *Nat. Rev. Rheumatol.* **13,** 87–99 (2017).
157. Chen, H. & Thorne, S. H. Practical methods for molecular in vivo optical imaging. *Curr. Protoc. Cytom.* **59,** 12.24.1-12.24.11 (2012).
158. Wang, W., Wang, E. Q. & Balthasar, J. P. Monoclonal antibody pharmacokinetics and pharmacodynamics. *Clin. Pharmacol. Ther.* **84,** 548–558 (2008).
159. Choi, H. & Lee, D. S. Illuminating the physiology of extracellular vesicles. *Stem Cell Res. Ther.* **7,** 55 (2016).
160. Imai, T. *et al.* Macrophage-dependent clearance of systemically administered B16BL6-derived exosomes from the blood circulation in mice. *J. Extracell. Vesicles* **9,** 26238 (2015).
161. Inoue, Y., Izawa, K., Kiryu, S., Tojo, A. & Ohtomo, K. Diet and abdominal autofluorescence detected by in vivo fluorescence imaging of living mice. *Mol. Imaging* **7,** 21–27 (2008).
162. van Deventer, S. J., Elson, C. O. & Fedorak, R. N. Multiple doses of intravenous interleukin 10 in steroid-refractory Crohn's disease. Crohn's Disease Study Group. *Gastroenterology* **113,** 383–9 (1997).
163. Tilg, H., Ulmer, H., Kaser, A. & Weiss, G. Role of IL-10 for induction of anemia during inflammation. *J. Immunol.* **169,** 2204–9 (2002).
164. Tilg, H. *et al.* Treatment of Crohn's disease with recombinant human interleukin 10 induces the proinflammatory cytokine interferon gamma. *Gut* **50,** 191–5 (2002).
165. Munagala, R., Aqil, F., Jeyabalan, J. & Gupta, R. C. Bovine milk-derived exosomes for drug delivery. *Cancer Lett.* **371,** 48–61 (2016).
166. Kim, M. S. *et al.* Development of exosome-encapsulated paclitaxel to overcome MDR in cancer cells. *Nanomedicine Nanotechnology, Biol. Med.* **12,** 655–664 (2016).
167. NHS England. NHS England » NHS set to save £150 million by switching to new versions of most costly drug. *News Article* (2018). Available at:

https://www.england.nhs.uk/2018/10/nhs-set-to-save-150-million-by-switching-to-new-versions-of-most-costly-drug/. (Accessed: 15th January 2019)

168. Cao, X., Pobezinskaya, Y. L., Morgan, M. J. & Liu, Z. -g. The role of TRADD in TRAIL-induced apoptosis and signaling. *FASEB J.* **25,** 1353–1358 (2011).
169. Ozes, O. N. *et al. Tumor necrosis factor-α/receptor signaling through the Akt kinase*. *Cell Signaling in Vascular Inflammation* (2005). doi:10.1007/978-1-59259-909-7_2
170. Fioranelli, M. & Roccia, M. G. Twenty-five years of studies and trials for the therapeutic application of IL-10 immunomodulating properties. From high doses administration to low dose medicine new paradigm. *J. Integr. Cardiol.* **1,** 2–6 (2014).
171. Naudé, P. J. W., Den Boer, J. A., Luiten, P. G. M. & Eisel, U. L. M. Tumor necrosis factor receptor cross-talk. *FEBS J.* **278,** 888–98 (2011).
172. Shouval, D. S. *et al.* Interleukin 10 receptor signaling: Master regulator of intestinal mucosal homeostasis in mice and humans. *Adv. Immunol.* **122,** 177–210 (2014).
173. Smyth, T. *et al.* Biodistribution and delivery efficiency of unmodified tumor-derived exosomes. *J. Control. Release* **199,** 145–155 (2015).
174. Wiklander, O. P. B. *et al.* Extracellular vesicle in vivo biodistribution is determined by cell source, route of administration and targeting. *J. Extracell. Vesicles* **4,** 1–13 (2015).
175. Pisetsky, D. S., Ullal, A. J., Gauley, J. & Ning, T. C. Microparticles as mediators and biomarkers of rheumatic disease. *Rheumatology (United Kingdom)* **51,** 1737–1746 (2012).
176. Sellam, J. *et al.* Increased levels of circulating microparticles in primary Sjögren's syndrome, systemic lupus erythematosus and rheumatoid arthritis and relation with disease activity. *Arthritis Res. Ther.* **11,** R156 (2009).
177. Walmsley, M. *et al.* Interleukin-10 inhibition of the progression of established collagen-induced arthritis. *Arthritis Rheum.* **39,** 495–503 (1996).
178. Urech, D. M. *et al.* Anti-inflammatory and cartilage-protecting effects of an intra-articularly injected anti-TNFα single-chain Fv antibody (ESBA105) designed for local therapeutic use. *Ann. Rheum. Dis.* **69,** 443–449 (2010).